Studies on Microdamage and Remodelling around Osseointegrated Oral Implants

Studies on Microdamage and Remodelling around Osseointegrated Oral Implants

Submitted for the degree of Doctor in Philosophy

University of Dublin

2007

Abdulhadi Warreth, BDS (Benghazi), MDentSc (Dublin)

Department of Periodontology and Restorative Dentistry

School of Dental Science

Trinity College

Dublin

Declaration

I hereby declare that this thesis has not previously been submitted for a degree at this or any other university and that, apart from where due acknowledgement has been made, it is entirely my own work.

I agree that this thesis may be lent or copied at the discretion of the Librarian, Trinity College Dublin.

Signed .....

Date 16.5.2007.....

Summary

Osseointegrated implants have become part of everyday dental practice. Their high success rate is due to the ability of the implanted material, titanium, to integrate with the surrounding bone. The study of the dynamic nature of this integration at the implant-bone interface gives a better understanding of the bond between the bone and the implant surface, and allows exploration of factors that may modify this biological activity. Several factors have been suggested to lead to integration. One factor that has been reported to stimulate bone remodelling in long bone is microdamage which is believed to activate bone remodelling and repair, although the mechanism for this is unclear.

It is the purpose of the first study to examine the occurrence and significance of microdamage (microcracks) as a result of different implant placement modalities. The mandibular premolar regions of four mature male beagle dogs were used as implant sites.

After the extraction of the four mandibular premolars of each side and a healing period of three months, four implants were installed in each jaw side using four different treatment modalities. One day after the implant placement one fluorochromic chelating agent (tetracycline) was administrated. One day later, the dogs were sacrificed. From each implant site three histological sections of 150-200μm thick were obtained and examined using epifluorescence microscopy. Microcracks were identified and measured. These sections represented the buccal and lingual cortical bone that surrounded the implant sites. Candidate microcracks were identified using modified criteria obtained from the criteria that were originally used

for identification of microcracks stained with fuchsin, and then later it was refined using chelating agents.

No significant difference in the number of microcracks were found between the four modalities. The control group (V) had significantly fewer number of microcracks compared to the four treatment modalities (F= 3.335, p =0.0125). The lengths of microcracks did not differ between the treatment groups. Diffusely stained areas were found in the osteotomy walls and in close contact with the implant surfaces irrespective of the treatment modality.

The conclusion of the first study is that the implant surgery mainly leads to generation of contact damage in the osteotomy wall close to the implant surface. Linear microcracks also occurred as a result of the surgery in an area distant from the implant surface/osteotomy site.

The second study used 2-dimensional finite element model to investigate stress and strain generation that may occur during implant placement due to the mismatches between the diameters of the osteotomy site and the implant. The effect of thickness of bone surrounding the osteotomy on the stress and strain around the implant was also studied. To simulate bone displacement that may be generated by the insertion of an implant of 3.75mm in diameter when the osteotomy diameter was 3 and 3.25mm, two models were generated: one when the osteotomy wall was displaced 0.375mm in the x-direction while in the second model the osteotomy wall was displaced 0.25mm. Several sub-models were generated and bone thickness around the osteotomy area was constructed to simulate 5mm and 10mm bone thickness.

The FEM indicated that the predicted stresses and strains were always concentrated along the osteotomy wall close to the implant surface. The predicted stresses and

strains were most of the time greater than the compact bone tensile strength. As the thickness of the surrounding bone increased the predicted stresses and strains also increased.

In this simulation, the disparities in diameters between implant and osteotomy were 0.5mm and 0.75mm. From the results obtained, it is reasonable to assume that mismatches between implant and osteotomy should be kept as low as possible compatible with obtaining adequate primary stability as catastrophic damage was demonstrated with the larger mismatches. It may also be important to prepare the osteotomy preparation deep enough and to use a shorter implant than the osteotomy to avoid generation of high stresses and strains at the apical end of the osteotomy while the implant threads are being engaged with the osteotomy wall. However, this study dealt with one factor that may generate stresses and strains. Other factors should be considered.

A third study was conducted on dogs in order to study bone modelling and remodelling around endosseous implants after a limited post surgical implant placement time. Four mature male beagle dogs were used in the study. The aims of the study are:

1) To investigate quantitatively the bone formation rate that occurs in the area one millimetre away from implant surfaces at baseline, 3, 6 and 10 weeks following implant placement using sequential bone labelling.

2) To study remodelling cycles in the area one millimetre away from implant surfaces at baseline, 3, and 6 weeks following implant placement using the same bone labelling.

3) To describe the histological features of bone remodelling activity at area ≤ one millimetre from implant surfaces for the different healing periods.

The study reported high bone remodelling increases in an area close to the implant surface as indicated by new bone formation in early stage of healing. Woven bone developd to more organised fibrolamellar bone as the healing time increased. Subperiosteal bone formation was also found to occur around the early placed implant. The number of remodelling cycles (events) per unit area was calculated as a number of different chelating agents. Remodelling cycles (Area 1) close to the implant when compared with those in the area away (Area 2) from the implant were found to be higher. The maximum bone remodelling was found to occur between 3 and 6 weeks following implant placement.

It was found that there was significantly more remodelling cycles in Area 1 than in Area 2 ($F = 6.294$, $P = 0.021$) when the implants were placed at week 6.

Bone formation rate was expressed as the amount of bone formed between any two consecutive fluorochromic chelating agents. It was expressed as a micron per day. Bone formation rate was found to increase with time and then decreased at the end of the study. The maximum bone remodelling was found to occur between 3 weeks and 6 weeks following implant placement. The surgical procedure was found to cause bone damage in the area close to the implant surface. This damage was stained with tetracycline. This damage was decreases one day after implant placement and remained up to at least one week after the implant surgery. This in accordance with the findings of the first study.

From the results of the three studies, it may be concluded that implant surgery caused bone damage, principally in the area close to the implant surface. This damage induced bone remodelling in order to replace the damaged bone. The newly formed

bone in its early stage was woven bone which is then replaced by more mature lamellar bone. It may also be reasonable to suggest that subperiosteal bone was formed as a result of the surgery; however, its fate is not known from the observations of this study.

Acknowledgements

I wish to acknowledge the dedication, expert advice and encouragement of my supervisor Professor Noel Claffey, Dublin Dental School and Hospital, Trinity College, Dublin. He was very encouraging and supportive.

I would like to thank my co-supervisor Professor Clive Lee, Department of Anatomy, Royal College of Surgeons in Ireland for his expert advice and assistance.

I would like to thank Dr. Danny Kelly, Department of Mechanical and Manufacturing Engineering, Trinity College, Dublin, for his help in the Finite Element Model construction.

I appreciate the assistance of Dr. Alan Kelly in the statistical analysis of the studies.

I would like to extend special thanks to Agnes Hagan for her help and support and to Mr. Declan Byrne for letting me use his computer.

I would also like to express my gratitude to Ms. Anne O'Byrne (librarian) for her continuous assistance and to Mr. Peter O'Reilly, Department of Mechanical and Manufacturing Engineering, Trinity College.

I am especially grateful to my wife (Najia), my children Nada, Shada, Ahmed and Shahed for their support.

Table of contents

List of Tables

List of Figures

Chapter 1. Review of the Literature

1.1 General Introduction

Generally, microdamage occurs naturally in bone due to overloading during day-to-day activities. It can also be produced experimentally by a cyclical loading (Forwood & Parker 1989, Huja *et al.* 1999b, Noble 2003). Microdamage generation in bone has been attributed to plastic deformation and shear failure (Chamay 1970). The microdamage can be seen histologically as cracks and as diffusely stained areas (Boyce *et al.* 1998, Cohen *et al.* 2003). The former type is known as a linear microcrack while the latter one is denoted as a diffuse damage.

It is believed that this microdamage can activate bone remodelling and repair (Burr *et al.* 1985, Mori & Burr 1993, Bentolila *et al.*1998, Verborgt *et al.* 2000, Weinlaender et al. 2006), although the mechanism for this appears unclear. Bentolila *et al.* (1998) presented evidence which suggested that microcracks cause the activation of intracortical remodelling in rat ulnae that does not normally have such remodelling activities.

A positive correlation between osteocyte apoptosis and microdamage was recently reported (Verborgt *et al.* 2000). Their results showed that (1) osteocyte apoptosis is induced by bone fatigue, (2) the apoptosis is localized in bone containing microdamage and (3) osteoclast resorption after fatigue was found to correspond with regions of osteocyte apoptosis. This study revealed a strong correlation between apoptosis and microdamage and between apoptosis and subsequent activation of bone remodelling. The decrease in osteocyte lacunar density was found to be associated with the increase in microdamage (Vashishth *et al.* 2000, Frank *et al.* 2002). This may have a negative effect on the ability of bone to remodel and repair this damage.

Bone remodelling is recognised as a coupling process in which when bone resorption starts it will be followed by new bone formation. However, the relationship between bone remodelling and the microdamage is not entirely understood. There is a general agreement that when microdamage occurs at a slow rate bone remodelling has the ability to repair the damage. This type of remodelling which specifically occurs to remove the microdamage is known as a targeted remodelling (Verborgt *et al.* 2000, Burr 2002, Parfitt 2002).

However, if the damage accumulates at a faster rate than repair, microdamage accumulates and weakens the bone and consequently could lead to a stress fracture. On the other hand, if the damage accumulates at normal rate but the bone's repair capacity is diminished, fragility fractures occur (O'Brien *et al.* 2003).

Bone activity subsequent to implant placement requires both bone modelling and remodelling (Roberts 1988, Davies 1998, Raghavendra *et al.* 2005). After implant placement the remodelling activity adjacent to the implant (within 1 mm) is greatest and substantially decreased with increasing distance from the implant-bone interface (Garetto *et al.* 1995). This phenomenon seems to occur irrespective of implant design. This elevation in remodelling activity has been attributed to several factors including the local biomechanical environment, material biocompatibility and host response (Garetto *et al.* 1995). The local biomechanical environment of the bone-implant interface may require continuous remodelling to avoid fatigue fracture. Results from a finite elements model assessing the bone-implant environment indicate that the region within 1 mm of the implant surface displays a persistent marked change in mechanical stress distribution resulting in both elevated stress levels and stress gradients (Chen *et al.* 1994, Chen *et al.* 1995, Chen *et al.* 1999). This pattern of

stress distribution is not caused by occlusal loading of the implant but apparently results from the implant placement. However, when an occlusal load was applied at the vertical axis of the implant, the most extreme stresses in the surrounding bone were located around the neck of the implant. These stresses decreased inversely with an increase in percentage of osseointegration (Lai *et al.* 1998).

Failure of oral implants as a result of occlusal overloading may be attributed to microdamage in the bone surrounding the implant which exceeds the repair potential of this bone and leads to the replacement of bone-implant interface with soft tissue. It has been experimentally demonstrated in monkeys that excessive occlusal force on endosseous oral implants can result in complete or partial loss of osseointegration with a narrow zone of soft tissue between them (Isidor 1996, Isidor 1997).

Generation of microdamage in bone during placement of screw-shaped implants in long bone has been reported and this microdamage decreased in a 4 week-healing time as a result of bone remodelling (Hoshaw *et al.* 1994b). In one study, Huja *et al.* (1999b) found that non-adapted bone (bone that was loaded immediately after implant placement) near the implant accumulated significantly more microdamage than adapted bone (loaded 12 weeks after implant placement). The non-adapted non-loaded specimens demonstrated approximately 20-fold more damage than the respective adapted specimens (crack density $\approx$ 10 crack/ mm^2 versus $\approx$ 0.5 crack/ mm^2). These findings indicated the ability of bone to repair the micro-damage created during the surgical procedure and implant placement.

The studies cited above may collectively indicate a positive role for microdamage generated around implants in achieving a rigid implant-bone interface. However, little direct data are available on the microdamage around endosseous implants.

Further investigations are required to explain the role of the microdamage in remodelling of that observed in the peri-implant bone.

1. 2 Bone structure

Bone is generally classified as either compact (cortical) or cancellous (trabecular). Both types differ in their detailed structures, but have the same basic histological structure (Kiuru 2002). The microstructure unit of cortical bone is known as the osteon (Haversian system) and that of cancellous bone is known as a trabicular packet (hemi-osteon).

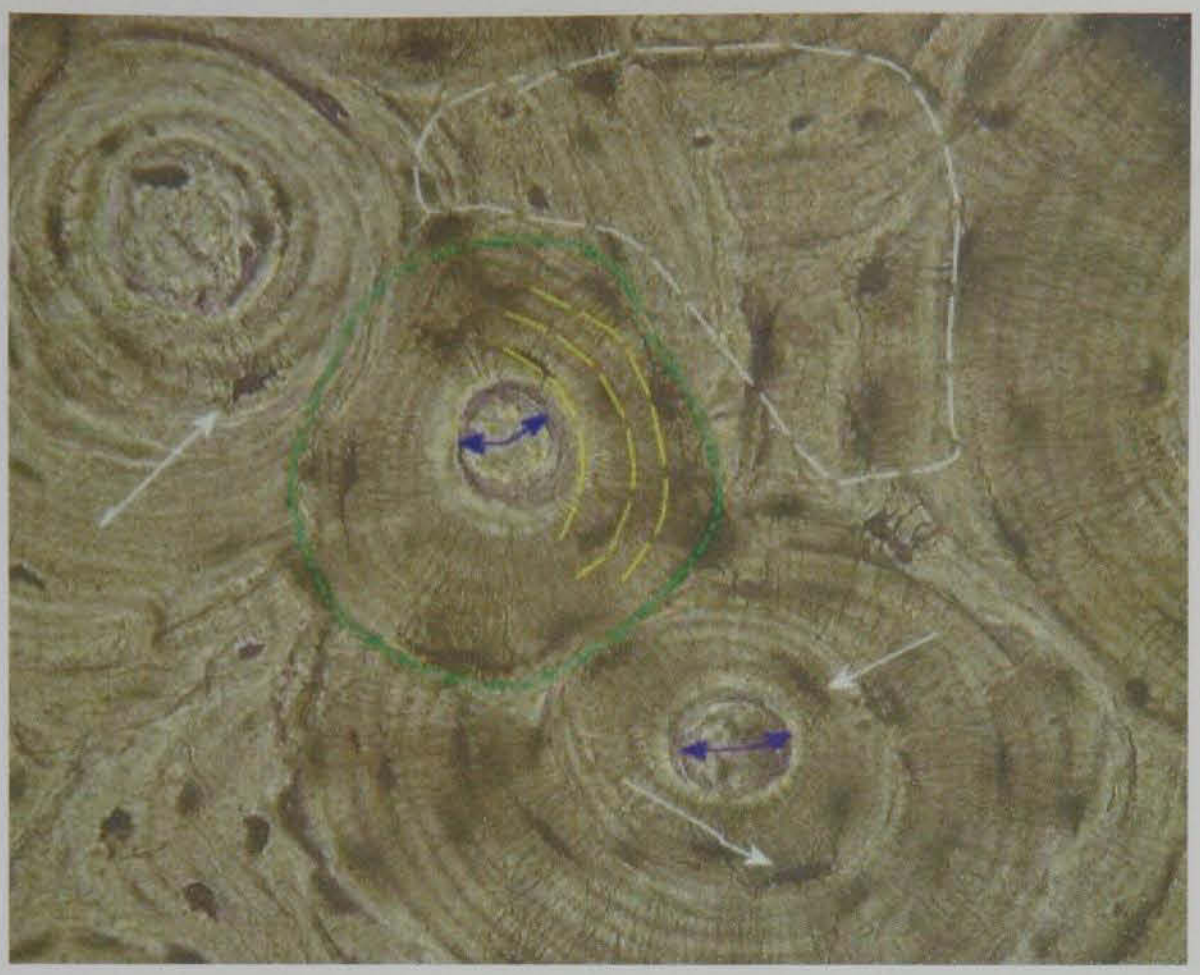

Figure 1.1 Cross section of compact bone: concentric lamellae (yellow dotted lines), Haversian canal (blue arrows), Cement Line (green line), interstitial lamellae (white dotted line) and osteocytes (white arrows).

Compact bone constitutes about 85% of bone in the body whereas cancellous bone forms the remaining 15%. Cortical bone is primarily found in the diaphysis; along the outer surfaces of long bones, while cancellous bone is found in the metaphyses and epiphyses of long bone [at the ends of long bone and internal to cortical bone] (Carter & Spengler 1978).

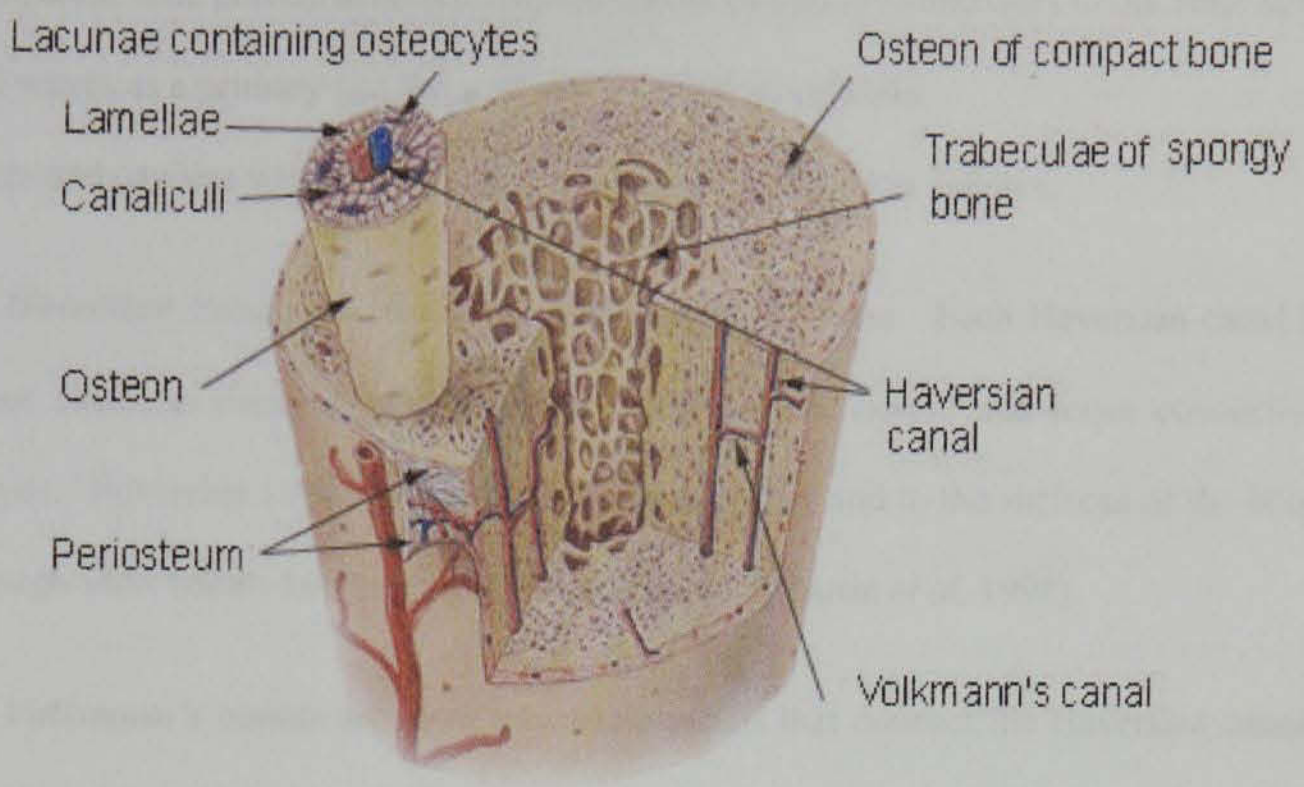

Figure 1.2 The basic structure of compact bone. (From http://training.seer.cancer.gov/module_anatomy/unit3_2_bone_tissue.html).

Compact bone (Figure 1.1 and 1.2) is dense and has a low surface area with a porosity of about 5-30%. Cancellous bone has a low density with a porosity ranging from 30 to 90% (Carter & Spengler 1978). It has a high surface area (Kiuru 2002, Ralston 2005), thus has a higher remodelling rate than cortical bone (Martin *et al.* 1998, Watzek & Gruber 2002). Although the calcified matrix of cancellous bone is similar to that of compactl bone, the apparent density (the ratio of bone mass to bulk volume) of cortical bone is higher than that of cancellous; range 1.8- 2.0 g/cm^3 versus 1.0-1.4g/cm^3. These differences in density are due to the presence of marrow filled spaces (Martin *et al.* 1998).

Porosity indicates the ratio of voids volume to the total volume (Martin *et al.* 1998).

The porous structure of cancellous bone acts as a shock absorber by which load is dissipated. The porous structure also facilitates diffusion of nutrients to the bone cells and serves as a primary site for production of red blood cells.

Pores and cavities within the cortical bone are categorised as follows:

1. ***Haversian canals*** run along the long axis of the bone. Each Haversian canal is about 50μm in diameter and contains blood vessels, nerves and loose connective tissues. Haversian canals are connected to each other and to the surfaces of the bone through short canals known as Volkmann's canals (Martin *et al.* 1998).

2. ***Volkmann's canals*** are short transverse canals that connect the Haversian canals to each other and to the surface of the bone. They contain blood vessels and probably nerves (Martin *et al.* 1998). They appear to be surrounded by concentric lamellae of bone, however their behaviour and structure are not fully understood (O'Brien 2000).

3. ***Resorption spaces*** are temporary cavities created by bone osteoclasts in the initial stage of remodelling. They are about 200 μm in diameter (Martin *et al.* 1998). When they present on the bone surface, they are known as Howship's lacunae (O'Brien 2000, Nanci *et al.* 2003), which are usually occupied by osteoclasts. The resorption spaces lead to stress concentrations within the bone that may aid in the generation of microcracks (Burr 2004).

4. ***Osteocyte lacunae*** and ***canalaculi***.

Bone is a mineralised connective tissue that is composed of organic and inorganic materials.

1.3 Organic Matrix

Organic matrix consists by weight of about 30%-33% of bone (Lee 1995, Guyton & Hall 2000, Nanci *et al.* 2003). About 90% of the organic matrix (osteoid) is collagen, which is predominantly type I collagen and accounts for about 85-90% of the organic matrix (Lee 1997, Currey 2002). Collagen, which is a fibrous protein, plays a principal role in determination of bone's mechanical properties. It also provides loci for the nucleation of bone mineral crystals, which gives bone rigidity and compressive strength (Martin *et al.* 1998). See arrangement of collagen fibres below.

The remaining 10% of the organic matrix (ground substance) comprises non-collagenous proteins such as proteoglycan, osteocalcin and osteopontin (Nanci *et al.* 2003). These non-collagenous proteins mediate attachment of bone cells to the matrix and regulate bone cell activity during remodelling (Ralston 2005). This matrix may act as glue that holds the mineralized fibrils together (Fantner *et al.* 2006).

As the osteoid calcifies, much of its water content is replaced by inorganic bone component that is almost entirely hydroxyapatite crystals (Martin *et al.* 1998). Both the collagenous and the non-collagenous bone matrix proteins are produced by osteoblasts in the initial stage of bone formation (Guyton & Hall 2000, Nanci *et al.* 2003).

1.4 Inorganic Matrix

Inorganic matrix (Mineral) consists by weight of about 70% of bone (Guyton & Hall 2000). About 95% of these inorganic components are in the form of hydroxyapatite (HA) crystals $\{(Ca_{10}\ [PO_4]_6[OH]_2)\}$, which are mainly composed of calcium and phosphate (Junqueira *et al.* 1998, Guyton & Hall 2000, Ralston 2005). Some other salts such as magnesium, sodium, carbonate and citrate are reported to exist (Martin *et*

al. 1998, Guyton & Hall 2000). For example, the phosphate groups are replaced by 4-6% of the carbonate changing the mineral to a carbonate apatite (dahllite) (Currey 2002).

The apatite crystal deposition usually increases during ageing and maturation of bone, which is associated with a change in bone mechanical properties. Although there is still controversy regarding the exact shape of the mineral crystals (Currey 2002), they are described as platelet-shaped (Sommerfeldt & Rubin 2001, Currey 2002). They deposit alongside collagen fibrils and bind tightly to them thus improving mechanical properties and prevent shear in the bone (Guyton & Hall 2000). However, a considerable variation in mineralisation degree between different bones exists (Currey 1984).

Using high electron microscopy and 3D imaging apatite crystals were seen oriented approximately parallel to one another and to the collagen fibrils with which they are associated. The crystals were separated by a minimum distance of 4.2nm and were observed in a distribution that suggested they were initially and preferentially deposited (nucleated) in gaps (hole regions) within collagen fibres. These gaps are distinct spaces between the heads and the tails of the protein molecules called *tropocollagen*, which aggregates to form microfibrils of collagen (Lee 1995, Currey 2002). The microfibrils combine to form fibrils (Currey 2002) (Figures 1.3 and 1.4).

These mineralised collagen fibrils are about 50-100nm in diameter and held together by a non-mineralized, non-fibrillar organic matrix (Fantner *et al.* 2006). The degree of mineralization as well as the amount of the non-fibrillar organic matrix were found to vary significantly between trabecular bone samples and within the same sample (Fantner *et al.* 2006). It was hypothesized that the non-mineralized, non-fibrillar

organic matrix might act as glue that binds the mineralized fibrils together and may result in a primary failure mode of de-lamination between the mineralized fibrils. The mineralized fibrils in turn span microcracks and crack tips and may also resist the growth and propagation of the cracks. They therefore, contribute to the fracture toughness of bone (Fantner *et al.* 2006).

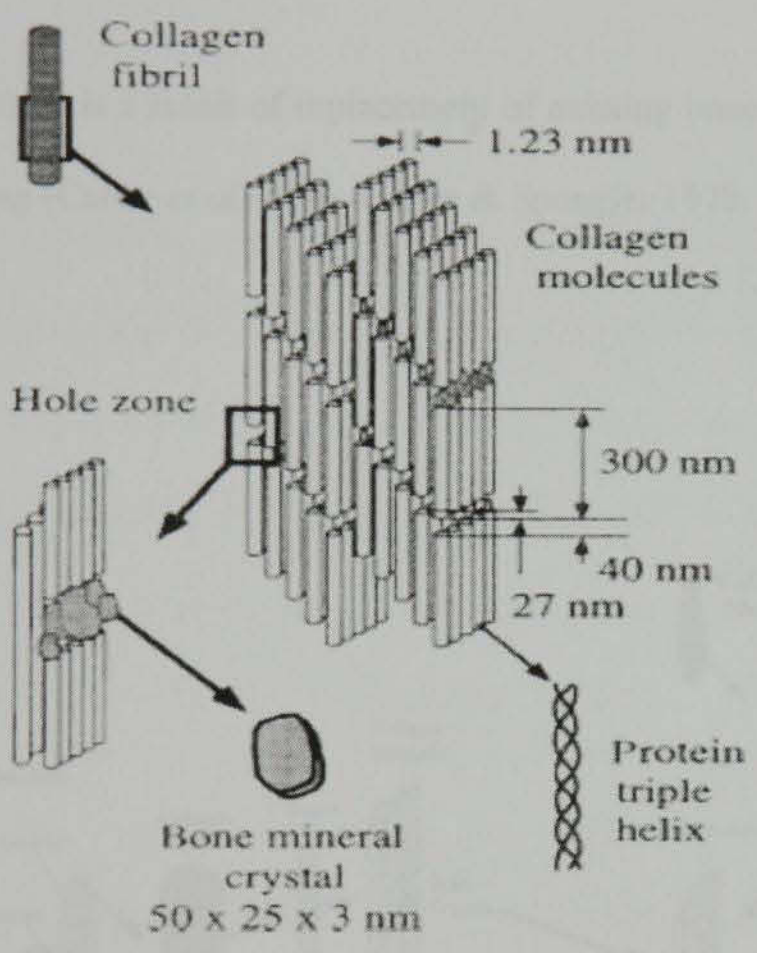

Figure 1.3 The structure of collagen fibril with hole regions and bone mineral crystals. Adapted from Ritchie *et al.* (2005).

In cortical bone, cells are primarily surrounded by bone matrix, whereas in the cancellous bone they lie between lamellae or on the surface of trabeculae adjacent to bone marrow.

1.5 Types of bone

1.5.1 Primary and secondary bone

In general, bone can further be classified as primary or secondary. Primary bone is formed by endochondral ossificationon or direct sub-periosteal deposition (Carter *et al.* 1976, Carter & Spengler 1978). It is usually transitory and is replaced by secondary osteonal bone tissue. It is less mineralised and has a higher proportion of osteocytes than secondary osteonal bone tissue (Junqueira *et al.* 1998).

Secondary bone tissue is a result of replacement of existing bone in a process known as bone remodelling (Carter *et al.* 1976, Carter & Spengler 1978, Jee 2001, Mohsin *et al.* 2006).

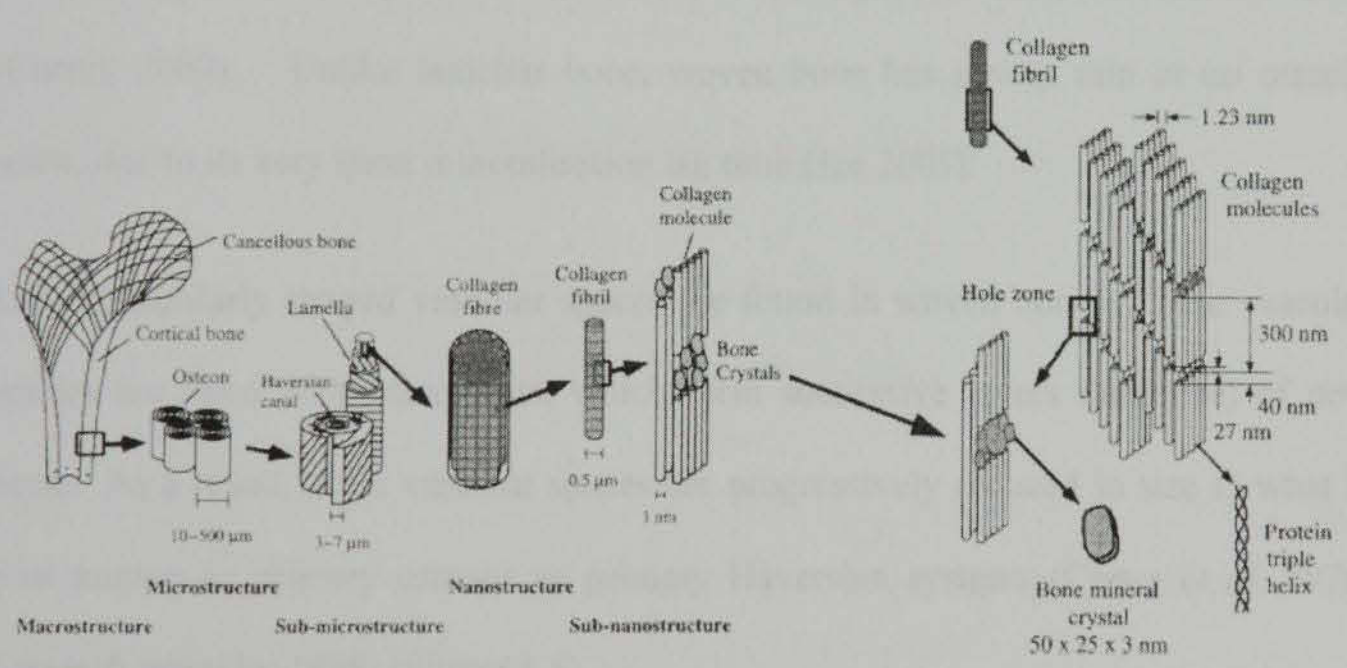

Figure 1.4 The hierarchical structure of human cortical bone from macrostructure to sub-nanostructure (Richie *et al.* 2005).

Bone can also be classified as woven (immature) bone or lamellar (mature) bone.

1.5.2 Woven bone

Woven bone is osteonless bone tissue that can be deposited *de novo* (no precursor bone). It is a newly formed bone in which collagen fibres are loosely packed in an irregular fashion and are almost randomly oriented (Roberts 1988, Martin *et al.* 1998, Currey 2002). It is formed more rapidly than lamellar bone. It is laid down at more than 4μm a day. Due to the way by which it mineralises, it is usually quite porous (Currey 2002). The final degree of its mineralisation is higher than that of the lamellar bone (Currey 2002); consequently it may be more brittle than the lamellar bone. Thus, its mechanical properties are inferior to that of other cortical bone. Woven bone also contains more osteocytes than lamellar bone and contains blood vessels (Carter *et al.* 1976, Currey 2002, Nanci *et al.* 2003). In woven bone, lacunae surrounding the osteocytes are wider thus differing from those in lamellar bone (Currey 2002). Unlike lamellar bone, woven bone has a very thin or no osteoid seam, due to its very short mineralisation lag time (Jee 2001).

Large irregularly shaped vascular spaces are found in woven bone. These vascular spaces are lined with osteoblasts, which form successive layers (lamellae) of new bone. As a result, these vascular spaces are progressively reduced in size to what is now known as primary osteons or primary Haversian systems (Carter *et al.* 1976, Carter & spengler 1978) (Figure 1.5).

Woven bone is most commonly found in immature, growing skeletons. When it is found in adult skeletons, it is usually a result of trauma or disease and indicates that it

was laid down in a very quick fashion. It also occurs as a normal adaptive response to elevated mechanical strains (Burr *et al.* 1998).

Woven bone was reported to exist around endosseous implants during the early healing stage (Roberts *et al.* 1984, Roberts 1988, Chappard *et al.* 1999, Berglundh *et al.* 2003, Abrahamsson *et al.* 2004). It is ultimately replaced by more mature, load bearing lamellar bone (Roberts 1988, Chappard *et al.* 1999).

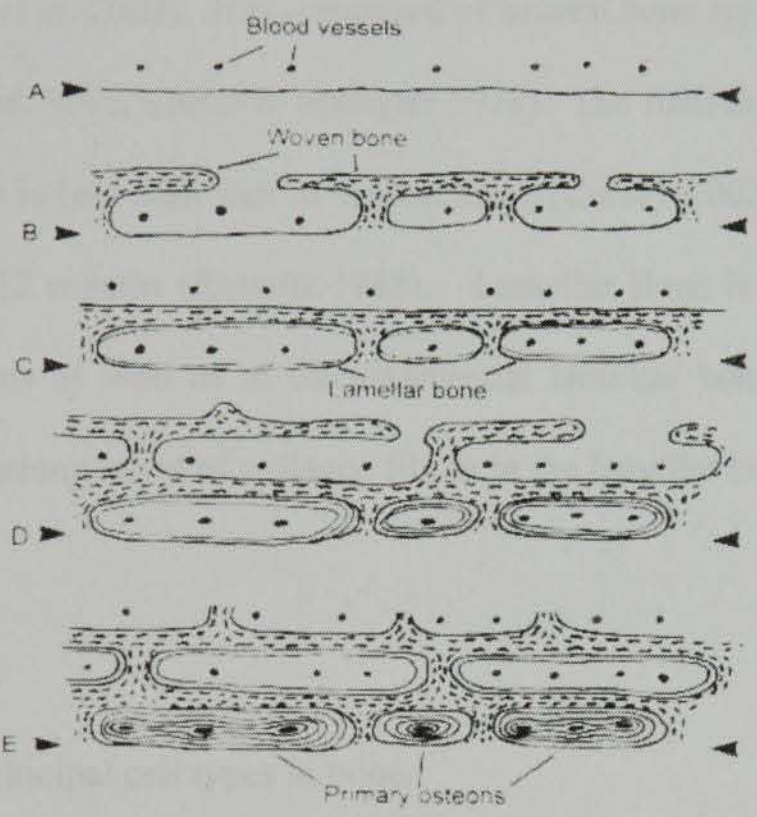

Figure 1.5 The formation of fibrolamillar bone. The arrow heads show the position of the original surface. A) The original section. B) Woven bone grows very quickly to form a scaffolding clear of the original surface. C) Lamellar bone shown by fine lines starts to fill in the cavities. D) As more lamellar bone is laid down, so is another scaffolding of woven bone. E) Formation of primary osteons (Currey 2002).

1.5.3 Lamellar bone

It is formed in adults and represents a mature type of bone. It is formed in a slow process at less than 1µm a day (Currey 2002). It is a highly organised type, consists of microscopic parallel sheets or lamellae. These lamellae are composed of an anistropic matrix of mineral crystals and collagen. The lamellae form a cylinder of bone within which a vascular canal runs. Numerous osteocytes reside in lacunae within the lamellae. The entire structure is known as a Haversian system or an osteon. The osteon is the basic organisational unit in lamellar bone and is particularly evident in cortical bone. The osteons are generally oriented parallel to the long axis of the bone (Nanci *et al.* 2003). It is composed of several bone layers with a thickness of 7 µm (Carter *et al.* 1976, Carter & Spengler 1978). The final degree of mineralisation of lamellar bone is less than that of woven bone (Currey 2002). Its full maturation may take up to 12 months (Roberts 1988). Lamellar Bone is found in primary and secondary osteons as well as in circumferential lamellar bone (Carter & Spengler 1978). [See the arrangement of collagen fibrils in the lamellar bone below].

1.6 Bone cells

There are four principal cell types in bone.

1.6.1 Osteoblasts (Bone forming cells)

They are mononuclear cells that are differentiated from mesenchymal cells or from their precursors at the periosteal or endosteal surface (Cooper 1998). They are responsible for the formation of the organic matrix (collagenous and non-collagenous proteins) (Cooper 1998, Nanci *et al.* 2003). They also secrete a range of cytokines that aid in regulation of cell metabolism (Nanci *et al.* 2003). Collagenous proteins are

released mainly along the surface of osteoblasts apposed to the forming bone and are assembled to form osteoid (uncalcified matrix) which, acts as a scaffold for deposition of bone minerals (Nanci *et al.* 2003). Osteoblasts produce the matrix at a rate of approximately 1 μm/day. Systemic hormones and local factors are believed to regulate their activity (Lee 1997).

When the osteoblasts get trapped in the matrix they produce, they become known as osteocytes (Martin *et al.* 1998, Currey 2002, Nanci *et al.* 2003).

1.6.2 Osteocytes

Osteocytes are found in spaces in the bone matrix known as osteocytic lacunae. From these lacunae numbers of small tunnels known as canaliculi extend. Each osteocyte has several long processes that are running in the canaliculi and by which osteocytes communicate with adjacent osteocytes and with osteoblasts or bone-lining cells (Sommerfeldt & Rubin 2001, Nanci *et al.* 2003). It was suggested that osteocytes have the ability to detect and to respond to mechanical stimuli: mechano-sensing cells (Mori *et al.* 1997, Hung & Lee 2001, Nanci *et al.* 2003, Ralston 2005). Osteocytes may also have a role to play in local degradation of bone (Nanci *et al.* 2003).

1.6.3 Bone lining cells

Bone lining cells are osteoblasts that are quiescent and inactive. They form a layer that covers the inner and the outer surfaces of bone as well as the surfaces of the Haversian and Volkman's canals (Currey 2002). In response to an appropriate stimulus, they differentiate into osteoblasts. The bone-lining cells may control the movement of ions to and from the bone (Currey 2002, Nanci *et al.* 2003). They are

like osteocytes play a role in sensing stress and strain on and within the bone and transmit the signals so bone formation/ resorption occurs.

1.6.4 Osteoclasts

Osteoclasts are bone-resorbing cells. They are highly migratory and multinucleated bone cells that are derived from hemopoietic stem cells (Sommerfeldt & Rubin 2001, Nanci *et al.* 2003). The attachment of osteoclasts to the mineralised bone surface is facilitated by several mechanisms such as the concentration of osteopontin on the bone surface leading to the formation of what is known as the sealing zone (Nanci *et al.* 2003). The osteoclasts make their way through bone by demineralising the adjacent bone with acids and expose the organic matrix, which is then dissolved by the action of released enzymes such as acid phosphatase (Martin *et al.* 1998, Nanci *et al.* 2003). An active osteoclast has the ability to resorb about 200,000 μm^3 of bone per day (Sommerfeldt & Rubin 2001). When osteoclasts occur on the bone surface, they are housed in small depressions known as Howship's lacunae (Nanci *et al.* 2003). After drilling and implant placement, osteocalsts resorb damaged bone and contribute to osseointegration of endosseous implants (Minkin & Marinho 1999).

1.7 Arrangement of collagen fibrils within osteons

The rate of bone formation determines whether the collagen fibrils are regularly or irregularly arranged. While the arrangements of collagen fibrils that are found in woven bone are irregular those found in the lamellar bone are regular.

The arrangement of collagen fibrils within the lamellae is a controversial issue. The most commonly cited models will be briefly explained below.

When a histologic section is illuminated with polarising light and viewed via a polarising filter, the collagen fibre bundles are seen as dark and/or bright bands. This illumination effect is highly dependent on the direction of the collagen fibres in relation to the light's plane. Thus, when the collagen fibres are vertically oriented to the viewing filter, the light will be blocked and the collagen bundle will be seen as a dark field. On the other hand, when the fibres are not vertically oriented (for instance transversely oriented) in relation to the viewing filter, they will be seen as a bright field (Martin *et al.* 1998). This phenomenon has been used to classify lamellae of Haversian system (osteon) into 3 classes (Ascenzi & Bonucci 1976, Martin *et al.* 1998):

1- **Type L osteons** indicates that the osteons with collagen fibres are parallel to the centre of the osteon.

2- **Type T osteons** contain collagen fibre bundles that are oriented in a transverse or circumferential manner perpendicular to the osteon axis.

3- **Type A osteons** contain collagen fibre bundles in a similar orientation to those found in Type L and T. Thus they are an alternating light and dark pattern (Figure 1.6).

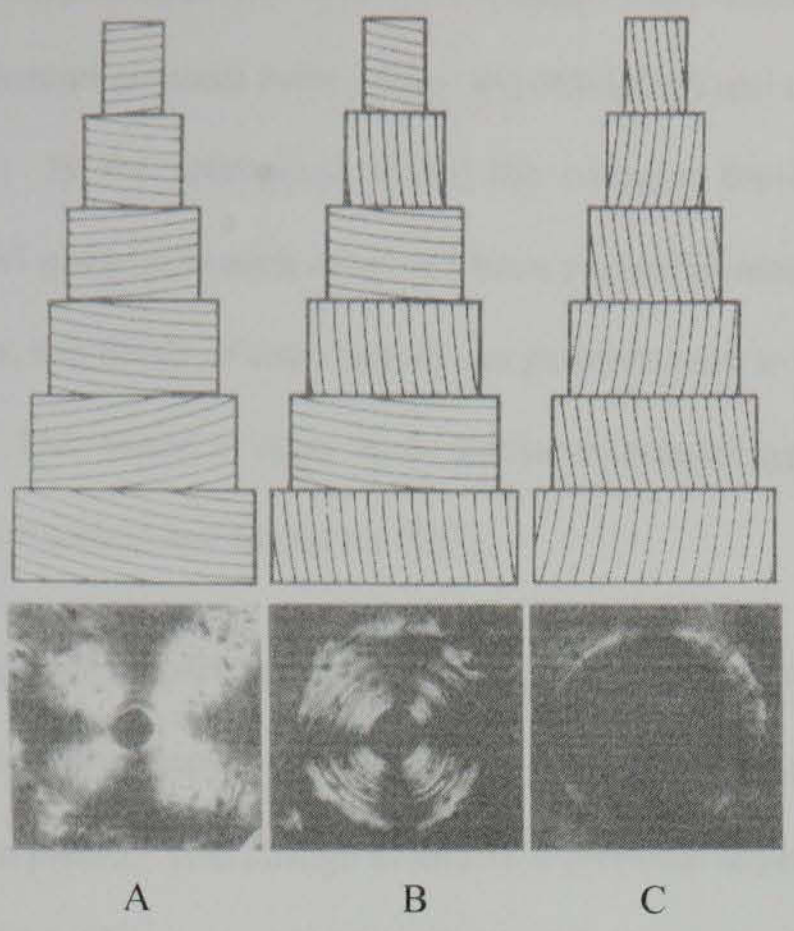

Figure 1.6 Fibre arrangements in lamellae of Haversian system. (After Martin *et al.* 1998). A) Type T osteons: collagen bundles oreinted in a transverse or circumferential manner perpendicular to the osteon axis. B) Type A osteons: collagen bundles are arranged in an alternating light and dark pattern. C) Type L osteons: collagen fibres are parallel to the centre of the osteon. Reproduced from Martin *et al.* (1998).

According to Marotti and Muglia (1988), the dark and light bands seen under polarised light are due to the different packing density of the collagen fibres and not as a result of the change in orientation of the fibres. Therefore, the collagen fibrils are tightly packed in the dark bands (collagen-rich lamellae) and are loosely packed in the light ones (collagen-poor lamellae) (Marotti *et al.* 1995).

Giraud-Guille (1988) presented two models of collagen fibril orientation that are most likely present in human compact bone. They are orthogonal and twisted (helicoidal) plywood models. In the orthogonal model the collagen fibrils of lamellae are arranged in parallel patterns to each other and have a specific orientation within each lamella. However, the fibrils of each lamella are perpendicular to those fibrils of the adjacent lamella. This model is most likely similar to osteons type L and T, which were described by Ascentzi and Bonucci (1967).

In the twisted (helicoidal) plywood model collagen fibrils are also parallel in each lamella but continuously change their direction with a constant angle (usually quite small) between the planes. This change in direction gives the impression that there is no individual lamella. They resemble type A (alternating) osteons that were described by Ascentzi and Bonucci (1967).

Lamellar bone may consist of four layering

1. Osteons are embedded in interstitial bone. They may be primary or secondary. Secondary osteons have a mean length of 3.1mm (3100 μm) and are 0.161 mm (161 μm) in width (Mohsin *et al.* 2002). Three-dimensional reconstruction of osteons during bone remodelling of bovine bone indicated that osteons are cylindrical structures with a gentle spiral course along the longitudinal axis of the bone. They intertwine with neighboring osteons and branch along their course producing a complex intertwining pattern of organization (Mohsin *et al.* 2002) (Figure 1.7).
2. Interstitial bone: is a remnant of old bone (remnants of circumferential or concentric lamellae) that previously occupied the area. Thus, it is composed of circumferential lamellar bone and fractions of primary and secondary

osteons (Carter & Spengler 1978, Nanci *et al.* 2003). It fills the regions in bone between adjacent Haversian systems (osteons) and takes different shapes (Nanci *et al.* 2003) (Figure 1.1)..

3. Circumferential: surrounds the entire bone surfaces adjacent to the *periosteum* and *endosteum.*
4. Trabecular: plates of lamellar bone perforated by marrow spaces forming cancellous bone of the medullary cavity (Lee 1997).

The external surface of compact bone is surrounded by a connective tissue layer known as the *periosteum* while the cancellous and the internal surface of the compact bone is surrounded by an essentially cellular membrane known as the *endosteum* (Nanci *et al.* 2003).

The age of the bone can be estimated from the amount of the interstitial lamellae found between complete secondary osteons as well as to the amount of secondary osteons. Younger bone has less interstitial lamellae and more intact secondary osteons than older bone. A greater percentage of microcracks were found in the interstitial bone (Boyce *et al.* 1998, O'Brien 2000, Martin 2003, O'Brien *et al.* 2003), which might be due to high mineralisation of such bone and to microstructural barrier. According to O'Brien and coworkers (2003), 91% of microcracks generated in the first 50.000 cycles were located in the interstitial bone. In microcracks formed between the 50,000 and failure, this figure dropped with 25% of microcracks found in osteons.

Secondary osteons are separated from the interstitial tissue by a thin sheath [line] (1 to 5 μm), which is formed during the initial stages of remodelling and occurs where

bone resorption ends and new bone formation begins (Figure 1.1). This thin line is known as cement line (Carter & Spengler 1978, Currey 2002, Nanci *et al.* 2003).

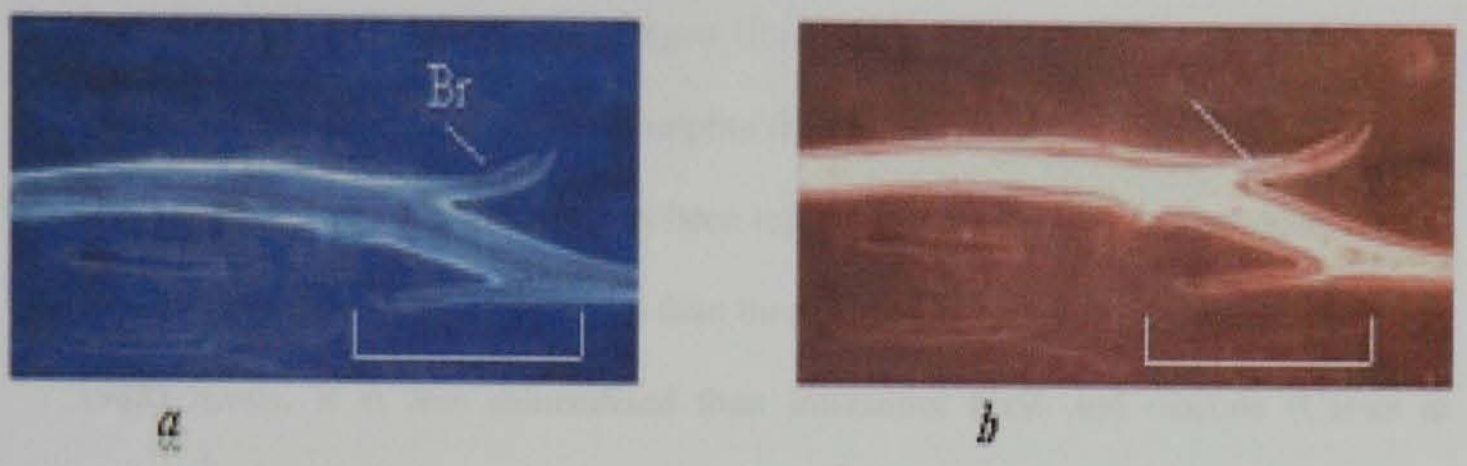

Figure 1.7 Example of a branching (Br) secondary osteon viewed with (a) UV (365) and (b) green epifluorescence (546 nm). Reproduced from Mohsin *et al.* (2002).

Osteons may affect the bone mechanical properties in several ways (Martin *et al.* 1998):

- By replacement of highly mineralised bone matrix with less calcified matrix
- By increasing cortical porosity introduced by new Haversian system
- Possibly by altering collagen fibres orientation and
- By the introduction of a cement line interface.

1.8 Cement line (CL)

CL is also known as reversal line. It is a sheath that surrounds secondary osteons (Figure 1.1). It is found only in secondary bone as a result of remodelling bone activity. It occurs where bone resorption ends and bone formation begins. It is a weak layer found between the osteon and the interstitial matrix (Burr *et al.* 1988).

The cement line is produced by the osteoblasts as a thin layer of glycoproteins (although its composition is still debatable) consisting of noncollagenous proteins such as sialoprotein and osteopontin that act as an adhesive between the old bone and new bone (Nanci *et al* 2003). It is a collagen-deficient structure with thickness ranges from 1 to 5μm. It has fewer collagen fibres than the surrounding bone. It is less mineralised and may contain more sulphur than the surrounding bone tissue (Schaffler *et al.* 1987, Burr *et al.* 1988). It has been reported that cement lines contained 10% to 15% less calcium and phosphorous than those found in surrounding bone (Burr *et al.* 1988) hence, it is less mineralised than interstitial bone and osteons (Carter & Spengler 1978, Martin *et al.* 1988) [Figure 1.1]. Cement lines may be penetrated by some canaliculi (Currey 2002).

There is a general agreement that CLs are weak regions within the normal bone structure and may be responsible for the observed stiffness variations in bone. CL may represent a region at which mechanical bone failure may occur (Zioupos & Currey 1994). However, it was difficult to conclude whether the CLs are regions of mechanical weakness or toughness (Mohsin *et al.* 2006).

CLs may provide a relatively weak interface within the surrounding bone matrix that permits crack initiation and provides a considerable resistance to crack growth (Burr *et al.* 1988). This property (ability of stopping crack-growth) has been attributed to the compliant (low stiffness) nature of cement lines (Burr *et al.* 1988, Schaffler *et al.* 1995) and may also reflect a possible microstructural barrier role to microcrack growth in bone (Martin & Burr 1989, Taylor 1998, Akkus & Rimnac 2001, O'Brien *et al.* 2003, O'Brien *et al.* 2005a, Mohsin *et al.* 2006). This nature may promote crack initiation but slow or even prevent crack growth in bone (Schaffler *et al.* 1995,

O'Brien *et al.* 2003, O'Brien *et al.* 2005a) and are more likely to absorb and dissipate energy (Burr *et al.* 1988). It has been reported that *in-vivo* microcrack may be initiated along the cement lines (Schaffler *et al.* 1995). However, the exact nature of cement line has not been completely understood (Currey 2002).

The ultrastructure of the bone-implant interface has been documented by a number of workers (Linder *et al.* 1983, Sennerby *et al.* 1991, Ohtsu *et al.* 1997, Puleo & Nanci 1999, Brunski *et al.* 2000). The study of implant-bone interface using electron microscopy indicated the presence of an electron-dense layer at the implant-bone interface similar to the cement line between a secondary osteon and pre-existing bone (Sennerby *et al.* 1991, Ohtsu *et al.* 1997, Puleo & Nanci 1999, Brunski *et al.* 2000). This interfacial layer occurs regardless of the implant material (de Bruijn *et al.* 1992, Puleo & Nanci 1999, Brunski *et al.* 2000). Early studies have indicated that this electron-dense interfacial layer was formed of glycoproteins 20nm thick (Hansson *et al.* 1983). However, latest investigations found that these interfacial layers are rich in noncollagenous proteins, such as osteopontin and bone sialoprotein (Puleo & Nanci 1999). Linder *et al.* (1983) observed in rabbit tibia an amorphous zone separating the collagen filaments from the implant surface by a gap of 100-500 nm.

Sennerby *et al.* (1991) studied the nature of the oral implant bone interface of seven clinically stable, "osseointegrated", titanium implants, inserted in human jaws for 1-16 years and concluded that the bone-implant interface was heterogenous and the mineralized bone was separated from the implant surface by an amorphous layer 100-400nm in thickness (Sennerby *et al.* 1991).

1.9 Bone formation

Bone formation occurs by two main mechanisms: a direct (*intramembranous*) or an indirect (*endochondral*) ossification.

Intramembranous ossification occurs during embryonic development directly within soft connective tissue. It is achieved by osteoblast cell recruitment from mesenchymal (marrow stem) cells or from their precursors cells at the endosteal or periosteal surfaces (Cooper 1998). These cells differentiate into osteoblasts and begin to secrete bone matrix (known as osteoid), which leads to formation of bone. The osteoid calcifies to form primitive cancellous or compact bone that is then converted into mature one. Bone formed by this process includes flat bones such as the clavariae of the skull, the maxilla and the mandible (Nanci *et al.* 2003, Ralston 2005). It is also reported to occur at the implant-bone interface (Cooper 1998).

Endochondral ossification is a more common type of bone developmental process. Bone formed by this process is a result of aggregation of mesenchymal cells that are transformed into chondroblastic cells. It takes place when a cartilaginous callus is invaded by vascular tissue containing osteoprogenitor cells and then replaced by bone (Ralston 2005). This bone formation process occurs at long bone of the limbs, vertebrae, ribs and the pelvis (Nanci *et al.* 2003, Ralston 2005). It also occurs in ectopic bone formation and fracture models (Cooper 1998).

1.10 Bone turnover

In order to maintain skeletal integrity and calcium homeostasis the quantity, quality as well as the shape of bone is continuously changing. Two processes are involved in bone turnover; modelling and remodelling.

1.10.1 Bone modelling

Modelling (change in shape and size) occurs on bone surfaces such as the periosteal and endosteal surfaces and leads to change in the bone's size and shape by adding or removing bone (Currey 2002, Nanci *et al.* 2003). It involves activation followed by either resorption (A-R) or formation (A-F) (Brunski & Hoshaw 1994). Thus, the process is not coupled biologically and is the result of independent sites of bone resorption and formation.

Activation → Resorption (A—R) OR Activation → Formation (A—F)

As a result of modelling processes lamellar or woven bone can be formed. It is believed that woven bone formation in the modelling process is a response to a larger stimulus than that required for formation of lamellar bone (Frost 1994). A modelling process activated by mechanical usage results in an increase in bone mass and strength and a decrease in its strain peak to the minimum effective strain under the same loading condition (Frost 1987, Frost 1994). "Presumably, this modelling process reduces strains in the weakened structure by increasing its cross-sectional area" (Martin *et al.* 1998). For example, during growth bone is formed at the periosteal surface in a faster rate than the resorption rate of the bone at the endosteal surface. Modelling allows development of normal architecture and if necessary it changes this architecture and mass (Jee 2001) (Table 1.1).

1.10.2 Bone remodelling

Bone remodelling (internal turnover or replacement of bone) is a process by which immature, damaged and old bone are resorbed and replaced by new lamellar bone

tissues. In remodelling processes the internal bone surfaces rather than the external are most likely to be affected. This leads to a change in the internal bone structure without a significant change in bone size or shape (Stanford & Brand 1999). Remodelling first occurs soon after birth when the primary osteons are replaced by the secondary ones. About 10% of the adult bone skeleton is remodelled at any one time (Ralston 2005). Bone is a dynamic tissue that requires continuous remodelling in order to remove the immature bone in the early age and the damaged old bone through life (Martin *et al.* 1998, Jee 2001). Furthermore, with remodelling, the balance of body mineral haemostasis (mineral exchanges between the bone and the blood) is achieved as well as adaptation of bone tissue to its mechanical environment. When bone is remodelled it is deemed metabolically and mechanically competent (Jee 2001). The remodelling rate of cortical bone is 2- 10% per year in human cortical bone (Roberts 1988) and about 30-40% in beagle dog's dentate mandible (Tricker *et al.* 1977). The rate of remodelling changes with age: it is high in children and reduced in young adults (Martin *et al.* 1998, Nanci *et al.* 2003). Bone remodelling rates of 30% to 100% per year are not uncommon in rapidly growing children (Nanci *et al.* 2003). Furthermore, bone formation rate (as expressed by % of turnover rate/year) and mineral apposition rate are substantially reduced with age (Tricker *et al.* 1977).

Table 1.1 Bone turnover (modelling and remodelling).

Modelling	Remodelling
1. Occurs on almost the entire peroisteal and endosteal surfaces. 2. Usually results in a change in the bone size, shape or both. 3. Involves - activation followed by resorption or by formation. 4. Resorption and formation occur in different sites. 5. Leads to formation of bone where there was no bone before. 6. Occurs at peroisteal and endosteal surfaces adjacent to the osteotomy of endosseous implants.	1. Involves less than 20% of the bone surface area. 2. Usually does not lead to a change in the size or shape of the involved bone. 3. Involves – activation, resorption followed by formation. 4. Resorption and formation occur in the same site. 5. Leads to the replacement of older and damaged bone by secondary osteons (Haversian Systems). 6. Occurs at endosseous implant-bone interface and extends a few microns away from the implant surface.

Each remodelling cycle is formed by coupling the activities of a group of osteoclasts and osteoblasts known as a *Basic Multicellular Unit* (BMU) or *Bone Remodelling Unit* (BRU) (Figure 1.8). Each BMU consists of about 10 osteoclasts and a higher number of osteoblasts (Martin *et al.* 1998). These coupling activities of osteoclasts and osteoblasts maintain the balance between bone resorption and formation; i.e., activation followed by resorption, which is then followed by formation (A-R-F).

The remodelling cycle is known as Sigma, which is estimated to be about 16 weeks in humans, 12 weeks in dogs (Frost 1985, Brunski & Hoshaw 1994) and six weeks in rabbits (Roberts *et al.* 1984, Roberts 1988).

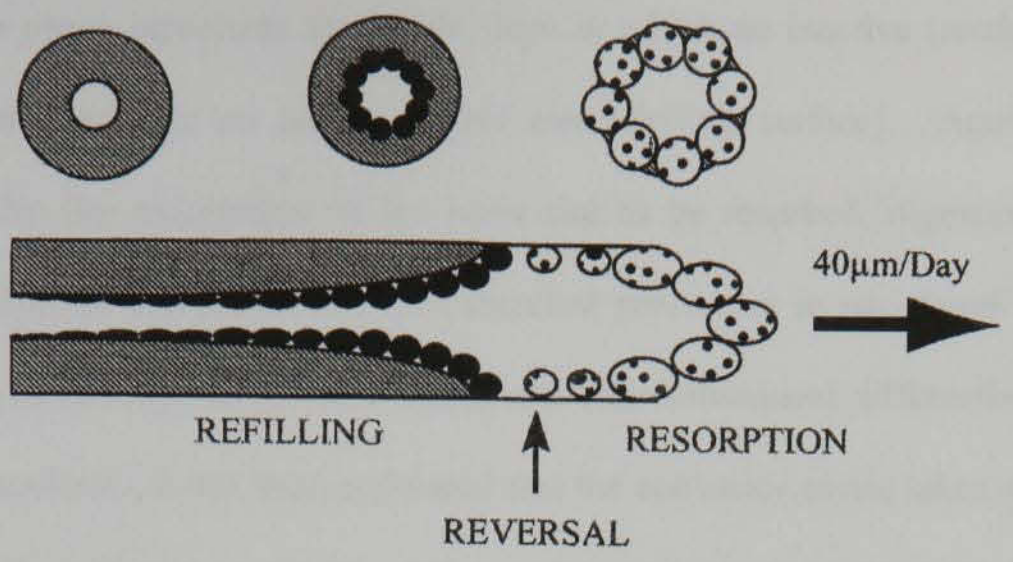

Figure 1.8 Basic multicellular unit (*BMU*) in bone. Larger multinucleated cells to the right are osteoclasts; smaller cells shown in black to the left are osteoblasts (Martin *et al.* 1998).

The remodelling process consists of 5 distinct phases or stages: resting, activation, resorption, reversal and formation (Frost 1973, Frost 1987, Roberts 1988, Lee *et al.* 2002).

1.10.2.1 Resting

It represents the stage at which the bone surface is in an inactive state. The resting bone surface is lined with a thin non-mineralised layer (endosteal membrane) and bone lining cells (osteoblasts which line the bone surface after bone formation is completed). During the remodelling processes the latter cells are altered from a resting state into a bone destructive mode and digest the un-mineralised layer to expose the mineralised bone to the osteoclasts where they can attach (Jee 2001). Osteoclasts can not attach to the non-mineralised layer, thus either mineralisation or resolution of this unmineralised layer is required before the initiation of the resorption phase can take place.

1.10.2.2 Activation

The activation phase represents the initial stage in which an inactive (resting) bone surface is converted into an active surface (remodelling surface). Activation is characterized by the recognition of the bone site to be resorbed, digestion of the endosteal membrane and recruitment of osteoclast precursors in peripheral blood to the site that is to be resorbed (Ralston 2005) and their subsequent differentiation into functional osteoclasts. It has been estimated that the activation phase takes about 3-4 days in dogs, about 7 days in monkey (Giannobile *et al.* 1994) and about 3-5 days in sheep (Lee *et al.* 2002).

1.10.2.3 Resorption

The activation phase is followed by the resorption phase in which osteoclasts (bone resorbing cells) come into direct contact with the bone surface and create a localised acidic environment. The osteoclasts attach to the bone surface by forming what is known as a sealing zone. They resorb bone by secreting hydrochloric acid and proteolytic enzymes into the space underneath the sealing zone (Ralston 2005). The osteoclasts dig within the pre-existing bone forming a microscopic tunnel (cone) of approximately 100 μm parallel to the involved cortical bone long axis. The formed cones are known as resorption cavities or cutting cones (Brunski & Hoshaw 1994, Currey 2002). The resorption cavities that form on the cancellous bone surface create saucer-shaped cavities (ditches), which are known, as Howship's lacunae (Brunski & Hoshaw 1994, Jee 2001, Nanci *et al.* 2003, Ralston *et al.* 2005). The resorption phase takes about 2 weeks in humans and monkeys and about 10 days in dogs (Giannobile *et al.* 1994).

1.10.2.4 Reversal

Reversal phase is a time between the end of resorption and the beginning of bone formation stage. Its length varies considerably depending on the lag between the resorption and the formation (Martin *et al.* 1998). It takes a few days in rabbits, one week in dogs and 2 weeks in humans (Roberts 1988, Giannobile *et al.* 1994) and in monkey (Giannobile *et al.* 1994). During this phase the resorbed surface contains mononuclear cells but not osteoclasts (Jee 2001). The cement line is believed to correspond with the location of the bone surface during this period (Martin *et al.* 1998).

1.10.2.5 Formation and mineralisation

The formation phase begins with the recruitment of osteoblast precursors which then differentiate into mature osteoblasts to form new bone (F) in order to fill the pre-existing resorption spaces (Martin *et al.* 1998, Jee 2000, Ralston 2005). During this phase, the osteoblasts produce bone matrix (osteoid: unmineralised matrix) (Currey 2002). The osteoid is then mineralized within few days (Martin *et al.* 1998, Jee 2001, Kapanen 2002). The formation period is estimated to be 4.5 weeks in rabbits, 10 weeks in dogs, 13 weeks in humans (Roberts 1988) and 7.5 weeks in sheep (Lee *et al.* 2002). Osteoblasts secrete alkaline phosphatase that promotes bone mineralisation by degrading the naturally occurring mineralisation inhibitor known as pyrophosphate (Ralston 2005).

There is a mineralisation lag time between the initiation of matrix formation and its mineralisation. The mineralisation lag time is about 10 to 15 days, which may lead to the formation of an osteoid seam of about 8 to 10 μm (Jee 2001). Complete mineralisation may take 3 to 6 months irrespective of the bone type (Jee 2001). About

70% of mineral deposition occurs early during the mineralisation phase while the remaining 30% takes several months (Sommerfeldt & Rubin 2001). Minerals in the form of hydroxyapatite are initially deposited in the hole regions between the heads and tails of the tropcollagen molecules and latter over and within the collagen fibrils (Lee 1995, Lee 1997). The rate of mineralisation appears to be controlled by a variety of inhibitors such as pyrophosphate that is found in the matrix. Osteoblasts secrete substances such as alkaline phosphatase that neutralises the inhibitory effect of pyrophosphate (Lee 1995, Lee 1997, Guyton & Hall 2000).

The degree of bone mineralisation affects its biomechanical properties. For example, increased mineralisation increases stiffness while ultimate displacement is decreased (Turner 2002). Poorly mineralised bone was found to be very weak while hypermineralised bone is brittle (Turner 2002) (Figure1.9). Meanwhile, bone mineralisation occurs when the remodelling rate is reduced (Misch *et al.* 2001).

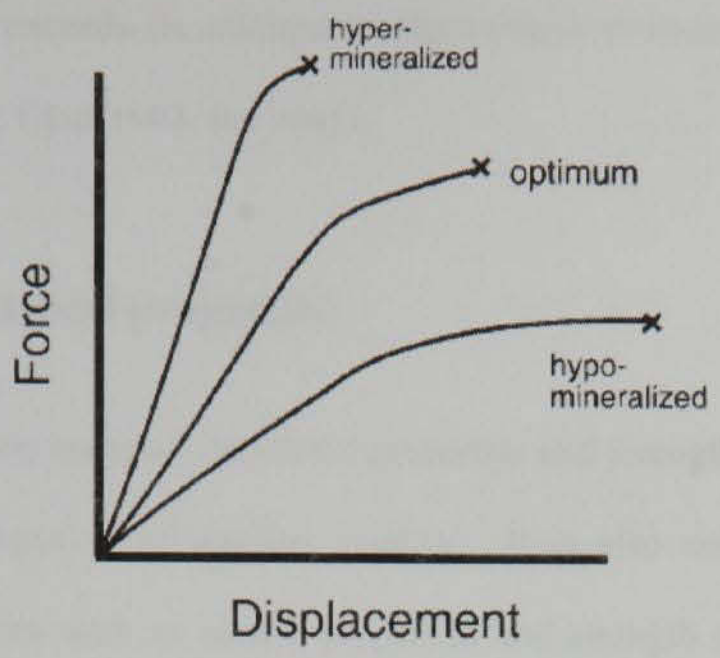

Figure 1.9 The relationship between degree of bone mineralisation and its biomechanical properties. Stiffness increases with increasing mineralisation, but bone becomes more brittle (after Turner 2002).

However, bone has a hierarchical structure, its composition and structure varies considerably with site, age, sex, physiological function and mechanical loading (Richie *et al.* 2005). This inconsistency should be considered when bone quality is investigated and comparison between results from different studies is made.

In normal conditions, bone remodelling can either maintain or remove bone (Frost 1994). Maintenance of bone occurs when the amount of bone resorbed is compensated for by an equal amount of newly formed bone, while the second event occurs when the amount of bone resorbed is more than the amount of newly formed one. Bone removal results in what is known as remodelling dependent bone loss as occurs in cases of reduced mechanical usage. It may result when strains within a bone remain below the minimum effective strain (Frost 1987, Frost 1994). On the other

hand, when strain exceeds its minimum effectiveness remodelling returns back to normal (Frost 1987, Frost 1994, Jee 2001).

1.11 Bone mechanical properties

Bone is a viscoelastic material; its elastic properties and strength are dependent upon the rate and the duration of applied loading. It is also anisotropic because its mechanical properties such as elastic properties and strength are dependent on the orientation of the bone microstructure with respect to the loading direction (Reilly & Burstein 1975, Carter & Spengler 1978, Misch *et al.* 1999).

Three principal factors that characterise some of the mechanical properties of bone: ultimate force, maximum deformation, and energy that can be dissipated before fracturing. The ultimate force represents the maximum load that the bone can sustain before fracturing. The ultimate force depends on several factors such as the type of load and the loading rate.

Stress-strain curves in tension and compression obtained from cortical bone showed a similar trend to that obtained from engineering materials. The stress-strain curve consists of an initial almost linear elastic region until the proportional limit is reached. This region indicates that the specimen will return to its original shape if the load is removed. The elastic phase is then followed by yielding at which the specimen begins to plastically deform until failure occurs. In the tensile specimen, after yielding point is reached the load increases gradually but at low rate until fracture occurs (Figure 1.10).

The curve of a compression specimen shows a linear proportion followed with a short yield region, the load soon dropping slightly and continuing at roughly the same level.

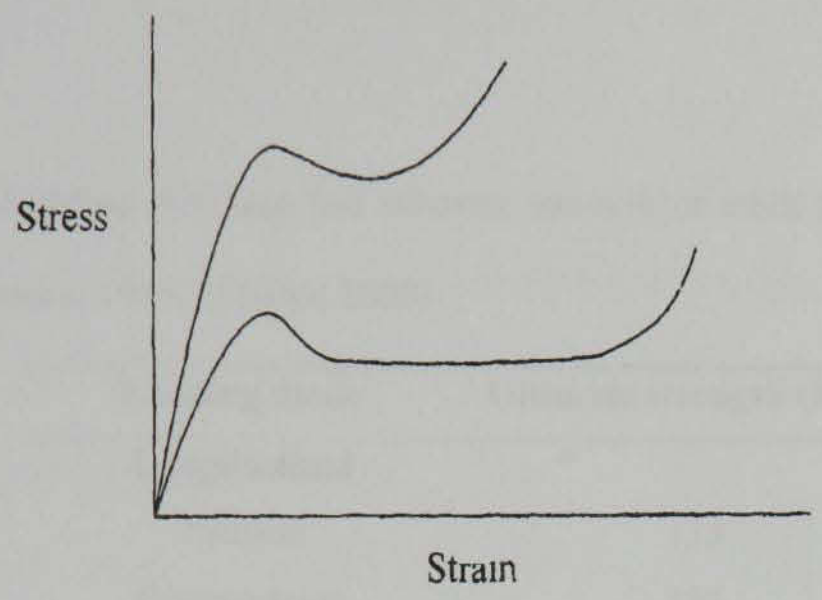

Figure 1.10 Load deformation curves for two specimens of cancellous bone having different properties. Yield and ultimate loads are apparent in the early portion of each curve. Subsequently, reduction and plateauing of the load occur. As void spaces collapse, the specimen densifies and the load rises steeply (Martin *et al.* 1998).

The deformation at failure depends on the loading rate as well as the loading direction.

The energy that bone absorbs before failure can be estimated from the area under the stress-strain curve. It therefore depends on the ultimate stress and strain and represents bone ductility.

Reilly and Burstein (1975) presented evidence of the anistropic nature of human femoral cortical bone. They used bone specimens obtained from a population ranging

in age from 19 to 80 years. The specimens were tested in compression and tension under wet conditions and at strain rates between 0.02 to 0.05 per second as measured with extensometers attached to the bone surface. The main results of the study are presented in tables 1.2 and 1.3.

Table 1.2 Loading direction and ultimate strength of adult femoral cortical bone (Reilly & Burstein 1975, O'Brien 2000).

Loading mode	Ultimate strength (MPa)
Longitudinal	
Tension	133
Compression	193
Shear	68
Transverse	
Tension	51
Compression	133

Table 1.3 Moduli of femoral cortical bone (Reilly & Burstein 1975).

Longitudinal modulus	17.0 GPa
Transverse modulus	11.5 GPa
Shear (modulus for torsion about longitudinal axis)	3.3 GPa

The two tables above indicate the following points:

1- Cortical bone is strongest in compression, 35% weaker in tension and 69% weaker in shear.

2- Compressive strength in both longitudinal and transverse directions was always greater than the corresponding tensile strength,

3- The specimens loaded in the longitudinal direction were stronger in both tension and compression than when transversely loaded,

4- The tensile strength in a longitudinal direction was equal to the compressive strength in transverse direction,

5- The mean value of the longitudinal modulus was approximately 50% greater than that of the transverse modulus,

6- In general, longitudinally loaded bone specimens are stronger than when transversely loaded in both compression and tension,

7- The strength anisotropy of cortical bone is less pronounced in compression than in tension (Reilly & Burstein 1975, Carter & Spengler 1978).

However, damage and failure of bovine cortical bone have been studied in static tensile experiments and have shown large variations of stress failure from 100 to 200MPa, and failure strain from 0.4% to 4% (Pithioux *et al.* 2004).

1.12 Responses of bone cells to biomechanical forces and the role of osteocytes

Bone is a load-bearing material that is able to adapt its inner structure and architecture to its mechanical environment (Huiskes *et al.* 2000). This ability is known as functional adaptation, which is probably controlled with a specific feedback mechanism, though the cellular mechanisms involved are not fully understood (Mosley 2000). However, several theories have been put forword to explain how bone recognises and reacts to such mechanical stimuli.

Osteocytes are the only living cells found within the bone matrix and are able to communicate with other bone cells including lining cells and osteoblasts due to their cytoplasmic processes within the canaliculi (Burger & Klein-Nulend 1999, Mikuni-Takagaki 1999). Thus, osteocytes are the appropriate "candidates" for mechano-sensors due to their location within the cortical bone and to their ability to communicate with other bone cells (Burger & Klein-Nulend 1999, Mikuni-Takagaki 1999). Osteocytes possess a number of cytoplasmic processes by which they can communicate with other cells and possibly play an important role in bone remodelling within the affected bone (Burger & Klein-Nulend 1999, Mikuni-Takagaki 1999).

It has been hypothesised that the three-dimensional network of lacunae and canaliculi containing osteocytes and their process is a mechano-sensing network by which the imposed loading can be detected and the loaded bone responds to such mechanical stimului (Burger & Klein-Nulend 1999). As a result, osteoblasts and osteoclasts are activated and bone tissue is either resorbed and/or formed.

The osteocytes and their processes are surrounded by a thin non-mineralised matrix through which the interstitial fluid (water and small molecules) flows as a result of local stress in the strained bone (load-induced fluid flow) (Weinbaum *et al.* 1994, Burger & Klein-Nulend 1999). Due to mismatches in diameter between the osteocytes process and the canaliculi an annular porosity is produced (Burger & Klein-Nulend 1999). Mechanical loading causes a change in pressure of these pores and causing the interstitial fluid to flow through them. As a result fluid shear stress at the osteocyte cell membrane is produced. Hence, the osteocytes are placed under shear stresses and drag forces. This flow provides the stimulus for the mechano-sensing cells (osteocytes) and informs the bone cellular network about adequacy of the existing bone structure (Srinivasan & Gross 2000, Hung & Lee 2001). The shear stress generated within the canaliculi was estimated to be in the range of 0.8-3 Pa (Burger & Klein-Nulend 1999). These values are sufficient to activate the neighbouring osteocytes. It is widely accepted that by this fluid flow shear stress the osteocytes are informed about their mechanical environment. Subsequently, bone modelling and/or remodelling will occur. If this shear stress is within a normal range the bone steady state will be maintained. Inversely, if the shear value is higher or lower the osteocytes will send signals and more bone is formed or resorbed (Burger & Klein-Nulend 1999). It has also been reported that canalicular fluid flow increases with the increasing of frequency of an applied stress in an avian ulna (Srinivasan & Gross 2000). Burger and Klein-Nulend (1999) assumed that the local strain of the osteocyte membrane resulting from the local fluid shear stress would be much higher than the bulk strain of the whole piece of bone.

However, this concept does not resolve inconsistencies that remodelling increases when the mechanical loading is extremely high or significantly low (Martin 2000).

Recently, another theory has been put forward to resolve the contradiction (Martin 2000). It suggests that lining cells are inclined to activate remodelling unless restrained by generated inhibitory signals that are generated by the osteocytes. Therefore, remodelling is activated when the inhibitory signal generation declines as a result of reduced loading such as in a state of disuse, or when signal generation or transmission is interrupted by micro-damage due to excessive loading (Martin 2000).

An association between the decrease in osteocyte lacunar density and the accumulation of microcracks has been reported in human cortical bone (Vashishth *et al.* 2000) as well as in dog humerus (Frank *et al.* 2002). Microcracks may disturb the canalicular network severing osteosytes processes (Burger and Klein-Nulend 1999) or may shield cells from local strains thus negatively affect the exchange of nutrients and waste affecting the homeostasis of cells (Lee *et al.* 2004). Furthermore, at a microstructural level microcracks may alter strain sensed by the osteocytes, which triggers bone remodelling (Prendergast & Huiskes 1996, Scannell & Prendergast 2005). Osteocytes have a suppressive effect on the activity of osteoclasts. This effect would be compromised by disuse and lack of loading and/ or disconnection of canaliculi as a result of microdamage (Huiskes *et al.* 2000) (Figure 1.11). The sequence of bone response to mechanical stimuli is depicted in Table 1.4.

Table 1.4 Bone response to mechanical environment (Duncan & Turner 1995).

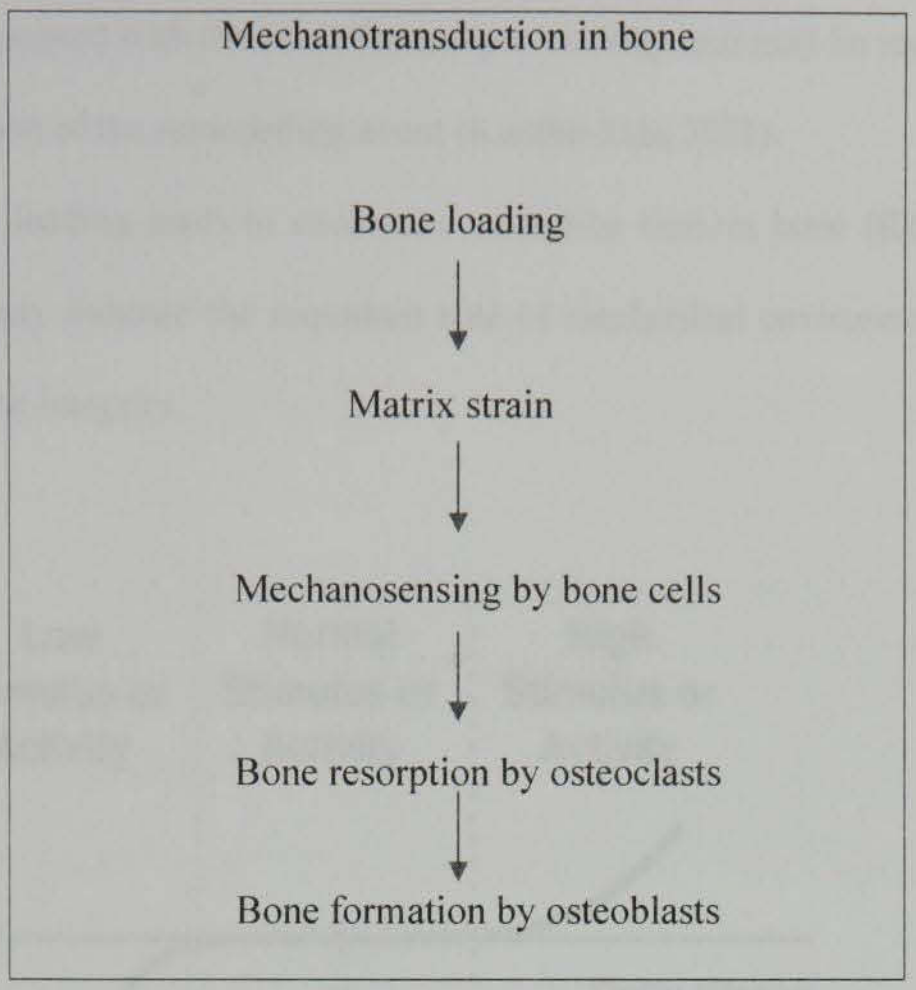

A positive correlation between osteocyte apoptosis (loss of osteocyte viability or planned cell death) and remodelling of bone has been reported (Bentolila *et al.* 1998, Verborgt *et al.* 2000). Osteocyte apoptosis can be induced by bone fatigue and localised to bone containing microcracks (Bentolila *et al.* 1998). After bone fatigue, bone remodelling (resorption) sites are found to be associated with regions of osteocyte apoptosis. These studies suggest that bone fatigue stimulates bone remodelling. Consequently, it was suggested that, "changes in osteocyte integrity play a key role in the signalling and/or targeting mechanism by which osteoclasts identify areas of bone to be removed after matrix injury" (Knothe-Tate 2001). Hence, impairment of interstitial fluid flow following matrix damage and osteocyte

apoptosis has been predicted as a cause of the remodelling in response to damage. The impairment of interstitial fluid flow due to inadequate mechanical load (disuse) was found to be associated with the loss of osteocyte viability and may be responsible for the rapid activation of the remodelling event (Knothe-Tate 2001).

Loss of mechanical loading leads to enormous resorption sites in bone (Knothe-Tate 2001). This may indicate the important role of mechanical environment in maintaining osteocyte integrity.

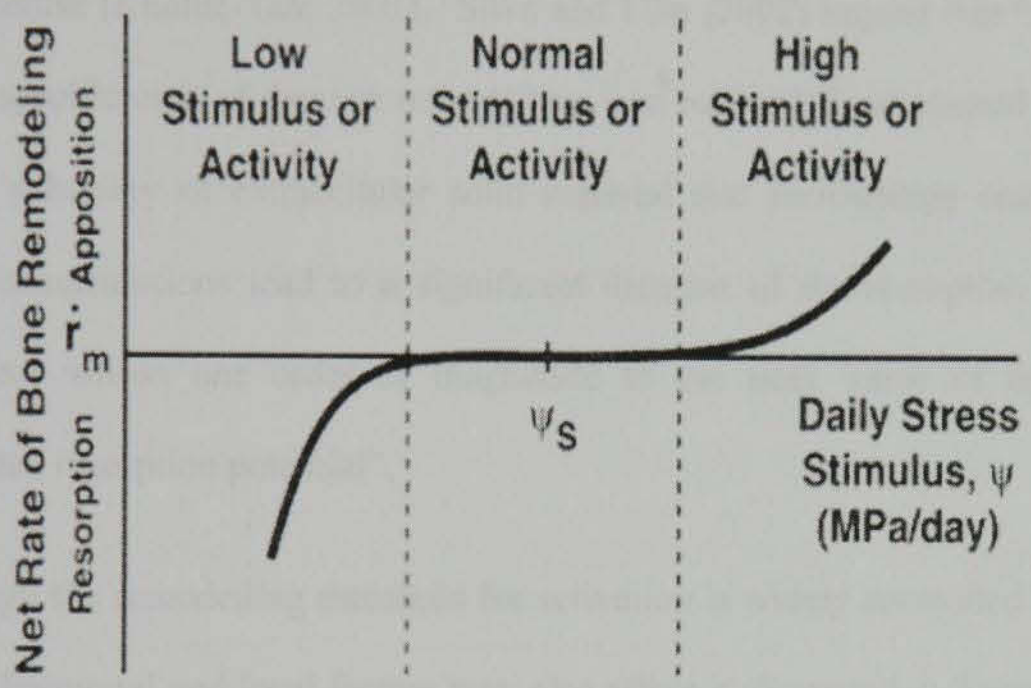

Figure 1.11 Theoretical net rate of bone apposition/resorption as a function of mechanical loading. When the daily stimulus is near the normal stress stimulus set-point, there is little resorption or apposition. When the daily stress stimulus loading is higher or lower than the stress stimulus set-point bone apposition and resorption respectively occurs (After Hernandez *et al.* 2000).

An association between bone resorption and osteocyte integrity in bone subjected to disuse has also been reported (Knothe-Tate 2001). In that laser scanning conofocal microscopy study, beagle dogs (female, 4-7 years old), were subjected to single limb

immobilization were used. Specimens of un-decalcified bulk-stained with basic fuchsin from metacarpal were examined after 1 and 6 weeks of immobilization. Osteocyte integrity was evaluated. The result of this study indicated that one week after immobilization, osteocyte integrity is reduced approximately 30% in comparison with controls. At 6 weeks of immobilization, osteocytes integrity is increased when compared with the one-week period values though are still reduced significantly relative to control values (Knothe-Tate 2001). This work suggests that a common pathway for signalling and timing of bone resorption occurs after both bone disuse and overuse (Knothe-Tate 2001). Silva and Ulm (2002) argued that "stress sensing" in the specific case of damage remodelling, can be partially explained by an increase of the solubility of extracellular solid material that surrounding cracks and flaws: stress concentrations lead to a significant increase of the resorption potential, that compares within one order of magnitude to the peak value of the biologically generated resorption potential".

Although the remodelling threshold for activation is widely controlled by mechanical usage, hormonal and local factors may also affect it (Forwood & Turner 1995). It is also reasonable to suggest that there is no way to remove microdamage from bone other than bone remodelling (Martin 2003).

1.13 Bone damage

Bone in general is not very ductile and cannot sustain very high plastic deformation (Turner & Burr 1993). When compact bone is subjected to cyclic (repeated) loading the mechanical properties are degraded gradually (Carter & Hayes 1977). If the load continues, the bone will ultimately fail at a value well below normal. This degradation in the mechanical properties has been attributed to microdamage accumulation (Carter

& Hayes 1977). The resistance of any material to fatigue failure is dependent on its resistance to both the initiation and growth of cracks (Martin *et al.* 1998). These two factors are in turn highly dependent on the microstructural characteristics of the material. Material that has a low resistance to crack initiation has, on the other hand a high ability to resist crack growth (Burr *et al.* 1988, Martin *et al.* 1998, Mohsin *et al.* 2006). Bone is one of many highly fatigue-resistant materials that obtain this property mainly from their resistance to crack growth rather than crack initiation (Martin *et al.* 1998, Mohsin *et al.* 2006). There are several microstructural factors that highly affect crack initiation and growth. These factors include porosity, mineralisation and collagen fibre orientation size, number and diameter. They affect initiation and growth in different ways (Martin *et al.* 1998, O'Brien 2002, Mohsin *et al.* 2006). In general, a decrease in the yield strength leads to an increase in the potential for crack initiation, but it also leads to an increase in the resistance to crack growth (Martin *et al.* 1998) (see loss of stiffness and microcrack accumulation below). The fibre size, number and diameter also affect the initiation and crack growth through a material. The interface between a fibre and the surrounding matrix is a source of weakness that can initiate cracks. Conversely, the cracks tend to remain small and follow the fibres instead of propagating across the structure (Martin *et al.* 1998).

Sections were found to have an effect on the density and length of microcracks (O'Brien *et al.* 2003). Microcracks that were found in the transverse sections were shorter than those found in the longitudinal ones, but their density was greater.

Microcracks accumulation in bovine tibiae that were exposed to an axial cyclic compressive load were found to develop rapidly during the first 10000 cycles and only slight accumulation occurred between 10000 and 50000 cycles. After 50000

cycles the accumulation increased rapidly (Figure1.12). This trend was observed irrespective of the sections; longitudinal or transverse (O'Brien *et al.* 2003). This was due to a microstructural barrier that was believed to govern the fatigue behaviour of bone (Akkus & Rimnac 2001, O'Brien *et al.* 2003, O'Brien *et al.* 2005a, Mohsin *et al.* 2006) which may facilitate microcrack generation but delay or even prevent microcrack growth.

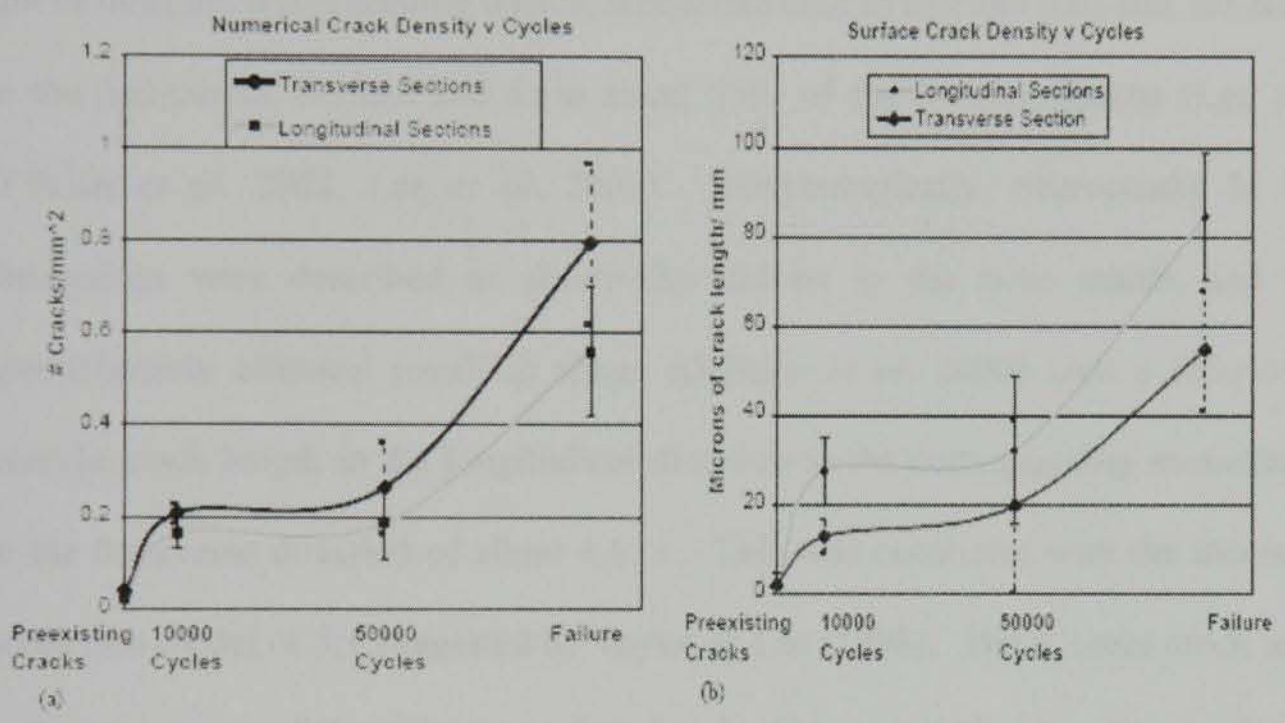

Figure 1.12 Microcrack accumulations during application of an axial compressive force to bovine tibiae using a series of chelating agents, (a) numerical microcrack density versus cycle (b) surface crack density versus cycle (Reproduced from O'Brien *et al.* 2003).

Both graphs show a similar trend, microcrack density increases rapidly during the first 10000 cycles but then there is a reduced rate of accumulation until 50000 after which there is a rapid rate of accumulation. The graph also indicates numerical microcrack

density for the longitudinal sections is lower than those for the transverse ones and vice versa in the case of surface crack density (O'Brien *et al.* 2003).

Microdamage is frequently defined as microscopic cracks (microcrack) in bone matrix, which can be stained with conventional stain techniques and detected using light microscopy (Frost 1960, Burr *et al.* 1985, Schaffler *et al.* 1994). It is also defined as a discontinuity in the calcium-rich bone matrix. It represents a fissure or a break in the hydroxyapatite, which comprises 60% of bone by weight. These features can be detected with chelating agents, which can bind to calcium ions that are present in the microcrack surface and form about 55% of the hydroxylapatite (Lee 1997, O'Brien *et al.* 2002, Lee *et al.* 2003). Morphologically, microcracks in three dimensions were described as sheath-like defects in the bone matrix and were approximately elliptical (oval) in shape (O'Brien *et al.* 2000) with a ratio of the average crack length in the longitudinal direction to the corresponding measurement in the transverse direction of about 4.6: 1. This was consistent with the theoretical prediction model of 5:1 suggested by Taylor & Lee (1998). The average crack length in the major axis of the ellipse was found to be 404μm ± 145 versus the crack width in the minor axis of the ellipse was 97μm ± 37.

Generally, microcracks occur naturally in bone during day-to-day cyclic activities (Burr *et al.* 1985, Frost 1991, Schaffler *et al.* 1994, Burr *et al.* 1997, Norman & Wang 1997, O'Brien *et al.* 2000, Zioupos 2001a, Norman *et al.* 2001, Lee *et al.* 2002). They can also be produced *in vitro* by cyclic loading (Burr *et al.* 1985, Schaffler *et al.* 1989, Forwood & Parker 1989, Schaffler *et al.* 1994, Burr *et al.* 1997, Huja *et al.* 1999b, O'Brien 2000, Lee *et al.* 2002, O'Reilly 2002, O'Brien *et al.* 2005a).

Microcracking appears to be greatly influenced by bone microstructure. The course of crack growth was most likely influenced by the Haversian systems and lamellar interface and they were most commonly found in interstitial bone (Wenzel *et al.* 1996, Norman & Wang 1997, O'Brien *et al.* 2000, Martin 2003, O'Brien *et al.* 2005a, Mohsin *et al.* 2006). Crack growth decreases rapidly with increasing length (Taylor 1998).

Microcrack generation and growth can adversely affect the mechanical properties of loaded bone (Forwood & Parker 1989, Schaffler *et al.* 1989, Turner & Burr 1993, Burr *et al.* 1997, Burr *et al.* 1998). For example, Forwood and Parker (1989) reported that microcrack generation in long bone (rat tibia) increased significantly with an increase in repetitive torsional loading, and this sequentially was associated with a decrease in bone stiffness (rigidity) and ultimate strength (maximum stress the bone can sustain before it breaks). Schaffler *et al.* (1989) found loss of stiffness associated with increased microcrack densities in cortical bone specimens, which were cyclically loaded uniaxially in tension. They found a strain rate dependency indicating that loading at lower strain rates is less damaging than loading at high strain rates (Schaffler *et al.* 1989).

1.13.1 Microcrack accumulation and loss of bone stiffness

It has been reported that a loss of stiffness is a result of microdamage accumulation (Carter & Hayes 1977, Burr *et al.* 1985, Zioupos *et al.* 1994, Reilly & Currey 1999) and stiffness is a primary predictor for ultimate strength in human trabecular bone in compression (Fyhrie & Vashishth 2000).

Reilly and Currey (1999) reported the occurrence of microcracks at the pre-yield region of the load deformation curve in specimens loaded in bending, and increased considerably at the yield point and post-yield region. This study suggests that the yield in bone is initiated by the generation of cracks (Zioupos *et al.* 1994).

Forwood and Parker's study supporting additional studies (Carter & Hayes 1977, Burr *et al.* 1985) suggested that the deterioration in bone mechanical properties and fatigue damage observed during repetitive loading is more likely to be caused by microcrack accumulation. Forwood and Parker (1989) stated "as few as 200 cycles were sufficient to cause a significant reduction in all mechanical properties at a load equivalent to 35% of the ultimate torque of the rat tibiae".

However, microcracks can absorb a significant degree of energy after the bone has been loaded. This may allow the bone to experience a large strain and deformation before fracturing. Thus, the direct effect of microcracks is in increasing bone compliance (ductility) (Reilly & Currey 1999).

1.13.2 Microcracks and bone toughness

Fatigue is defined as the progressive loss of strength and stiffness that occurs prior to failure in materials subjected to cyclic loading, while toughness is a measure of a material's ability to resist fracture (O'Brien *et al.* 2000). Toughness is defined as the amount of energy required for a fracture to occur, therefore, the more the overall amount of energy dissipated, the "tougher" the material (Zioupos 2001b). Toughness is an important material biomechanical property as a tough material will be more resistant to fracture, albeit it may be less resistant to plastic deformation (Turner & Burr 1993).

The energy will be dissipated in three major steps. Some energy is absorbed by generation of diffuse damage before a major crack is generated. This was denoted as the "pre-fracture" toughness, or damage tolerance level of the material. Some energy is dissipated to create the final fracture crack; the rest is consumed to drive the crack through the tissue in order to break the material (Zioupos 1998, Zioupos 2001a).

Microcrack generation in bone may also be a bone toughening mechanism by which the bone fatigue life may be extended as cracking in bone involves rising fracture resistance with crack extension (Vashishth *et al.* 1997, Vashishth *et al.* 2003, Wang 2003, Richie *et al.* 2005). The major part of bone toughness is determined by its post-yield behaviour (Wang 2003).

When a microcrack propagates through stiff material, stress will be generated and concentrated at the crack tip to a high degree that enables the crack to propagate at applied stresses lower than that of the theoretical fracture stress. In bone (as it is often considered a two-phase), lamellar interfaces lead to stress concentration (enhancement) at a propagating crack tip to be relieved as the crack enters the interface. Thus, the microcrack will first be accelerated when it is within a stiffer one, then it will be slowed down by the complaint interface and finally it will be arrested as it propagates towards a stiffer face. In order to overcome the last event (arresting of microcracks) an increased threshold stress is required (Burr *et al.* 1988, O'Brien *et al.* 2000). This provides evidence of the difficulty for crack propagation in bone as a composite material.

The accumulated damage *in vivo* relates more to bone toughness than to bone stiffness and strength (Zioupos 2001a) and the fracture toughness and the cumulative number of microcracks increased linearly in human and bovine cortical bone (Vashishth *et al.*

1997). Thus, "bone toughness is determined by its ability to form microcracks during crack propagation" (Vashishth *et al.* 2003) and stiffness loss is associated more with microcrack generation than growth (Burr *et al.* 1998). Toughness of human and bovine cortical bone was found to rise linearly with crack extension (Vashishth *et al.* 1997, Nalla *et al.* 2003, Nalla *et al.* 2005, Ritchie *et al.* 2005) and crack growth resistance (fracture resistance) was found to increase with crack extension (Vashishth *et al.* 2003).

The fracture resistance of cortical bone is primarily influenced by the orientation relationship between the bone and the crack. For instance, cracks with transverse directions have been reported to be consistently tougher than those oriented longitudinally (Ritchie *et al.* 2005).

Generation of small microcracks i.e. diffuse microcracks, which have a limited capacity to extend, may reduce the strain energy and play an important role in bone toughening (Ritchie *et al.* 2005). It has been suggested that control of microcrack length appears to be essential to prevent more severe damage and fracture (Sobelman *et al.* 2004).

Several studies (Vashishth *et al.* 1997, Nalla *et al.* 2003, Nalla *et al.* 2005, Ritchie *et al.* 2005) have suggested that crack propagation is a mutual competition between two types of material toughening mechanisms: intrinsic and extrinsic. The intrinsic mechanism (microstructural damage mechanism) operates ahead of the crack tip. An example of this type of mechanism is deflection of microcracks along the cement line when encountering osteons and crack deflection happens along the cement line because it provides a weak path for the propagation of the crack. This mechanism was considered as the main source of toughening in the transverse orientation (where

the osteons run along the specimen) (Nalla *et al.* 2003, Nalla *et al.* 2005, Ritchie *et al.* 2005) (Figure 1.13).

The second toughening mechanism is an extrinsic one and acts principally behind the crack tip in the crack wake and/or in the surrounding material (Ritchie *et al.* 2005). It acts as a crack shield from the driving force. It is the principal toughening mechanism in the longitudinal orientation (the plane of the crack and the crack front are parallel to the long axis of the osteons) and causes a local reduction in the magnitude of the stress experienced at the crack tip. An example of this mechanism is a crack bridging by uncracked ligaments and by collagen fibrils (Figure 1.13).

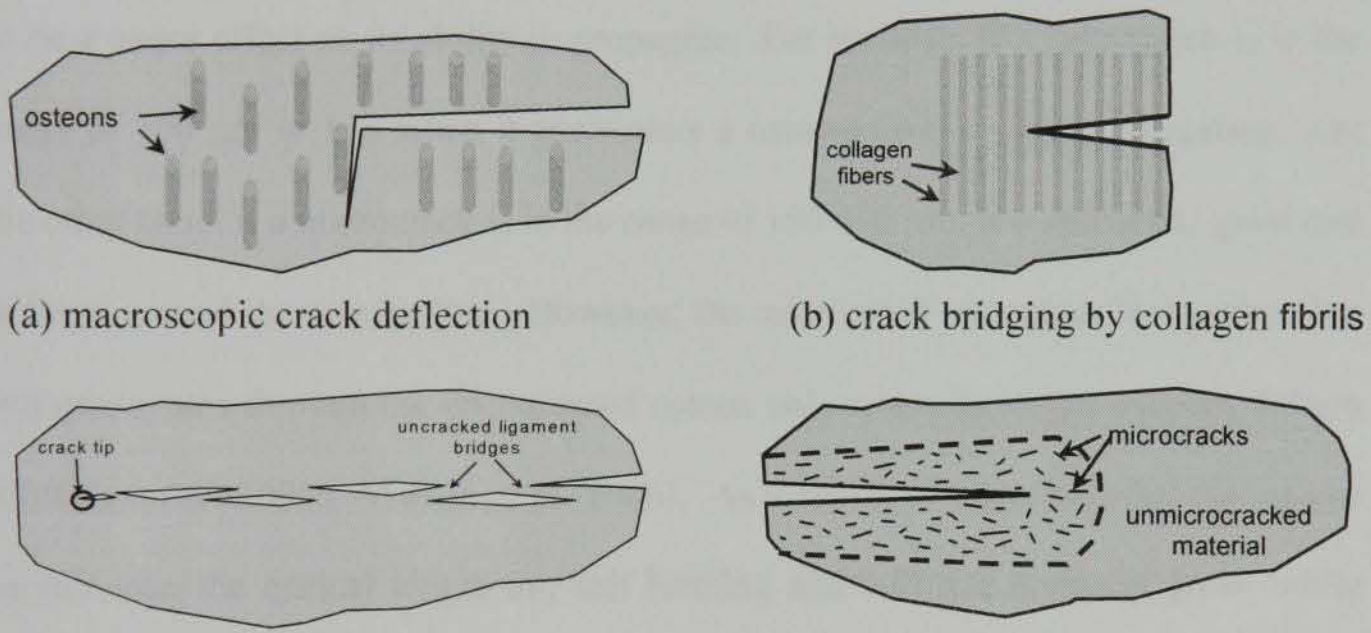

(a) macroscopic crack deflection

(b) crack bridging by collagen fibrils

(c) crack bridging by uncracked ligaments

(d) constrained microcracking

Figure 1.13 Schematic illustrations of some of the toughening mechanisms possible in cortical bone: (a) crack deflection (by osteons), (b) crack bridging (by collagen fibres), (c) uncracked ligament bridging, and (d) constrained microcracking by diffuse microcracking (Ritchie *et al.* 2005).

It has been proposed that the post-yield behaviour of bone most likely involves three mechanisms (Wang 2003). First, microcrack formation that generates new surfaces in the mineral (hydroxylapatite crystal) and in the collagen phase. Second, generation of diffuse damage at nano scales that leads to denaturation of collagen due to stress concentration around the diffuse damage tip. The energy consumed to achieve this denaturation is probably related to the plastic deformation of bone. Third, the viscoelastic behaviour of bone. This behaviour is observed during the post-yield deformation and is most likely due to the reversible collagen deformation (Wang 2003).

In accordance with two *in vitro* studies (O'Brien *et al.* 2005a, Mohsin *et al.* 2006) microcrack length at the time at which the microcrack encounters the osteon appears to be a major effect on its ability to propagate. For instance, if a microcrack is in the range of 100 μm or less when it encounters a cement line, it stops propagating. On the other hand, if a microcrack is in the range of 150-300 μm, it continues to grow and deflects around the cement line. However, the microcrack penetrates the cement line and propagates through the encountered osteon only when its length exceeds 400μm (O'Brien *et al.* 2005a, Mohsin *et al.* 2006). As a result, it was concluded that cracks shorter than the critical length are self limiting and will not normally grow, while those longer than the critical length will propagate and could lead to failure (Mohsin *et al.* 2006). In order for short cracks that are below the critical length to propagate, energy input into the material is needed. Beyond this point, the cracks grow in a faster manner under the effect of the release of strain energy from the material. Thus, when such short cracks hit an osteon, they are stopped as they have less surface energy than the longer cracks. Inversely, when longer cracks (>400μm) hit and penetrate the cement line and propagate through an osteon. Whereas, microcracks of

intermediate length (100-300 μm) follow the path of least resistance and are deflected around cement lines (Mohsin *et al.* 2006).

It has been theoretically predicted and experimentally shown that microcrack growth rate decreases with increasing microcrack length in antler of Red Deer (Vashishth *et al.* 2003). This trend has been previously observed in human cortical bone (Vashishth *et al.* 1997), which may suggest that compact bone tissue resists fracture at the micro-scale by slowing down microcrack growth and arresting them (Akkus & Rimnac 2001). Nevertheless, antler is in essence a less mineralized bone, but is much tougher than ordinary bone (Zioupos *et al.* 1994).

Microcracks, as a result of fatigue compression, were found to develop rapidly in bovine tibiae and then the rate of accumulation slowed down until the period prior to failure where they accumulate in a significant degree until failure (O'Brien *et al.* 2003). In this study pre-existing microcracks were first stained with alizarin dye. The specimens were also stained with xylenol orange for the first 10,000 cycles, followed with calcein to 50,000 cycles and finally with calcein blue between 50,000 and failure (O'Brien *et al.* 2003).

Schaffler *et al.* (1996) used specimens obtained from human compact bone, which were fatigued using uniaxial loading until stiffness loss of 18-30% was achieved. They found that visible microcracks did not increase until a 30% stiffness loss has been achieved, while diffusely stained areas of bone matrix increased in a linear pattern with the increase in degradation of the stiffness (Schaffler *et al.* 1996). This trend was also observed by Burr *et al.* (1998) who found that linear relationship between the damaged (diffuse staining) area and stiffness loss but the relationship between microcrack density and stiffness loss was approximately quadratic. Also,

Burr *et al.* (1998) did not detect significant microcrack generation until the bone had lost 15% of its elastic modulus (stiffness). In Burr and coworker's study canine femurs were tested using a 4-point cyclic bending under a controlled load and microcracks were stained with basic fuchsin and examined using light microscope.

The amount of damage in cancellous bovine tibia was found to depend on the generated strain level (Wachtel & Keaveny 1997). They found damage density for cancellous bone specimens which were loaded to about 0.4% strain level (pre-yield group) were not statistically different from that for bone specimens loaded to 1% strain level (yield group) ($p<0.66$). However, when the specimens were loaded to a strain level of 2.5% (post-yield group) the damage density was significantly greater than the pre-yield group ($p<0.0008$) and the yield group ($p<0.006$). This may indicate that the damage may occur below the level that can be detected at x200 magnification when the 10% silver nitrate bulk stain was used as a bone label (Wachtel & Keaveny 1997).

Bone however, may undergo significant stiffness loss and its mechanical properties may be compromised before microcracks can be detected under light microscope.

These studies may be evidence of a sub-microscopic level of bone damage (diffuse damage) that can not be detected using light microscope because they are beyond the resolution capabilities of light microscopy (Schaffler *et al.* 1989, Schaffler *et al.* 1994, Burr *et al.* 1997, Reilly & Currey 1999). Hence, they may be generated before production of larger microcracks (Schaffler *et al.* 1994, Jepsen *et al.* 2001, Norman *et al.* 2001).

This finding supports the idea that there is an ultra-structural level of damage in bone in addition to the microscopic level. This diffuse damage has been considered as

evidence of a damage process zone, which is an area of ultra-structural damage defined by increased molecular permeability in composite materials (Schaffler *et al.* 1996, Burr *et al.* 1998).

In bone, these diffuse staining areas may represent ultra-structural level of disruption in the bone matrix, as indicated by a change in bone matrix permeability to lead-uranyl acetate, because intact bone matrix is not stained by lead-uranyl acetate (Schaffler *et al.* 1994).

In vivo microcracks observed in human rib samples had little collateral diffuse staining patches, while other microcracks were associated with marked diffuse staining that extended from microcrack tip or from sides (Schaffler *et al.* 1994).

It has been suggested that bone matrix ultra-structural feature, such as the collagen fibre-bone mineral interrelationship, may play a major role in minimising the formation of principal microcracks and it may also facilitate the formation of marked diffuse damage which does not propagate as readily to complete fracture (Schaffler *et al.* 1994).

Diffuse damage in human cortical bone was found to be small, averaging about 3% of total bone area and did not influence bone fracture toughness *in vivo* (Norman *et al.* 2001).

Three different histological morphologies of bone damage were reported in the literature (Vashishth *et al.* 2002). The first type represents a microscopic level of bone damage. It is long (approximately 100 μm), has sharp distinct edges and a well-defined outline. This is usually denoted as a linear microcrack and is most commonly observed in interstitial bone (Frost 1960, Schaffler *et al.* 1994, Martin *et al.* 1996,

Martin 2003). Frost (1960) was the first to describe this type of bone damage in human ribs.

The second type of damage represents the ultra-structural and molecular level of bone damage. It occurs as a diffuse staining area within the bone matrix (Schaffler *et al.* 1994, Boyce *et al.* 1998) that has been disrupted by locally intense deformation (Martin 2003). Using conofocal microscopy these staining areas are found to be composed networks of fine, ultrastructural level cracks (Boyce *et al.* 1998). This type of damage may rise from the edges or from the tip of the linear microcrack or can also occur on its own (Schaffler *et al.* 1994, Burr *et al.* 1998, Reilly & Currey 1999, Norman *et al.* 2001).

The linear microcracks may or may not be associated with the second type. The reason for the association or lack of such association between the two bone damage types remains a speculative and "may be related to the energy with which cracks propagate or to the relative degree of brittleness of the region of bone matrix through which cracks propagate" (Schaffler *et al.* 1994).

The diffuse damage, consisting of tiny cracks may occur at the sub-microscopic level, which is beyond the resolution capabilities of light microscopic evaluation (Schaffler *et al.* 1989, Schaffler *et al.* 1994). It has been speculated that sub-microscopic features of the bone matrix, such as collagen fibre associated with bone minerals, might have the capacity to reduce microcrack generation and encourage the formation of numerous diffuse areas of damage which do not propagate rapidly to complete fracture (Schaffler *et al.* 1994). The diffuse damage may represent cracks in bone apatite crystals, mineral/collagen de-bonding or an organic matrix deformation. It has

also been proposed that the diffuse damage is possibly an early formation stage of the linear microcrack (Schaffler *et al.* 1994, Reilly & Currey 1999, Jepsen *et al.* 2001).

A similar intensely (diffusely) stained area as well as linear microcracks were also reported to occur *in vitro* in the bone adjacent to external skeletal fixation pins used in orthopedic surgical treatment as a result of pin insertion. Diffuse damage was found to extend beyond a 1.5 mm zone next to the pin-bone interface (Cohen *et al.* 2003). Similar diffuse staining areas were also observed by Lee (1997) on the machined bone surface as a result of the cutting procedure.

The third type of damage has a fine, tear-like appearance. They most commonly occur near and in the plane of the neutral axis of the tested specimen. These fine cracks are extensively branched and cross cement lines, lamellae and are found within osteonal regions. In another words, they are not affected by microstructural boundaries of the tested bone (Boyce *et al.* 1998).

In cancellous bone three patterns of bone damage have been observed *in vivo*. They are linear microcracks, cross-hatched and diffuse damage (Wenzel *et al.* 1996, Fazzalari *et al.* 1998). The linear microcracks were most commonly found in the cement line, within the interstitial bone matrix and near the surface of the trabeculae (Wenzel *et al.* 1996). The cross-hatched damages were observed primarily in vertically oriented trabeculae and were surrounded with diffuse staining areas (Wenzel *et al.* 1996).

Wachtel & Keaveny (1997) reported a strong dependence of damage morphology on the apparent strain level in cancellous bone in bovine samples. Accordingly, they classified the generated damage into four types: transverse cracks, shear bands, parallel cracks and complete fracture. The transverse cracks are perpendicular to the

long axis of the trabeculae. Some of these cracks were found to be completely or partially crossing horizontal trabeculae. The shear bands are characterised by criss-cross pattern which are oriented at approximate ± 45° to the long axis of the trabeculae and are most commonly found in vertical trabeculae. The parallel cracks are running parallel to the long axis of the involved trabeculae and are detected in both horizontal and vertical trabeculae. The complete fracture indicates a clear displacement of trabecular segments and are found in both horizontal and vertical trabeculae (Wachtel & Keaveny 1997).

Microcracks are most commonly observed in the interstitial bone matrix (Boyce *et al.* 1998). This would be expected because the interstitial bone contains more minerals compared with other type of bone matrix such as osteons, thus it is more brittle and is the site of increased damage.

Bone microcracks may be easily generated; yet, their growth is highly resisted by bone structure (Turner & Burr 1993). It has also been suggested that microcracks may be generated in brittle regions of bone and arrested by other tougher regions (Forwood & Parker 1989).

1.13.3 Fatigue life of bone

Thus, in general, the fatigue life of bone (as other fibre composite materials) is divided into three phases" [Figure 1.14 and Table 1.5] (Turner & Burr 1993, Matrin *et al.* 1998, O'Brien *et al.* 2000).

Phase I: Crack initiation

The first phase is characterised by the initiation of numerous of small microcracks associated with a relatively rapid but limited loss of stiffness. It usually begins at a

weak area and high stress concentration such as cement lines and structural discontinuities. At this stage, the microcrack is self-limiting because it is confined to a single lamella and stops at lamellar interface (Matrin *et al.* 1998). This rapid stiffness loss and its stabilization are due to a rapid crack generation but without further crack growth (Lee 1997, Matrin *et al.* 1998, O'Brien *et al.* 2000). The generated cracks reduce stress in the material along side the crack and increase the stresses near the crack tips at the lamellar interface (Matrin *et al.* 1998). As the number of cracks increase, the distance between their sides reduces as well as the peak stresses in these regions, thus new cracks cannot be generated. This phase occurs in the first 25% of the materials fatigue life (Figure 1.14).

Phase II: Crack growth

This phase is characterised with shifting of damage accumulation to interlamellar debonding or delamination. The stress field or plastic zone in front of a growing microcrack leads to inter-lamellar debonding at the interface. This debonding blunts the tip of the growing microcrack. Consequently, the microcrack will follow the path of least resistance (the debonding interface) and becomes parallel to the lamellar interface which is usually aligned in the direction of the principal stress. Secondary cracks may grow between lamellae and act as an energy sink and prevent the growth of large dangerous cracks (O'Rielly 2002). Thus, the fatigue life is extended without a considerable change in its stiffness. The reduction in stiffness loss and the rate of damage accumulation are both maintained until just before failure although the microcracks begin to grow.

However, Boyce and associates (1998), after conducting a 4-point bending test on a human tibia observed that phase II was characterised with a continuous and gradual decrease in stiffness (Figure 1.15).

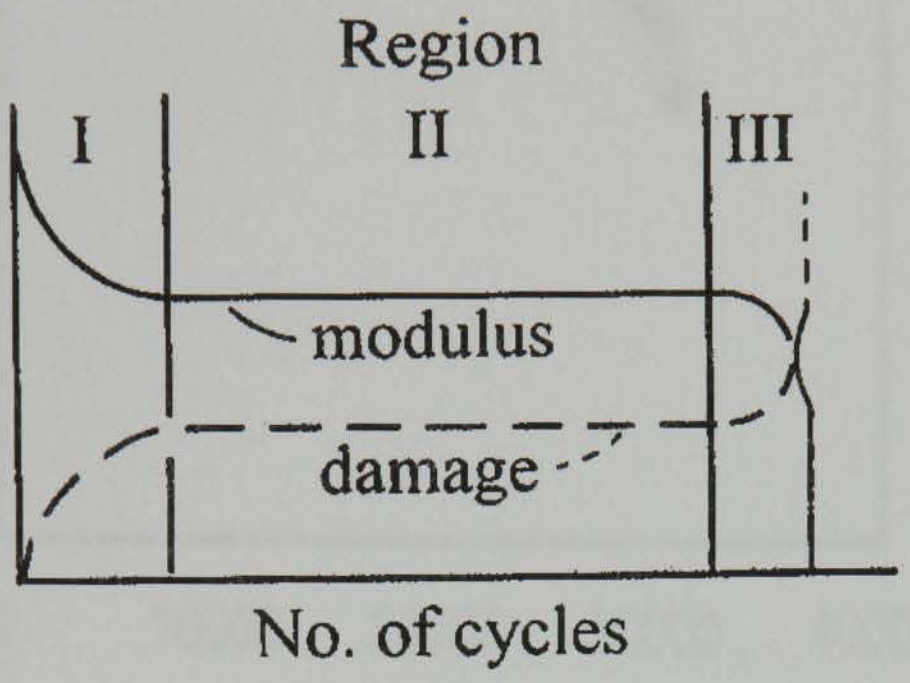

Figure 1.14 The process of fatigue failure for a typical composite material. In region I, elastic modulus declines as damage begins under the initial loading. In region II, the rates of change of modulus and damage are much less. In region III, damage builds up rapidly to failure and the modulus decreases rapidly as well (Martin *et al.* 1998).

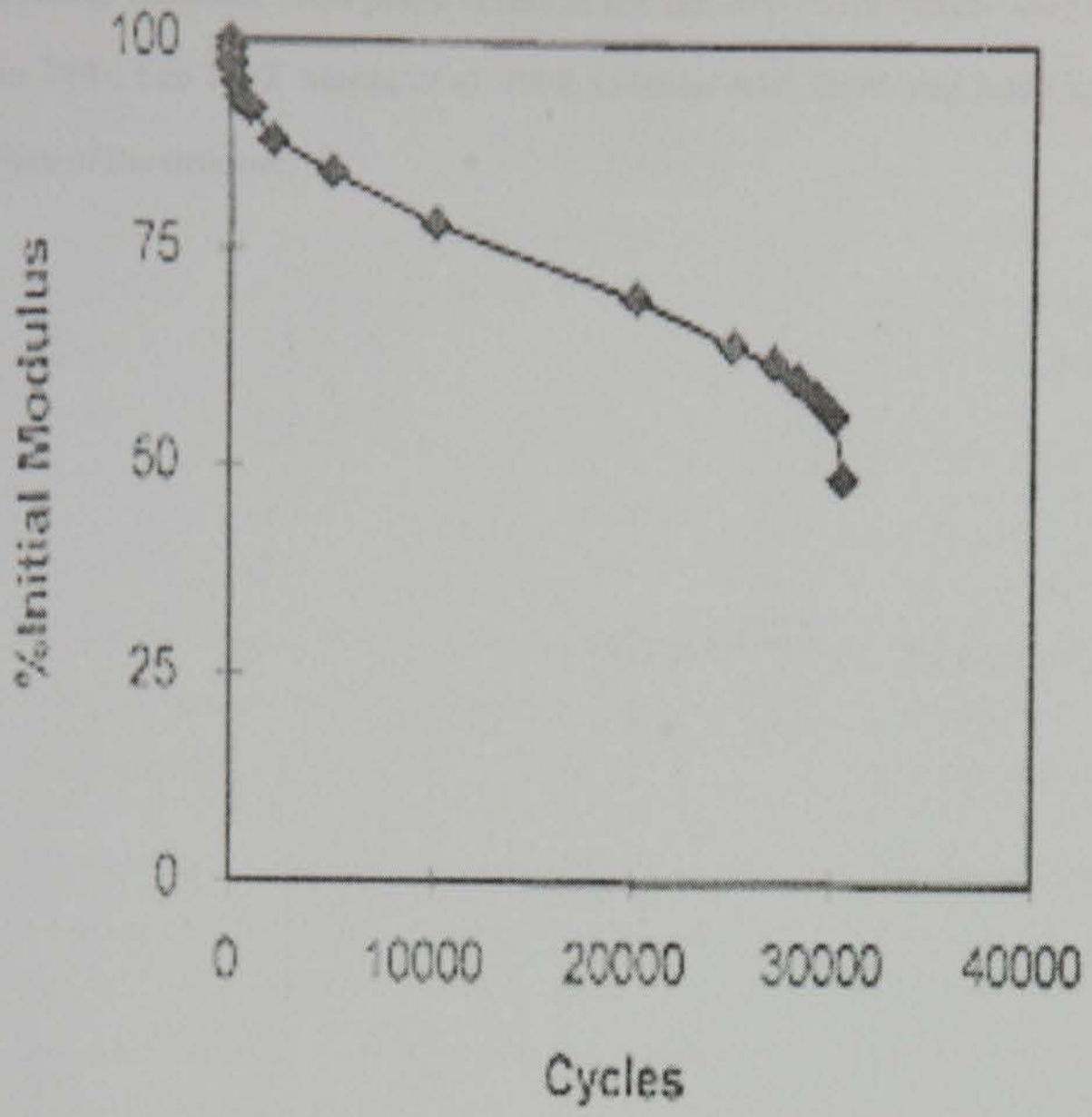

Figure 1.15 phase II was characterised with a continuous and gradual decrease in stiffness (Boyce *et al.* 1998).

Phase III: Failure

It is a relatively short phase during which the stiffness declines rapidly. This is attributed to the coalescence of accumulated damage in the matrix coupled with debonding of lamellar interfaces which allows fibres that align in the direction of the applied stress to break. Because the lamellae begin to break, thus increasing the stress in the elements remaining intact which, subsequently fracture. As a result of an increase in size and to the fusion of the growing microcracks, the loaded material

eventually fractures. This phase occurs at the last 10% of the fatigue life (Turner & Burr 1993, Lee 1997, Martin *et al.* 1998, O'Brien *et al.* 2000) and leads to ultimate failure of the structure.

Table 1.5 Features of the three phase of failure in composite materials.

Phase I	Phase II	Phase III
Associated with a relatively rapid but limited decline in material stiffness. (self limiting)	No significant decrease in the stiffness.	Associated with fast decline in stiffness. It is relatively short. (self feeding)
Rapid initiation of microcracks associated with a limited or no microcrack propagation.	The rate of change in damage accumulation is very limited.	The damage accumulation increases significantly.
Microcrack is usually confined to a single lamella and propagates to the adjacent one where it is stopped.	Microcracks tend to propagate and follow the least resistant path between lamellae (de-bonding).	Further debonding of lamellae takes place.
Occurs at the first 25% of the material fatigue life.		Occurs at the last 10% of the material fatigue life and leads to material failure.

It is important to recognize factors that may play an important role in the generation and growth of microcracks such as the type of load applied on bone. For example, Burr *et al.* (1998) detected more microcracks in tensile cortices, but longer ones in compressive cortices when dog's femurs were tested using a 4-point cyclic bending. Furthermore, different loads and magnitude may influence the nature and character of generated microcracks in dissimilar manners. For instance, microcracks occur due to

compressive loadings and those that occur as a result of tensile loadings are different (Carter & Hayes 1977, Boyce *et al.* 1998). The microcracks that are a result of compression loadings are relatively long, straight and are generally oriented at approximately 30-40° to the long axes of the bone. They start at obvious stress-concentration regions such as Haversian channels.

In Boyce *et al.* (1998) 4-point bending study stresses were applied to introduce fatigue damage to tibial beam specimens. The specimens were bulk-stained with basic fuchsin to mark damaged surfaces and then were examined histologically under conofocal microscopy to describe damage morphologies and position relative to tensile and compressive strains that were generated in response to the bending stresses. Diffuse damage (seen as focal regions of diffusely increased stain) was found in regions of the beam that were subjected to tensile strains. On the other hand, linear microcracks were found in the regions that were subjected to compressive strains (Boyce *et al.* 1998). The latter crack type was principally found in the interstitial bone, running from cement line to cement line and was stopped at the osteonal boundaries (Martin *et al.* 1998).

Burr *et al.* (1998) found that microcracks accumulate more rapidly in tensile than in compressive loads. They found about 25% more damage in tensile than in compressive cortices, but on average the microcracks were significantly shorter in tensile than in compressive.

The above mentioned studies collectively indicate that the microcracks are stopped better in tensile fatigue than in compression (Martin *et al.* 1998). A possible explanation is that in a tensile loaded specimen, the Poisson stress acting across the fibres is compressive and more likely to close the generated cracks than propagate

them. This makes it easier for a cement line to stop them. On the other hand, in specimens loaded in compression, the Poisson stress generated is tensile and tends to open up the crack and make it more difficult for the cement lines to stop the crack (Figure 1.16). This is consistent with the observation that such microcracks travel from Haversian canal to Haversian canal, crossing cement lines (Martin *et al.* 1998).

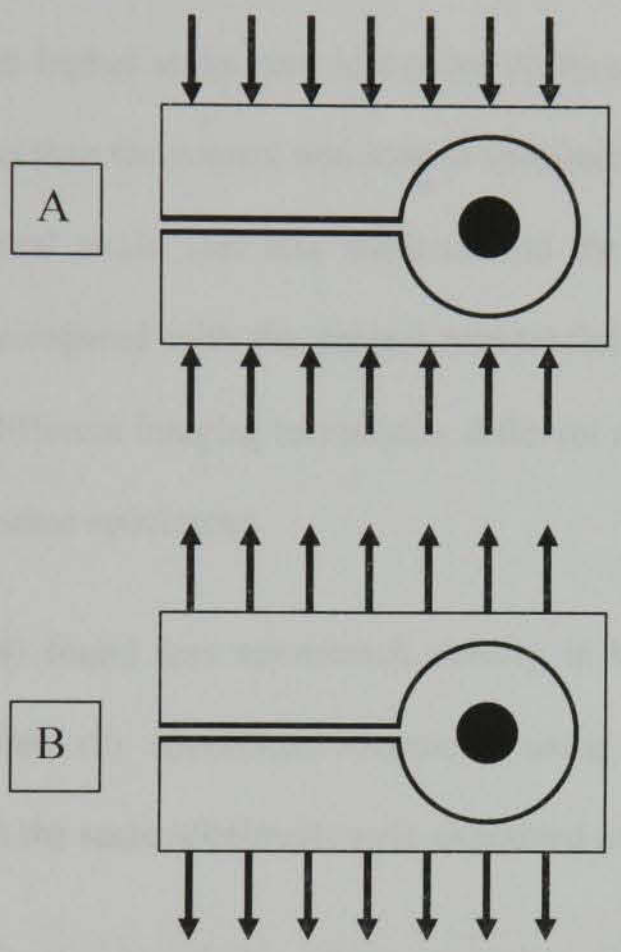

Figure 1.16 Hypothetical bases for differences in crack growth in tensile and compressive fatigue. In tensile loading (A), Poisson stress is compressive, closing cracks and making them more likely to stop at cement lines. In compressive loading (B), Poisson stress is tensile, opening cracks and making them less likely to stop at cement lines. Reproduced from Martin *et al.* (1998).

Because stiffness loss is associated with microcrack initiation rather than microcrack growth, the stiffness loss of tensile cortices should decline more quickly than that of compressive, and have a shorter tensile fatigue life (Burr *et al.* 1998).

Microcrack densities observed in transverse sections were significantly greater than those in longitudinal sections in bovine bone (O'Brien *et al.* 2001, O'Brien *et al.* 2003). Furthermore, the strain to which the bone was exposed has a major role to play in the generation of the microdamage. Schaffler *et al.* (1989) found that specimens loaded at a higher strain rate lost more stiffness and had approximately 50% more microcracks than the control non-loaded specimens. The specimens loaded at a lower experimental strain lost less stiffness and the number of microcracks increased only 35% compared with the control non-loaded specimens. When bone was examined using different imaging techniques, different microcrack density values were reported for the same specimens.

Schaffler *et al.* (1994) found less microcrack density in heavy metal (lead-uranyl acetate) stained human rib specimens examined using back-scattered electron microscopy than when the same specimens were examined using light microscopy.

In contrast to light and scanning electron imaging, back-scattered electron imaging is highly affected by section thickness. Thus only microcracks open onto or very close to the surface were detected (Schaffler *et al.* 1994).

A study has been conducted to investigate compression-induced microdamage accumulation in bovine cancellous bone (Moore & Gibson 2003). These authors did not detect significant test-induced microcracks until the specimens were strained by 0.5% through which the stress-strain was linearly elastic. When the strain on the specimens reached about 0.5% the strain-stress curve becomes non-linear and

microdamage parameters increase rapidly and at a strain of about 1.3% regions of localised damage coalescence and damage bands formed. With increasing strains the curve becomes flat and the damage band widens. After that the damage progresses until the specimens fracture.

Reilly and Currey (1999) studied the relationship between microcrack density and change in mechanical properties of bovine bone using a laser scanning conofocal microscope. The bone was loaded in four-point bending. Microcracks were stained with a fluorescence dye, which was then exited with a laser light. They found that microcracks appeared at the yield point but not in the linear part of the stress-strain curve. Microcracks also developed considerably before a significant decline in modulus (stiffness) could be detected (Reilly & Currey 1999).

Generation of microcracks and their fate in long bone may vary according to the loading mode to which the bone is usually subjected (Martin *et al.* 1996, Reilly & Currey 1999). In an animal study (using horse radius) Reilly and Currey (1999) reported that microcracks that developed as a result of compressive load developed first at the bone that is adapted more commonly to tensile stress and tensile microcracks occur afterwards and at higher strain values. On the contrary, the microcracks that developed by tensile loading generated first at the bone that is adapted to compressive stress, then compressive microcracks occur later and at higher strain values. In Reilly and Currey's study tensile microcracks first occurred at a strain of approximately 0.004, and all specimens showed considerable growth in microcrack density once the tensile strain had passed approximately 0.008. In the bone, which is more often subjected to compressive loading, there are little, small and diffuse microcracks. Furthermore, these bones failed on the tensile side first. In

contrast, cortex that is habitually subjected to tensile loading (adapted to tensile force), compressive microcracks were more numerous, longer and less diffuse, and they failed initially in compression. They concluded that the patterns of failure in bones are what would be expected assuming they were adapted to the mode of loading to which they are usually subjected (Reilly & Currey 1999).

The lamellar structure plays a significant role in determining bone's mechanical properties. For instance, in long bone cortices the regions thought to be habitually subjected to more longitudinal compression *in vivo* were found to have more transversely oriented collagen (Riggs *et al.* 1993, Martin *et al.* 1996). This aspect of bone structure is controlled during bone formation so as to adapt the bone tissue to stress habitually experienced in a particular location (Martin *et al.* 1996).

Reilly and Currey (2000) studied microcracks that were generated when bovine bone specimens were exposed to bending and tensile loading to stiffness losses of up to 27%. Depending on the loading mode, they reported tensile and compressive type of microcracks. The tensile loading generated diffuse microdamage of 2-20μm in length characteristic of tensile loading on all surfaces. The bending load usually exposes the loaded bone to compression as well as to tension. Thus, the bending specimens showed long, straight and cross-hatched compression cracks on the compressive surface and tensile microcracks on the tensile surface (Reilly & Currey 2000). They further divided the specimens that had been damaged in bending into two groups, in one group the part of the specimen that had undergone compression damage was placed in tension, and in the other group the tensile damage was placed in tension. They found that tensile damage loaded in tension did not reduce the bone's energy-absorbing ability in impact until a modulus reduction of over 20%. In contrast,

compression damage loaded significantly lost their energy absorption capabilities when exposed to tensile loading (by an average of about 40%) (Reilly & Currey 2000).

It has been hypothesized that the mechanism leading to cortical bone fatigue-induced microcrack generation and propagation is determined (in a similar way of composite materials) by bone architecture and composition (Burr *et al.* 1988).

Lee *et al.* (2002) reported a mean microcrack length of 49μm with a standard deviation of ±10μm in skeletally mature female sheep. The microcrack length did not differ significantly among the groups of ulnar osteotomy, groups with Steinman pins and control groups in which ulna was exposed and the periosteum disrupted in a sham operation procedure (Lee *et al.* 2002).

1.14 Microcracks and bone remodelling

Microcracks have been reported to be associated with remodelling (resorption) sites and they may act as a bone remodelling stimulator (Burr *et al.* 1985, Mori & Burr 1993, Lee 1997, Burr *et al.* 1997, Bentolila *et al.* 1998, Lee *et al.* 2002, O'Brien *et al.* 2003, O'Brien *et al.* 2005a, O'Brien *et al.* 2005b) that leads to the repair of the microdamage and prevents its accumulation (Carter & Hayes 1977, Burr *et al.* 1985, Frost 1991, Mori & Burr 1993, Frost 1994, Hoshaw *et al.* 1994a, Bentolila *et al.* 1998, Verborgt *et al.* 2000).

Bentolila *et al.* (1998) presented evidence that microcracks cause the activation of remodelling. They used ulnae of rats, which do not usually remodel to study generation of micro-damage in bone. Right ulnae were fatigue-loaded to a pre-failure

stopping point of 30% decrease stiffness. Ten days later left ulnae were loaded in a similar manner as the left ones. Both the right and the left ulnae were harvested immediately to compare the immediate response of the right ulnae and the biological response of the right ulnae to the loads. Basic fuschin-stained specimens were examined histo-morpho-metrically and under conofocal microscopy. They observed linear microcracks as well as diffuse stained patches in the fatigue loaded ulnae. Microcrack density was reduced to almost 40% by the 10 days post-loading period. Intra-cortical resorption was found to occur in preferential association with linear microcracks but not with diffuse damage (Bentolila *et al.* 1998).

Lee and coworkers (2002) reported in sheep that when the ulna was removed in order to overload the radius, microcracks and bone remodelling were observed in the radius bone.

In order to repair the damage and to avoid a stress fracture, the initiation of the remodelling should occur within a few days after the damage generation (Burr *et al.* 1985). Moreover, as microcracks occur, resorption progresses in a fast manner and more intensely around microcracks. Ultimately this will decrease the stress intensity, and therefore the risk of crack propagation will be limited. Damaged bone, therefore, appears to be more likely to be resorbed and secondary osteons to be formed (Silva & Ulm 2002). It has been demonstrated in dogs that 44 times as many as microcracks were associated with resorption spaces in a greater rate than would be expected by chance alone (Burr *et al.* 1985).

Verborgt *et al.* (2000) found that in the ulnae of rats subjected to fatigue loading in vivo, that in bone immediately surrounding microcracks, a large number of TUNEL-positive osteocytes were found (almost 400% over control levels ($p< 0.005$) and in

bone surrounding intracortical resorption spaces (about 300% increases over controls, $p< 0.005$). On the other hand, in bone regions of fatigue-loaded ulnae distant from microcracks, the number of TUNEL-positive osteocytes was similar to that in nonloaded control bones (15 and 13% of total cells, respectively). The study indicates that the strong association between osteocyte apoptosis and bone microdamage (Verborgt *et al.* 2000).

However, the association between microcracks and resorption sites is not a "one-to-one" process, which may be attributed to the ability of microcracks to induce more than one resorption site and/ or to the inability of bone damage marker; such as basic fuchsin, to stain all generated microcracks. It is also reasonable to speculate that some of resorption sites may be a result of other stimuli, such as hormonal and metabolic changes (Mori & Burr 1993, Lee *et al.* 2002). Furthermore, the orientation of bone sections to the course of microcracks may be a contributory factor (Lee *et al.* 2002).

Martin and Burr (1989) put forward a theory that explained the relationship between the generation of bone damage and its removal by the remodelling process. It is assumed that the microdamage stimulates bone remodelling to repair this damage by BMUs that are activated in a proportional rate to the amount of damage in the tissue. However, since the initial stage of any remodelling is resorption which creates more pores in the affected bone, the increased porosity decreases the elastic modulus and subsequently increases strains within the local tissue. Consequently, the damage formation rate increases although the remodelling is removing the damage at a faster rate.

Bone remodelling is a coupled process in which resorption occurs and followed by bone formation. Thus, it is logical to suggest that if targeted bone remodelling is suppressed or inhibited microdamage will accumulate over time in normally loaded bone (Martin 2002, Martin 2003). A series of animal studies were conducted by Mashiba and colleagues (Mashiba *et al.* 2000, 2001a and 2001b) to investigate the effects of bisphosphonates on bone remodelling activity and its consequential effect on bone mechanical properties and microdamage accumulation. Bisphosphonates are compounds that act as osteoclastic inhibitors. The first study (Mashiba *et al.* 2000) investigated the effects of suppressed bone remodelling that was produced by bisphosphonates on microdamage accumulation in rib cortex of beagle dogs. The dogs were divided into three groups. One group served as a control and was treated daily for 12 months with saline vehicle. The other two groups were treated daily with risedronate at a dose of 0.5 mg/kg per day or alendronate at 1.0 mg/kg per day orally. These doses were six times the clinical doses recommended for treatment of osteoporosis in humans. Both compounds are oral forms of bisphosphonate used in the treatment of osteoporosis and to prevent bone loss in patients at risk of developing osteoporosis (Melo & Obeid 2005). After one year, risedronate or alendronate were found to significantly suppress intracortical remodelling to 53% and 68% respectively. Microdamage accumulation was also found to increase significantly in risedronate (155%) and alendronate (322%) compared to the control group. This suppression of bone remodelling was also found to be associated with reduction in bone toughness.

A similar effect of bisphosphanate on bone was also reported in the second study (Mashiba *et al.* 2001a) in the same animal model using the same treatment dose for the same treatment period (Mashiba *et al.* 2001a). They observed a suppression of

tarbecular remodelling in vertebra (ranged 90-95%) and ileum (76-90%) without impairment of mineralisation. The authors also observed a significant increase in microdamage accumulation in all the sites studied for the presence of microdamage (Mashiba *et al.* 2001a).

In the third study Mashiba *et al.* (2001b) used low- and high-dose etidonate to study microdamage accumulation and mechanical properties in beagle bone. They found that both doses led to suppression of bone remodelling and production of microdamage. However, the high dosage treatment was associated with accumulation of osteoid (unmineralised matrix) caused by mineralisation deficit which reduced production of microdamage (Mashiba *et al.* 2001b).

Bisphosphonates are potent inhibitors of osteoclast-mediated bone resorption and are a group of synthetic analogues of inorganic pyrophosphate which is produced by the body (Flint *et al.* 2006). They are classified into two types: nitrogen–containing and non-nitrogen-containing bisphosphonates. The former ones are more potent and are not metabolised (Marx 2003). It was reported that bisphosphonates have a strong affinity to bone minerals around active osteoclasts (Marx 2003, Flint *et al.* 2006). They have a very long half life of up 10 years (Flint *et al.* 2006). For instances, alendronate binds to bone and its elimination from bone tissue is ranging from 200 days in rats, 3 years in dogs and 12 years in humans (Lin *et al.* 1999).

Bisphosphonates are widely used for the management of bone disorders, osteoporosis, hypercalcemia associated with malignancy, multiple myeloma and Paget's disease (Ficarra *et al.* 2005). They have suppression effects on the osteoclast activities and imbalance the osteoclasts/osteoblast axis (Hellstein & Marek 2005). However, their precise effect and mechanism of action are not completely understood.

The use of bisphosphonates was found to be associated with a recently recognised pathologic condition more likely to affect the jaws and known as osteonecrosis (ONJ) or osteochemonecrosis of the jaw. It is characterised by painful exposed alveolar bone in the mandible and less frequently in the maxilla with intra- or extra-oral drainage and does not respond to conventional treatment (Flint *et al.* 2006). However, ONJ has been reported in patients with cancer taking not only bisphosphonates but also other treatments such as chemotherapy, steroids and/or had previous radiotherapy (Hellstein & Marek 2005).

ONJ has been reported to occur after a minor surgical procedure such as tooth extraction and even spontaneously without trauma or surgery (Marx 2003, Assael 2004, Ficarra *et al.* 2005, Flint *et al.* 2006).

The condition was first reported to be associated with intravenous forms of bisphosphonate i.e. Pamidronate and Zoledronate (Ruggeiro & Mehrotra 2004, Ruggeiro *et al.* 2004) however; it was also found in patients on the oral bisphosphonate (Flint *et al.* 2006).

The presence of teeth and periodontal ligaments in the alveolus and the chronic low grade trauma associated with mastication render the jaws very active areas of turnover. Bisphosphonates were reported to accumulate in areas of high bone turnover such as jaws. This may give an explanation to why this bone necrosis was solely reported in the jaws (Flint *et al.* 2006).

The association between bisphosphonate treatment and the occurrence of ONJ raises the question of safety with placement of denntal implants into jaws of patients who are on bisphsphonate treatments or who are at risk of developing bone disorder and

will need further treatment with bisphosphonates. A definitive answer was not found in the literature. Stark and Epker (1995) reported failure of osseointegrated implants approximately six months after treatment with bisphosphonate (Etidronate) was commenced. However, the failed implants might have been overloaded as the patient had developed a parafunctional clenching habit in order to retain her upper conventional complete denture. The authors recommended that dental implants should not be placed in patients on bisphosphonate therapy and bisphosphonate should not be prescribed for patients with dental implants (Stark & Epker 1995).

Microdamage has been reported to generate as a result of implant placement and around osseointegrated implants. Bone remodelling is induced in order to replace and repair such damage (targeted remodelling). If the major therapeutic action of bisphosphonate is to inhibit osteoclast-mediated bone resorption (Russell *et al.* 1999) which is one of the main steps of bone remodelling, then it is logical to suggest that the damage will accumulate leading eventually to implant failure.

1.15 Microcracks and endosseous implants

Bone activity subsequent to implant placement requires both bone modelling and bone remodelling. After implant placement the remodelling activity adjacent to the implant (within 1 mm) is greatest and substantially decreased with increasing distance from the implant-bone interface. This phenomenon seems to occur irrespective of implant design (Hoshaw *et al.* 1994b, Huja *et al.* 1999a). This elevation in remodelling activity has been attributed to several factors including the local biomechanical environment, material biocompatibility and host response (Garetto *et al.* 1995). The local biomechanical environment of the bone-implant interface may

require continuous remodelling to avoid fatigue damage. Remodelling activities have been observed even after two years of implant placement in dog mandibles (Steflik *et al.* 1995, Steflik *et al.* 1996) and after five years in humans (Garetto *et al.* 1995). A three to four fold increase in the bone remodelling rate in the area the adjacent areas (<1mm) compared to distant areas (1-3mm) has been observed for the rabbit, dog and monkeys increasing to about 9 fold in humans (Garetto *et al.* 1995).

Although based on assumption, results from a finite elements model assessing the bone-implant environment indicate that the region within 1 mm of the implant surface displays a persistent change in mechanical stress distribution resulting in both elevated stress levels and stress changes (gradients) (Chen *et al.* 1995). This pattern of stress distribution may occur as a result of bone flexure. When an occlusal force was applied to the cantilever part of a superstructure, a stress was found to be generated in the bone surrounding the implant. The location and magnitude of such stresses were reported to be influenced by complex factors such as the thickness of the surrounding bone and the relationship between adjacent implants (Nagasato *et al.* 2002). Transmission of occlusal forces from the implant is affected by the percentage of osseointegration. The 3-dimensional finite element method indicated that there is an inverse relationship between the percentage of osseointegration and the stresses in the implant bone interface (Lai *et al.* 1998).

Microcracks have in recent publications been shown to occur in bone surrounding implant after implant placement and decreased in a 4-week healing period because of bone remodelling (Hoshaw *et al.* 1994a, Hoshaw *et al.* 1994b, Hoshaw *et al.* 1995). Hoshaw *et al.* (1995) studied the effect of Brånemark implant placement and design on generation of microcracks in rabbit bone. They measured the area fraction of

microcracks, as detected by basic fuchsin staining, immediately after implant placement and at a 4-week healing period. They studied the microcrack generation in a 1.2 mm-wide region of the interface adjacent to the implant. They found that the mean area fraction of microcracks detected at the 4-week healing period was significantly ($p< 0.03$) lower than that detected at the base line time. The values were 9.5%± 2 and 12.5%± 2 respectively. This report is in agreement with other works which suggested that microdamage in bone stimulates bone remodelling (Frost 1991, Mori & Burr 1993, Cohen *et al.* 2003).

In one study, Huja *et al.* (1999a) found that non-adapted bone (bone that was loaded immediately after implant placement) near the implant accumulated significantly more micro-damage than adapted bone (loaded 12 weeks after implant placement). The non-adapted non-loaded specimens demonstrated approximately 20-fold more damage than the respective adapted specimens (crack density ≈ 10 crack/mm^2 versus ≈ 0.5 crack/mm^2). These findings indicated the susceptibility of pre-implant bone to generation of microcracks as a result of the implant placement procedure. It may also indicate the resilient nature of the newly formed bone at the pre-implant area (Huja *et al.* 1999a).

Trisi and Rebaudi (2002) reported existence of microcracks in bone around oral implants that were previously orthodontically loaded in humans. It was found that the remodelling rate was elevated even after 18 months (Trisi & Rebaudi 2002).

Cohen and co-workers (2003) reported the generation of diffuse damages as well as linear microcracks due to insertion of external skeletal fixation pins into sheep tibia *in vitro*. The authors suggested that these types of microdamage may be the principal factor which may regulate bone reparative remodelling in the early period after

surgery (Cohen *et al.* 2003). This study also shed light on the possible deleterious effects of excessive microdamage generation on the healing process around the fixation pins. It also indicated that different external pins induced quite different patterns of microdamage (Cohen *et al.* 2003).

The studies cited above may indicate a positive role of the microcracks in achieving a rigid implant-bone interface. However, little direct data are available on the microcracks around endosseous implants. Further investigations are required to explain the role of microcracks in remodelling of peri-implant bone.

A progressive marginal bone loss around endosseous implants was observed and this loss may be due to several factors including infection and implant overloading (Isidor 1996, Isidor 1997, O'Mahony *et al.* 2001).

Adell *et al.* (1981) speculated that marginal bone loss which occurred months or even years after uneventful osseointegration could be attributed to inadvertent stress or unfavourable stress distribution from a number of factors such as trauma from occlusion and defective bridge retained design which resulted in overloading with microfractures of the peri-implant bone leading to implant failure.

However, implant surgery and its consequence such as elevation of the flap, heat generation, and excessive pressure on the marginal bone during the surgery, may all contribute to the observed early marginal bone loss (Adell *et al.* 1981, Oh *et al.* 2002).

Surgical trauma and bone damage during implant placement may also lead to implant failure (Adell *et al.* 1981).

Controlling of the heat generated during implant surgery is important in order to achieve uneventful healing and to avoid impairment of bone regeneration (Tehemar

1999). Eriksson and Albrektsson (1984) investigated the effect of increased temperature on the regenerative capacity of bone in implants placed in long bone of rabbit. They reported that heating the test implants to 47°C or 50°C for one minute led to a significant reduction in bone formation around the implants. In the mean time no such effects could be perceived when the temperature reached 44°C for the same duration (Eriksson & Albrektsson 1984). In this experimental study the temperature was measured in the bone located 0.5 mm from the osteotomy wall.

Drilling during osteotomy site preparation causes mechanical damages due to compression and vibration as well as heat induced bone injury due to overheating (Eriksson & Albrektsson 1983, Eriksson & Albrektsson 1984). Overheating of alveolar bone during osteotomy site preparation may result in a formation of soft tissue between the implant and the surrounding bone, which ultimately may lead to implant failure (Eriksson & Albrektsson 1984).

When bone temperature was measured during osteotomy preparation in bovine bone, drill temperature was found to rise beyond that of the surrounding bone. In the meantime, irrigation greatly reduced drill temperature and bone density was reported to play a greater role in temperature elevation than did osteotomy depth. When the osteotomies were enlarged from 2 to 3 mm the generated heat was found to be as much as the 2-mm-wide osteotomy (Yacker & Klein 1996).

Bone heating may also be generated by excessive pressure on bone during the surgery and pressure applied was found to have more effect on heat generation than the speed of the drill (Matthews & Hirsch 1972). However, when the applied force and the speed of the drill were both increased, elevation in temperature was minimal while the

rate of cutting was maximised (Brisman 1996). Thus, heat control during the surgery is needed in order to achieve osseointegration and to avoid implant failure.

Bone necrosis was reported to occur at the peri-implant bone as a result of surgery (Eriksson & Albrektsson 1984, Clokie & Warshawsky 1995, Berglundh *et al.* 2003, Abrahamsson *et al.* 2004). Fractured spongiosal trabeculae have been observed histologically in peri-implant bone when the osteotome technique was applied and not the standard technique. These fractures were found one week after surgery but not after four weeks (Büchter *et al.* 2005).

Failure of oral implants as a result of occlusal overloading may be caused by microdamage generation in the bone which exceeds the repair potential of this bone, leading to the replacement of bone-implant interface with soft tissue (Adell *et al.* 1981, Isidor 1996, Isidor 1997). It has been experimentally demonstrated in monkeys that excessive dynamic occlusal force on endosseous oral implants can result in complete or partial loss of osseointegration with a narrow zone of soft tissue between the implant and the bone with bone crest located near the implant margin without significant crestal bone loss and implants failed without preceding marginal bone loss (Isidor 1996, Isidor 1997).

Using finite element (FE), Tada and colleagues (2003) reported a significantly increased stress generated just above the bone crest irrespective of the implant design and at the root of the first thread (placed just below cortical bone level in the model) in the screw-type implant (Tada *et al.* 2003).

Other FE reports indicated that an increase in implant length and diameter were found to result in a reduction in crestal bone strain while an increase in the degree of taper increased the strain (Pertie & Williams 2005). High density cancellous bone showed

lower crestal bone strain when compared with low density bone (Tada *et al.* 2003, Pertie & Williams 2005).

Using three-dimensional finite element models of a mandibular first molar and a titanium implant Ishigaki *et al.* (2003) studied biomechanical stress distribution in supporting bone around them under simulated chewing. The tooth model showed smooth stress distribution in the surrounding bone with low stress concentration around the neck of the tooth. However, the implant model showed stress concentration in the surrounding bone around the implant neck, especially the buccal area. (Ishigaki *et al.* 2003). This may attribute bone loss to bone strain beyond the effective strain (Frost 1994).

Load transfer at the bone-implant interface depends on several factors including 1) type of loading; 2) material properties of the implant and prosthesis; 3) implant geometry, length and diameter; 4) implant surface characteristics; 5) nature of bone implant-interface and 6) quality and quantity of the surrounding bone (Geng *et al.* 2001).

Holmgren and coworkers (1998) used an FE parasaggital model that was digitised from computed topography (CT)-generated patient data with various single-tooth two-dimensional dental implant models to examine the effect of implant diameter variation of both a press-fit, stepped cylindrical implant type and a press-fit, straight cylindrical implant type as osseointegrated in the posterior mandible and to compare the stress-dissipating characteristics of the two implant designs. The results suggested that stress is more evenly dissipated throughout the stepped cylindrical implant when compared to the straight implant type and using the widest diameter implant is not necessarily the best choice when considering stress distribution to surrounding bone.

When FEA is used in dental implants it is important to consider axial forces (vertical loading) and horizontal forces (moment-causing loads), as well as combined loads (oblique occlusal forces), because the latter forces represent the more realistic occlusal forces that are encountered in real clinical situations. It is also because the oblique occlusal force may cause the highest localized stress in cortical bone (Holmgren *et al.*1998). The authors concluded "whenever possible, an optimum, not necessarily larger, dental implant should be used based on the specific morphological limitations of the mandible and that a stepped cylindrical design for press-fit situations is most desirable from the standpoint of stress distribution to surrounding bone".

The validity of FE models is difficult to estimate objectively, however, it may be assessed experimentally by relating the obtained results with other comparable FE models results and with *in vivo* observations. In this regard, a strong correlation between the stress distributions in the peri-implant bone as obtained throughout FEA and the remodelling phenomena in the comparative animal model was observed (Barbier *et al.* 1998).

1.16 Modelling, remodelling and bone strain

There is a general agreement on the existence of a relationship between the bone modelling and remodelling processes and mechanical usage of bone, as reflected in bone strain or deformation. *In vivo* and *in vitro* studies indicate that mechanical stimuli play a major role in bone functional adaptation. Consequently, this relationship governs the shape, architecture and mass of the bone (Lanyon *et al.* 1982). When bone is subjected to an external force, it becomes strained (deformed

from its original shape and size). In order to balance this force, an internal stress will be generated. The generated internal stress is equal to but in an opposite direction to the external forces (Kiuru 2002). Frost (1987) proposed a theory that describes the dynamic relationship between bone loading and its biologic response to that load. It explains the interrelationship between the modelling and remodelling. This theory has been known as the mechanostat and proposed that modelling and remodelling would be initiated at some critical level in order to maintain bone minimum effective strain. The minimum effective strain is defined as the level of strain necessary to maintain bone mass (Lanyon 1987). The mechanostat theory suggests that bone has 4 microstrain zones that are related to the bone mechanical adaptation strain. Accordingly, bone mass is highly affected by the use of the skeleton (Frost 1987, Frost 1994, Stanford & Brand 1999, Wiskott & Belser 1999, Misch *et al.* 2001, Mellal *et al.* 2004). These microstrain zones include disuse zone (bone loss or resorption), adapted zone (lazy zone, normal load, the steady state or homeostasis), mild overload zone (bone gain), and pathologic overload zone (irreversible bone damage). For instance, in a case of acute disuse such as micro-gravity and immobilisation (due to lack of physical exercise) and alveolar bone resorption after tooth loss, when strains within a bone remain below the minimum effective level (Frost 1987, Misch *et al.* 2001) a loss of bone mass occurs as a result of its resorption and an increase in its porosity. On the other hand, when strain exceeds its minimum effectiveness remodelling returns back to normal level. The disuse atrophy has been suggested to occur when peak strains drop below 50με [microstrain] (Frost 1987, Frost 1994, Stanford & Brand 1999).

According to Rubin and coworkers (2001) low magnitude, high frequency stimuli may be enough to maintain bone mass. This could be useful in the treatment of metabolic disease.

The adapted zone (steady state) occurs when the load was within the adaptive capacity of the loaded bone that is in the range of 50 to 1500 με (Frost 1994). In this situation the remodelling activity tends to stay within its normal range and no modelling would occur. During this zone bone strength and mass will be preserved. The adapted window is more likely to induce formation of organized and highly mineralised lamellar bone (Frost 1987, Frost 1994, Misch *et al.* 2001). It has been suggested that the adapted window would be the ideal strain condition next to the dental implant in order to achieve a long-term osseointegration (Misch *et al.* 2001).

The mild overload (physiological overload) creates strain that ranges from 1500 to 3000με and leads to new bone formation (modelling) and bone mass tends to increase. The remodelling tends to stay near its normal value. The new bone formation continues until the generated strain within the affected bone returns to its normal value i.e. minimum effective strain.

The pathological overload zone i.e. when the strain is above 3000με, could lead to generation of microdamage, which is consequently targeted and replaced by remodelling. It could lead to a net bone resorption (Stanford & Brand 1999).

Thus, both the pathological overload and the acute disuse window will result in a net bone loss. While the mild overload zone induces a higher remodelling rate than the adapted window, it also leads to the formation of more woven bone (Frost 1987, Misch *et al.* 2001). It has been reported when a part of ulna in a mature sheep was

removed causing an increase in the principal strain in the radius that long bone subjected to increased mechanical strain will develop woven bone as a result of the adaptive response in order to offset the increase in the strain (Lanyon *et al.* 1982). However, strain magnitude, distribution and rate as well as non-mechanical influences should be considered to understand the nature of adaptive bone remodelling (Lanyon 1987).

Nevertheless, it should be mentioned that there is no general agreement about borders of each zone and where each one ends the next one starts.

When the mechanostat theory was applied to bone surrounding the oral implant, Misch and associates (2001) suggested that when strain conditions to the interfacial bone are in the mild overload zone, an increased bone remodelling response occurs, which leads to formation of woven bone that is less organised, less mineralised and weaker. The presence of woven bone at the interfacial area increases the biomechanical mismatch between the stiffness of the titanium and bone and consequently increases the magnitude of strain between the bone and the implant (Misch *et al.* 1999). When the interfacial strain reaches the pathologic overload zone it may cause microfracture of the bone, resorption and/or fibrous tissue formation (Misch *et al.* 2001). Therefore, the endosseous implants should be designed so that normal and shear strain on the implant-bone interface are kept below the pathologic or mild overload zones in order to reduce the risk of woven bone formation or bone loss (Misch *et al.* 2001). However, according to Morris and coworkers (2004) if occlusal stress is directed toward the cancellous bone, a long term osseointegration could be achieved because when damaged it repairs much faster than the cortical bone due to its great regenerative capacity (Morris *et al.* 2004).

The relationship between the remodelling and mechanical circumstances is probably controlled by a "feedback" mechanism (Lanyon *et al.* 1982, Mosley 2000). This "feedback" mechanism adjusts the bone strain level and maintains it at a predetermined and probably optimum level (Lanyon *et al.* 1982). Therefore, the aim of skeletal design is not the production of minimal strain levels, but to maintain an optimum level (Lanyon *et al.* 1982, Mosley 2000, Sommerfeldt 2001). Furthermore, Laynon *et al.* (1982) stated that "the adaptive remodelling is influenced by the distribution of strain rather than the peak strain phase customarily achieved".

1.17 Bone labelling

In 1736, John Belchier observed red streaks in bones of pigs that had been fed madder, a dye obtained from Eurasian herb *Rubia tinctrom*. Meanwhile, in the 1770s, using madder-fed pigs John Hunter reported that bone is subject to endosteal resorption and peroisteal deposition (Martin *et al.* 1998). However, in the 1800s, synthetic alizarin was used and found to be as effective as natural dyes in preferentially labelling actively mineralising bone sites. These dyes are chelating agents, which bind to calcium ions. Milch *et al.* (1958) found that tetracycline was incorporated into actively mineralising bone and fluoresced yellow when histologic sections were observed in ultraviolet light (Martin *et al.* 1998). Once tetracycline is combined with calcium in bone it remains until the marked bone is renewed by remodelling (Milch *et al.* 1957, Milch *et al.* 1958, Aaron *et al.* 1984) and tetracycline is reincorporated in the mineralising bone (Stewart 1973).

In addition to alizarin and tetracycline compounds, other compounds such as xylenol orange, calcein blue and calcein green are also used *in vivo* (Sun *et al.* 1992,

Marcaccini *et al.* 2003). These bone labels are *fluorochromes* (also called fluorophores) which are excited by irradiating light and eventually emit light of a greater intensity. They fluoresce under ultra-violet (UV) giving different colours that can be detected using UV epifluorescence microscopy (Harris 1960, O'Brien *et al.* 2000 Lee *et al.* 2003, Marcaccini *et al.* 2003).

Fluorescence is defined as the property of certain materials by which short wavelengths of light are converted into radiation of longer visible wavelengths (Marcaccin *et al.* 2003). Fluorescence may be primary or secondary. Primary fluorescence (also known as autofluorescence) is described as the ability of a substance to fluoresce when irradiated with light of shorter wavelength (Rost 1992, Rost 1995). It is a material with a self-fluorescence capacity (Rost 1992, Rost 1995). Secondary fluorescence (also called induced fluorescence) is produced by adding fluorescent substances to non-fluorescent ones in order to make the latter substances fluoresce (Rost 1992, Rost 1995).

Tissues may be stained with fluorescent agents (fluorochromes) in a process known as fluorochromy, e.g. incorporation of tetracycline in bone surface which can then be seen glowing under UV light (Stewart 1973, Rahn 1977, Aaron *et al.* 1984, Rost 1992 and 1995, O'Brien *et al.* 2000, O'Brien *et al.* 2001, O'Reilly 2002, Lee *et al.* 2003, Mohsin *et al.* 2006). Fluorochromes work by absorbing energy in the form of light that is emitted as a result of movement of electrons between the energy shells.

In general, movement of electrons from one energy level to another is associated with either gain or loss of energy. If an electron moves from a low level shell (ground state) around the nucleus to a higher one (excitation state) it gains energy, however when it returns back to its original shell it loses the acquired energy (Rost 1992,

O'Reilly 2002). When energy in the form of light is supplied to an atom the electrons absorb a certain amount of energy. This moves electrons into a higher energy level away from the nucleus. The electrons remain in the higher energy levels (the excitation state) and then return back to more stable, lower energy shells (the ground state). When this occurs a definite amount of energy is dissipated as both heat and light (Rost 1992, Rost 1995, O'Brien *et al.* 2000, O'Reilly 2002). Bone remodelling, microcracks in bone (O'Brien *et al.* 2000, Lee *et al.* 2002, Lee *et al.* 2003), bone formation around endosseous implants (Gotfredsen *et al.* 2001) as well as the effect of loading on bone surrounding the implants (Lubberts & Turley 1982, Ogiso *et al.* 1991) have been studied using fluorochromes and fluorescence microscope.

Fluorescence microscopy preferentially permits the excitation light of a short wavelength e.g. UV light, to illuminate the specimen which absorbs part of the excitation light and re-emits it as a fluorescence. The re-emitted light has a longer wavelength than that of the excitation one (Rost 1992). The resulting fluorescing area of the specimen glows against a dim background with sufficient contrast in order to facilitate detection. The higher the intensity of the non-fluorescing material background, the more apparent the image of the fluorescing material. Barrier filters are applied to improve fluorescence and permit polychrome analysis of a single image (Martin *et al.* 1998). In epi-fluorescence microscopes UV light is used. The filtered UV light irradiates the specimen, which emites fluorescent light of longer wavelengths. Visible light emitted from the specimen is then filtered through a barrier filter that does not allow the passing of reflected UV light. The barrier filter is required to be entirely transparent at the re-emitted light wavelength and entirely opaque at the excitation light wavelength (Rost 1992).

Several fluorchromes were used as bone markers to study the rate of bone formation (Módis *et al.* 1969, Treharne & Brighton 1979, Barbier & Schepers 1997), bone remodelling activity, percentage of new bone formation for diagnosis or research purposes and to study the healing process around endosseous implants (Lubberts & Turley 1982, Ogiso *et al.* 1991, Barbier & Schepers 1997, Gotfredsen *et al.* 2001, Nkenke *et al.* 2002, Marcaccini *et al.* 2003). They were also used to investigate microcrack initiations *in vivo* (Stover *et al.* 1993) and their growth in bone (Lee 1997, O'Brien *et al.* 2000, O'Reilly 2002, Lee *et al.* 2003).

1.18 Detection of microcracks and Bone remodelling

To detect microcracks in bone reflected light photomicrography was used. Carter and Hayes (1977) showed the difference in damage pattern on tensile and compressive surfaces. Bulk stain technique and light microscope were used to study microcracks by Frost (1960), Burr *et al.* (1985) and Schaffler *et al.* (1994).

Zioupos and Currey (1994) studied the extent of microcracking and the morphology of test induced microcracks using laser scanning conofocal microscopy. Boyce *et al.* (1998) used laser scanning confocal microscopy to study damage in human tibiae and Fazzalari *et al.* (1998) studied microcracks in tabicular bone. Reilly and Currey (1999) used a laser scanning conofocal microscope to investigate the relationship between microcrack density and change in mechanical properties of bovine bone. Zioupos (1994) used acoustic emission tests and laser scanning conofocal microscopy to study the micromechanics of failure in bone and antler.

Schaffler *et al.* (1994) used both light microscopy and back-scattered electron microscopy to examine compact bone microcracks in sequential sections of human ribs than when the same specimens were examined under a light microscope.

However, transmitted light microscopy is the most common method applied to detect microcracks. This can be completed on stained and unstained bone (O'Reilly 2002).

Epifluorescent microscopy with chelating agents have been used extensively in order to study generation and growth of microcracks (Lee 1997, O'Brien *et al.* 2000, O'Reilly 2002, Lee *et al.* 2003, O'Brien *et al.* 2005a, O'Brien *et al.* 2005b, Mohsin *et al.* 2006).

It has been reported that chelating agents such as tetracycline deposit and bind to calcium ions of mineralising tissues and fluoresce under UV light (Suzuk & Mathews 1966, Módis *et al.* 1969, Lee 1997, O'Brien *et al.* 2000, O'Reilly 2002, Lee *et al.* 2003). Chelating agents work by sequestering ca^{2+} and binding it into a ring (Lee 1997). Calcium ions are also exposed at resorption cavities, Haversian canals and blood vessels. (O'Reilly 2002). Thus, these sites will fluoresce and may complicate the detection of miroccracks (Figure 1.18).

Tetracycline compounds are a well-known group of antibiotics with a common basic structure and activity. Chlorotetracycline was available since 1948. Oxytetracycline was introduced in 1950. They are derived from *Streptomyces* bacteria. Tetracyclines are used as bone labelling agents due to their ability to strongly bind calcium ions (chelation) and to their fluorescent properties (Lee 1997, O'Brien *et al.* 2000, Lee *et al.* 2003). They fluoresce bright yellow in ultra-violet light wavelength of 360 nm.

Tetracycline compounds bind to newly formed bone at the bone–osteoid interface but do not bind to inactive bone surfaces and osteoid tissue (Aaron *et al.* 1984) thus bone-

remodelling activity becomes possible to study (Suzuki & Mathews 1966, Módis *et al.* 1969, Sun & Mosekilde 1978, Sun *et al.* 1992, Aaron *et al.* 1984, Trisi & Rebaudi 2002). They can be used *in vivo* as well as *in vitro* (Aaron *et al.* 1984, Lee *et al.* 2002).

In the actively mineralising bone, incorporated tetracycline or other fluorochromes is seen as linear fluorescence bands. If more than one fluorochrome is given intermittently (separated by a certain numbers of days) a series of fluorescent bands are observed. The distances between these bands can be used to estimate the net amount of bone formed during that period (Olerud & Lorenz 1970, Fallon 1982, Suzuki & Mathews 1966, Módis *et al.* 1969, Lee *et al.* 2002, Lee *et al.* 2003). However, when one fluorochrome such as tetracycline is used two or more times in the same animal, correct interpretation is difficult (Olerud & Lorenz 1970).

Several tetracycline compounds may be used to study the kinetic nature of bone. These compounds include: oxytetracycline hydrochloride, demeclocycline hydrochloride and rolitetracycline. However, tetracycline compounds have the potential to demonstrate comparable fluorescence characteristics ranging from yellow to green (Lee *et al.* 2003). Thus, differentiation between the bands becomes difficult and tetracycline compound such as chloretetracycline may interfere with bone mineralization (Harris 1960) and certain types of tetracycline such as demethychloretetracycline are tissue irritants and are unsuitable for long term investigations (Stewart 1973). When tetracycline hydrochloride was used after calcein a significant underestimation of mineralising surface in rats was reported (Sun *et al.* 1992). Módis *et al.* (1969) found that prolonged use (five weeks) of tetracycline inhibited calcification of bone in dogs.

The use of tetracycline as a bone labelling agent has several limitations (Treharne & Brighton 1979):

1 Tetracycline compounds may interfere with the rate of bone formation. High doses of tetracycline partially inhibited bone mineralisation in dogs (Harris 1960).

2 Tetracycline can be leached out during specimen preparation, storage or as a result of bone resorption

3 Multiple tetracycline doses are required in order to maintain a high serum level and also to avoid fluctuation (Stewart 1973).

4 Fluorescence may come from other sources rather than from tetracycline itself:

A- auto-fluorescence (primary fluorescence) of phosphate that is present in a newly calcified area,

B- diffuse fluorescence of tetracycline; it may bind to other bone components such as collagen and other tissues that contain calcium,

C- artifactual fluorescence due to binding of tetracycline to calcium-rich deposits such as hypermineralised bone.

Tetracycline is maximally excited by UV light of wavelength 390 nm and emits maximal yellow fluorescence of wavelength 515 nm (Rost 1995, Lee *et al.* 2003).

Some other compounds such as xylenol orange, calcein, calcein green and alizarin complexone have been also used to study the dynamic nature of bone (Adkins 1965, Rahn 1977, Sun *et al.* 1992, Lee *et al.* 2002) and in detecting bone microcracks (Garetto *et al.* 1995, Lee *et al.* 2000, O'Brien 2000, O'Brien *et al.* 2000, Lee *et al.* 2003). They are site-specific labels with various affinities for calcium ions, which line the microcracks. They also fluoresce under ultra-violet (UV) giving a different

colour that can be detected using UV epifluorescent microscopy (Lee 1997, O'Brien *et al.* 2000, Lee *et al.* 2003). However, simultaneous excitation and visualisation of all these fluorochromes from blue to red requires excitation in the UV range and an almost colourless barrier filter (Rahn 1977).

Calcein, alizarin and xylenol were used in twelve-week-old rats and found to provide comparable histomorphometric information (Sun *et al.* 1992).

Suzuk and Mathews (1966) tried to find a suitable combination of fluorochrome substances for bone labelling. They used tetracycline hydrochloride followed by alizarin red S, but they detected that both compounds fluoresced in the yellow range and were difficult to differentiate. They also used different combinations of tetracycline compounds in a sequential manner, but again all compounds fluoresced yellow and were difficult to distinguish from each other. They further used tetracycline and 2,4-bis [N, N´(carbomethyl) aminometyl] fluorescein (DCAF). The two agents were deposited in newly mineralised sites. They were distinguishable as tetracycline fluoresced yellow while DCAF fluoresced green (Suzuk & Mathews 1966). Earlier, Harris (1960) used a double colour fluorescent technique combining tetracycline with alizarin red S that is detectable under transmitted light and fluorescence microscope. Módis *et al.* (1969) combined tetracycline, alizarin red S and DCAF. In an attempt to facilitate the interpretation of a histological bone specimen excited with UV light, Rahn (1977) recommended an *in vivo* dosage and sequence regime for UV excitation of the 5 well-known bone fluorochromes (Table 1.6).

Table 1.6 *In vivo* dosages, sequence of bone fluorochrome chelating agents, their excitation and emission maxima (After Rahn 1977, Rost 1995, O'Brien *et al.* 2000, Lee *et al.* 2003)

Fluorochrome	**Dosage** (intravenous) (mg/kg)	**Excitation wavelength** (nm)	**Emission wavelength** (nm)	**Colour**
Calcein blue	30	375	445	Blue
Xylenol orange	90	377	615	Orange
Calcein	10	495	540	Green
Alizarin complexone	30	580	625	Red
Oxytetracycline	30	365	520	Yellow

1.19 Bone remodelling and fluorochrome chelating agents

In general, when a given BMU has already started before the first label has been administrated, all labels with a mineralised bone matrix in between them are observed provided that the time period between each succeeding label is long enough to avoid substitution. These labels will arrange in a sequence starting with the first label and ending with the last one (Figure 1.17).

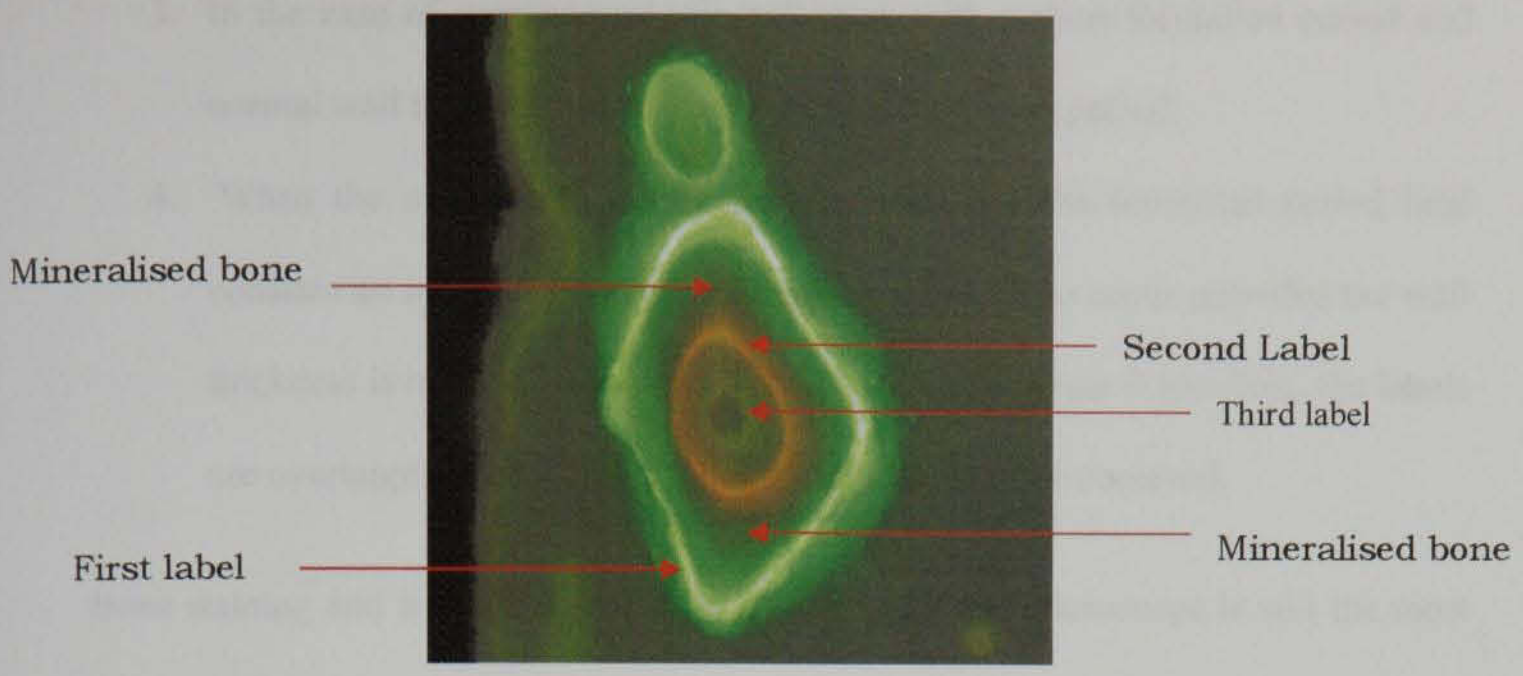

Figure 1.17 A representation of an osteon with three labels stained with three different chelating agents and examined under blue incident light (450nm) at x100. The image was obtained from the 3rd study of the thesis.

When polylabels (for example four labels) were used and some BMU has already started the first three labels can be seen but not the last label, because these BMUs have been completed before the last label was adminstrated. While when only the first two labels were observed, some BMU has been completed before the third label was adminstrated.

There is a predictable relationship between the uptakes of polyfluorochromes (Hori *et al.* 1985, Nölke 1995). For examples, the ratios of double labelled BMUs to single labelled ones depends on the rate of mineralisation, interlabel periods and the wall thickness of the BMU as follows (Hori *et al.* 1985):

1. When the interlabel periods is too long and exceeds the formation period (i.e. one Sigma) only a single label can occur even following a double or a polylabelling procedure.
2. If the interlabel period between successive labels is too short, the labels can overlap. To avoid this problem, the interlabel period should exceed 10 days.

3. In the case of supranormal mineralisation with a short formation period and normal wall thickness, more single labels could be expected.
4. When the mineralisation rate is subnormal and the interlabel period held constant an increase in polylabelling is more likely to occur provided the wall thickness is normal. However, if the mineralisation rate is too slow, the labels are overlapping and a single label is more likely to be observed.

Bone staining and its histological examination under the microscope is still the most commonly used method to study microcracks.

Using an *en bloc* staining with basic fuchsin to study microcracks in bone was first described by Frost (1960) validated by Burr and Stafford (1990) and later modified by Burr and Hooser (1995). In this method, fresh bone is immersed in a dye medium (i.e. basic fuchsin with an ethanol-soluble dye 6% at 26 °C) for several weeks to enable the dye to penetrate cracks that existed before the immersion procedure. Afterwards, the cutting and grinding process is carried out in an aqueous medium. The specimen is then examined under light microscopy. Variation of light intensity, depth of focus and magnification are required to distinguish between unstained and partially stained cracks from pre-existing cracks. The pre-existing cracks are usually stained through the depth of the section and have a sharp border (Lee *et al.* 1998). This technique is difficult and time consuming as a large number of cracks need to be examined and false positive cracks eliminated (Lee *et al.* 1998, Lee *et al.* 2003).

However, dehydration (de-fatting) of the bone specimen in alcohol may introduce some artefacts (cracks) due to differential shrinkage. To address this issue, Burr and Stafford (1990) compared cracks detected in human rib specimens. The specimens were either cut and ground under water and then stained with basic fuchsin after being

mounted on slides or bulk stained in basic fuchsin before preparation of a thin section. They found no difference in cracks detected for both experimental groups (Burr & Stafford 1990). They confirmed the validity of a bulk-staining method as a technique to differentiate between artefactual and *in vivo* microcracks (Burr & Stafford 1990, Lee 1997).

However, basic fuchsin penetrates by diffusion; consequently it may not mark all microcracks and leads to an underestimation (a false negative) of damage quantification. It is also not suitable to study the damage at its sub-microscopic level (Burr & Hooser 1995). The ability of the *en bloc* staining with basic fuchsin method is highly affected by density of bone being investigated; it over-stains bone of lower density and under-stains those with a higher one. Basic fuchsin is a single stain, so it cannot be used to study microcrack growth. It is also not a site-specific stain because it enters voids in bone such as vascular channels, canaliculi as well as microcracks and settles there (Lee *et al.* 2003). Furthermore, it can bind to proteins and collagen. Collagen forms about 30% of bone by weight and is unlikely to line the walls of microcracks (Lee 1997).

In order to distinguish between pre-existing and test-induced microcracks and to study their growth *in vitro*, different stains are required and should be used in a sequential manner (Lee 1997, Lee *et al.* 2000, O'Brien *et al.* 2000, Lee *et al.* 2003).

In one study (Lee *et al.* 2000) basic fuchsin and five fluorochromes were investigated and proved equally effective in labelling microcracks. The tested agents (in additional to basic fuchsin) were oxytetracycline, xylenol orange, calcein, calcein blue and alizarin complexone (Figure 1.18). All agents were able to label the microcracks and neither crack density nor length differed significantly between them. Several

chelating agents were also tested and found to be as effective as basic fuchsin in staining microcracks (Lee 1997). A comparison between basic fuchsin and fluorochromes is displayed in Table 1.7.

Table 1.7 A comparison between properties of basic fuchsin and fluorochromes.

Basic Fuchsin	**Fluorochrome chelating agents**
It is a single stain.	Multiple stains.
It is a space-filler and not site-specific; it can be lodged into voids such as microcracks and resorption spaces.	They are site specific.
It can bind to collagen that comprises 30% of bone by weight and is unlikely to line the walls of microcracks.	They can bind to calcium ions which line the walls of microcracks, resorption cavities and Haversian canals.
It is a single stain thus it cannot be used to study growth of microcracks.	They can be used in a sequence to study growth of microcracks.

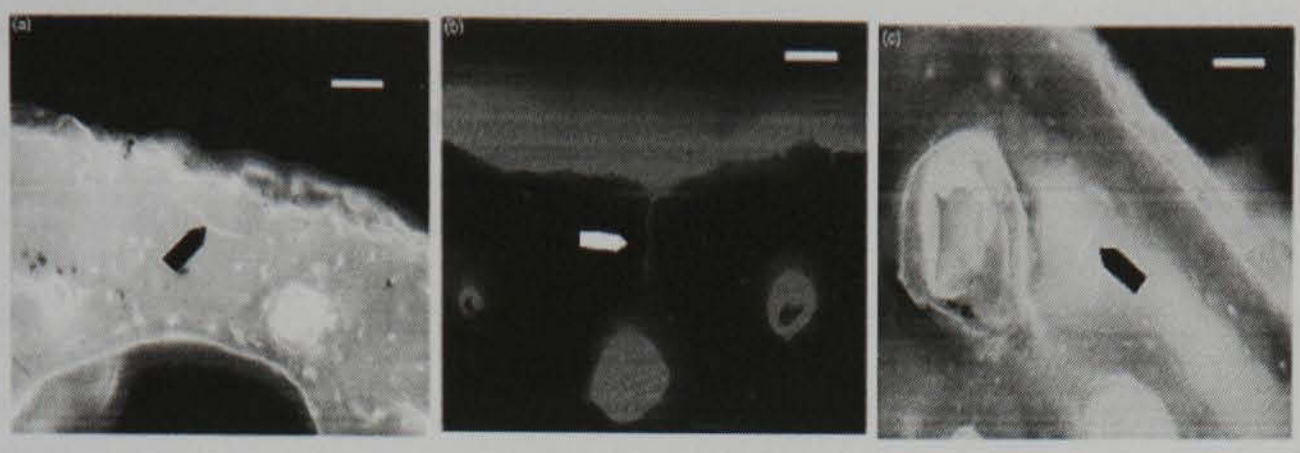

Figure 1.18 Labelled microcracks. Microcracks labelled with (a) calcein blue (UV epifluorescence, λ = 365 nm), (b) alizarin complexone (green epifluorescene, λ = 545 nm) and (c) oxytetracycline (UV epifluorescene, λ = 365 nm). Scale bar = 50 μm. Resorption cavities are also stained with these used chelating agents. [Reproduced from Lee *et al.* 2003].

Lee *et al.* (2000) further investigated microcrack generation and growth in bovine bone using a sequential labelling technique. Bovine bone sections were immersed in tetracycline for 16 hrs and were then fatigue tested. Pre-existing microcracks were labelled with the tetracycline but test induced microcracks were unstained. In order to monitor microcrack generation and growth, other sections were bulk stained after each test period. Firstly, the specimens were cyclic fatigue tested in compression for the first 75% of the test and then stained with calcein blue. The same specimens were then exposed to the final 25% of the test and stained with xylenol orange. At the end of the study, some microcracks stained with calcein blue indicating that they were formed during the first 75% of the test period. Some microcracks stained with two labels, which indicate that microcracks propagated, while some other microcracks were stained with xylenol orange indicating that they were generated during the last 25% of the test

period (Lee *et al.* 2000). However, evidence of dye substitution was obvious. In a recent experimental study by O'Brien *et al.* (2002) optimal sequence of label application was determined and refined. This sequence was alizarin complexone followed by xylenol orange, calcein and calcein blue. However, "oxytetracycline was excluded from the study after recurring problems were found with its ability to chelate when applied in sequence with other agents" (O'Brien *et al.* 2002).

Lee *et al.* (1998) used both transmitted light and epifluorescence microscopy to study *in vivo* microcracks in human rib specimens, which were bulk stained with basic fuchsin. The authors found no difference in crack number, density or length between the two techniques indicating comparable accuracy. Under green incident light (λ = 546nm) microcracks containing basic fuchsin fluoresced orange and the intensity of the fluorescence was directly related to the amount of stain lodged in a microcrack. The fully stained microcracks (i.e. microcracks that stained through the full depth of the section) appeared brighter than those artifactual cracks partially lodged with basic fuchsin debris. Unstained or partially stained artefactual cracks could be screened out. Under ultraviolet incident light (λ = 365nm) only microcracks that stained through the depth of the section fluoresced purple while the artefactual microcracks, partially stained with basic fuchsin were not seen (Lee 1997, Lee *et al.* 1998).

The differences in fluorescence between any two agents are due to the differences in their wavelength. The wavelength of the green incident is higher than that of the UV one (546nm versus 365nm).

The green filter allows green incident light of wave length of 546 nm to impinge upon the specimen while the UV filter allow UV light to impinge on the specimen (Lee 1997, O'Brien 2000, O'Reilly 2002). Under the green light bone appears red while the

microcracks that are stained with tetracycline chelating agent fluoresce dull orange. Under the UV light bone appears blue and the microcracks fluoresce yellow/ green (O'Reilly 2002). Table 1.8 displays different chelating agents and their fluorescent colours.

Table 1.8 Colour of fluorchrome chelating agents under different light sources (O'Reilly 2002).

Chelating agent	**Transmitted light**	**UV epifluorescence**	**Green epifluorescence**
Alizarin	purple	dark red	dull orange
xylenol	red	orange	bright orange
Calcien green	orange	light green	bright orange
Oxytetracycline	yellow	yellow/ green	dull orange

Thus, green incident light has the capacity of maximum absorption and emission compared with the UV incident light. Lee (1997) used epifluorescence with green filter (G – 2A filter block, λ = 546nm) and candidate cracks were identified by their dull orange fluorescence, linear shape and their size being larger than canaliculi and smaller than vascular channels. Candidate cracks were also observed using UV incident light (UV – 2A filter block, λ = 365nm). The basic Fuchsin stained microcracks were identified by their purple fluorescence. Under transmitted light, candidate cracks were identified using the criteria set by Burr and Stafford (1990) for identification of *in vivo* microcracks that were stained with Fuchsin (Table 1.9). The candidate microcrack sizes were intermediate between canaliculi and vascular channels with sharp borders. By varying the light intensity, the edges of the candidate cracks were found to be more deeply stained than the intervening space. Only cracks that satisfied Burr and

Stafford's criteria were considered to be *in vivo* microcracks and not artefacts. The author also observed some artefactual cracks that were not stained with Fuchsin and thus were created during the cutting and grinding processes.

Table 1.9 Criteria and methodology for identification of microcracks using Basic Fuchsin (After Burr & Stafford 1990, Lee 1997, Lee *et al.* 1998, O'Brien 2000).

1.	They are intermediate in size, being larger than canaliculi but smaller than vascular channels • Method: fluorescent green incident light (λ = 546nm).
2.	They have sharp borders with a halo of basic fuchsin staining around them. • Method: fluorescent green incident light (λ = 546nm).
3.	They are stained throughout the depth of the section • Method: UV incident light (λ = 365nm).
4.	When the depth of focus is changed, the edges of the crack can be observed to be more deeply stained than the intervening space • Method: light microscopy, X 225 magnification.

In his study Lee (1997) reported that the amount of Fuchsin in a microcrack influences the intensity of fluorescence when examined using green incident light (λ = 546nm). Therefore, the microcrack, which stained throughout the depth of the section, was brighter than those partially stained with Fuchsin. The latter artefactual cracks were most probably filled with fuchsin during the cutting and grinding processes while the cracks that did not fluoresce contained no fuchsin. However, all microcracks that fluoresced under UV light (λ = 365 nm) were found to be stained

throughout the depth of the section when they were examined using transmitted light thus they are *in vivo* microcracks. In this study (Lee 1997) microcrack number as well as microcrack density was found to be higher when using the epifluorescence method than when using light microscopy, although these differences were not statistically significant.

The protocol used by Burr and Stafford (1990) was refined and used with fluorochrome chelating agents (Lee 1997) as displayed in Table 1.10.

Table 1.10 Criteria and methodology for identification of microcracks using chelating agents (After Lee 1997, Lee *et al.* 1998, O'Brien 2000, O'Reilly 2002).

1.	They are intermediate in size, being larger than canaliculi but smaller than vascular channels
2.	They have sharp borders with a fluorescence of chelating agent within crack border evident.
3.	They are stained throughout the depth of the section
4.	When the depth of focus is changed, the edges of the crack can be observed to be more deeply stained than the intervening space

Chelating agents were found to be effective at labelling microcracks in cancellous (Lee *et al.* 2000) and compact bone (O'Brein 2001) when used individually. They can also be used to study microcrack growth (propagation) when applied in a sequence (O'Brien

2000). However, problems may arise when the chelating agents are applied in the sequencing technique. For example, tetracycline compounds have similar colours, ranging from yellow to green, which makes differentiation between them difficult (Lee *et al.* 2003). When tetracycline was used with calcein and examined under UV epifluorescence (λ = 365 nm) tetracycline was found to fluoresce yellow-green while calcein fluoresced green making differentiation between them problematic. Nevertheless, when they were examined under green incident light (λ = 546nm) the calcein fluoresced but the tetracycline did not. This was attributed to the differences in their excitation maxima (λ = 365nm versus λ = 495nm) (Lee *et al.* 2002).

Tetracycline agents were found *in vitro* to substitute (agents cover other agents applied prior to them) other chelating agents such as calcein blue and xylenol orange. These agents may also substitute the tetracycline. Xylenol orange substituted calcein and to a certain extent alizarin that were applied prior to it. Alizarin and xylenol orange were found difficult to differentiate between because both agents appeared as a red/orange. It was hypothesised that this substitution is due to the differences in binding strength of each agent for calcium ions as well as to the concentration of each dye (Lee 1997, Lee *et al.* 2000, O'Brien 2000). To test this hypothesis O'Brien (2000) studied the affinity of five chelating agents for free calcium ions in a calcium chloride solution using chromatography. According to this study, the five chelating agents were then used in order beginning with the agent of the greatest affinity for calcium, down to the agent with the least affinity (O'Brien 2000). A preliminary sequence was established from the chromatography test. The Alizarin complexone has the greatest affinity, followed by xylenol, calcein blue, calcein and oxytetracycline (O'Brien 2000). Scratch tests of bovine bone were then carried out to optimise the sequence and to determine the most efficient concentration which allowed each chelating agent to fluoresce under UV light.

Upon application of this sequence calcein blue was found to displace calcein and xylenol orange to a lesser extent. So the sequence was revised and the concentration of calcein blue was reduced to avoid the substitution problem (O'Brien 2000). Oxytetracycline was excluded from the study because it was found to substitute other dyes and to be substituted by them.

It is difficult to differentiate between the agent used in the study and pre-existing tetracycline that might be found in the tested specimen prior to testing (O'Brien 2000) as tetracycline is commonly used in treatment of infectious diseases in animals. This led the author to modify the sequence as well as concentration of the chelating agents, which had been previously set by Rahn (1977). Table 1.11 below describes the recommended sequence and concentration of the most commonly used chelating agents (O'Brien *et al.* 2000).

Molecular structures of different chelating agents are displayed in figures 1.19-1.23.

Table 1.11 Sequence of chelating agents according to their affinity to calcium ions and the *in vitro* recommended concentrations (O'Brien *et al.* 2000).

Fluorochrome sequence	Concentration
Alizarin	0.0005 M
Xylenol orange	0.0005 M
Calcein	0.0005 M
Calcein blue	0.0001 M

Oxytetracycline was excluded.

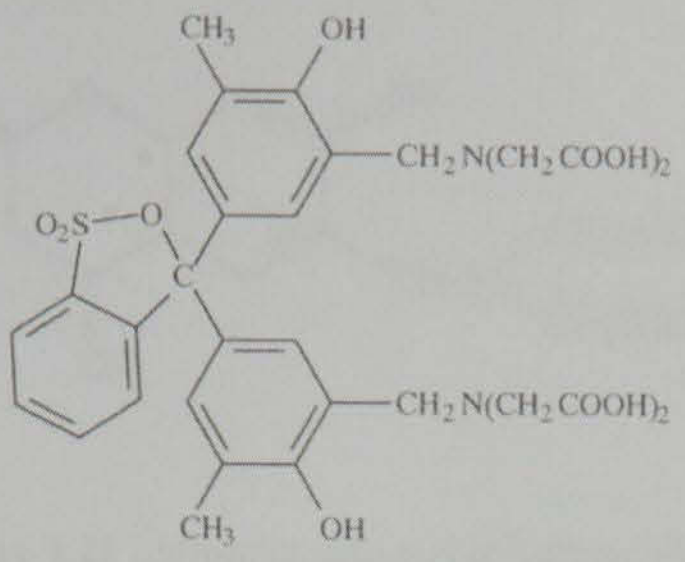

Figure 1.19 Molecular structure of xylenol orange.

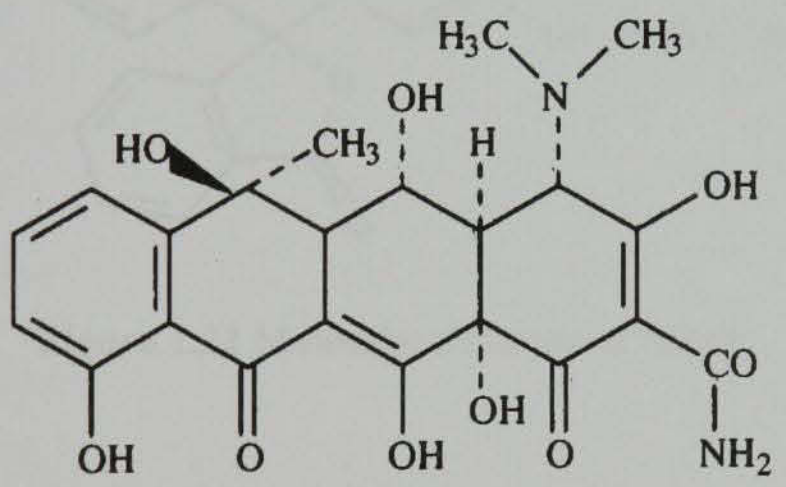

Figure 1.20 Molecular structure of oxytetracycline.

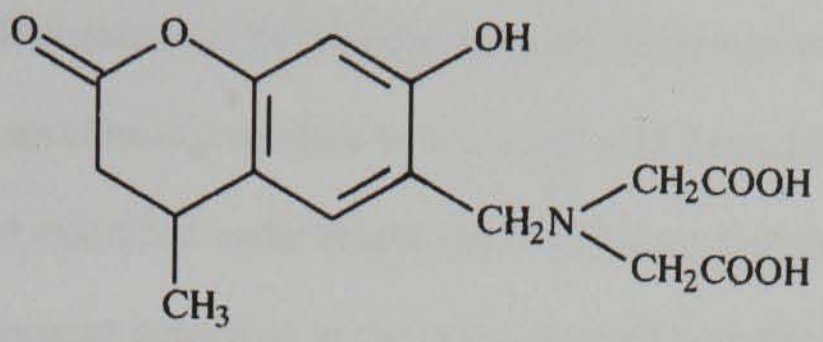

Figure 1.21 Molecular structure of calcein blue

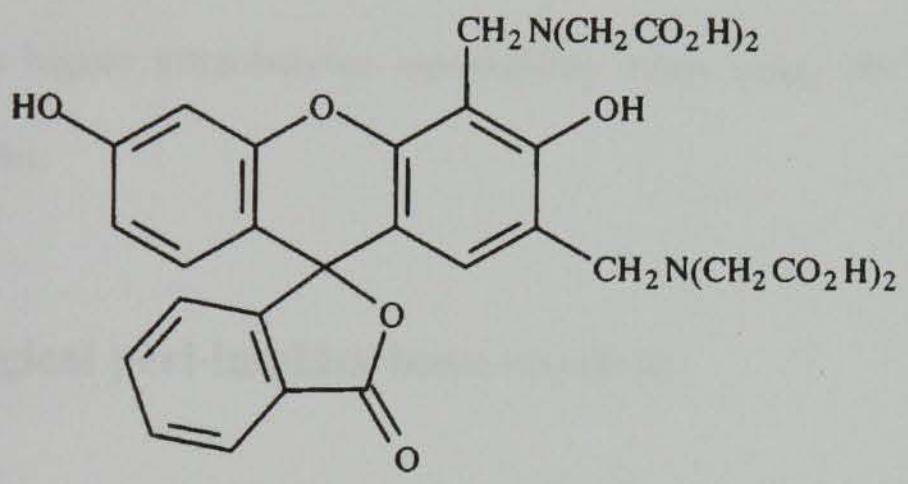

Figure 1.22 Molecular structure of calcein.

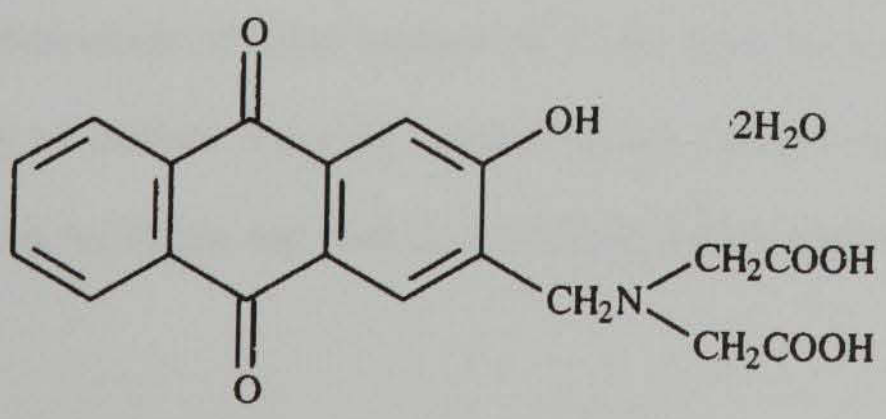

Figure 1.23 Molecular structure of alizarin.

Huja *et al.* (1999b) used canine femurs to study bone microdamage. The bone specimens were subjected to four-point cyclic bending until they had lost between 5 and 43% of their stiffness. The specimens were then bulk stained with basic fuchsin for the presence of microdamage and examined under bright-field and fluorescent microscopy. They also investigated microdamage generated in the bone adjacent to endosseous implants, which were subjected to fatigue loading. The bone around the implant was either allowed to heal (adapted specimen) for 12 weeks after placement in dog mid-femoral diaphyses prior to testing or was loaded immediately to simulate non-healed bone surrounding endosseous implants (non-adapted). They reported that significantly more microdamage was detected using the fluorescent technique than by the brightfield method and observed a trend towards higher intraobserver repeatability when using the fluorescent method (Huja *et al.*1999b).

1.20 Post-surgical peri-implant bone reaction

The connection between implant surfaces and bone can either be mediated by connective tissue fibres or by intimate contact of bone and implant surface. While the first outcome indicates a failure of any implant system, the second one is the objective of the implant surgery and is known as osseointegration or functional ankylosis. However, commencement of either mechanism is influenced by many factors such as biocompatibility of implant materials, implant design, implant surface topography, host bed, surgical technique and loading conditions during healing (Albrektsson & Isidor 1994).

Osseointegration is defined as a direct structural and functional connection between living bone and the surface of a load-carrying implant (Brånemark 1985, Brånemark *et al.* 2001).

Osseointegration as reported in a wide range of animal studies or from retrieval of osseointegrated and failed implants in humans using light microscopic analyses revealed a direct apposition of bone on the implant surface without an intervening of organised collagenous and fibroblastic matrix (Masuda *et al.* 1998). However, under the electron microscope a zone of 100μm in thickness rich in non-collagenous proteins, similar to cement lines at the natural bone interface, has been found between the implant surface and the surrounding bone (Sennerby *et al.* 1991, Clokie & Warshawsky 1995, Brunski 2000).

Osseointegration may be experimentally evaluated quantitively and mechanically. The quantitive evaluation is a morphometric measurement of the amount (percent) of implant surface covered by bone (Ivanoff *et al.* 1996, Masuda *et al.* 1998, Ivanoff *et al.* 1999, Albrektsson *et al.* 2000a, Albrektsson *et al.* 2000b, Uehara *et al.* 2004). Conversely, mechanical evaluation such as resistance to removal torque, measures the strength of bone-implant interface (Wong *et al.* 1995, Ivanoff *et al.* 1996, Albrektsson *et al.* 2000a). A correlation between the histomorphometric values and mechanical measures for screw-shaped titanium implants has been reported (Johansson & Albrektsson 1987, Cordioli *et al.* 2000).

Earlier studies mainly considered the amount (quantity) of bone surrounding the implant and how much bone is required for an implant to be clinically successful. These investigators used static measurement of bone, which is not necessarily an index for living bone (Garetto *et al.* 1995). However, recent studies investigated the

dynamic nature of bone at the implant-bone interface, which gives an insight to better understanding of the bond nature between the bone and the implant surface, and explore factors that may modify this biological activity.

Study of the tissue-implant interface involving various animal models such as dog, rabbit, goats, rat, and installed in different anatomical sites (e.g., maxilla, mandible, femur, tibia and knee) were reported. Varying results were found. These differences may be caused by factors such as characteristics of the implant, type of surgery, the healing period, location of the implant and relative health and functional state of the implant at the time of analyses as well as methods of analyses and the animal species (Wennerburg *et al.* 1997; Masuda *et al.*1998, Shirakura *et al.* 2003). Table 1.12 displays these factors.

Table 1.12 Factors that should be considered when a comparison between different study results is made (Modified from Sykaras *et al.* 2000).

Implant material	Implant design	Implant length	Implant diameter
Implant surface topography	Implant surface chemistry	Implantation time	Implantation site
Analysed length	Biomechanical loading	Animal model	Orientation of histological section

All of these factors may lead to confusion in the interpretation of various study results and should be considered as has been pointed out by various investigators.

The implant surface is far from being considered totally covered by bone, and values for coverage reported in the literature vary (Albrektsson & Johansson 1991). The percentages of bone-to-implant contact have varied between different studies. For

instance, the morphometric measurements of implant-bone interface have shown differences between mandible and maxilla (Carr *et al.* 1997) as well as between varies jaw regions in autopsy jaw specimen (Friberg *et al.* 1995). One such study indicated the ratio of compact to cancellous bone was higher for mandible than maxilla (Friberg *et al.* 1995).

Although an increase in bone formation around implants with time has been found in several animal studies, this increase was not linear (Takeshita *et al.* 1997, Masuda *et al.* 1998). When the bone apposition around implants in rat tibia was examined at one month and after two years after implant placement, Takeshita *et al.* (1997) reported a rapid bone formation after one month followed by progressive bone formation in the following two year-healing period (53% versus 89% bone-implant contact). In minipigs the value was 78 ± 5.8% after a four-month period of unloading healing (Nkenke *et al.* 2003). In rabbits in a four-week healing period, the value was 59 ± 6.3% for one surgical implant placement technique (osteotome method) versus 71.1± 7.2% when another surgical technique (conventional method) was used (Nkenke *et al.* 2002). However, the method by which the bone implant contact was estimated should be considered. For instances, Nkenke and coworkers (2002) calculated the implant bone contact percentage when the implant and its surrounding bone were cut perpendicular to the implant. This could not be compared with results that were obtained when the implant and the surrounding bone were cut vertically.

Morphometric analysis of the bone-implant interface by Hipp and colleagues (1987) has revealed that 59% and 49% of screw-shaped titanium implant surface was found to be in close contact with bone after 4 to 7 months in canine mandibles and radii respectively.

Bone to implant contact was reported to increase with time (a 12-week healing period compared with a 6-week period) (Ivanoff *et al.* 1996). Another morphometric analysis of the bone-implant interface (Abron *et al.* 2001) reported that 54% of screw-shaped grit-blasted and acid etched titanium implant surface was found to be covered with bone following a 3-week experimental period in rat tibia. The value for machined implant surface was significantly lower (34%). Sennerby and coworkers (1991) found that the threads of the implants in vivo were packed (79-95%) with dense lamellar bone when examined by light microscopy and that the bone-implant contact was 56 to 85% (Sennerby *et al.* 1991). However, this study consisted of seven clinically stable retrieved implants, which some of them had bone resorption and could be considered as failing implants. Therefore, the figures reported by the authors only represented the threads that were osseointegrated at the implant removal time. The result should be interpreted with caution. Nevertheless, the implant surface of clinically stable and osseointegrated titanium implants were not 100% in contact with the mineralised bone as these studies suggested (Sennerby *et al.* 1991).

The definition of osseointegration based on the stability of the implant within the bone rather than on histomorphometric analyses has been described as "a process whereby a clinically asymptomatic rigid fixed of alloplastic materials is achieved and maintained in bone during functional loading" (Zarb & Albrektsson 1991).

1.20.1 Bone-implant interface

Several clinical studies have reported that under optimum circumstances, a long-term rigid union between the implant surface and the surrounding bone can be achieved and maintained for indefinite periods of time (Garetto *et al.* 1995). Therefore, to

maintain the rigid union, continuous remodelling of the bone supporting the implant in the presence of functional loading is essential (Misch *et al.* 2001).

The adaptive capacity of bone surrounding loaded implants is demonstrated as changes in size, shape and mass of the loaded bone. However, the rigid bony interface does not necessarily indicate that the total implant surface is in direct contact with bone and soft tissue may be present between the implant surface and the supporting bone (Roberts *et al.* 1984, Ericsson *et al.* 1994).

Bone responds to implant in a similar way it responds when it fractures. Early events that were reported to occur after implant placement are: vascular disruption, serum protein deposition on the implant surface and formation of blood clot with fibrin-rich materials within the small gap between the implant surface and the surrounding bone (Watzek & Gruber 2002). Attachment of mesenchymal cells to the implant surface and their proliferation, secretion of osteoid and then its mineralisation as early as two weeks were reported (Raghavendra *et al.* 2005).

Development of a histologically successful rigid implant-bone interface with an intimate implant-to-bone contact (osseointegration) has been described (Roberts *et al.* 1984, Roberts 1988, Sennerby *et al.* 1991, Davies 1998, Shirakura *et al.* 2003, Berglundh *et al.* 2003, Abrahamsson *et al.* 2004, Raghavendra *et al.* 2005). In general, features such as angiogenesis, formation of woven bone at the periosteal and endosteal surfaces as well as at the implant-bone interface, remodelling of the interface and its maturation (continuous remodelling of the interface and supporting bone) have been reported to occur around successful implants (Roberts *et al.* 1984, Garetto *et al.* 1995, Davies 1998) (Table 1.12).

Understanding the mechanism by which the biomaterials integrate with their surrounding tissues is a key in explaining its long-term success. However, in spite of several studies on the mechanical and biological properties of implant biomaterials when used as a medical device, the mechanism by which they integrate with bone is not completely understood. The way by which bone forms around implants is debatable. Meanwhile, it is assumed (although more research is required) that formation of bone around implants occurs through two distinct mechanisms: *Distance Osteogenesis* and *Contact Osteogenesis* (Davies 1998, Raghavendra *et al.* 2005, Weinlaender *et al.* 2006). In the first mechanism, *distance osteogenesis*, (appositional bone formation) new bone arises from the old bone (the osteotomy walls) towards the implant surface while in the second mechanism (*contact osteogenesis*) bone forms directly on the implant surface. In the first mechanism cement lines were found to separate the newly formed bone and the pre-existing old bone (Shirakura *et al.* 2003).

In contrast to Davies (1998), Sennerby and coworkers (1993) observed that bone formation proceeded from the pre-existing bone towards the implant (*distance osteogenesis*) *in vivo* and that the newly formed bone was separated from the implant surface by a layer of amorphous material of 100 to 400 nm wide (Sennerby *et al.* 1991). Clokie and Warshawsky (1995) reported that bone was deposited only on previously existing bone and extended toward the available space between the bone and the implant surface. The implant surface was also found separated from the surrounding bone by an amorphous layer, a granular electron-dense layer, or a layer of uncalcified collagen fibrils when the implant bone interface was examined using electron microscopy. Furthermore, Ohtsu *et al.* (1997) used the rat femur to study cortical bone response to titanium implants and failed to find any evidence of *contact*

osteogenesis as described by Davies (1998). Thus, it was suggested that titanium is biocompatible, but not necessarily osteoinductive (Clokie & Warshawsky 1995).

It may be argued that implant initial stability and whether a gap present between the implant surface and the surrounding bone may affect the mechanism by which bone forms around the implant. For example, when the implant design provides a space between its surface and the osteotomy walls *contact osteogenesis* may occur. On the other hand, when there is an intimate contact between the implant surface and the osteotomy walls bone may be formed by *distance osteogenesis* (Sykaras 2000). Similar findings were also reported by Weinlaender and co-workers (2006) in dogs. They reported that bone formation around machined and plasma sprayed titanium surfaces was most likely to rise from the old bone (*distance osteogenesis*) However, on HA ceramic coated implants and occasionally on plasma sprayed titanium surfaces new bone was found to form simultaneously by *contact* and *distance osteogenesis* (Weinlaender *et al.* 2006). The authors also indicated that in the area of the cortical layer, two different bone reactions could be seen depending on the implant initial fit in the cortical bone. According to Weinlaender and coworkers (2006), the newly formed bone in the tightly seated implant, was usually preceded by old bone resorption and could be seen three weeks after the implantation time. On the other hand, when there was a gap between the implant surface and the surrounding bone, newly formed bone could be seen as early as one week after the implantation time and starting from the old bone (Weinlaender *et al.* 2006). Nevertheless, figures that were included in the above article may indicate a mis-interpretation of the findings. In one figure the area which was believed to be new formed bone on the surface could have been just debris from the grinding procedure since the criteria by which newly formed bone was distinguished from the old one was not set.

It has been suggested that implant surface roughness may promote *contact osteogenesis* by both increasing surface area for fibrin attachment and by providing surface features with which fibrin could become entangled (Davies 1998). In an animal study, Botticelli *et al.* (2003) reported that bone formed by the two mechanisms was also found to occur in marginal bone defects around implants. However, the *distance osteogenesis* may occur first followed by the *contact* osteogenesis once the newly formed bone reaches a certain distance from the implant surface (Botticelli *et al.* 2003).

Shirakura *et al.* (2003) claimed that tissue response in rat maxilla to titanium differs from that to HA. While the HA-coated implants induced bone formation by *contact osteogenesis*, the bone was formed by the *distance osteogenesis* on implants that were sandblasted with $Al_2 O_3$. This difference was attributed to the osteoconductivity of the HA. In the case of the sandblasted implants, they observed that the new bone was separated from the old one by the cement line and that the implant surface was separated from the newly formed one by fibroblast-like cells. On the other hand, no cell element was found to intervene between the implant surface (HA) and the newly formed bone.

The response of the host to the implant material and the behavior of these materials in the host are considered as the two main factors that significantly affect the performance of these materials when they are implanted (Puleo & Nanci 1999).

Bone formation around implants relies on the recruiting of potentially osteogenic cells, on their attachments to the implant surface, on their proliferation and differentiation into mature cells (Cooper 2000). Once osteogenic cells differentiate, they start secreting matrix and stop migrating. On the other hand, non-differentiated

osteogenic cells have the ability to migrate and once they reach the surface they initiate matrix synthesis and secretion at the implant surface (Davies 1998).

The migration of osteogenic cells through blood clot matrix causes contraction of the fibrin strands in the clot matrix which can detach the strands from the implant, disturbing or stopping contact osteogenesis and osteoconduction (Davies 1998, Lazzara *et al.* 1999). Attachment of the blood clot to the implant surface is required in order to enable the migrating cells to reach the implant surface. Thus, it is reasonable to suggest that enhancement of such attachment may occur on a rough implant surface rather than on a smooth one. For instance, in an *in vitro* study, Davies (1998) demonstrated a superior attachment of blood clot to a rough implant surface (a dual acid etched surface; Osseotite) when compared with a relatively smooth one (Davies 1998). The rough surface may enhance fibrin attachment and consequently improve bone to implant contact. When the fibrin is well attached to the implant surface (which most likely occurs when a rough surface implant is used) migrating osteoblasts are able to reach the surface implant. This phenomenon was also illustrated histologically when the Osseotite implant was compared with a relatively smooth surface implant after 6 months of healing in the posterior region of human maxilla (Lazzara *et al.* 1999). In the same human histological study of the maxilla, Lazzara *et al.* (1999) reported a mean percentage of bone-implant contact of 72.96% for acid etched-implant surfaces and 33.98% for machined surfaces (Lazzara *et al.* 1999).

1.20.2 Stages of osseointegration

Immediatelly after implant installation tips of threads are usually in close contact with host bone providing initial stability for the implant. The implant surface is not completely in contact with the host bone and spaces also exist. The spaces are

initially filled with blood that comes from injured blood vessels forming a fibrin network (Watzek & Gruber 2002). As early as two hours after implantation a large number of erythrocytes, some neutrophils and macrophages were found to be embedded in the fibrin network. Small proportions of bone remnants dislodged during surgical preparation were also found surrounded by the blood elements (Berglundh *et al.* 2003, Abrahamsson *et al.* 2004). Protein depositions were also seen on the implant surface (Table 1.13).

Table 1.13 Bone healing events

Events
• Protein adsorbtion to implant surface • Blood clot formation and platelet activation • Formation of granulation tissue; angiogenesis and fibroplasia • Woven bone formation • Replacement of woven bone with lamellar bone • On-going bone remodelling

In a 4-day period, within regions which are in contact with the implant surface large numbers of erythrocytes remained while the blood clot is replaced with fibroblast-like (mesenchymal) cells, which surrounded vascular structures (Berglundh *et al.* 2003, Abrahamsson *et al.* 2004). Inflammatory cells are also seen in several regions in the spaces as well as around the vascular structures. A lining of mesenchymal cells can be seen oriented parallel to and in close contact with rough-surface implants. Osteoclasts were seen on the proximal bone surface associated with areas of bone resorption.

Osteoclasts were also found on the surface of some bony remnants (Abrahamsson *et al.* 2004).

Woven bone was reported to occur as early as one week after implantation irrespective of the implant surface texture (Abrahamsson *et al.* 2004) and material: HA or titanium (Shirakura *et al.* 2003). Clokie and Warshawsky (1995) suggested that large blood vessels surrounded by woven bone could occur in the spaces between the implant surface and the host bone in rat tibia as early as 3 to 4 days after implantation. These vessels eventually will be reduced in diameter as more bone deposits around them.

Around machined implants, woven bone was found as a continuation of the cut bone surface, extending within a provisional tissue matrix toward the implant surface. The latter observation characterised the appositional type of bone formation or *distance osteogenesis* (Davies 1998). According to Futami *et al.* (2000) and Shirakura *et al.* (2003) different patterns in bone formation were recognized between lateral and base areas of implant cavities.

Futami *et al.* (2000) concluded that bone formation proceeds at different modes around the titanium implant in rat maxilla, depending on the nature of the recipient bones and the dimensions of the gap between the implant and osteotomy margin.

Distance osteogenesis (as a reparative reaction) may be stimulated as a result of microdamage generation, which is believed to occur around the implant site (Hoshaw *et al.* 1994a). As it has been reported, about 1mm of compact bone adjacent to the implant site was found to experience necrosis after implant placement and as a result of implant loading.

New bone formation which occurred from the pre-existing bone toward the implant, was found to be preceded by active bone resorption in the lateral areas with narrow gaps between the implant surface and the old bone (Shirakura *et al.* 2003). However, this was not the case when the bone at the base was observed. Bone in the latter region was found to form without any evidence of bone resorption when titanium implants were implanted into the rat maxilla (Futami *et al.* 2000, Shirakura *et al.* 2003). Futami and coworkers (2000) concluded "ossification proceeds at different modes around the titanium implant in rat maxilla, depending on the nature of the recipient bones and the dimension of the gap between the implant and osteotomy margin".

Several layers of densely compact osteoblast-like cells were also found in the periphery of the tissue surrounding the machined implants. The blood clot remnants can occasionally be seen in contact with the implant surface. According to Davies (1998) and Abrahamsson *et al.* (2004) woven bone was found to be laid down directly onto rough surface implants with a distance from the old bone [*contact osteogenesis*] and from the old bone towards the implant surface [*distance osteogenesis*] (Davies 1998). The latter mechanism is the way by which bone forms around smooth surface implants (Davies 1998, Berglundh *et al.* 2003, Abrahamsson *et al.* 2004). Primary osteons are also obvious at this stage and are lined with osteoblasts and lacunae containing osteocytes. On the osteotomy wall, reversal lines were observed (Abrahamsson *et al.* 2004).

The formation of woven bone increased over two weeks irrespective of the implant surface; machined or rough. Trabeculae of woven bone could be seen filling up the spaces around the implants. As opposed to the bone formation in the spaces around

frame of mineralized tissue. Remodelling activities including the formation of secondary osteons could be observed at this time in regions close to the old bone (Abrahamsson *et al.* 2004).

After a six-week healing period, the previous spaces adjacent to the implants are filled with a mixture of woven, parallel-fibred and lamellar bone. Large areas of this bone are characterised with the presence of secondary osteons. Such bone tissues were also found in close contact with implant surfaces (Berglundh *et al.* 2003). Signs of remodelling are also obvious at this time (Abrahamsson *et al.* 2004). Bone mineral apposition rates of 1.7 ± 0.1μm/day at two weeks increased in average to 1.8 ± 0.2μm/day at six weeks in minipigs (Nkenke *et al.* 2003) and slightly. Between week 10 and 14 a minimal decrease was observed (1.6 ± 0.4μm/day).

The lattice of formerly formed woven bone is then filled with lamellar bone. This results in the formation of primary osteons and eventually matures and has sufficient strength for loading. The latter event is known as lamellar compaction of immature woven bone callus (Roberts 1988). The maturation of formed woven bone is achieved in about six weeks in rabbits and 18 weeks in humans (Roberts 1988). At this time the formerly formed woven bone reduced in size and reoriented itself as internal maturation and strength were attained (Roberts *et al.* 1984, Roberts 1988).

After 8 and 12 weeks the mineralised tissue increases around smooth and rough surface implants and only small differences can be observed between them (Abrahamsson *et al.* 2004). Remodelling of newly formed bone occurs with formation of secondary osteons (Berglundh *et al.* 2003, Abrahamsson *et al.* 2004).

These healing events indicate that osseointegration is a dynamic process at its early stage as well as during the maintenance period (Berglundh *et al.* 2003; Abrahamsson *et al.* 2004). Bone remodelling is an essential mechanism for replacing immature, damaged, or over-stressed bone on a continuous basis (Roberts *et al.* 1984). Despite the optimal surgical technique used for preparation the osteotomy site compact bone adjacent to implant (about one millimetre) undergoes necrosis. Remodelling starts at the area adjacent to the implant surface in order to replace the necrotic bone, which unavoidably occurs in the implant surrounding bone probably as a result of severed blood vessels, trauma caused by the drilling procedure and heat generation at the time of implant surgery (Eriksson & Albrektsson 1983, Clokie & Warshawsky 1995). The sequence of such necrosis may be reflected in one of the following three outcomes: 1) formation of fibrous tissue; 2) necrotic bone remains as a sequester without repair or 3) bone remodelling and formation of new bone (Albrektsson 1985).

The remodelling is achieved by cutting/filling cones originating from the endosteal surface. The cutting/filling cones are almost oriented perpendicular to the long axis of the bone (unlike the physiogical remodelling which usually occurs along the long axis of the bone). In rabbit, from 6 to 16 weeks after implant placement remodelling of a part of the woven bone to well-organised and mature secondary osteons is routinely observed (Roberts *et al.* 1984).

1.21 Bone loss around endosseous implants

1.21.1 Early bone loss

An implant is unlike a natural tooth, which when loaded concentrates large stresses/strains at the crest of surrounding alveolar bone. The direction and the magnitude of chewing forces on teeth and oral implants are not the same owing to the

differences in the system by which the oral implant and the teeth are connected to the surrounding bone. While the teeth are surrounded with the periodontal ligaments that work together as a shock absorber, the implant is in an intimate contact with the surrounding bone and the chewing force is dissipated by bone deformation. The absence of the periodontal ligaments around the implants leads to loss of the proporioception. Consequently, the periimplant bone is much more endangered by the excessive chewing forces when compared with the natural teeth (Gaggl & Schultes 2001).

When a load of equal magnitude and direction is applied to both an implant and a tooth, the implant sustains a higher proportion of the load that it is not dissipated to the surrounding bone (Misch *et al.* 1999).

An average of one millimetre of marginal bone loss is commonly seen after the first year of function (Adell *et al.* 1986, Oh *et al.*2002, Steigenga *et al.* 2003). This may be followed by an annual loss of less than 0.1 mm thereafter (Adell *et al.* 1986). At least six possible factors are assumed to cause bone loss around implants, including surgical trauma, occlusal overload, perimplantitis, the micro-gap that is present between the implant-abutment interface, biologic width, and implant crest module (Oh *et al.* 2002). However, the exact cause of this bone loss is still debatable. Currently available literature indicates that the reformation of a "biologic width" around dental implants, development of a micro-gap if placed at or below the bone crest, occlusal overload, and implant transosteal region (crest module) are the most likely causes of early implant bone loss. Nevetheless, other contributing factors, such as surgical trauma and perimplantitis may have a role to play in the process of early implant bone loss as well (Oh *et al.* 2002, Steigenga *et al.* 2003). According to

Hermann *et al.* (2000), during the early healing phase after implant placement the marginal bone loss is dependent on the surface characteristics of the implant and the presence/absence as well as the location of an interface (micro-gap). However, the bone loss was not dependent on the surgical technique (submerged or non-submerged). In another animal study conducted by the same group, Hermann *et al.* (2001) concluded that crestal bone changes around 2-piece submerged titanium implants are most likely influenced by possible movements between implants and abutments, but not by the size of the micro-gap. Thus, a significant crestal bone loss occurs in 2-piece implant configurations even when the micro-gaps are less than ten microns in combination with possible movements between implant components.

A biomechanical factor was thought to determine the nature of implant-bone interface and whether fibrous tissue or bone will develop to cover the implant surface.

Occlusal force applied to an implant-supported restoration is transferred to the tissue of the mandible or maxilla through the supporting implant. Therefore, mechanical properties of the implant-bone interface play a major role in the outcome of any implant system. These mechanical properties are related to the structural characteristics of the bone and/or soft tissue surrounding the implants, and the degree of fixation between the bone and the implant (Elias *et al.* 1996). Irrespective of implant surface or design, two theories have been suggested to explain peri-implant crestal bone loss (Block *et al.* 1996). First is the mechanical overloading of the implant during function, and second is microbial-based leading to a periodontal disease-like process and crestal bone loss. Thus, placement of a short implant in poor-quality bone (posterior region of the mandible) may lead to marginal bone loss through microtrauma to the bone trabeculae and down-growth of soft tissue creating

an infra-bony pocket, which collects plaque and other debris. This will eventually lead to periodontal disease-like destruction (Block *et al.* 1996). A short implant in the posterior region of the mandible is more likely to be overloaded due to high occlusal force and to its low surface area.

In the presence of parafunctional activity or lacking of anterior occlusal contact failing and failed fixtures were more commonly observed than in patients with osseointegrated supported prosthesis in one jaw (27% versus 2.2%) (Quirynen *et al.* 1992). These findings concur with the earlier report, presented by Naert (1991), in which patients with maxillary and mandibular osseointegrated supported-prosthesis had more bone loss than those with osseointegrated supported-prosthesis in one jaw. These studies suggested the importance of implant loading on consequent peri-implant bone loss. This may reflect differences in the loading values imposed on the two groups. In patients with osseointegrated implants in both jaws, there would be a reduction in number of exteroreceptors due to the missing of teeth and their periodontal ligament when compared with patients with osseointegrated implants in one jaw (Quirynen *et al.* 1992).

Hermann *et al.* (1997) radiographically studied crestal bone changes around unloaded non-submerged and submerged titanium implants in five dogs. Standardized radiographs were used to calculate the distance between the top of the implant/abutment and the most coronal bone-to-implant contact. Bone density changes were also evaluated using a computer-assisted densitometric image analysis (CADIA). Six different implants were used in the study. Two implants were 1-part implants and four implants were 2-part types. One stage technique (non-submerged) was used for one of the 1-part implants and one of the 2-part implants. Two-stage

technique (submerged) was applied for the remaining 2-part implants. The results revealed that in 1-part, nonsubmerged implants, the most coronal bone-to-implant contact followed at all time points the rough/smooth implant interface while in all 2-part implants, nonsubmerged and submerged, the most coronal bone-to-implant contact appeared to be affected by the location of the microgap. It was located approximately 2 mm below the microgap. This study demonstrated that the location of the microgap and the rough/smooth implant interface have a significant effect on marginal bone formation. In addition, bone remodelling occurs rapidly during the early healing phase after implant placement for non-submerged implants and after abutment connection for submerged implants (Hermann *et al.* 1997). This finding was latter supported by (Assenza *et al.* 2003) who concluded that during the first year of function bone crest level changes depended on the location of the microgap.

Hoshaw *et al.* (1994a) used male canine tibia and demonstrated an increased bone resorption around the neck of loaded osseointegrated implants and a decreased percentage of mineralised tissue around these implants after 12 weeks of application of a high cyclic tension when compared with control unloaded implants. They found that bone that formed on the original periosteal and endosteal surfaces were on both loaded and control implants. They also reported bone closely contacting the implants for both the loaded and control ones in the intra-cortical region. However, most notably, within about 1mm of the necks of the loaded implants a zone of non-mineralised tissue was often found and this tissue extended and often went below the first threads. This did not occur for unloaded implants. There was a significant difference in surface bone loss between control and loaded implants. Overall there was a higher percentage of nonmineralised tissue, which surrounded the loaded implants than the unloaded controls. The latter finding may indicate an increase in

remodelling activities stimulated by the mechanical stress as a result of implant loading.

In an animal study in dogs Gotfredsen *et al.* (2001) studied peri-implant bone response to static loading. In this study, marginal bone level was not found to be affected by the static load but by the implant surface characteristics. The study indicated that amount of mineralised peri-implant bone increases as a consequence of this load when the relatively smooth surface implants were compared with the rough surface implants (TPS implants) after both types were subjected to static loading for 24 weeks. This led the authors to suggest that implant surface characteristics has a major effect on the stress transformation from the implant to the surrounding bone and a rough surface transfers a more favourable stress than that transferred by the relatively smooth surface (Al-Sayyed *et al.* 1994, Gotfredsen *et al.* 2001). Angular bony defects were frequently observed in the machined but not at the TPS implant sites (Gotfredsen *et al.* 2001). Higher levels of mineralizations were observed at the bone-implant interface. Furthermore, a higher percentage of mineralised bone density was observed at the implants with a TPS compared to the machined surface (Gotfredsen *et al.* 2001).

Placement of the polished neck of dental implants under the peri-implant bone was found to be associated with crestal bone loss when compared with a textured neck implant (Wiskott & Belser 1999). The authors suggested that in order to maintain its level, crestal bone must be subjected to suitable levels of mechanical stimulation. It follows that implants with a smooth surface neck may ultimately be associated with crestal bone loss due to its lack of ability to provide adequate biomechanical coupling with the surrounding bone. This was in accordance with clinical observations, which

indicate that crestal bone loss appears to be stopped by threads or textured surfaces (Quirynen *et al.* 1992, Wiskott & Belser 1999).

Barbier and Schepers (1997) used fluorochromes to study peri-implant bone reaction to axial and nonaxial loading in the dog mandible. They used three bone labels; tetracycline, xylenol orange and DCAF. Each bone label was injected three times in one week and a one-week interval was allowed between the successive labels. Barbier and Schepers observed that bone contact with the smooth collar of implant was not maintained after 7 weeks of loading, but decreased to a level just coronal or apical to the coating border.

A "steady state" between the forces acting on the implant and the remodelling capacities of the anchoring bone is required to maintain the rigid implant-bone interface. On the contrary, lacking of this "steady state", may lead to an adverse effect of these forces on the surrounding overloaded bone. This imbalance may explain the excessive marginal bone loss around overloaded implants and probably their loss of osseointegration when implant overload goes beyond a certain limit (Hoshaw e*t al.* 1994a). A long-term clinical study of 467 patients treated with Brånemark implants (Quirynen e*t al.* 1992) indicated that excessive marginal bone loss in the absence of plaque accumulation correlated well with occlusal overloading.

The mechanism of loosening osseointegration by overloading has been explained as a consequence of micro-damage generation in bone when its potential to repair these damages has been exceeded (Frost 1994). The end result is formation of soft tissue between the bone and the implant that ultimately leads to failure of the affected implant. This is consistent with "an increased number of resorption cavities and

newly formed bone tissue which is less mineralised than mature bone" (Hoshaw *et al.* 1994a).

Microdamage is believed to occur at the loaded bone-implant interface and is caused by high strains in bone that are high enough to over come yield and fracture limits for bone (Hoshaw *et al.* 1994a). These authors proposed the following scenario by which the influence of micro-damage on bone modelling and remodelling around overloaded implants was explained: the microdamage generated in the bone around overloaded implants activates a repair response involving bone modelling and remodelling (Mori & Burr 1993, Hoshaw *et al.* 1994a, Verborgt *et al.* 2000, Burr 2002).

Resorptive bone modelling which occurs on damaged periosteal surfaces leads to crestal bone loss. At the same time remodelling occurs at increased levels at damaged intracortical regions. Thus, the modelling occurs and leads to resorption of the damaged periosteal bone via activation of osteoclasts (A) followed by bone resorption R (A-R). Likewise, remodelling activities through the activation of osteoclasts (A) followed by bone resorption (R) and then bone formation (F) (A-R-F activity) is enhanced to restore bone, which is damaged at a more apical location (Hoshaw *et al.* 1994a). Due to this increased remodelling, the cortex should be more porous and less mineralised in the loaded cases compared with the controls. This is consistent with an increased number of resorption cavities and newly formed bone tissue which is less mineralised than mature bone (Hoshaw *et al.* 1994a).

Hoshaw *et al.* (1994a) demonstrated what they believed was evidence of microdamage after implant loading. This damage may stimulate remodelling activities. In their study the small number of detected microdamage may be attributed

to the inability of the used histological technique to detect microdamage and/or to healing of this damage, as the animals were sacrificed 12 weeks after load application.

In an experimental study in monkeys, Ogiso and coworkers (1994) demonstrated that increased occlusal loading of dense apatite implants led to remodelling and thickening of the surrounding bone and intrusion of the opposing teeth. To the contrary, Isidor (1996) found that overloaded osseointegrated implants lost their osseointegration. This discrepancy between the two studies may be due to the differences in the implant materials and to the direction of the occlusal forces. In the latter study the implant material was titanium and the occlusal force was in the lateral rather than in the axial direction (Isidor 1996). The surrounding bone may be strained above the 4000με postulated as the mild overload level beyond which irreversible bone damage could occur (Wiskott & Belser 1999).

Hürzeler *et al.* (1998) histologically evaluated in five monkeys the effect of a repetitive mechanical trauma on peri-implant tissues when it was applied alone and when it was combined with a ligature-induced peri-implantitis. They observed no significant effect of such trauma in both cases following 16 weeks. The contradiction between this study and that conducted by Isidor (1996 and 1997) may be due to the difference in the experimental study period and to the forces applied to induce the trauma. In Isidor's studies the forces were applied in a lateral direction to the implants. However, plaque accumulation around implants may aggravate the negative effect of the excessive occlusal load (Isidor 1996, Oh *et al.* 2002).

Implants with complete loss of osseointegration and those with partial loss of osseointegration as a result of overloading, have marginal bone loss resulting in a narrow zone of fibrous tissue between the implant and surrounding bone (Isidor

1997). The epithelium was found to extend slightly apical to the implant margin rather than covering the whole osseointegrated implant and unless a superimposed plaque-related infection was present marginal soft tissue level remained unaffected (Sanz *et al.* 1991).

An experimental study in a dog, Heitz-Mayfield and co-workers (2004) were not able to observe negative effects of occlusal trauma on osseointegrated implants. The occlusal load was applied for a period of eight months and in the presence of healthy peri-implant mucosa. The results of this study are in direct contrast to those described by Isidor (1996). This contradiction may be attributed to the differences in the animal models (Dogs versus Monkeys) as it is believed that the occlusal forces in monkeys are greater than that in dogs. So it is fair to claim that the two studies are not comparable. Bacterial plaque was also allowed to accumulate around the implant in Isidor's study but not in Heitz-Mayfield *et al.* study which may explain the reported crestal bone loss observed by Isidor (1997).

It is also important to recognize that animal models differ distinctly from one another and may not be representative of human function.

Miyata and associates (1998, 2000, and 2002) conducted a series of experimental studies to investigate the influence of occlusal trauma on the peri-implant tissue in monkeys. In one study, occlusal overload was applied by a superstructure with an excess height of about 100μm (Miyata *et al.* 1998) while plaque control was carried out to maintain a healthy peri-implant tissue. The superstructure was left in place for one to four weeks to provide occlusal trauma. Histopathologic examinations of the peri-implant tissue were performed. They found that occlusal trauma around the implants did not cause peri-implant bone loss. However, when occlusal trauma was

induced by placement of a superstructure similar to that used in the previous study and combined with an experimental inflammation induced by using ligature, peri-implant bone loss was observed. These results suggest that peri-implant bone loss is accelerated when both trauma from occlusion and inflammation in the peri-implant tissues are present.

In another study (Miyata *et al.* 2000) the authors observed peri-implant bone loss when oral hygiene was maintained but the occlusal heights exceeded 180μm, but not when the occlusal heights were 100μm. This may indicate the existence of a critical value of excessive occlusal height on the prosthesis for bone peri-implant bone loss (Oh *et al.* 2002). These results suggest that peri-implant bone loss may occur under severe occlusal overload or under co-existence of inflammation and occlusal overload (Oh *et al.* 2002). However, according to Barbier and Schepers (1997) the bone remodelling rate in animals may be affected by the load direction while an axial loading maintains a lamellar bone and showed a lower remodelling rate when compared with a non-axial one.

In contrast, Vaillancourt *et al.* (1995) reported that the crestal bone loss is not induced by overloading but by bone disuse atrophy as determined by a two-dimensional finite element analysis. In this study dog mandibular premolar regions were modelled with one of two designs of porous-coated dental implants: one fully porous-coated design which had a porous coating covering the entire implant surface, while a partially porous-coated design had a porous coating that covered implant apical two-thirds. The first implant type represented a complete interface bond while the second implant type had a bond in the apical two-thirds. Occlusal forces with axial and transverse components were assumed to act on the implant with interface bonding and effective

force transfer at all porous coat-bone interfaces and no bonding for the non-porous-coated regions. Vaillancourt *et al.* (1995) suggested that 1.6 Mpa stress is sufficient to avoid bone loss due to disuse atrophy in the dog mandibular premolar region. This would reflect a microstrain range of 137-360με which depends on the Young's Modulus of the chosen value (Wiskott & Belser 1999).

A phenomenon known as "stress shielding" is believed to occur in long bone when the bone adjacent to the implant is isufficiently loaded. This is because the implant materials have a higher Young's modulus (stiffer) than bone, thus are more likely to carry a larger portion of the load than would normally be transmitted into the bone (Turner 2004, Scannell & Prendergast 2005). In a recent study using finite element analysis, Scannell and Prendergast (2005) demonstrated that the strain reduction in femoral bones caused bone loss at the periphery (stress shielded area) while bone resorption at the bone-implant interface was caused by damage accumulation.

This phenomenon was also suggested, as one of the causes of crestal bone loss around endosseous implants. At the alveolar bone crest the implant surface is smooth, hence adaptation and bonding may not occur in this area and is said to be protected (shielded) from stress (O'Mahony *et al.* 2001).

Failure of oral implants as a result of occlusal overloading may be attributed to microdamage generation in the bone surrounding the implant which exceeds the repair potential of this bone and leads to the replacement of bone-implant interface with soft tissue. Thus, it may be speculated that if microdamage is generated and bone remodelling is induced to tackle the damage for repair and if there is a positive feedback between damage and remodelling of the peri-implant bone, loss of implant

osseointegration will be the end result of this interrelated response (Trisi & Rebaudi 2002).

Plaque accumulation around dental implants can cause marginal bone loss (Isidor 1996, 1997) and implants with plaque accumulation but without overloading demonstrated a progressive marginal bone loss in monkeys. On the other hand, only the overloaded implants (5 out of 8) were found to de-osseointegrate at 4.5 months to 15.5 months after being overloaded. However, none of the implants with plaque accumulation were found to de-osseointegrate, although an average loss of 1.8 mm in the radiographic bone level was found after 18 months. This may indicate that, the excessive occlusal force is a major reason for this loss of osseointegration.

Other factors such as implant placement method and bone quality may compromise the crestal bone level leading to its resorption. For example, Strietzel *et al.* (2002) found that the osteotome method was not suitable for type 1 and 2 bone.

1.22 Factors affecting bone implant interface status

Several factors have been found to affect bone-implant integration (osseointegration). These factors include: material biocompatibility, surface macrostructure (design) and microstructure (roughness), host bed, surgical technique and loading conditions (Albrektsson *et al.* 1981). Bone reaction to implantation was also found to vary depending on the area being investigated as well as on the time after implantation (Shirakura *et al.* 2003). Available bone volume and bone density are also influencing factors for implant success (Steigenga *et al.* 2003).

Since the body mainly interacts with the surface of the implant several factors that relate to implant surface are suggested to play a major role in implant bone integration. Some of these factors are chemical composition, topography, roughness and surface energy. These properties are highly interrelated and it is not always easy to separate their effects (Gottlander *et al.* 1997).

1.22.1 Material biocompatibility

Biocompatibility is the ability of a material to perform with a suitable response in a specific application and does not indicate total inertness (Equivel-Upshaw 2003). Therefore, reaction of bone peri-implant, which results in formation of osseointegration as described earlier, is a clear indication of material compatibility. Incompatible materials are usually encapsulated by a thick connective tissue and these materials will be eventually rejected by the body. Thickness of proteoglycan found interposed between implant surface and the surrounding bone was related to implant material compatibility (Ellingsen 1991). While a thick proteoglycan layer was

associated with a low compatible implant material a thin proteoglycan layer was associated with a more compatible one (Ellingsen 1991).

The thickness of the proteoglycan layer surrounding the Ti-6Al-4V alloy was in the range of 500 to 1000 Å, while that surrounding the CP titanium was in the range of 200 to 400 Å (Johansson *et al.* 1989). Zirconium demonstrated a thicker collagen-free zone than that found at titanium-bone interface, which may suggest that titanium is more compatible than zirconium (Albrektsson & Jacobsson 1987).

The most commonly used materials in endosseous implants are either bioinert such as commercially pure titanium (CP Titanium) and titanium alloy, or bioactive ceramics such as HA, tricalcium phosphate, tetracalcium phosphate and bioglass (Sykaras *et al.* 2000).

For more than three decades, titanium was the most commonly used material in dental implants due to its biocompatibility, as well as its mechanical and physical properties such as resistance to corrosion, high strength and low weight. Depending on its oxygen content, commercially pure titanium may be categorised into four grades grade one contains the least oxygen while grade four contains the most (0.18% versus 0.4%) (Sykaras *et al.* 2000).

Titanium is a non-noble metal which has the ability to form a very adherent self-repairing and protective surface oxide layer, which prevents further titanium corrosion. This layer forms immediately when the titanium is exposed to oxygen. An oxide layer thickness of 7-10nm before implantation has been reported (Ellingsen 1991). This oxide layer may increase 2 to 3 times after implantation (Larsson 2000). However, Esposito *et al.* (1999) did not observe changes in thickness or compositions of the oxide layer after implantation.

TiO_2 forms the main constituent of this oxide layer, however other oxides such as TiO and Ti_2O_5 may exist too. Incorporation of other chemical elements such as calcium, phosphorus and sulfur into the oxide layer have been reported (Ask *et al.* 1989). Releasing of metallic from the implant surface *in vivo* is minimal due to the protective oxide layer. However, titanium particles were detected in peri-implant bone, regional lymph nodes, as well as in lung, liver, kidney and spleen. These particles could not be detected in the pre-implant bone after a five-month period of implant placement (Schliephake *et al.* 1993). Meanwhile, this increased release of titanium from the implant surface may be associated with increases in the implant surface area (Cooper 2000).

It has been suggested that titanium release may interfere with the normal periimplant bone mineralization and remodelling, which could lead to loosening of the implant (Blumenthal & Cosma 1989). However, when titanium fibres were implanted into the tibia of rabbits and were left for up to one year the titanium concentration in serum and urine was not found to increase when compared with controls (Bianco *et al.* 1996). Nevertheless, it is difficult to conclude that these ions unquestionably come from the implant titanium since they may come from other sources such as food. The effect of such titanium release may be biologically insignificant because of its compatibility and tolerance (Schliephake *et al.* 1993).

Titanium is used in oral implants in a pure form (99.75% pure). It is also used as an alloy (Ti-6-AL-4V alloy) (90% Ti, 6% AL and 4%V). However, titanium is a very active material and is rapidly passivated once exposed to air or water. The latter event results in formation of a layer of titanium oxide, primarily titanium dioxide (TiO_2) but other oxides are also present. This layer is relatively stable and its thickness increases

with time. One of the potential advantages of the oxide layer is its ability to interfere with or reduce titanium ion release (Equivel-Upshaw 2003). Thus, the peri-implant tissue reacts with the oxide layer and not with the titanium substrate per se. An *in vitro* study (Ellingsen 1991), suggested that calcium ions from body fluid are adsorbed to the titanium oxide layer through electrostatic interaction between the negatively charged oxide layer (anions) on the implant surface and positively charged calcium (cations) in the body fluid. This interaction induces a further adsorption of calcium-binding macromolecules proteins (such as albumen) on the implant surface. By this mechanism the non-cellular electro-dense layer of proteoglycan, which was reported to occur between the bone and the titanium implant surface (Albrektsson *et al.* 1983) might bind to the titanium oxide (Ellingsen 1991) through its hydroxyl groups (Albrektsson *et al.* 1983).

Investigations were carried out in rabbits by Galassini *et al.* (1995) to evaluate a possible release of titanium from implants into the tissues and to measure other elements at the bone-implant interface. Preliminary results of this investigation suggested that a minor diffusion of titanium and a possible deposition of calcium and phosphorus on the titanium surface may occur. The latter finding might indicate good biological behaviour of titanium (Galassini *et al.* 1995).

To conclude, titanium release could occur as a result of chemical diffusion, biological processes (i.e. phagocytosis) and mechanical wear of the implant surface (Galassini *et al.* 1995).

Cp titanium and titanium alloys can make up the entire implant or can be used as a substrate to which a coating of bioactive material such as HA is attached. Available literature indicates that cp titanium has a long-term successful performance (> 5

years). This may be due to the ability of cp titanium on the formation of the surface oxide layer, which prevents further titanium corrosion. Intimate contact between the titanium implant surface and the surrounding bone under light microscopy was reported (Albrektsson *et al.* 1981, 1984, Hansson *et al.* 1983) and re-osseointegration of a previously contaminated titanium surface implant was also achieved after the implant surface was treated to remove the contaminant (Kolonidis 2001).

Ceramics are a compound made of a mixture of metals and non-metals. As an example hydroxyapatite (HA) is a calcium phosphate ceramic. During the formation of the ceramics, energy is released giving them a chemically stable structure, which means further spontaneous reactions are unlikely to occur. As a result of this chemical stability, ceramics are considered to be the most inert of all materials. HA is a calcium phosphate ceramic (Sandén 2001). It has been claimed that HA is capable of forming a direct biochemical bond with bone due to its chemical similarity to the natural bone mineral (Thomas 1994, Sandén 2001). HA is found to be more efficient than titanium in absorbing proteins such as vitronectin and fibronectin from human body fluids. This may promote attachment of human mesenchymal stem cells to the HA and consequently their proliferation and differentiation will be facilitated (Kotobuki *et al.* 2005). HA has been used as an implant coating material due to its ability to accelerate bone healing and improve bone apposition around HA-coated implants as compared with uncoated titanium implants, thus better implant-bone integration can be achieved (Weinlaender *et al.* 2006).

It is believed that HA is biocompatible, non-toxic, osteoconductive and capable of providing a strong biomechanical bond with bone (Cook *et al.* 1987, Thomas *et al.* 1987, de Lange & Donath, 1989, de Lange *et al.* 1990) and the active nature of HA

coatings was reported by several investigators (Gross *et al.* 1997, Anselme *et al.* 1997).

According to some authors (Wie *et al.* 1995; Wie *et al.* 1998; Shirakura *et al.* 2003) the mechanism by which bone is formed around titanium and HA-coated implants differs. While bone formed around titanium implants arises by the *distance osteogenesis* process, bone formed around HA-coated implants appears to come simultaneously by both *distance* and *contact osteogenesis* (Wie *et al.* 1995, Wie *et al.*1998).

The bone around the HA-coated implants was found to be more complete and more uniform than that formed around the cp titanium (Wie *et al.*1998). The difference in the bone-implant contact was as low as 28.8% for cpTi, compared with 76.2% for HA-coated implants (Wie *et al.* 1995). The *contact osteogenesis* was attributed to the similarity in crystal and lattice parameters of HA and bone, and this property of HA seems to be found irrespective to the HA-coating method (e.g Plasma-spray or Hot isostatic pressing (HIP) (Wie *et al.* 1998). This difference may also be as a result of the mechanisms by which bone forms around HA-coated implants and cpTi implants as indicated by a demarcation (although it was not specified) found between the two newly formed bone.

Gottlander *et al.* (1997) compared bone formation around plasma-sprayed HA implants with uncoated cp titanium implants after one and six months of implantation in rabbit bone. They reported more bone contact with the coated implants in both healing periods. However, at the six-month healing period the amount of bone inside and/or outside the coated implants showed significantly lower percentages of bone

than around the uncoated ones. This was attributed to HA macrophage-induced resorption.

The difference in bone formation (if it exists) may be as a result of different cellular and tissue responses and to the implant surface character and possibly the animal model.

It has been postulated that pre-osteoblasts in the tissue derived from old bones, which are capable of transformation into osteoblasts, may have been introduced into the HA surface. Owing to the similarity in the crystal structure, a possibly enhanced proliferation and bone formation may have started. The HA surface may thereby have acted as a scaffold for bone formation from the implant toward the bone, thus creating a seemingly epitaxial bone growth (Wie *et al.* 1998). However, using a high power electron microscope a thin (20-100Å) electron dense layer of non-mineralised organic bone materials was detected at the HA-coated implant-bone interface (de Lange *et al.* 1990, Piatteli *et al.* 1993). These materials resembled the lamina limitans of organic bone matrix and was also seen lining of the osteocyte lacunae. This layer was also reported to occur when the implant material was titanium implanted in the rat tibia (Clokie & Warshawsky 1995).

Several studies (Thomas *et al.* 1987, Buser *et al.* 1991, Cook *et al.* 1987, Wong *et al.* 1995, Wie *et al.* 1995, Wie *et al.* 1998) have shown that HA-coated surfaces achieve very intimate bone to implant contact and have been claimed to reduce the healing period (Block *et al.* 1987, Cook *et al.* 1987). Thomas and coworkers (1987) showed that attachment to bone was achieved for HA-coated implants in half the time required for non-coated implants, but this difference diminished over the next ten weeks. Another study in baboons (Carr *et al.* 1997) reported that after a three-month

healing period, plasma spray HA-coated implant gained greater percentages of bone integration than Cp Titanium but bone area did not differ. Nevertheless, in another study and after a six-month healing period, Carr and colleagues (2000) demonstrated that the percentage integration and the bone area of HA-coated implants were similar to the titanium implant. Gottlander and Albrektsson (1991) reported that one year after placement of implants in rabbit tibia, significantly more bone was found to be in contact with the uncoated implants than the coated ones (76% versus 52.6%), while after six weeks, more bone was found to be in contact with the coated ones.

Bioactive ceramics such as HA have poor mechanical properties, which preclude its use in load-bearing situations (Denissen *et al.* 1990, Sandén 2001). Therefore, a combination of good mechanical properties and biocompatibility is required in order to achieve a long term osseointegration. Thus, HA coated implants have been developed to modify the surface of a metallic implant substrate for better implant-tissue integration. Different types of metal have been used as substrates including titanium alloys, cobalt chrome alloys or stainless steel. However, adherence of the HA coating material to the metal substrate is a concern (Denissen *et al.* 1990).

HA is basically applied to the titanium implant surface by one of two methods: plasma spray technique and fabrication of a sintered HA cylinder into which a titanium core is cemented. High bond strength between the HA and the substrate is required to withstand functional stresses and to avoid fragmentation of the coating materials (de Groot *et al.* 1987, Wie *et al.* 1998). However, the risk for HA-coat degradation and loosening (delamination) are still a remaining concern. It was found that HA mechanical failure occurred primarily at the metal substrate-HA irrespective to the implant design (Cook *et al.* 1993a, 1993b).

Although all HA-coatings are not the same (Kim *et al* 1994, Tufekci *et al.* 1997), bone formation on the HA-coated implants was reported to increase by the release of calcium and phosphate ions in the area around the implant as a result of a HA-coat degradation (Daculsi *et al.* 1990). This issue is still debatable.

Completion of the active bone turnover (remodelling) at the implant-bone interface was found to occur at a quicker rate around HA-coated implants than around rough and smooth surface titanium implants (Block *et al.* 1987).

Other investigators (Anselme *et al.* 1997, Chang 1999) reported no effect of these ion releases on the osteoblastic cell adherence to implant surfaces, which were believed to play an essential role in the potential bone formation in the implant-bone interface. For example, Anselme *et al.* (1997) found a relatively low level of cell attachment and growth on HA coating. This may be due to the bioactivity of the HA that rendered the implant surface unstable and prevented the cellular attachment and growth. Cellular attachment requires protein adsorption on to the implant surface.

Although HA has a higher affinity for osteoblasts *in vitro* than does titanium, HA's stability is a very important factor for cellular attachment (Chang *et al.* 1999). It has been speculated that HA has strong adsorptive properties for protein, so that serum proteins are adsorbed to HA and then mediate specific adhesion of osteoblasts. Although Chang and coworkers (1999) did not find significant differences in the percentage of cell attachment among various degrees of crystallinity; they reported a higher level of cell attachment on pre-treated surfaces than on un-treated ones. Using HA as a coating material may reduce mobility of osseointegrated implants and by addition of surface macro-texture (such as grooves, dimples or threads) to HA-coated implants it does not significantly increase interfacial shear strength in mechanical

axial pull out or torsional shear in either the femur or the mandible of dogs. Torsional shear strength of a smooth HA-coated cylindrical implant was significantly greater than grooved HA-coated implants (6.16MPa and 4.61MPa respectively) (CooK *et al.* 199b). The mobility of HA-coated implants, as tested using periotest recorder, was significantly lower than cp titanium and titanium alloy implant irrespective to the implant design (bullet, basket, platform or screw) (Ochi *et al.* 1994).

In a pilot study involving two dogs (Strnad *et al.* 2000) osteoconductivity of sandblasted titanium implants were compared with plasma-sprayed HA-coated implants, which were installed in unfavourable clinical situations (i.e. gaps ranged from zero to 1 mm and a poor primary implant stability). When the implants and their surrounding bone were examined using light microscopy, most of the sand-blasted implant surfaces were found to be encapsulated with a layer of fibrous tissues and only 15% of these surfaces were in direct contact with newly formed bone. On the other hand, 72% of HA plasma sprayed implant surfaces were surrounded with newly formed bone. Furthermore, when the implants were installed in a press-fit fashion the HA-coated implants demonstrated more implant-bone contact than the sand-blasted implants did (79% versus 54%). The *in vitro* part of this pilot study also revealed deposition of calcium phosphate crystals on the surface of HA-coated discs after their exposure to a simulated blood plasma fluid. This deposition was accompanied with a decrease in calcium ions (ca^{++}) and Phosphate ions ($PO3^{-}$) in the simulated blood plasma fluid. In contrast, the sand-blasted titanium was not affected by this exposure. This may indicate the degree of osteoconductivity of pure titanium and HA (Strnad *et al.* 2000). Gottlander and coworkers (1997) found significantly more bone in contact with the HA-coated implants than those in contact with Cp titanium implants (Nobelpharma) in rabbits after a 4-week healing period. However, when the amount

of bone inside the threads was considered, there was no significant difference between the two systems (p= 0.2). In a 24-month healing period, although the same trend was observed, the percentage of bone in the threads revealed a lesser value for HA-coated implants than for titanium ones. This has been attributed to resorption that might be induced by macrophages as a response to loosened HA particles (Gottlander *et al.* 1997).

The substrate surface roughness and implant design may have a detrimental effect on the uniformity of the HA-coating thickness. Unevenness of the coating may cause mismatching between the surgical drill and the outer surface of the implant, which will lead to removal of HA particles if not well attached and/or may cause unnecessary trauma to the bone (Gross *et al.* 1998).

However, there is much controversy concerning the long-term stability of HA coating and the bond between the HA-coating and the substrate (core).

HA is used as a coating attached mechanically or may be chemically to the implant metallic substrate (Gross *et al.* 1998). HA-coating detachment was observed (Cook *et al.* 1993a, Cook *et al.* 1993b) and was more frequently seen on Hot Isostatic Pressing (HIP) implant surfaces than on the HA-plasma-sprayed ones, which may reflect the effect of the coating method (Wie *et al.* 1998).

Bone response to HA may differ according to the bone type. For example, Piattelli *et al.* (1993) used light and conofocal laser scanning microscopy and found that HA resorption on implant surfaces was minimal in areas embedded in cortical bone; where as greater resorption was observed in medullary spaces. The implant surfaces in the medullary space were lined by a fibrous tissue capsule, and in some areas a thin basophilic material was observed adjacent to the HA surface. In some sites, the HA-

coating was absent or detached from the metal surface, dispersed in the extra-cellular fluids, or covered by soft tissue with macrophages.

The amount of the amorphous phase should be reduced in order to increase the longevity of the coat and equally important is the location and distribution of the amorphous phase within the coat. In an *in vitro* study, stability and dissolution of HA-coatings on dental implants were investigated by Gross and coworkers (1997). They reported that both crystalline and amorphous HA coatings underwent degradation by cracking and dissolution after immersion in Ranger's solution (a simulated inflammatory media). Degradation was followed by precipitation of crystalline apatite which modified the coating topography. This change in the surface may influence the initial attachment to the HA surface (Chang *et al.*1999). Crystalline HA, however, is less prone to degradation than amorphous HA (Lemons & Dietsh-Misch 1999). *In vitro*, HA-coat dissolution and possibly its stability is determined by its composition and its surface roughness (Zurita *et al.* 1994).

Elemental exchange between HA-coating and the implant may occur during the plasma spraying procedure (Tufekci *et al.* 1997). Scanning electron microscopy and x-ray energy-dispersive spectroscopy were used to analyse the elemental composition at the coating substrate interface of two commercial plasma-spray HA-coating titanium alloy (Ti-6AL-4V) dental implants. There was no significant difference in the mean coating thickness between the two investigated implants (Bio-Vent and Integral) with coating thickness of 72μm and 71.4μm respectively (Tufekci *et al.* 1997). They found that titanium and aluminium diffused into the coating and calcium diffused into the substrate during the HA attachment coating procedure (Tufekci *et al.* 1997). Accordingly, it has been suggested that the HA-coating should be considered

in two layers, the amorphous outer layer to promote faster bone attachment and the crystalline as an inner layer (adjacent to the substrate) so resorption of the later layer will occur slowly under conditions of bone remodelling (Gross *et al.* 1997).

Roughness, thickness and the crystalline nature of twenty-four commercially available HA-coated implants from four manufacturers were investigated by Kim *et al.* (1994). The thickness of the coatings ranged from 50 to 80 μm. All groups showed cracks and porosity in the HA-coats. They also observed differences in the amount of crystalline phase and coating composition (Kim et *al.* 1994).

Resorption of HA-coating is believed to occur in two ways: biological fluid-mediated and cell-mediated mechanisms. The fluid-mediated resorption results in a corrosion-like dissolution. This dissolution occurs along the grain borders of HA crystals. By this mechanism detachment of HA crystals from the main bulk of coatings occurs. The detached crystals are then engulfed by cells in a phaygocytotic process (Piatteli *et al.* 1993). The degree of HA resorption may be affected by TCP content, its manufacturing method, degree of crystallinity, surface texture (microporosity) and type of bone in which it is located (Piatteli *et al.* 1993b). The microporosity of HA may be due to inclusion of foreign particles within the coating or due to the speed by which the HA particles cool during the coating procedure. The titanium substrate is cold, causing the first layer to

Correlation between the mechanical anchorage values of implant to bone and histomorphometric measurements have been reported (Gotfredsen *et al.* 1995, Wong *et al.* 1995). A good correlation ($r^2 = 0.90$) was found between the average roughness of the implant surface and pushout failure load (Wong *et al.* 1995).

However, Gotfredsen *et al.* (1995) reported a significantly lower removal torque value for machined implants than for TiO_2-blasted implants. HA-coated implants were reported to show superior osseointegration in terms of both push out failure load and surface coverage by bone (Wong *et al.* 1995).

The non-tapping method of implant installment was recommended in order to reduce stress concentration on the bone around the implant. Nevertheless, when either screw type oxide-coated or non-coated titanium alloy implants were tapped more bone apposition percentage was observed than for non-tapped (manually inserted) implants (Satomi *et al.* 1988). Furthermore, no clear difference was observed between coated (74.5%) and non-coated tapped implants (68.4%). The non-tapping approach resulted in formation of connective tissue at the bone implant interface. However, in this study, the implants which were installed by the non-tapping approach were loosely fitting because the implant sites were 0.1 to 0.3 mm larger in diameter than the actual implants (Satomi *et al.* 1988). It was assumed that this interfacial gap was wide enough to be bridged by new bone and adverse connective tissue was formed at the interface. This study involved only two monkeys and eight unloaded implants; four implants in each dog. Two implants were tapped and the other two were not. After a healing period of three months, the area around the implant was histologically evaluated (Satomi *et al.* 1988). In a more recent animal study by the same authors (1990) using HA as a coating material on titanium alloy substrates allowed formation

of bone at the implant-bone interface irrespective to the insertion technique (tapping or non-tapping) and no adverse connective tissue was observed. The implants were coated by means of a modified plasma-spray technique. The HA thickness was approximately 20μm. The histological and histomorphometrical evaluation revealed the consistency of the HA coats and the lack of HA resorption. The results of this study may indicate the biocompatibility and capability of HA materials on enhancement of bone formation at the bone-implant interface.

A positive effect of HA on the amount of new bone formation in simulated bone defects has been reported by Strnad *et al.* (2000). This study concurs well with earlier results from Knox *et al.* (1991) who reported such a positive effect of HA, when used in unfavourable clinical situations such as gaps and/or compromised primary implant stability. Knox *et al.* (1991) concluded that the presence of HA on the implant surface appears to have a positive effect on the amount of bone fill within the defects.

In 1991 Knox and colleagues compared the height and the percentage of direct bone to implant contact in simulated extraction sockets in dogs. The results indicated that gaps larger than 0.5 mm produced a smaller amount of direct bone to implant contact.

In conclusion, the literature indicated the following drawbacks that should be considered when HA is used as coating materials:

- There is no coating technique that provides a titanium surface perfectly covered with pure ceramic.
- Due to inadequate biomechanical stability, detachment of HA coatings from the substrate may occur (Cook *et al.* 1993a, 1993b).
- Detached HA particulates may induce an adverse reaction at the bone-implant interface area.

- HA biodegradation may explain the reported high failure rate of HA-coated implants.
- A HA-coat is a good substrate for bacterial colonisation.
- Success could be predicted when using cp titanium implants than when using HA-coated ones.

1.22.2 Implant design (surface macrostructure)

Implant design is one of three important reported factors on which implant primary stability depends (Martinez *et al.* 2001). Implant primary stability plays a major role in achieving osseointegration (Albrektsson *et al.* 1981, Martinez *et al.* 2001).

In addition to implant design, implant surface roughness, bone quality and quantity and surgical technique are reported to play a major role in implant primary stability (Sennerby & Roos 1998, Martinez *et al.* 2001).

Implant design seems to be of grater importance in soft bone (type 3 and 4) (Lekholm & Zarb 1985) than in the dense one (O'sullivan *et al.* 2000) and this stability in soft bone can be improved by surgical preparation technique as well as by implant design (Siddiqui *et al.* 2001).

The long term success rate of any implant system depends on many factors, implant design plays an essential role in maintenance of osseointegration. A continuous marginal bone loss and high failure rates of cylindrical implants has been reported (Isidor & Kaaber 1988). This bone loss may occur slowly and continuously around cylindrical implants which have no threads. This maybe due to generation of shear

stresses at the bone-implant interface (Misch *et al.* 1999). In contrast, screw-shaped (threaded) implants demonstrate a steady state bone.

Currently, screw-shaped (threaded) implants are the most commonly used implant designs while smooth cylinder implants (press-fit) are eliminated. In an experimental study on dogs screw implants were found to have a better bone anchorage than the cylindrical implants (Gotfredsen *et al.* 1992).

The threads are usually incorporated into the implant design in order to transform destructive forces such as shear forces into more resistant ones at the implant-bone interface (Misch *et al.* 1999, Steigenga *et al.* 2003). They are also used to improve initial stability and increase implant surface area and also to dissipate interfacial stress in a more favourable way. Thread features such as thread depth, thread thickness, face angle, pitch and helix angle are considered as factors that determine the functional thread surface and effect the biomechanical load distribution of the implant (Steigenga *et al.* 2003).

The most commonly cited thread shapes are v-shaped, square shaped or reverse buttress (Misch *et al.* 1999, Steigenga *et al.* 2003, Steigenga *et al.* 2004). The standard v-shaped is comparable to the buttress thread and has 10 times an increase in shear stresses at the implant-bone interface when compared with a square thread (Misch *et al.* 1999).

The v-shaped thread is called a fixture in engineering and is principally not load transfer. The buttress thread shape is optimised for pull loads. The square thread shape is called a power thread. It provides an optimised surface area for intrusive, compressive load transmission, resulting in a lower strain in bone and reduces the shear loading (Misch *et al.* 1999, Steigenga *et al.* 2004). Steigenga *et al.* (2004)

studied effects of implant thread geometry on osseointegration and resistance to reverse torque in tibia of rabbits and reported that the square thread design implants have more bone to implant contact and greater reverse torque measurements compared to the v-shaped and reverse buttress thread designs.

Another thread-type implant design known as Ankylos® (Friadent Gmbh, Mannheim, Germany) is available in the market. According to the designer the theory is based on the difference in the response of the cortical and cancellous bone to functional stress. Ankylos has a rough surface with progressive threads. Both features are aimed at the direction of the functional stresses to the cancellous bone, which is more resilient and has a greater regenerative capacity when damaged (Morris *et al.* 2004).

The thread designs have been extensively investigated and positive results on their long term clinical function have been reported. However, a long term documentation of other implant designs is not available.

Two of Brånemark's implant systems were available in 1987: a self-tapping and conical fixture. The self–tapping was developed to be used in situations when the bone was of low density. The conical one was indicated for an immediate implant placement in fresh extraction sockets. The conical implant has a coronal non-threaded area which will eventually be denuded of bone after unavoidable bone resorption which usually occurs following tooth extraction. This smooth part would facilitate oral hygiene procedure and be less irritating to peri-implant soft tissue (Quirynen *et al.* 1992).

In one study by Quirynen *et al.* (1992) the failure rate of self-tapping fixtures was lower than that of standard Brånemark implant systems before and after loading. This has been attributed to the exceptional primary self-tapping fixtures stability at the time

of implant placement. This primary stability is a function of diameter mismatch between the self-tapping fixture and its bone osteotomy.

It is believed that occlusal forces must be dissipated over a large implant area in order for the bone to be preserved (Lum 1991). However, the importance of implant length is obvious in its initial stability and overall amount of bone in contact with the implant. The length also provides resistance to torque or shear forces when the initial implant stability is assessed (Steigenga *et al*. 2003).

Through the use of engineering statistics, the amount of force transferred to the crestal bone from a horizontal occlusal load, relative to the implant length necessary to support that load, was analyzed for hypothetical instances when the implant was embedded in a uniform mass of bone and when it was bicorticated. The analysis demonstrated that implants longer than 12 mm will not significantly reduce force transfer proportionately to the increased length. The amount of force transferred is directly proportional to the height of load application from the crestal bone (Lum & Osier 1992).

1.22.3 Implant surface texture (topography)

Increasing of implant surface roughness increases surface area of the implant (Wennerburg *et al* 1995, 1996, 1997). Early endosseous integration is important for long-term implant stability particularly in areas with low bone density such as maxillary molar area. Therefore, increasing the rate of early integration is valuable to increase implant success rates in such circumstances. Several methods have been used to alter the implant surface texture in order to facilitate and encourage early osseointegration.

In general, two methods for alteration of implant surface roughness (texture) have been described in the literature. These methods are; additive and subtractive. In the former method, a biocompatible material is added to the implant surface substrate (titanium plasma-sprayed coating) (Klokkevold *et al.* 2001), while in the latter method a material is removed from the implant surface, i.e. by blasting (Wilke *et al.* 1990, Wong *et al.* 1995) and acid etching (Klokkevold *et al.* 1997, Cordioli *et al.* 2000, Klokkevold *et al.* 2001).

Several advantages are believed to be an outcome of increased implant surface roughness (Cooper 2000, Testori *et al.* 2001), which leads to a better wetability and therefore improved cell adhesion to the implant surface. It also exhibits an increase in the strength of the implant-bone bond and also increases the biomechanical interaction of the implant with bone when compared with smooth surfaces.

A series of investigations (Wennerburg *et al.* 1995, 1996, 1998) have shown that implant torque removal was significantly higher for rougher surface implants than it was for relatively smooth (machined) surface implants. Wennerburg and coworkers (1995) reported that after a healing period of 12 weeks in rabbits, a significantly higher removal torque was required to remove implants blasted with 25μm or 75μm particles compared with the torques for the smooth surface implants. The average surface roughness of the implants of this study was 0.88μm, 1.27μm and 0.39μm respectively. However, when the implants were blasted with 25μm or 250μm and installed in rabbits for 4 weeks, there was a significantly less bone-to-implant contact for implants blasted with 250μm than those, which were blasted with 25μm (Wennerburg *et al.* 1996). This may be due to an increase in ion release and reduction in corrosion resistance of the titanium surface as the implant surface area increases by

roughness (Wennerburg *et al.* 1996). Nevertheless, comparison of the same surface treatment after 12 weeks revealed no such difference (wennerburg *et al.* 1995). In another study Wennerburg and coworkers (1997) demonstrated that blasting an implant surface with 25μm or 250μm created surfaces that were more resistant to removal torque than machined surface. Their histomorphometric analyses also revealed a significantly higher bone-to-implant contact for 25μm-blasted implant than smooth ones, 62% versus 50% respectively. On the other hand, when the bone area inside the threads was evaluated (Wennerburg *et al.* 1997), significantly less bone was found in the thread area of blasted implants than of the machined surfaces (42% versus 60% respectively). They stated, "This is a finding of yet unknown implication".

Roughening of cp titanium implant surface can also be achieved by thermal acid etching (Hydrochloric and Sulphuric acid) surface treatment, i.e. dual acid etching. The resulting surface of one of the commercially available implant system (Osseotite®) is characterised by small peaks and valleys with peak-to-peak distances ranges from 1μm to 3μm and peak-to-valley distances that generally ranging from 5μm to 8μm. A series of pits are superimposed onto the peak-and-valley landscape with a range of 1μm to 2μm, which leads to a complex three-dimensional surface texture.

A number of mechanical, histological and clinical studies have evaluated osseointegration of the rough implant surfaces. Furthermore, histomorphometric and removal torque studies with roughened surface have revealed greater bone apposition (Buser *et al.* 1991) and higher removal torque values than implants with smoother surfaces (Cordioli *et al.* 2000, Klokkevold *et al.* 2001).

Klokkevold *et al.* (2001) observed an enhancement of bone-implant interfacial strength when dual acid etched screw-shaped implants (Osseotite®), as measured by resistance to reverse torque removal following a 2 month healing period in the femur of New Zealand white rabbits, were compared to machined-implant surfaces (Klokkevold *et al.* 2001). The mean torque values were 20.50 ± 6.59Ncm for the chemically etched and 4.95 ± 1.61Ncm for the machined implants. These values were lower than that reported by Cordioli *et al.* (2000). The differences have been attributed to differences in the implant size and to structural differences at the bone implantation sites. The latter study (Cordioli *et al.* 2000) may reflect the effect of implant surface treatment on the type of bone formed around implants. For instance, Cordioli *et al.* (2000) observed formation of compact bone along the parts of acid etched-implant surface (Osseotite®) which were previously located in the cancellous bone. However, this was not observed around smooth, blasted- or plasma sprayed-implant surfaces. This may be due to the micro-topographic nature of the acid-etched implant surface (Cordioli *et al.* 2000). Their result also revealed a positive correlation between the percentage of bone-implant contact and the reverse torque removal. However, despite the surface roughness of (osseotite), which was significantly less than those of the plasma-sprayed implant surfaces, the removal torque and bone-implant contact percentage values of the former were higher (Cordioli *et al.* 2000). This was attributed to the micro-topography of the surface obtained by the acid etching method. This was, in part, contradicted by Klokkevold *et al.* (2001) who found that dual acid-etched (Osseotite®) implants had always lower values of torque resistance at all observation times than those of TPS implant surfaces.

These findings (Klokkevold *et al.* 1997) were later confirmed by the same investigating group using the same animal model (Klokkevold *et al.* 2001).

Roughening implant surface by acid etching enhanced the strength of osseointegration as tested by the reverse torque removal. They found that the dual acid-etched implants had 3-4 times greater resistance to reverse torque removal than the machined ones irrespective of the healing period (1, 2, or 3 months). When the dual acid-etched implants were compared with TPSs, the acid-etched ones had lower values than the TPSs at all the observation times.

In an *in vitro* study, Davies (1998) reported that surface complexity as a result of dual acid etching such as the osseotite, improves fibrin attachment to the rough implant surface when compared with smooth implant surfaces. When fibrin is anchored to the implant surface, migrating oseoblasts are able to reach the implant surface and produce bone directly on the implant surface (contact osteogenesis). This phenomenon is illustrated histologically using a dual-surface implant design in a human model comparing the osseotite to a machined surface after 6 months of healing in the posterior maxilla (Lazzara *et al.* 1999). With Osseotite®, it was also possible to reduce the healing period to 8 weeks instead of 12 to 24 weeks, which is recommended for machined implants (Lazzara *et al.* 1998).

One study presented by Gottlow *et al.* (2000) indicated that the Osseotite® surface resulted in a significantly lower bone-to-implant contact and less removal torque when compared with TiUnite® implant system. TiUnite is a type of implant with an oxidized rough surface. Albrektsson *et al.* (2000b) observed that TiUnite implants had a significantly higher bone-to-implant contact and higher removal torque values than machined surface implants in rabbit tibia and femur after a healing period of six weeks.

Human fibroblast and epithelial cell attachment and also proliferation were found to be affected by surface characteristics of titanium *in vitro* (Cochran *et al.* 1994). For instances, surface titanium altered osteoblast proliferation, differentiation, and matrix production when osteoblast-like cells (MG63) were used (Martin *et al.* 1995). On the other hand, Castellani *et al.* (1999), who worked with titanium surfaces of differing roughness exposed to rat bone marrow cells "could not clearly confirm the effect of surface roughness on the proliferation, differentiation and calcification of rat bone marrow". Säuberlich *et al.* (1999) studied human gingival fibroblast on the surface of titanium subjected to different surface treatments and concluded "a marked correlation between the cellular compatibility of the modified titanium and surface modification made did not become apparent".

In vivo studies also created an inconclusive picture of the role of surface texture. For example, Buser *et al.* (1991) placed titanium implants with six different surfaces into metaphyses of the tibiae and femora of miniature pigs for 3 and 6 weeks. Surface treatments of the titanium included electropolishing (E), sandblasting with medium grit acid pickling (hydrofluoric acid/ nitric acid) (SMP), sandblasting with large grit and acid attack with hydrochloric acid/ sulphuric acid (SLA), titanium plasma spray (TPS), and also Hydroxyapatite (HA) flame spraying. These surfaces had not only different roughness, but also different surface composition; the SL surface had some of the grit-blasted particles embedded in the "highly distorted" metal surface. The key finding was that all the implants revealed" direct bone-implant contact" but with differing percentages of bone contact in the cancellous bone. The bone-implant contact was in the SLA and HA cases, with contact percentages of 50% to 60% (SLA) and 60% to 70% (HA). The authors reported that "the extent of the bone-implant interface is positively correlated with an increasing roughness of the implant surface.

Chehroudi *et al.* (1997) worked with titanium-coated epoxy replicas of 19 different micromachined grooved or pitted surfaces in the parietal bones of rats and reported that "surface topography influenced the frequency and amount of bone deposition adjacent to the implants".

Wong and coworkers (1995) examined bone reaction to press-fit cylindrical implants made of three materials and given different surface treatments in trabicular bone sites in knees of mature miniature pigs. After 12 weeks of healing time, (HA) coated implants had the highest push-out loads and the largest surface coverage by bone i.e., a mean of 79.9% versus 38.5% for all metal groups. There was a highly significant correlation ($r^2 = 0.9$) between the average roughness of the implant surface and push-out failure load (Wong *et al.* 1995).

Ericsson *et al.* (1994) studied reactions of peri-implant bone to machined screw-shaped implants and titanium-oxide blasted implants in dog maxillae. At two months, both types of implant had a mean bone to implant contact percentage of about 40% (40.5% for rough surface implants versus 39.4% for the smooth ones). However, at four months the histomorphometric analysis revealed a higher mean percentage of bone to implant contact for the rough surface implants ($p < 0.05$) than that percentage for the machined surface (65.1% ±17.3% versus 42.9%±31.2%). In this study the bone implant contact was expressed as a percentage in the three best consecutive threads on each side of the implant (Ericsson *et al.* 1994).

In contrast with the foregoing studies, other work did not reveal a major effect of roughness in vivo. Jansen *et al.* (1993) tested cylindrical plugs of three different titanium alloys (cp Ti with 0.2 wt% palladium, Ti6Al4V, and titanium-aluminium-iron [Ti-5Al-2.5Fe]) and HA-coated Ti6Al4V alloy in rabbit tibiae for 6 and 16

weeks. The materials did not have identical roughness. After measuring the amount of bone apposition and other aspects of the bone reaction to the implants, the authors noted that "the results demonstrated no marked differences in bony reaction to the different implant materials" and "that HA coatings showed a loss of thickness". Caulier *et al.* (1997) tested the response of "low density" bone to threaded, uncoated, cp Ti implants as well as the same metal plasma-sprayed with three different types of calcium/phosphorus-containing material (fluoroapatite, HA, and heat-treated HA). After implantation times of 3 to 6 months in the maxillae of goats, differences were found between the histomorphometric measurements that were made. The authors found no significant differences" in the bone reaction among the various implant materials" although all coatings showed some decrease in thickness.

Successful long term maintenance of osseointegration is achievable by the ability of the peri-implant bone to respond and adapt to the functional loading throughout continues repair and remodelling. Overloading was proposed to occur when prolonged excessive forces that were imposed on the implant exceeded the ability of the bone-implant interface to withstand and adapt to these forces. This subsequently leads to formation of fibrous tissue between the implant surface and the peri-implant bone (Adell *et al.* 1981).

Long term retrospective and longitudinal studies have provided strong evidence to support high survival rates of osseointegrated implant (Adell *et al.* 1981, Albrektsson *et al.* 1988). However, despite the high survival rates, implant failures do occur. Consequently, implant failures were characterised into two classes: early and late failure. While early failure indicates that failure occurs before the implant is put to function, the late failure denotes the failure that occurs months or even years after implant loading. The early failure indicates failure to establishment of

osseointegration and in the late failure osseointegration occurred but later deteriorated and leads to failure (Esposito *et al*. 1998a, Esposito *et al*. 1998b).

Chapter 2. Generation of microdamage around endosseous implants

2.1 Introduction

In general, microdamage occurs naturally in bone due to overloading during day-to-day activities. It can also be produced experimentally by cyclic loading (Forwood & Parker 1989, Huja *et al.* 1999a, Huja *et al.* 1999b, Lee *et al.* 2002, Noble 2003). Microdamage generation in bone has been attributed to plastic deformation and shear failure (Chamay 1970). The microdamage can be seen histologically as cracks and as diffusely stained areas (Boyce *et al.* 1998). The former type is known as a linear microcrack while the latter one is denoted as diffuse damage.

It is believed that this microdamage can activate bone remodelling and repair (Burr *et al.* 1985, Mori & Burr 1993, Bentolila *et al.*1998, Verborgt *et al.* 2000, Lee *et al.* 2002), although the mechanism for this appears unclear. Bentolila *et al.* (1998) presented strong evidence that microcracks cause the activation of intracortical remodelling in rat ulnae that do not normally have such remodelling activities.

There is a general agreement that, when microdamage occurs at a slow rate bone remodelling has the ability to repair the damage. This type of remodelling which specifically occurs to remove the microdamage is known as a targeted remodelling (Parfitt 2002, Verborgt *et al.* 2000, Burr 2002). Nevertheless, if the damage accumulates at a faster rate than repair, microdamage accumulates and weakens the bone and consequently could lead to a stress fracture. On the other hand, if the damage accumulates at normal rate but the bone's repair capacity is diminished, fragility fractures occur (O'Brien *et al.*2003, O'Brien *et al.* 2005).

Bone activity subsequent to implant placement requires both bone modelling and remodelling (Roberts1988, Berglundh *et al.* 2003, Abrahamsson *et al.* 2004). After implant placement the

remodelling activity is greatest adjacent to the implant (within 1 mm) and substantially decreases with increasing distance from the implant-bone interface (Garetto *et al.* 1995). This phenomenon seems to occur irrespective of implant design. This elevation in remodelling activity has been attributed to several factors including the local biomechanical environment, material biocompatibility and host response (Garetto *et al.* 1995). The local biomechanical environment of the bone-implant interface may require continuous remodelling to avoid fatigue fracture. Results from a finite elements model assessing the bone-implant environment indicated that the region within 1 mm of the implant surface displayed a persistent marked change in mechanical stress distribution resulting in both elevated stress levels and stress gradients (Chen *et al.* 1993, Chen *et al.* 1994, Chen *et al.* 1995, Chen *et al.* 1999). This pattern of stress distribution is not caused by occlusal loading of the implant but apparently results from implant placement.

Generation of bone damage as well as an increase in remodelling activity around endosseous implants has been reported. This remodelling activity may be induced by the generated bone damage generated. It is reasonable to investigate the generation of bone damage surrounding endosseous implants as well as the remodelling activity to find out the association between them.

It is the aim of the first study to examine the occurrence of microdamage (microcracks) as a result of osteotomy preparation and/or insertion of endosseous screw-shaped titanium implants.

2.2 Materials and methods

2.2.1 Experimental animals

The protocol followed was in accordance with the animal research policies of the Department of Health and Children in Ireland.

Four beagle dogs; about two years old and weighing approximately 16 kg were included in the study.

The mandibular premolar regions of the four dogs were used for the study. Food was withheld for 12 hours prior to each procedure. The animals were pre-medicated 30 minutes pre-operatively with 0.1mg/kg of acetyl promazine by subcutaneous injection. Anaesthetic induction was achieved with phenobarbitone 25mg/kg intravenously, an endotracheal tube was inserted, and anesthesia was maintained with halothane and oxygen. A local anaesthetic (Lignospan special® (Lidocaine Hydrochloride 2% and epinephrine 1:80000) (Septodont; Cidex, France) was administrated to areas undergoing surgery for analgesia and to aid in haemostasis.

The lower premolars (P_1, P_2, P_3, and P_4) were extracted on each side of the mandible and the bony prominences were trimmed using a large round bur to facilitate healing. The surgical sites were sutured and the dogs were allowed to recover from the anaesthetic. They were reinstalled in kennels, where they were kept for a healing period of three months. The sutures were removed after one week.

Following the three months healing period, general anaesthesia was again administered as described earlier. An incision was made at the crest of the lower ridges from the distal surface of the canine to the mesial surface of the first molar of each side. Full thickness buccal and lingual mucoperiosteal flaps were reflected to a level approximating the lower border of the mandible. The neurovascular bundles from both mental foramina were identified and protected. Figure 2.1 shows one of the experiment site.

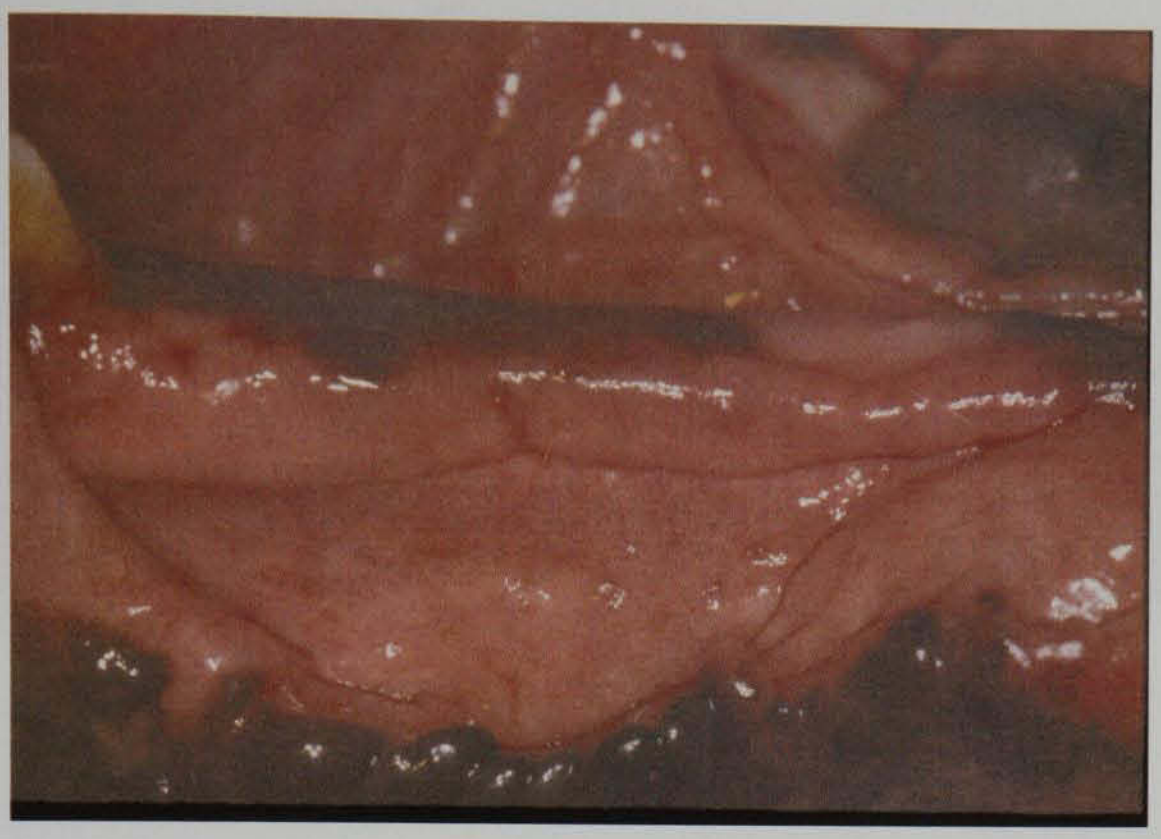

Figure 2.1 One of the experiment sites

Nobel Biocare machined implants, 3.75mm diameter and 10mm length (Fixture MK III ∅ 3.75 x 10 mm RP, star grip, Nobel Biocare®), were used in the study. The implants were installed according to the manufacturer's instructions. Four implant sites were prepared in the edentulous area of each mandible on each side. All implant sites were a minimum of 5mm apart. The osteotomies were initiated using a guide drill and saline irrigation and then were further enlarged with a 2mm twist drill and a 2/3mm pilot drill. In the case of groups I and III (see below) the final enlargement was made with a 3-mm twist drill while in groups II and IV the sites were further tapped using a screw tap of 3mm diameter (Figure 2.2, 2.3, 2.4 and 2.5). The screw tap matched the diameter of the implant; 3.75mm.

Figure 2.2. Four osteotomy preparations

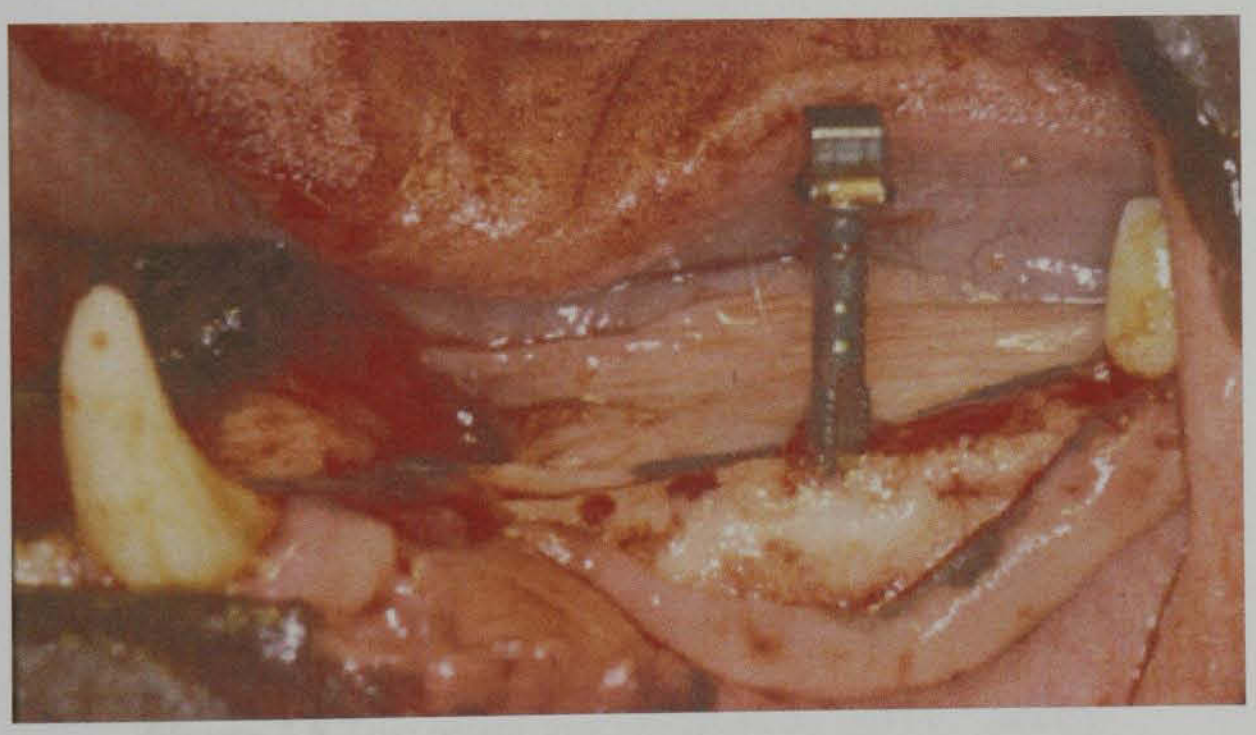

Figure 2.3 An illustration of the tap

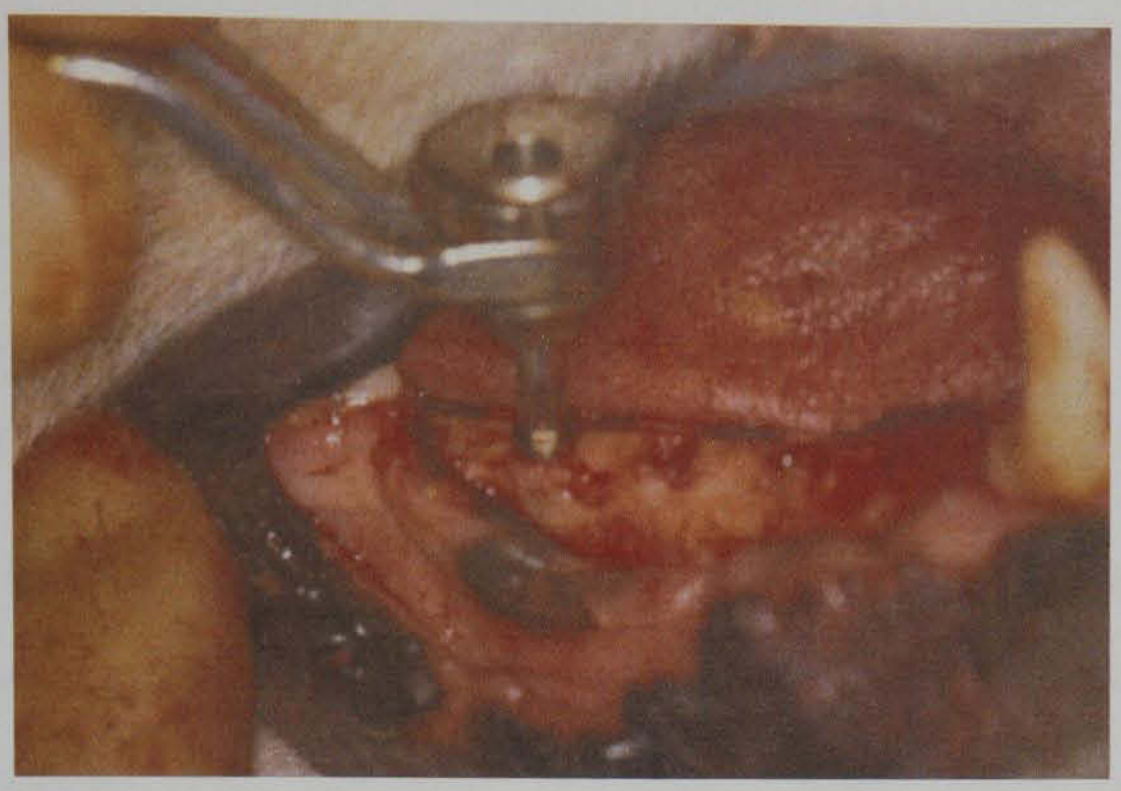

Figure 2.4 Implant placement

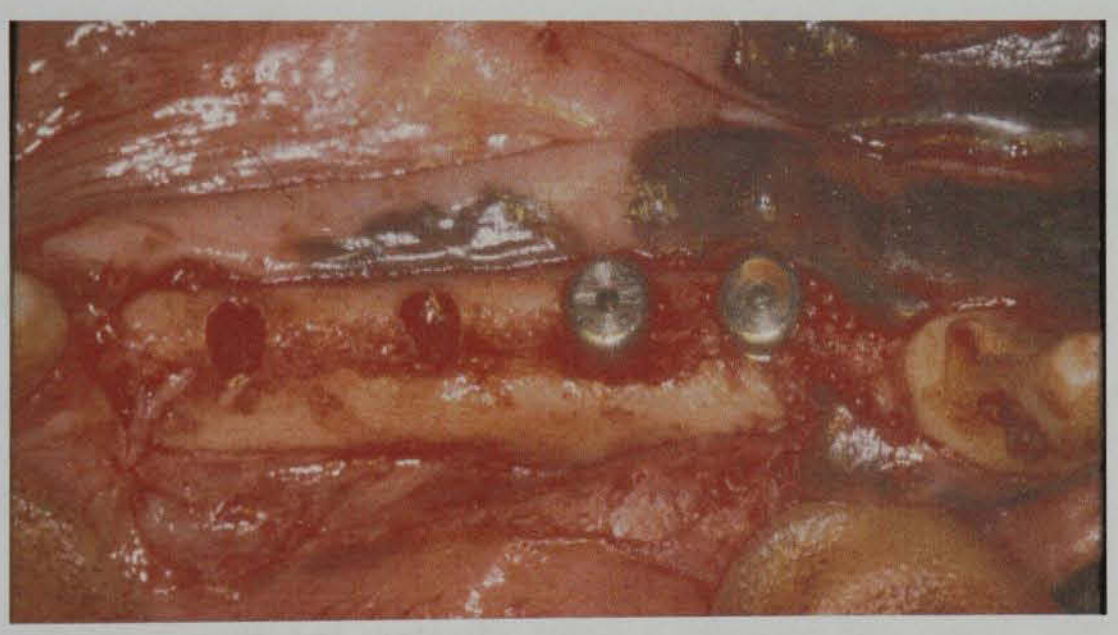

Figure 2.5 Two osteotomy preparations and two implants

The sites were divided into four experimental groups as following:

Group I: included sites that contained an osteotomy preparation only (no tapping or implant placement)

Group II: included sites that contained an osteotomy preparation and were tapped but did not receive any implant

Group III: included sites that contained an osteotomy preparation and were not tapped but received an implant

Group IV: included sites that contained an osteotomy preparation and were tapped before implant placement.

The sites were rotated to get an even balance throughout the four dogs (Table 2.1).

The flaps on both sides were then sutured by using 3.0 black silk interrupted sutures and complete wound closure was achieved. Immediately after the surgical procedure a single intravenous injection of oxytetracycline (50 mg/Kg) [Aldrich Chemical Company, Inc., Milwaukee, WI, USA] was administered to each dog.

Two days after implant placement the animals were sacrificed by an intravenous injection of 200 mg/kg of phenobarbitone. Each mandible was then sectioned at the mandibular body between the first and the second molar of the right and the left sides using a disc (Superflex®, Edenta AG, Switzerland) mounted in a straight hand piece at 100 round per second using water as a coolant. The right and left side were separated at the symphysis between the two central incisors using a scalpel with a number 15 blade.

The mandible was also sectioned vertically using a diamond saw which was mounted on a Minitom® cutting tool (Struers, Copenhagen, Denmark) to obtain four blocks from each side (Figure 2.1). Each block contained the implant and/ or the osteotomy area and about 3 mm of the surrounding bone mesially and distally (group I and II) and (group III and IV). The blocks were then rinsed in running water and stored in 90% ethanol (Aldrich Chemical Company, Inc., Milwaukee, WI, USA) until the embedding procedure.

Table 2.1 experimental group distributions according to dog sides and implant site

		Implant site			
Dog's Number	Dog' side	1st Pre-molar	2nd Pre-molar	3rd Pre-molar	4th Pre-molar
Dog 1	Left	Group I	Group II	Group III	Group IV
	Right	Group II	Group III	Group IV	Group I
Dog 2	Left	Group III	Group IV	Group I	Group II
	Right	Group IV	Group I	Group II	Group III
Dog 3	Left	Group I	Group II	Group III	Group IV
	Right	Group II	Group III	Group IV	Group I
Dog 4	Left	Group II	Group III	Group IV	Group I
	Right	Group III	Group IV	Group I	Group II

2.2.2 Dehydration and embedding procedures

The dehydration and the embedding procedures are in accordance with the protocol used at the Royal College of Surgeons in Ireland (RCSI) and it was described in details by O'Brien (2000) and O'Reilly (2002).

2.2.2.1 Dehydration procedure

Before embedding, a block of bone containing the implant and or the osteotomy preparation and about two millimetre of its surrounding bone was obtained for each experimental site. The soft tissue surrounding the mandibular bone was completely removed using a scalpel with a number 15 blade. The bone specimens were then dehydrated. Each specimen was first completely immersed in a vial containing 80% ethanol for four days. The 80% ethanol

solution was then changed with 95% and 100% ethanol respectively for one day each. A fresh solution of 100% ethanol was used for one more day. Finally, the specimens were immersed in acetone for two days.

2.2.2.2 Embedding procedure

Each side of the mandible was separately embedded in a methylmethacrylate polymer (MMA) (Sigma-Aldrich). The MMA consisted of a monomer (pure methylmethacrylate), a softener (dibutyl phthalate) and a catalyst (benzoyl peroxide). The softener was added to the monomer to avoid brittleness of the finished polymer while the catalyst causes the solution to polymerise when the temperature is increased. The solution was made up using the following protocol (O'Brien 2000): methylmethacrylate 200ml, dibutyl phthalate 50 ml and benzoyl peroxide 7g. Each mandibular block was placed in a separate vial and infiltrated with the MMA solution at room temperature and in a vacuum desiccator (50 mm Hg) over a period of three days. The polymer was changed with a fresh MMA solution every day. They were then placed into an oven at 55°C for four days to polymerise.

2.2.3 Preparation of ground sections

1. In order to obtain three sections of 150-200μm thickness from each experimental site, the embedded blocks were mounted on a diamond saw (Minitom®, Struers, Copenhagen, Denmark) to obtain an approximately a thickness of 300μm (Figure 2.6). The implant sites were oriented so that the diamond saw was parallel to the experiment site and perpendicular to the body of the mandible. The cuts were made vertically through the centre of the experiment sites. Three sections (of 300 μm thickness) were obtained; one in the centre, one mesial to and one distal to the central specimen (Figure 2.7).

Another piece of carbide paper was wrapped around a glass slide and the section was manually ground down under running water.

3. The thickness was checked regularly using a micrometer screw until a thickness of 150-200 μm was obtained.
4. Specimens were washed using tap water and then placed in a test tube and washed with distilled water.
5. Specimens were then dried using tissue paper and mounted on glass slides using mounting medium DPX® (Eukitt's mounting medium, Germany) under a glass cover slip.

One implant site (group I) was accidentally fractured. Only two sections were obtained from group II from one dog and one section from another dog represented group III. So, eighty nine sections were obtained to represent the experimental sites. Control sites were randomly selected from different mandibular sites (Group V).

Figure 2.6 The minitom® machine

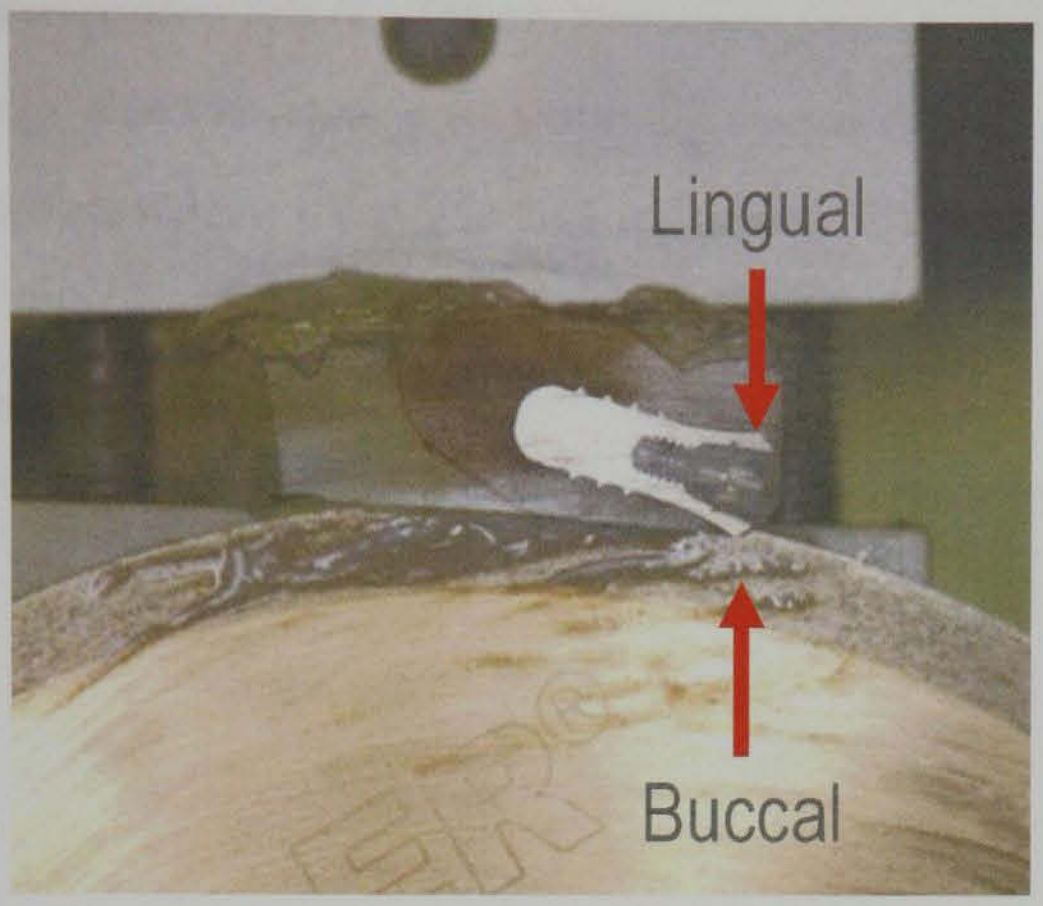

Figure 2.7 An embedded implant and its surrounding bone mounted on the minitom® machine.

2.2.4 Histological examination of ground sections

The ground sections represented the buccal and lingual cortical bone that surrounded the implant sites and were examined using epifluorescence microscopy. Candidate microcracks were identified using modified criteria obtained from the criteria that were originally used for identification of microcracks stained with fuchsin (Burr & Stafford 1990, Lee1997, O'Brien 2000, O'Brien *et al.* 2000, O'Reilly 2002, Lee *et al.* 2003) (Table 2.2) and then later it was refined to be used with chelating agents (Lee1997, O'Reilly 2002).

Table 2.2 Criteria for the identification of microcracks

1. Fluorescent green incident light (λ = 546nm): Microcracks should be intermediate in size, being larger than canaliculi but smaller than vascular channels.
2. Epifluorescence microscopy- UV (λ = 365nm), and green (λ = 546nm) incident light at X100 magnification: Candidate microcracks should be stained through the depth of the section

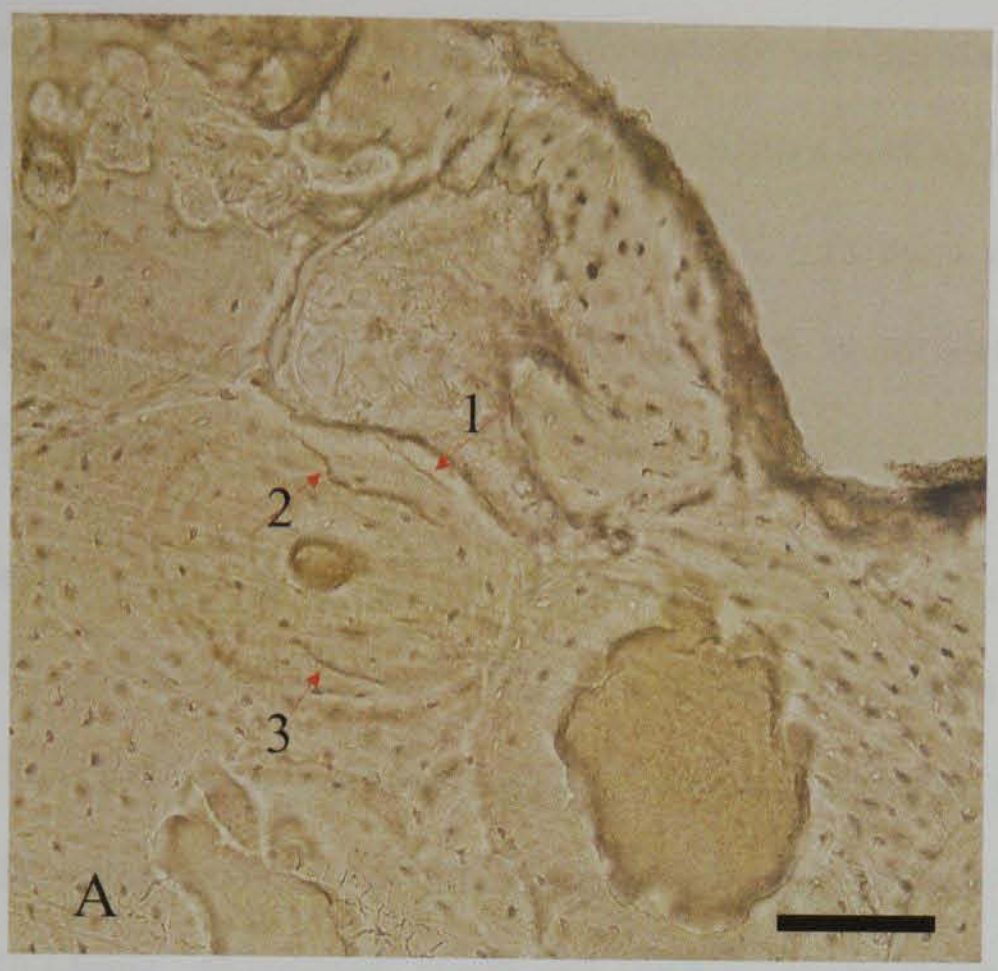

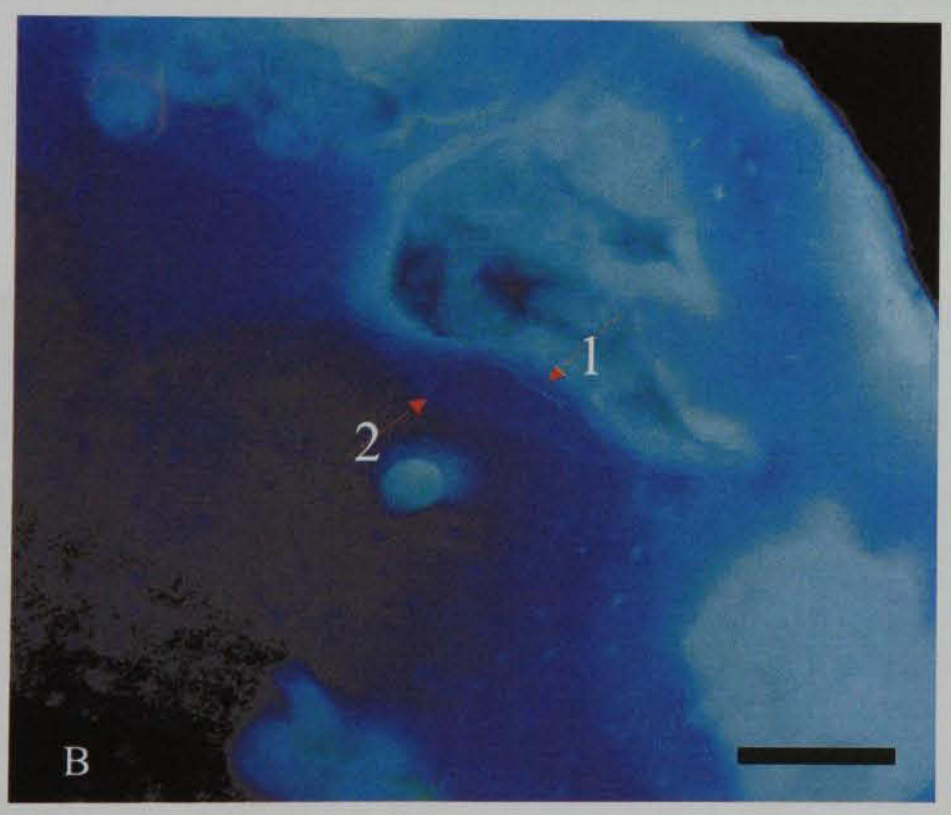

Figure 2.8 Three microcracks can be seen under transmitted light microscope (A) but only two can be seen using epifluorescent microscope and UV incident light (B); one is stained through the depth of the section (1) while the other is partially stained (2). Microcrack no. 1 is brighter than microcrack no.2. Magnification X100. Scale bar = 50μm.

An area in the cortical bone surrounding each experiment site was examined and microcracks recorded. About a 200μm zone in close contact with the implant surface, an area between the thread peaks (interthread) and about 200μm adjacent to the periostium were not examined owing to their intense staining with oxytetracycline that made identification of microcracks difficult (Figure 2.9 and 2.10).

Each glass slide was examined using epifluorescence microscopy (Olympus Optical Co., Ltd, London EC1Y, United Kingdom) under UV (λ = 365nm) and green incident light at magnification of X100 and then confirmed at X200. Microcrack images were captured and transferred to a PC using an Olympus® CCD camera (Olympus Optical Co., Ltd, London EC1Y, United Kingdom). Microcrack length and number of microcracks were measured, tabulated and then compared for different treatment modalities and experiment sites.

Figure 2.9 Oxytetracycline diffuse stained area (Black arrows) and one microcrack (Red arrow) examined using epifluorescent microscopy using UV light (365 nm). A white arrow indicates the implant. Scale bar = 50μm.

The resultant data were expressed as the mean ± standard deviation. Total number and length of microcracks for each side were compared (left vs. right) using unpaired Student's *t*-test. One-way analysis of variance (ANOVA) was used to test significant differences in the number and length of microcracks when the slide numbers, regions and treatment modalities were compared. Differences between group means were considered significant at a level of $p< 0.05$. Where there was a difference in mean number of microcracks, *Dunnett's post hoc* test was used to verify this difference.

It was planned to obtain 3 specimens from each experimental site in order to get ninety-six slides. However, due to technical difficulties some specimens were unsuitable for examination. Therefore, group I was represented by 21 slides. Eighteen slides were obtained from sites that represented group II. Group III was represented by 22 slides and IV by 21 slides. The control group (group V) was represented by 10 slides. The number of slides per each group is shown in Table 2.3.

All measurements were carried out by one investigator. Intra-examiner reproducibility was not carried out which may have been a weak point in the reported results. Also bias could have been introduced and false positive and/or false negative could not have been eliminated.

Table 2.3 Number of slides obtained for each treatment modality

Test Groups	**Number of slides**
Group I	21
Group II	18
Group III	22
Group IV	21
Group V (Control)	10
Total	**92**

There were diffuse stained areas along bone forming the osteotomy walls and extending for a few microns away from the osteotomy walls (Figure 2.9). These areas were produced as a result of the surgical procedure and the various types of the treatment modalities. This type of damage was defined as contact damage generated as a result of the osteotomy preparation and/ or implant placement. The nature of contact damage (seen as diffuse stained areas) precludes detection of individual microcracks and requires viewing by electron microscopy to find out if these areas are actually diffuse damages. However, because the bone label (oxytetracycline) was found to bind to the calcium ions lining the microcrack wall, they were considered as a type of diffuse damage (Figure 2.9). Linear microcracks were found in the four treatment modalities as well as in the control group (Figure 2.9 and 2.10).

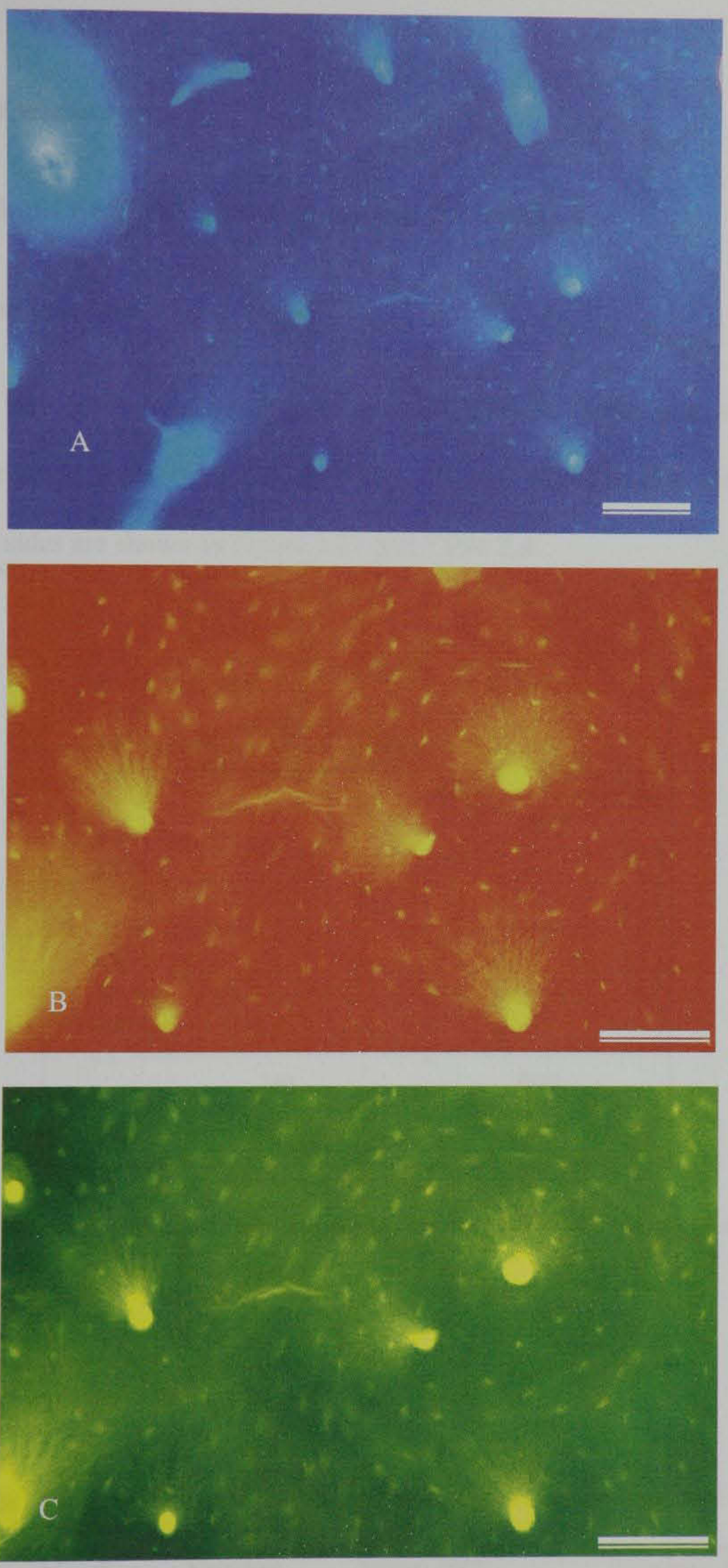

Figure 2.10 Oxytetracycline stained microcracks viewed with (**A**) UV (365 nm), (**B**) green (546 nm) and (**C**) blue incident light (450nm). Scale Bar =100μm.

2.3 Results

2.3.1 Number of microcracks

2.3.1.1 Comparisons when the control group was not included

2.3.1.1.1 Effect of jaw side

The right side had fewer microcracks on average and the difference was regarded as statistically significant (t-test = 1.973, p=0.05). Descriptive statistics for the difference between the jaw sides are shown in Figure 2.11 and Table 2.4.

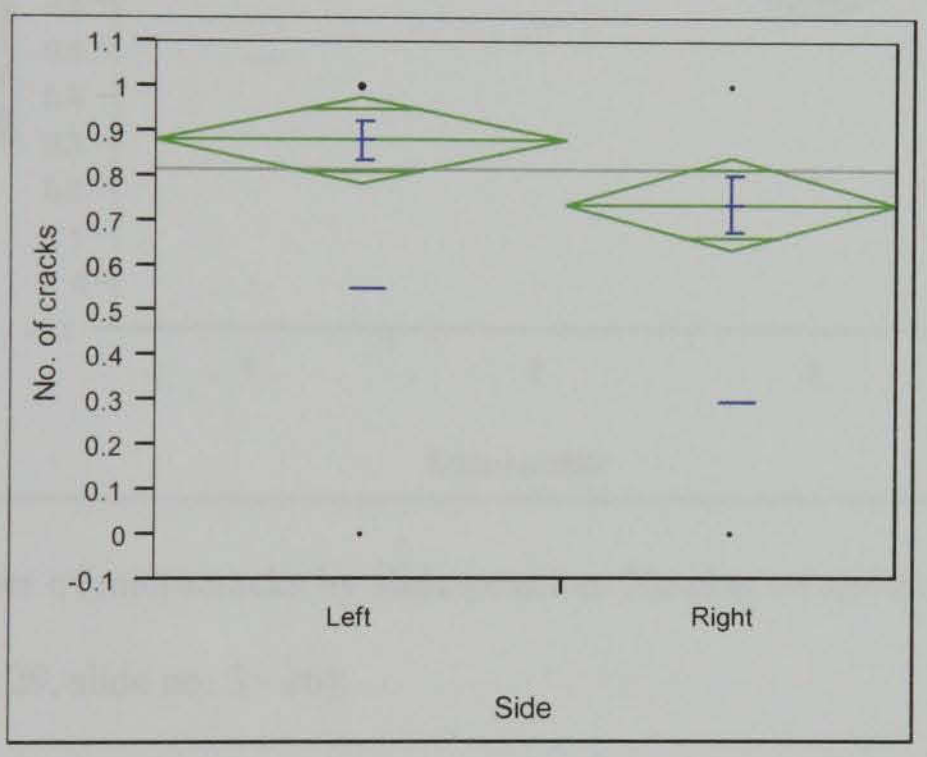

Figure 2.11 Mean and standard deviation of microcracks per side. Number of slides examined slides (left side 43, right side 39).

Table 2.4 Number of microcracks for jaw sides, mean, standard deviation and standard error.

Jaw side	Number of slides	Number	Mean (SD)	Standard Errors
Left	43	65	0.88 (0.33)	0.048
Right	39	53	0.74 (0.45)	0.054

2.3.1.1.2 Effect of slide position

Although position 3 (the distal one) tends to have fewer microcracks on average, the differences were not statistically significant (F= 2.564, p=0.08).

Descriptive statistics for the difference in microcrack number between the three specimens are shown in Figure 2.12 and Table 2.5.

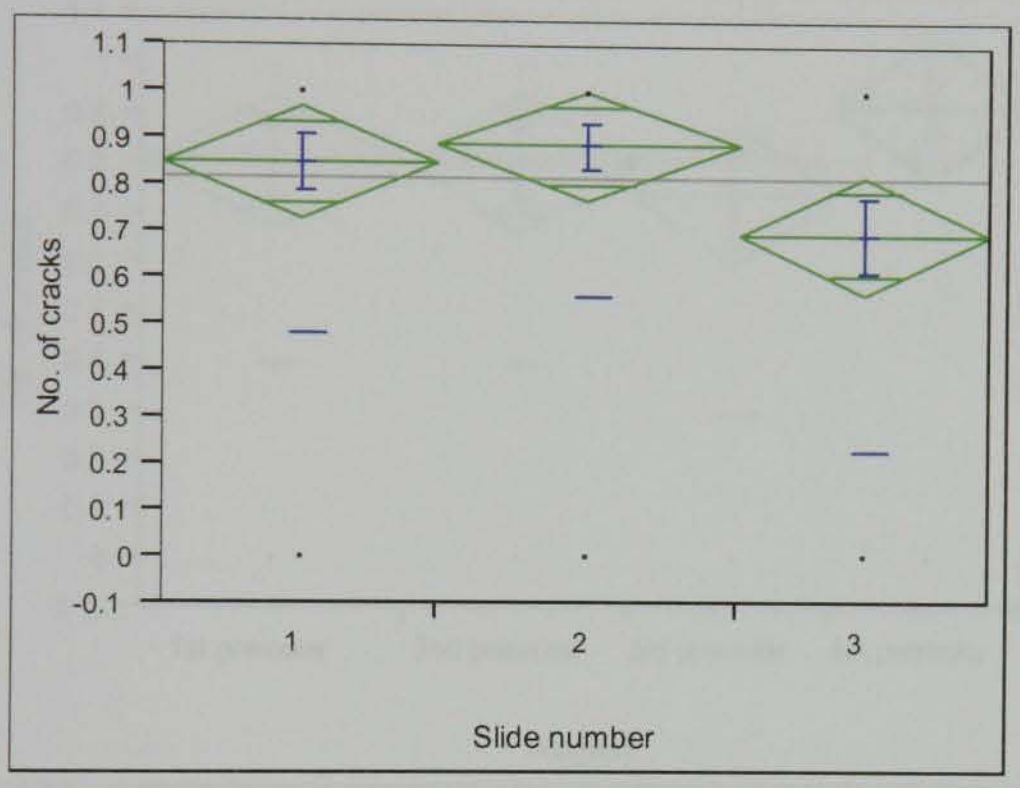

Figure 2.12 Number of microcracks by slide position. Number of slides examined (slide no. 1 = 27, slide no. 2= 29, slide no. 3= 26).

Table 2.5 Number of microcracks, means and standard deviation by slide position

Slide number	Number of slides	Number of microcracks	Mean (SD)
Mesial (1)	27	39	0.846 (0.366)
Middle (2)	29	43	0.883 (0.324)
Distal (3)	26	36	0.694 (0.467)

2.3.1.1.3 Effect of jaw region

The 4th premolar region had the highest number of microcracks while the 3rd premolar region had the lowest, however, the differences across regions were not statistically significant (F= 1.018, p=0.388). The difference in microcrack number between the regions is shown in Figure 2.13 and Table 2.6.

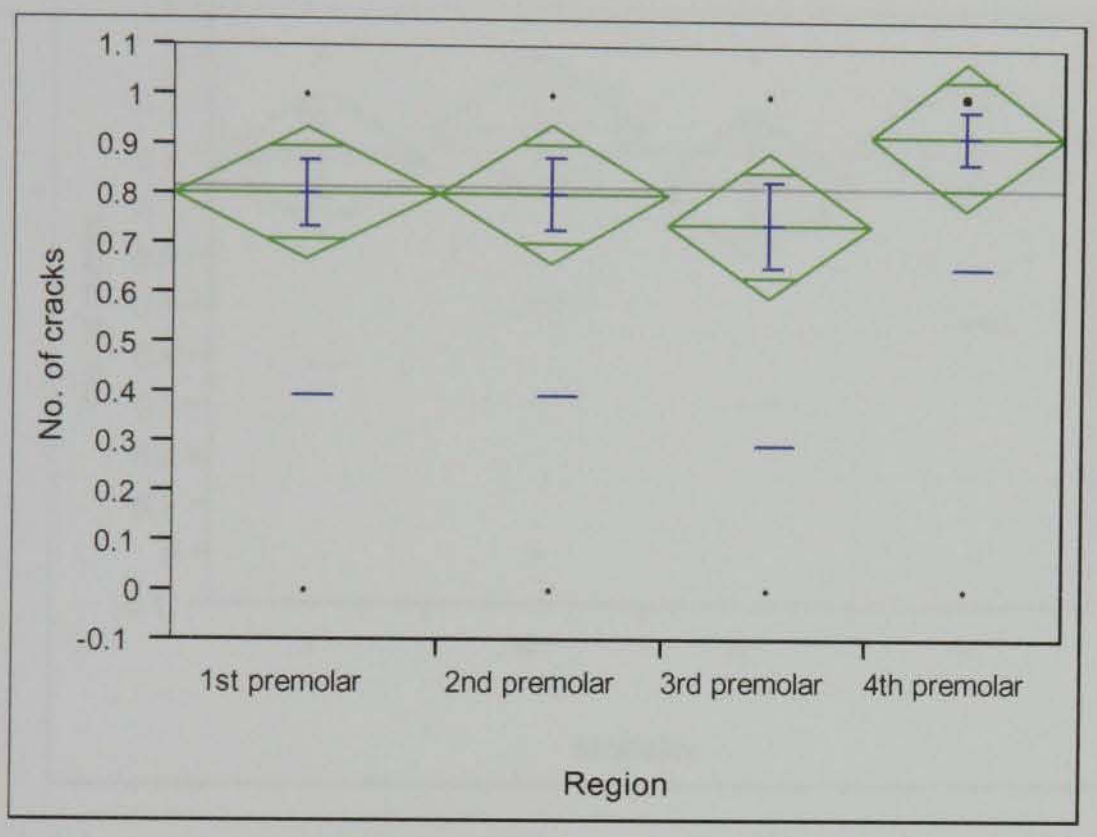

Figure 2.13 Number of microcracks for each site. Number of slides examined (1st premolar = 19, 2nd premolar = 22, 3rd premolar = 20, 4th premolar =21).

Table 2.6 Number of microcracks for each region, mean, standard deviations and standard errors

Regions	Number of slides	microcracks	Mean (SD)	Standard Error
1st premolar	19	35	0.80 (0.41)	0.07
2nd premolar	22	30	0.80 (0.41)	0.07
3rd premolar	20	27	0.74 (0.45)	0.08
4th premolar	21	26	0.92 (0.27)	0.08

2.3.1.1.4 Effect of treatment modality

Modality IV tends to have a higher number of microcracks on average but the difference across modalities was not statistically significant (F= 0.49, p= 0.698) (Figure 2.14 and Table 2.7).

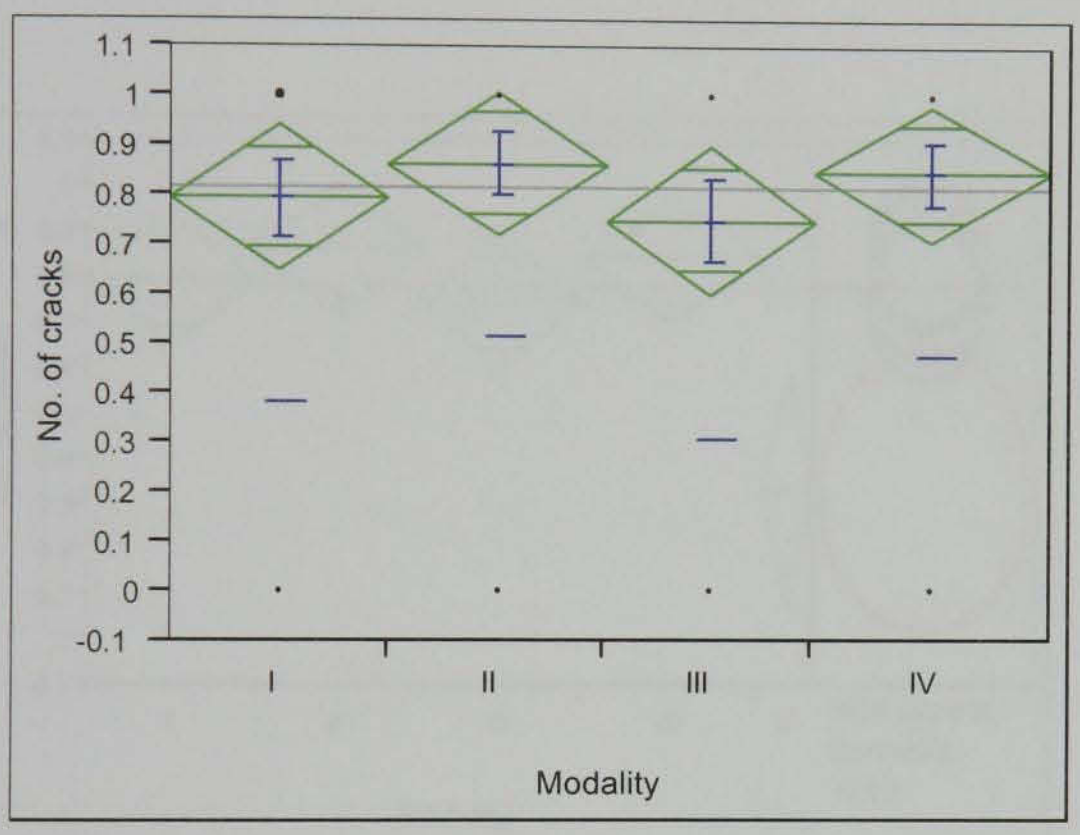

Figure 2.14 Number of microcracks by modality. Number of slides examined (modality I= 21, modality II= 18, modality III= 22, modality IV= 21).

Table 2.7 Number of microcracks for each treatment modality, mean, standard deviation and standard error

Treatment Modality	Number of slides	Number	Mean (SD)	Standard Error
I	21	29	0.793 (0.412)	0.073
II	18	29	0.862 (0.351)	0.074
III	22	28	0.750 (0.441)	0.073
IV	21	32	0.844 (0.369)	0.069

2.3.1.2 Comparison with the control group

The data were pooled and compared with the control. The control group (V) had significantly fewer microcracks compared to the modalities I –IV (F= 3.335, p =0.0125). On comparison with the control group using *Dunnett's post hoc* test, the number of microcracks obtained in the various treatment modalities was significantly different from those obtained in the control group (Figure 2.15).

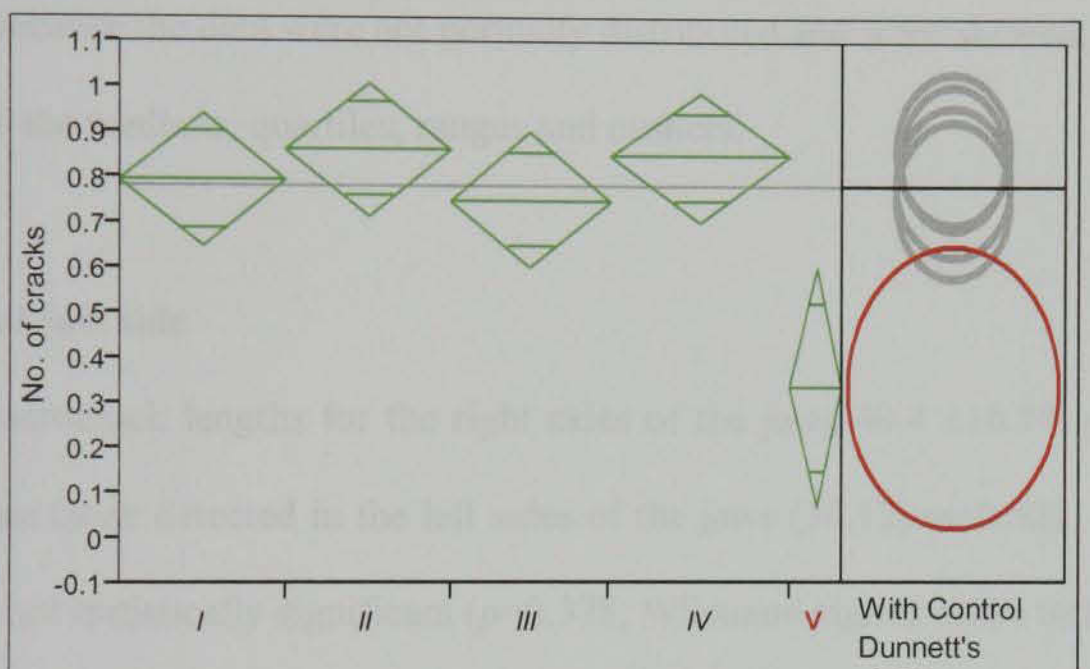

Figure 2.15 The gross number of microcracks by modality and control. Number of slides examined (modality I= 21, modality II= 18, modality III= 22, modality IV= 21, modality V= 10).

2.3.2 Microcrack lengths

Objectives: To determine if the jaw sides, regions and treatment modalities affect the microcrack lengths.

Null Hypothesis #1: There is no difference in microcrack lengths between the jaw sides.

Null Hypothesis #2: There is no difference in microcrack lengths obtained by the different modalities.

Null Hypothesis #3: There is no difference in microcrack lengths obtained from the different jaw regions

Null Hypothesis #4: There is no difference in microcrack lengths obtained by the different modalities and the control group.

Box plots were used to compare between microcracks detected in the jaw sides, by different treatment modalities, the slide number and the comparison with the control group. The box plot was used because the data were not normally distributed and were skewed.

Box plots show the medians, quartiles, ranges and outliers.

2.3.2.1 Effect of jaw side

The average microcrack lengths for the right sides of the jaws 40.4 ±16.79 μm (mean±SD) were longer than those detected in the left sides of the jaws (36.12μm±9.82). However, this difference was not statistically significant (p=0.378, Wilcoxon signed ranks test).

A box plot illustrating the microcrack lengths of the two jaw sides is presented in Figure 2.16.

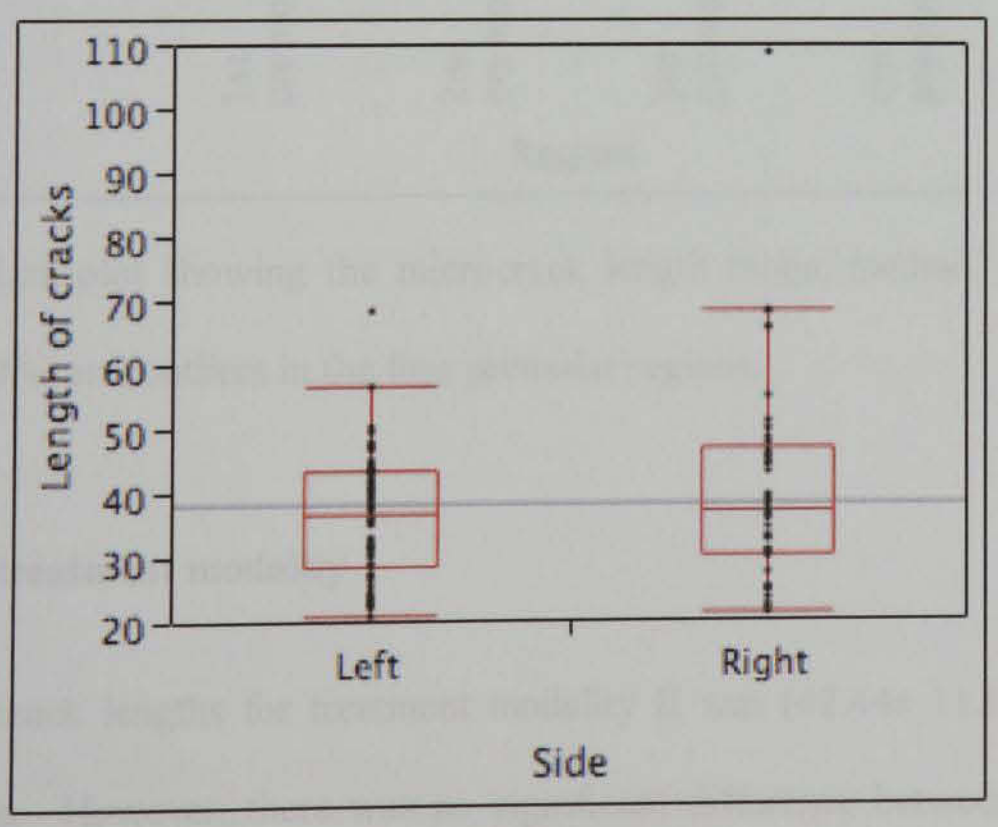

Figure 2.16 A box plot showing the microcrack length range, median, percentiles (10%, 25%, 75% and 90%) and outliers by the jaw sides.

2.3.2.2 Effect of jaw region

On average the microcracks detected in the 2nd premolar region (39.56± 18.45μm) were longer than the other microcracks that were detected in the 1st, 3rd and 4th premolar regions (37, 38.77 and 35.25 respectively). However, the difference was not statistically significant (p=0.637).

The length of microcrack range, median, percentiles (10%, 25%, 75% and 90%) and outliers obtained by the four premolar regions are displayed in Figure 2.17.

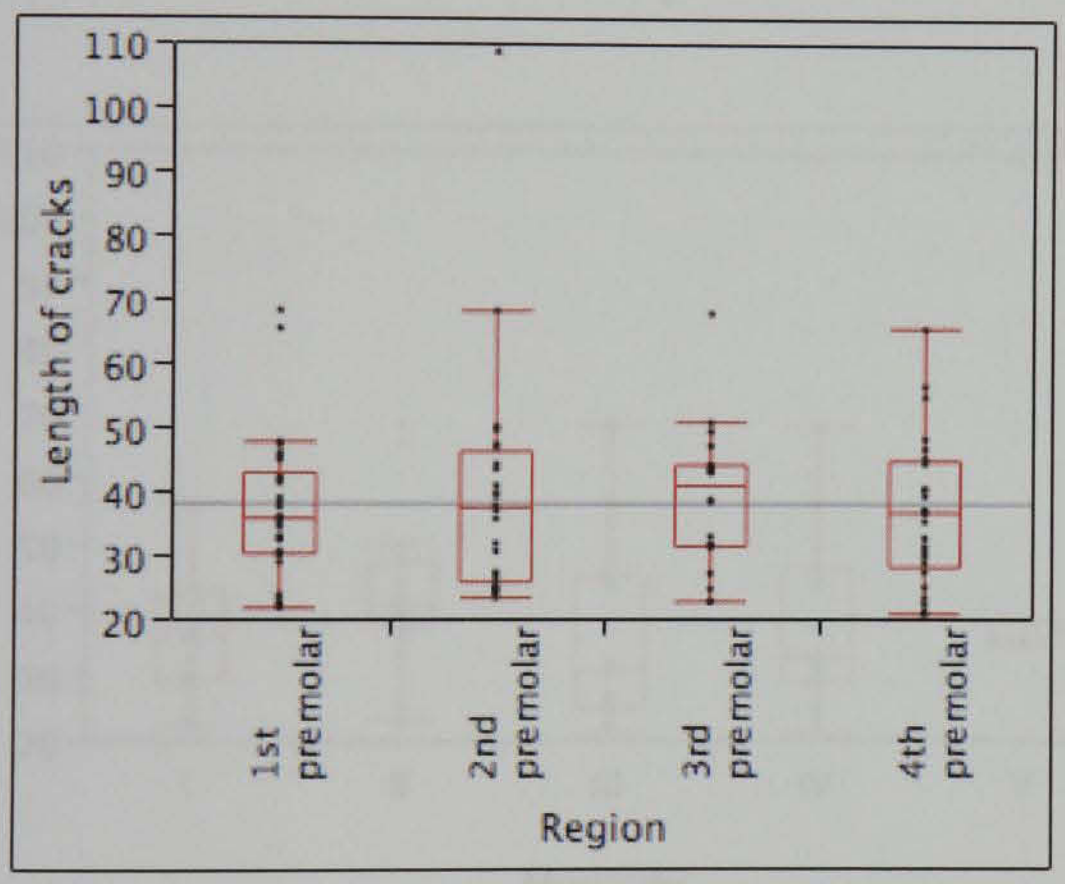

Figure 2.17 A box plot showing the microcrack length range, median, percentiles (10%, 25%, 75% and 90%) and outliers in the four premolar regions.

2.3.2.3 Effect of treatment modality

The mean microcrack lengths for treatment modality II was (42.44± 11.05μm) the highest among the groups. However, there was no significant difference between modality II and other modalities (p=0.126, Wilcoxon signed rank test). Table 2.8 shows means and standard deviations of the four groups.

Table 2.8 Means and standard deviations of the four groups

Treatment modality	Modality I	Modality II	Modality III	Modality IV	Modality V
Mean	35.57μm	42.44μm	34.85μm	38.26μm	35.82μm
Standard Deviation	9.39	11.05	12.47	17.90	1.96

A box plot illustrating the microcrack lengths of the four treatment modalities and the control group (V) is presented in Figure 2.18.

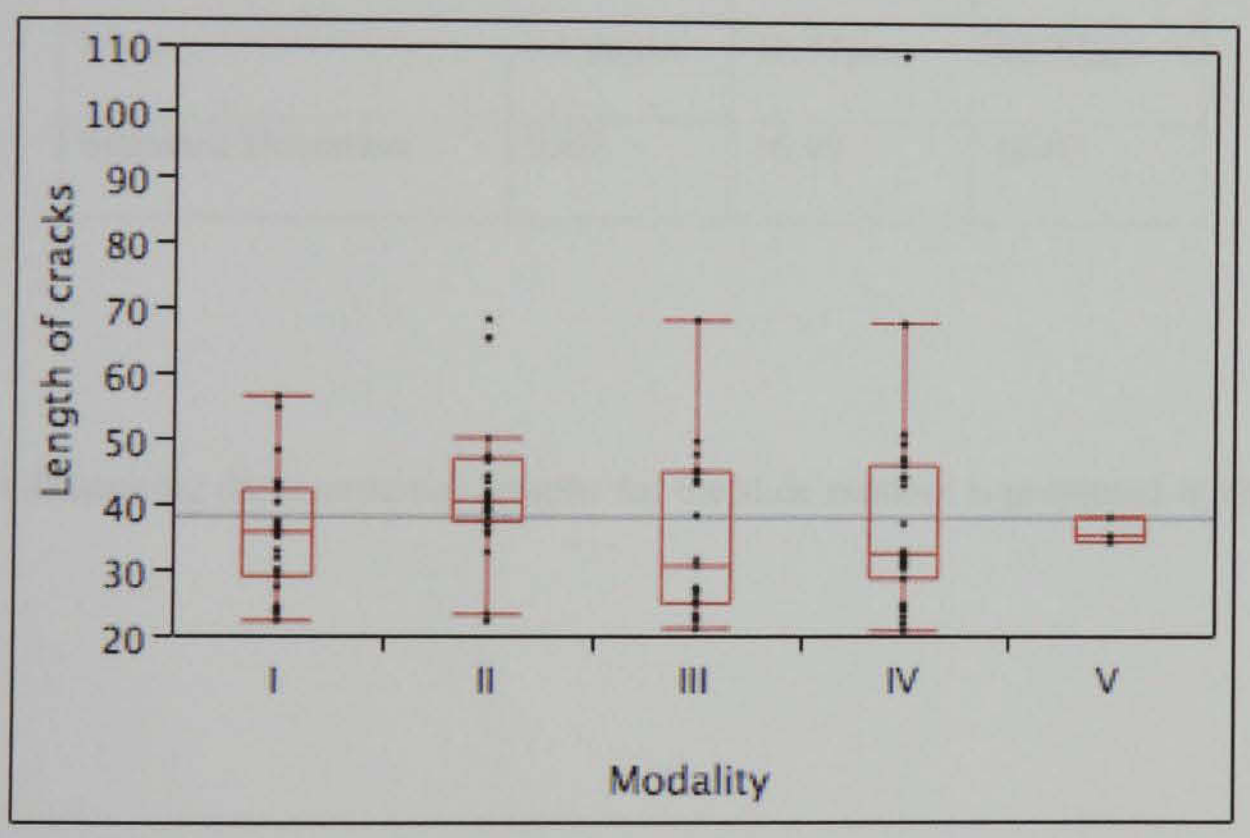

Figure 2.18 A box plot illustrating the microcrack lengths of the four treatment modalities and the control group (V).

2.3.2.4 Effect of slide number (position)

The obtained slides were denoted as number 1, 2 and 3. Number 1 represented the slides obtained from the mesial, number 2 represented the middle while number 3 the distal. On

average slide number 3 had (40.32μm±10.03) longer cracks than the other two slides. Slides number 1 had the shortest crack length. However these differences were not found to be significant (P=0.095).

Table 2.9 shows means and standard deviations of the microcrack lengths as obtained from each slide.

Table 2.9 Means and standard deviations of the microcrack lengths

Treatment modality	Slide 1	Slide 2	Slide 3
Mean	34.06μm	39.77μm	40.32μm
Standard Deviation	9.69	16.99	10.03

A box plot illustrating the microcrack lengths for the slide number is presented in Figure 2.19.

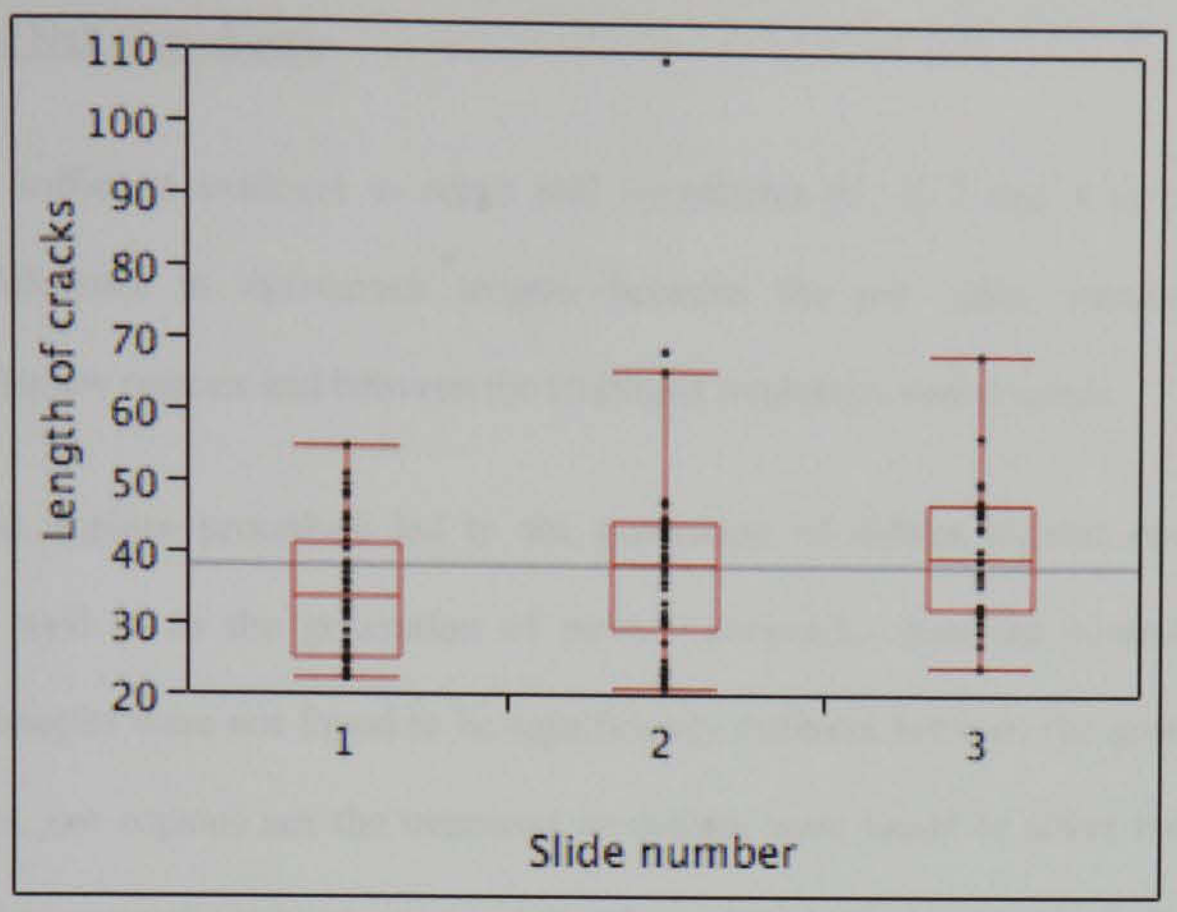

Figure 2.19 A box plot showing the microcrack length range, median, percentiles (10%, 25%, 75% and 90%) and outliers for slides no. 1, 2 and 3.

Table 2.10 Summary of microcrack length

Level	Minimum	Maximum	25%	Median	75%
Left side	20.62	68.12	28.27	36.4	43.15
Right side	20.97	108.59*	29.87	36.74	46.56
1st premolar	21.62	68.09	30.10	35.64	42.74
2nd premolar	23.2	108.59*	25.68	37.33	46.07
3rd premolar	22.56	67.74	31.23	40.745	43.99
4th premolar	20.62	65.38	27.93	36.49	44.63
Modality I	22.13	56.33	28.84	35.59	40.04
Modality II	22.09	68.12	37.26	40.34	46.88
Modality III	20.97	68.09	24.77	30.50	44.93
Modality IV	20.60	108.59*	28.60	32.35	45.90
Control (V)	34.24	38.01	34.24	35.20	38.01
Slide No. 1	22.09	54.65	24.98	33.53	40.97
Slide No. 2	20.62	108.59*	29.01	38.16	44.09
Slide No. 3	23.74	67.74	32.03	39.17	46.77

* The only microcrack that was found to exceed the critical length.

Evaluation of Null Hypotheses:

There is no sufficient evidence to reject null hypotheses #1, 2, 3 and 4 as there was no statistical difference in microcrack lengths between the jaw sides, between treatment modalities, the jaw regions and between the treatment modalities and controls.

Although the implant procedure led to the generation of diffuse stained areas (diffused damage) as well as to the generation of more microcracks than the control group, the microcrack lengths were not found to be significantly different between the groups. Neither the jaw sides, jaw regions nor the treatment modalities were found to affect the microcrack lengths. All microcracks (except one crack (modality IV)) had a length which did not exceed the critical microcrack value, i.e. 100μm (O'Brien *et al.* 2005, Mohsin *et al.* 2006).

2.4 Discussion

Microcracks are defined as a discontinuity in the calcium-rich bone matrix and represent fissures or breaks in the hydroxylapatite that comprises 60% of bone by weight (Lee *et al.* 2003). These features can be detected with chelating agents, which bind to calcium on the microcrack surface (Lee 1997; O'Brien *et al.* 2000; Lee *et al.* 2003). *In vivo*, microcracks were reported to exist in human ribs (Frost 1960; Lee *et al.* 1998; O'Brien *et al.* 2000), human femurs (Shaffler *et al.* 1995), bovine tibiae (Lee *et al.* 2000), sheep radii (Lee *et al.* 2002) and in dog mandibles in the present study. Microcracks can be detected in calcified sections using tetracycline compounds (Lee *et al.* 1998; O'Brien *et al.* 2000; Lee *et al.* 2000).

Microcracks have been reported to be associated with remodelling sites and they may act as a bone remodelling stimulus (Burr *et al.* 1985, Mori & Burr 1993, Lee 1997, Burr *et al.* 1997, Bentolila *et al.* 1998, Lee *et al.* 2002, O'Brien *et al.* 2005) that leads to the repair of the microdamage and prevents its accumulation (Carter & Hayes 1977, Burr *et al.*1985, Frost

1991, Mori & Burr 1993, Frost 1994, Hoshaw *et al.* 1994, Bentolila *et al.* 1998, Verborgt *et al.* 2000). Following this initial stimulus osteoclasts come into direct contact with the bone and resorption begins. The osteoclasts dig out their way forming either a cutting cone within the cortical bone or Howship's lacunae on its surface. Osteoblasts are then attracted to the site and produce bone matrix (osteoid), which is mineralised to form secondary osteons. In this way the damaged area is repaired with new secondary bone (Lee 1997).

In the present study detection of microcracks was limited to the cortical bone adjacent to osseointegrated root form dental implants. Due to the lack of cancellous bone as a result of cutting and grinding procedures, examination of the surrounding cancellous bone was not carried out. The examination was also limited to the inner portion of the cortical bone to avoid edge artefacts. Furthermore, the bone in close contact with the implant surface or that forming the osteotomy walls was intensely stained with tetracycline indicating either artifactual damage during slide preparation or diffuse damage during the surgical procedure, which makes detection of microcracks impossible. Thus, about a 200μm wide area adjacent to the implant surface or that outlining the osteotomy walls were excluded from the examination. A similar intensely stained area was also reported to occur *in vitro* in the bone adjacent to external skeletal fixation pins used in orthopaedic surgical treatment and extended beyond a 1.5 mm zone next to the pin-bone interface as a result of pin insertion (Cohen *et al.* 2003). Similar diffuse staining areas were also observed by Lee (1997) on the machined bone surface as a result of the cutting procedure. This intensely stained area may be evidence of a sub-microscopic level of bone damage that cannot be detected using light microscope because they are beyond resolution capabilities (Schaffler *et al.* 1989, Schaffler *et al.* 1994; Reilly & Currey 1999). It has been suggested that these areas may be generated before production of larger microcracks (Schaffler *et al.* 1994; Norman *et al.* 2001).

Schaffler *et al.* (1996) studied specimens obtained from human compact bone, which were fatigued in uniaxial loading until stiffness loss of 18-30% was achieved. They found that visible microcracks did not increase until a 30% stiffness loss had been achieved, while diffusely stained areas of bone matrix increased in a linear fashion with the increase in degradation of the stiffness (Schaffler *et al.* 1996). This trend was also observed by Burr *et al.* (1998) who found a linear relationship between the damaged (diffuse staining) area and the stiffness loss. Also, Burr *et al.* (1998) did not detect significant microcrack generation in canine femurs until the bone had lost 15% of its elastic modulus (stiffness). This supports the idea that an ultrastructural level damage in bone occurs in addition to a microscopic level. Schaffler *et al.* (1994) suggested that the bone matrix's ultrastructural features, such as the collagen fibre-bone mineral interrelationship, may play a major role in minimising the formation of principal microcracks and it may also facilitate the formation of marked diffuse damage which does not propagate as readily to complete fracture. *In vivo* microcracks observed in human rib samples had little collateral diffuse staining, while other microcracks were associated with marked diffuse staining that extended from the microcrack tip or from the sides (Schaffler *et al.* 1994).

In the present study this diffusely stained area may represent foci of diffuse damage as a result of implant placement and/or osteotomy preparation. It is reasonable to suggest that the osteotomy preparation and the implant placement may concentrate the damage in the area close to the implant without significant generation of microcracks in areas farther away from the osteotomy wall. This may be an explanation for the lower values of microcrack number observed in that area. It is in accordance with the previously reported finding which indicated that bone remodeling is reduced with increasing distance from the implant site (Garetto *et al.* 1995).

The diffuse damage in human cortical bone was found to be small, averaging about 3% of total bone area and did not influence bone fracture toughness *in vivo* (Norman *et al.* 2001).

In the current study, the low number of microcracks detected may also be attributed to the criteria that were used to include candidate microcracks. Candidate microcracks were observed using UV incident light ($\lambda = 365$ nm). The UV stained microcracks were identified by their yellow-green fluorescence. The candidate microcrack sizes were intermediate between canaliculi and vascular channels and had sharp borders. Only cracks that satisfied the set criteria were considered to be *in vivo* microcracks and not artefacts.

Furthermore, it is possible that microcracks were so small as to be detected using the epifluorescence microscope. It is also possible that not all microcracks were successfully stained with tetracycline. Furthermore, intensely stained areas were observed at perimeters of resorption spaces as well as within and around the Haversian systems, making identification of microcracks challenging (Figure 2.20).

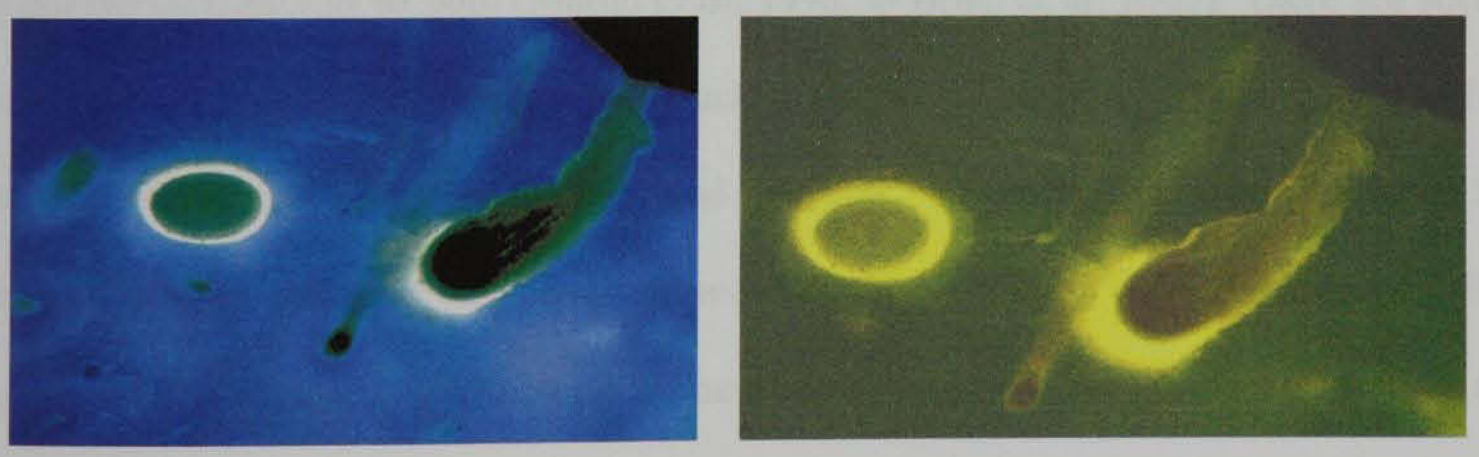

A B

Figure 2.20 Tetracycline stained areas observed at perimeters of resorption spaces under UV (A) and blue incident light (B).

The degree of mineralisation is believed to play a role in the generation of microcracks. For example, microcracks were most likely to occur in interstitial bone (O'Brien *et al.* 2003, O'Brien *et al.* 2005) due to its high mineralisation leading to less ductility than newly formed

bone. Hypomineralised bone might be strained at a higher value than normally mineralised bone (Currey 1990). In the present study, the low number of detected microcracks may have been due to incomplete mineralisation of bone (more flexible), as the implants were placed three months after extraction. At three months the bone may not have been fully mineralised and was therefore flexible. The osteotomy preparation and/or implant placement may have strained the bone but to a lesser extent than its yield strain. In other words, it may be strained to a lesser degree than to its elastic limit. Consequently, the bone could be deformed but without significant generation of microcracks. This is in accordance with an earlier observation made by (O'Brien *et al.* 2001). Lee and coworkers (2002) could not find microcracks in the newly formed peroisteal or endosteal bone while they were found in the original cortex near the peroisteal surface. In this animal study mechanical loading in the sheep radius was increased by ulnar osteotomy, altered by Steinmann pinning or unaltered in sham operated controls.

The resistance of any material to fatigue failure is dependent on its resistance to the initiation and growth of cracks or to both (Martin *et al.* 1998, O'Brien *et al.* 2003). There are several microstructural factors that highly affect crack initiation and growth. These factors include material strength and fibre size, number and diameter. In general, material that has a low resistance to crack initiation has, on the other hand a high ability to resist crack growth (Burr *et al.* 1988; Martin *et al.* 1998). Bone is one of many highly fatigue-resistant materials that obtain this property mainly from their resistance to crack growth rather than crack initiation (Martin *et al.* 1998).

Decrease in the yield strength leads to an increase in the potential for crack initiation, but it also leads to an increase in the resistance to crack growth (Martin *et al.* 1998). The interface between a fibre and the surrounding matrix is a source of weakness that can initiate cracks. Conversely, the cracks tend to remain small and follow the fibres instead of propagating

across the structure (Martin *et al.* 1998). This may explain the lower average length of the microcracks reported in the present study. The mean microcrack length reported in the present study (range 35-42μm) did not significantly differ from the 49 μm reported by Lee *et al.* (2002). The length of microcracks detected in the present study was found to be below the critical length. The critical or Griffith length for microcrack formation is the length beyond which the crack become energetically unstable and propagate to failure. The critical length for microcracks was found to be approximately 100 μm (Lee 1997). This finding suggests, in agreement with the general belief, that bone has the ability to resist microcrack growth rather than crack initiation (Martin *et al.* 1998; O'Brien 2000).

Microcracks have been found to be associated with the insertion of endosseous implants into long bone (Huja *et al.* 1999a) and with external skeletal fixation pins (Cohen *et al.* 2003). The number of microcracks was seen to decrease during a 4-week healing period following implant placement in long bones due to bone remodelling (Hoshaw *et al.* 1994a, Hoshaw *et al.* 1994b). Hoshaw *et al.* (1994b) studied the effect of Brånemark implant placement and design on generation of microcracks in rabbit bone. The density of microcracks, as detected by basic fuchsin staining, immediately after implant placement (baseline) and after a 4-week healing period. They studied microcrack generation in a 1.2 mm-wide region at the interface adjacent to the implant and found that the mean area fraction of microcracks detected at the 4-week healing period was significantly ($P< 0.03$) lower than that detected at the baseline. The values were 9.5± 2% and 12.5± 2% respectively. These data suggest that bone remodelling may repair some of the microcracks generated.

In one study, Huja *et al.* (1999a) found that non-adapted bone (bone that was loaded immediately after implant placement) near the implant accumulated significantly more microcracks than adapted bone (loaded 12 weeks after implant placement). The non-adapted non-loaded specimens demonstrated approximately 20-fold more damage than the respective

adapted specimens (crack density ≈ 10 crack/ mm^2 versus ≈ 0.5 crack/ mm^2). These findings indicate the susceptibility of pre-implant bone to microcrack generation as a result of the implant placement procedure. It may also indicate resilience of the newly formed bone at the pre-implant area (Huja *et al.* 1999a). It has been suggested that after a 3-month post implantation period bone remodelling has repaired the microcracks incurred by the surgery. The resultant bony structures may have a decreased level of mineralisation and be relatively more compliant. This may limit further generation of microcracks because microcracks are more likely to occur in highly mineralised bone (Huja *et al.* 1999a; O'Brien 2000).

High remodelling rates at bone adjacent to implants have been reported (Garetto *et al.* 1995). This elevation in the remodelling process was found even after one year of the implant placement. High remodelling activity could lead to formation of bone with a relatively low level of mineralisation, and which is more compliant. In one study (Tricker *et al.* 1977), high remodelling rates and mineral apposition in dentate dog mandibles were reported. They found that the remodelling rate was of about 30-40% a year, which represents a 10-fold difference from the standard accepted rates of cortical bone and is substantially higher than the accepted 2-10% per year in the appendcular skeleton and rib.

It is also possible that such bone when loaded can undergo a significant deformation without major microcrack generation. The results of the present study correspond partially with the results reported earlier by Huja *et al.* (1999a) who observed that fatigue-loaded tibiae in dogs which react to the loading imposed on them depended on whether the bone has adapted or not. The adapted bone was allowed to heal for 12 weeks after placement of the implant before it was loaded while the non-adapted one was loaded immediately *in vitro*. They observed few microcracks in the non-loaded adapted specimens, when compared with the non-loaded, non-adapted specimens (CrDn ≈ 0.5 microcrack/mm^2 Versus CrDn ≈ 10 microcrack/ mm^2). Even after loading, the adapted specimen groups were found to have half

as many microcracks as the non-loaded, non-adapted specimen groups (5 Versus 10 microcracks/ mm^2). However, Huja *et al.* studied the microcracks generated in a very limited area close to the implant surface.

In the current study, the staining method does not differentiate between pre-existing and experimentally generated microcracks. Thus, a control group was used. The control group was also used to prevent any systemic errors.

There was strong evidence for effect of treatment modalities when compared the control. The control group (V) has significantly fewer number of microcracks on average compared to the modalities I –IV ($F= 3.335$, $p=0.0125$). It was also found that the experimental groups contained areas of intensely stained regions adjacent to the implant. Such diffuse damage could not be found in the control site. Thus it is reasonable to assume that the detected microcracks as well as the intensely stained areas were generated as a result of the experimental procedures.

The analysis showed no significant differences among treatment groups for number or length of microcracks.

The technique used in the present study to obtain ground sections is the most commonly used technique to study microcracks in bone. However, it may give an accurate estimation of microcrack densities, but microcrack lengths may be underestimated unless a larger sample size is used (O'Brien *et al.* 2003). This underestimation may occur because of the cutting and grinding procedures. In the present study, in order to obtain a slide of 150-200 μm, a section of 300-350 μm thickness was prepared to avoid slipping of the blade during the cutting procedure. If the 300 μm blade thickness was added to the previous loss of bone due to grinding procedure, it could be possible to estimate that about 450-500 μm of bone was most likely wasted in the cutting and grinding procedures.

The ground sections in the present study represented vertical sections taken from the bone surrounding the implant. According to O'Brien *et al.* (2003) who reported that shorter microcracks were found in transverse sections when compared with those found in longitudinal sections but their density was lower which may be due to the anisotropic nature of bone (O'Brien *et al.* 2003). This is in accordance with the present study where the crack lengths were found to be below the critical lengths, as was mentioned earlier. O'Brien *et al.* (2003) found that in bovine tibiae that were cyclically loaded in compression, microcracks developed early during the first 10000 cycles and only slight accumulation occurred between 10000-50000 cycles. After 50000 cycles microcracks increased rapidly. This trend was observed irrespective of bone sections: longitudinal or transverse. Shorter microcracks were found in transverse sections when compared with those observed in longitudinal sections but their density was lower (O'Brien *et al.* 2003).

2.5 Conclusion

The presence of microcracks in the control group indicates the presence of such microcracks *in vivo* as has been reported in the literature. The increased number of microcracks in the treatment groups indicates that the implantation procedure generates microcracks in bone surrounding implants. Diffusely stained areas were found in all specimens obtained from the different treatment modalities (I- IV). These areas may indicate diffuse damage generated during the osteotomy preparation and/ or implant placement. No significant differences in the number of microcracks were found between the different modalities or regions. Most of the microcracks were generated by the first treatment modality (preparation of osteotomy) and other modalities appear to have had no major additional effect.

Chapter 3. Finite Element Method

3.1 Introduction

The Finite Element Method (FEM) has been used in engineering since 1943 to provide analytical solutions to problems of complex geometric forms. FEM applications have been extended to be used in medicine and dentistry. It is a useful tool in analyzing biomechanical structures and it has been used to evaluate and improve implant designs to optimize the peri-implant bone reaction to the functional forces imposed on the implants and the prosthesis. Prediction of the life of an implant material or structure can be achieved using FE fatigue analysis.

FEM has also been used to evaluate functional load transfer characteristics of different implant systems (Lozada *et al.* 1994, Carvalho *et al.* 2003, Bozkaya *et al.* 2004) and to simulate the effect of implant loading on the surrounding bone (Hoshaw *et al.* 1999a, Mellal *et al.* 2004, Akagawa *et al.* 2003). FEM was also used to study several problems that may be encountered in various clinical situations, such as the functional loads on the restorations and tooth deflection under occlusal loads (Geramy & Sharafoddin 2003).

FEM has many advantages that are appreciated by professionals due to its ability to include irregularity and heterogeneity of the body of the model design as well as to the relative ease with which loads can be applied at different directions and magnitudes for a more complete analysis. It is a highly precise technique that can be used to study structural stresses on the basis of its physical properties. It is a cost effective method

that allows designers to observe all the theoretical stresses and strains within the materials or structures without the need to build them up to their actual size.

Finite Element Analysis (FEA) is a numerical technique; it is a mathematical representation of a physical system, thus its accuracy is highly dependant on the model construction and on its ability to simulate the geometric form and the applied forces. A detailed description regarding deformation, stress and strain, within a complex elastic form can be estimated by stress analysis.

In the FEM, the body is divided into small parts (elements), which are joined by nodes (Geramy & Sharafoddin 2003) (Figure 3.3). The reaction of each element can be described with a relatively simple set of equations. These equations, which are derived from each element, are then joined together to obtain a very large set of equations that describe the behavior of the body as a whole. A software program is used to solve these equations simultaneously.

When the element is subjected to a load under specific boundary conditions (constraints), the element will be deformed and each point within the element, including the nodes, will be displaced. Each node is an associated unknown to be solved. The displacement of the nodes (translation and rotation) is known as a degree of freedom (DOF). For example, for a 2-dimensional model, the nodes are displaced in the x and y directions and are considered unknowns. This means that each node has two DOF. Once the nodal displacement has been computed, the stress and strains can be calculated and the solutions for all the elements are united to obtain a result for the body as a whole (Geramy & Sharafoddin 2003).

FEM may be classified as 2-Dimensional (2-D) or 3-Dimensional (3-D) models. The 2-D model limits the investigation to a longitudinal simulation of the stress distribution within the objective under investigation. However, its use may save computer memory and it is less time-consuming than the 3-D model.

It has been recognized that bone remodeling in the peri-implant region occurs following implant placement as a part of the healing process that leads to osseointegration of the implant. It is also documented that microcracks generated in the peri-implant bone as a result of implant placement and functional loading may induce such a remodeling process to repair these damages (Hoshaw *et al.* 1994a, Hoshaw *et al.* 1994b).

In our first study, we reported the generation of excessive diffuse damage in the osteotomy wall and a few microcracks in the remote area surrounding the implant irrespective to the surgical procedure. In implant dentistry, it is known that in order to achieve primary stability, there should be a mismatch between the implant diameter and the osteotomy, i.e. the implant is wider than the osteotomy. Consequently, it could be speculated that further damage may occur as a result of compressing the bone (generation of compressive stress on the osteotomy walls) due to this disparity. However, the reaction of the bone to such an event is difficult to study practically. Nevertheless, construction of FEM that can simulate bone response to its displacement during implant placement may shed light on the stresses and strains that may occur and lead to generation of bone damage which is believed to stimulate the remodeling activity that was reported to occur at this critical area.

The purpose of the present FEM study was to investigate stress and strain generation that may occur during implant placement due to the mismatches between the diameters of the osteotomy and the implant. Effect of thickness of bone surrounding the osteotomy on the stress and strain around the implant was also studied

3.2 Model construction

3.2.1 Geometry

FEA was found to be significantly affected by the modeling details and depends on the accuracy by which the model was constructed to mimic the real object or body under study (Teixeira *et al.* 1998, Akagawa *et al.* 2003). However, in the present study, for simplicity, 2-dimensional models were used. The models were constructed to simulate a mandibular segment in mesio-distal direction that contains an osteotomy preparation using an FE package (ANSYS® version 8.1, ANSYS, Canonsburg, PA).

The osteotomy was either 3mm (model 1) or 3.25 mm (model 2) in diameter and 10mm in depth. Only half of osteotomy diameter and half of the surrounding bone were simulated due to the symmetry of the generated stresses and strains. Two sub-models were constructed from each model as follows:

1). Model 1. The distance from the osteotomy wall outward was 5mm in the mesio-distal direction. This model consisted of two sub-models as follows:

a). Osteotomy preparation diameter of 3mm

b). Osteotomy preparation diameter of 3.25mm.

2). Model 2. The distance from the osteotomy wall outward was 10mm in the mesio-distal direction. This model also consisted of two sub-models as follows:

a). Osteotomy preparation diameter of 3mm

b) Osteotomy preparation diameter of 3.25mm.

3.2.1.1 Model 1

3.2.1.1.1 sub-model 1

Only half of osteotomy and half of the surrounding bone were simulated due to the symmetry of the generated stresses and strains. The osteotomy diameter was 3 mm. The osteotomy preparation was simulated as a 10mm deep and 1.5mm wide area surrounded by bone 10mm in height. Thus, the two millimeter coronal part of the osteotomy was surrounded by cortical bone while the remaining eight millimeters were encased in cancellous bone. These two areas extended five millimeters from the osteotomy wall in the bucco-lingual direction.

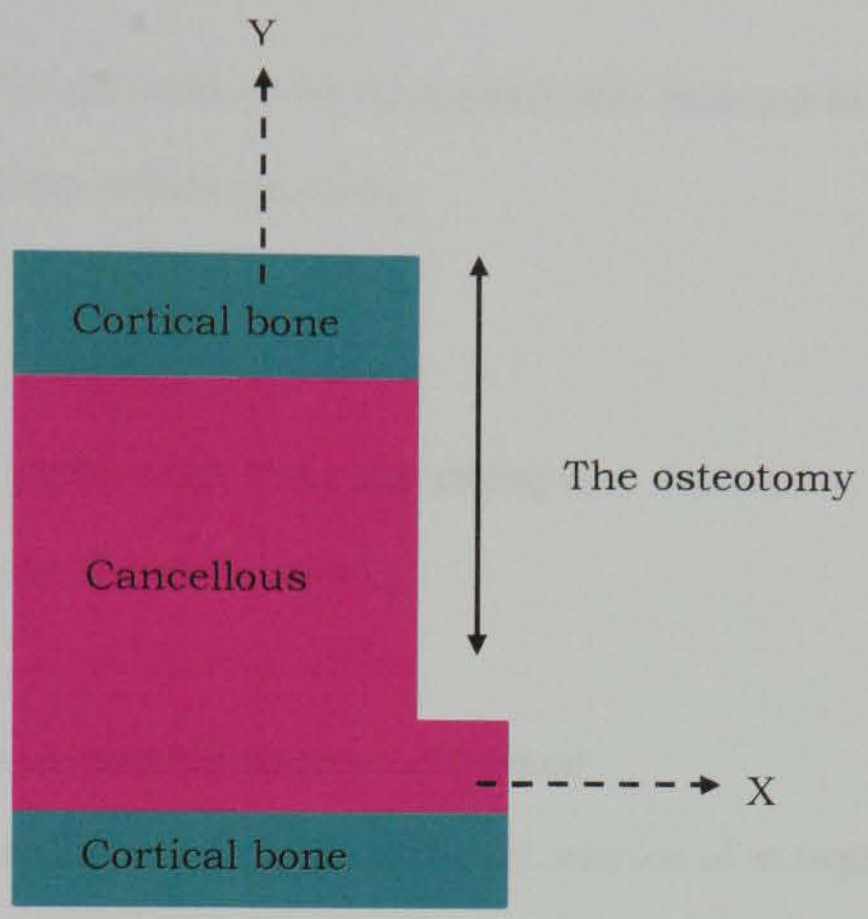

Figure 3.1 A view of half of the osteotomy preparation and the surrounding bone of sub-model 1.

The cancellous bone also extended two millimeters in the apical direction just above 2-mm of cortical bone, which formed the lower border of the mandible. This cortical and cancellous bone was 6.5 mm in the bucco-lingual direction.

3.2.1.1.2 sub-model 2

It is similar to sub-model 1, but with an osteotomy preparation of 3.25mm. Thus, the bone was displaced 0.25mm in the x-direction.

3.2.1.1.3 sub-model 3

It is similar to sub-model 1, but the width of the surrounding bone increased to 10mm (the bone was displaced 0.375mm in the x-direction).

3.2.1.1.4 sub-model 4

It is similar to sub-model 2, but the width of the surrounding bone increased to 10mm (the bone was displaced 0.25mm in the x-direction).

3.2.2 Boundary conditions and modeling insertion of implant

To simulate bone displacement that may be generated by the insertion of an implant of 3.75mm in diameter (when the osteotomy preparation was 3 mm in diameter), 18 serial models with a -0.375mm displacement in the x-direction were constructed. The displacement was applied on the keypoints that formed the osteotomy wall. This wall was made of 51 keypoints. Each two consecutive keypoints were 0.2mm apart. The displacement was applied to the next three consecutive keypoints to simulate the distance (0.6mm) between each two consecutive threads in the Brånemark® implant system. First, the displacement was applied to the first coronal keypoint. Second, the displacement was applied to the 1^{st} and the 4^{th} keypoint. Third, the displacement was applied to 1^{st}, 4^{th} and the 7^{th} keypoint. The same pattern was applied to the other keypoints. Figure 3.2 illustrates positions of the keypoints that were displaced. Table 3.2 shows the number of keypoints at which the displacements were applied.

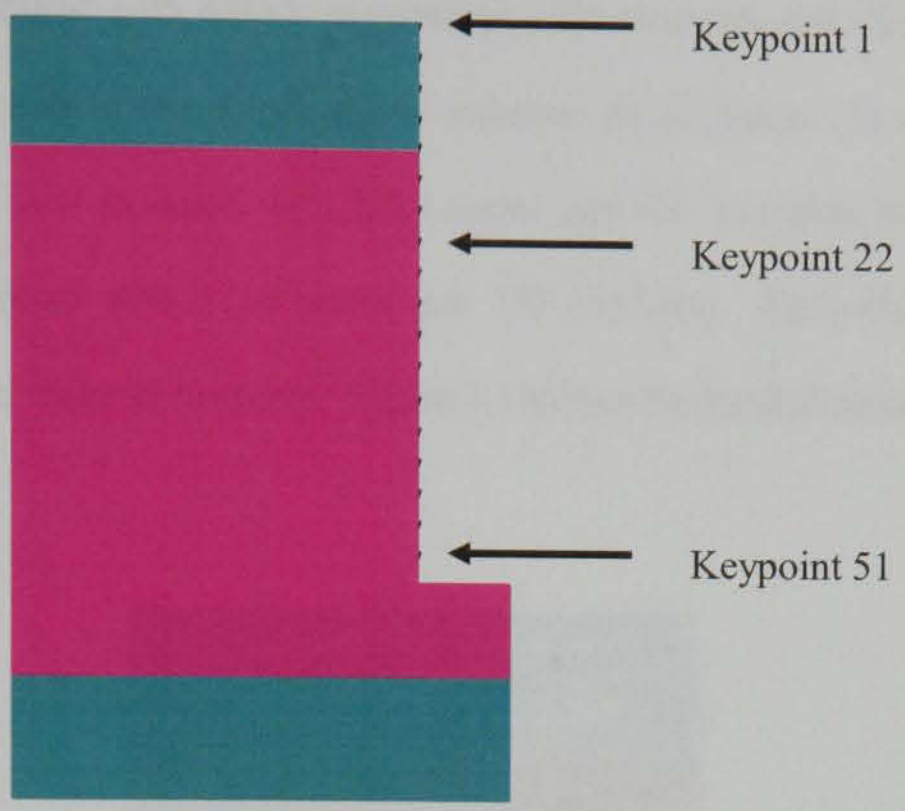

Figure 3.2 An illustration of the displaced keypoints.

Table 3.1 Displaced keypoints and their depth in the osteotomy preparation.

Displacement model	Displaced keypoins	Depth in the osteotomy
1	1	0 (on the crest)
2	1,4	0.6mm
3	1,4 and 7	1.2mm
4	1,4,7 and 10	1.8mm
5	1,4,7, 10 and 13	2.4 mm
6	1,4,7,10,13 and 16	3mm
7	1,4,7,10,13,16 and 19	3.6mm
8	1,4,7,10,13,16,19 and 22	4.2mm
9	1,4,7,10,13,16,19,22 and 25	4.8mm
10	1,4,7,10,13,16,19,22, 25 and 28	5.4mm
11	1,4,7,10,13,16,19,22, 25, 28 and 31	6mm
12	1,4,7,10,13,16,19,22, 25, 28,31 and 34	6.6mm
13	1,4,7,10,13,16,19,22, 25, 28,31, 34 and 37	7.2mm
14	1,4,7,10,13,16,19,22, 25, 28,31, 34, 37 and 40	7.8mm
15	1,4,7,10,13,16,19,22, 25, 28,31, 34, 37, 40 and 43	8.4mm
16	1,4,7,10,13,16,19,22, 25, 28,31, 34, 37, 40, 43 and 46	9mm
17	1,4,7,10,13,16,19,22, 25, 28,31, 34, 37, 40, 43,46 and 49	9.6mm
18	1,4,7,10,13,16,19,22, 25, 28,31, 34, 37, 40, 43,46, 49 and 51	10mm

The FEM was meshed with 4-node tetrahedral solid elements and finer meshes were generated at the wall of the osteotomy to enhance its accuracy. In all of the 5mm models, the bone was modeled with 2209 nodes and 690 elements, while the 10mm models were modeled with 1254 nodes and 373 elements. Each element was then assigned a specific material property. Figure 3.3 shows the meshed model 1.

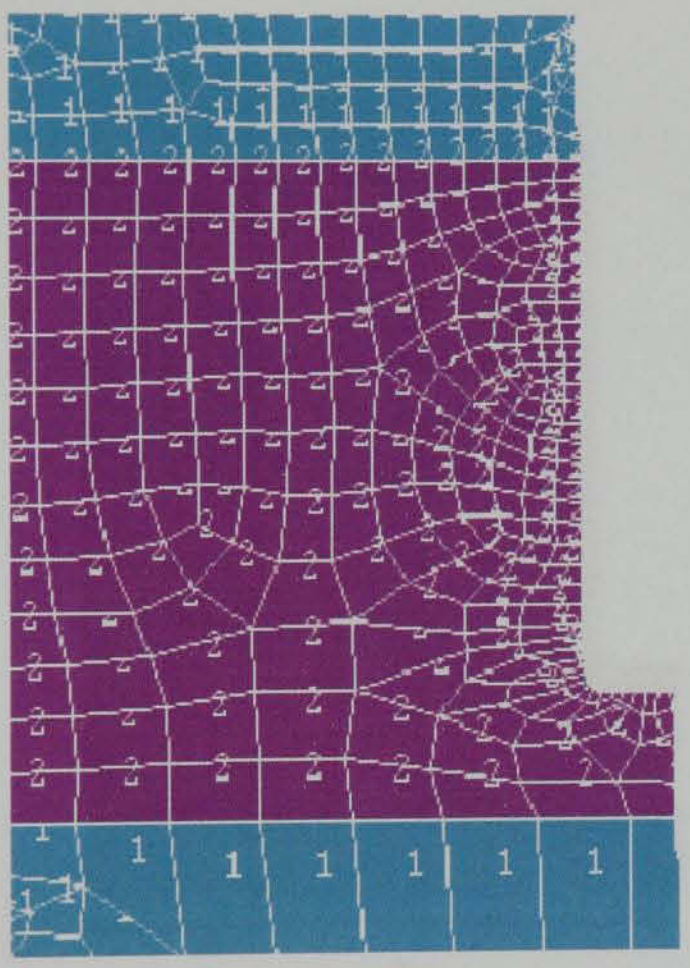

Figure 3.3 The meshed model 1.

After the model was constructed, boundary conditions were defined on the bottom and side of the jaw at the following lines with zero degrees of movement in both directions (fixed in the x- and y-axis).

1. Two lines which made the cancellous and the cortical bone apical to the osteotomy preparation were constrained in the x-direction (Figure 3.4).
2. One line that made the lower border of the mandible was constrained in the y-direction (Figure 3.4).

The constrained conditions were used to avoid deflection of the geometry in the x- and y-direction.

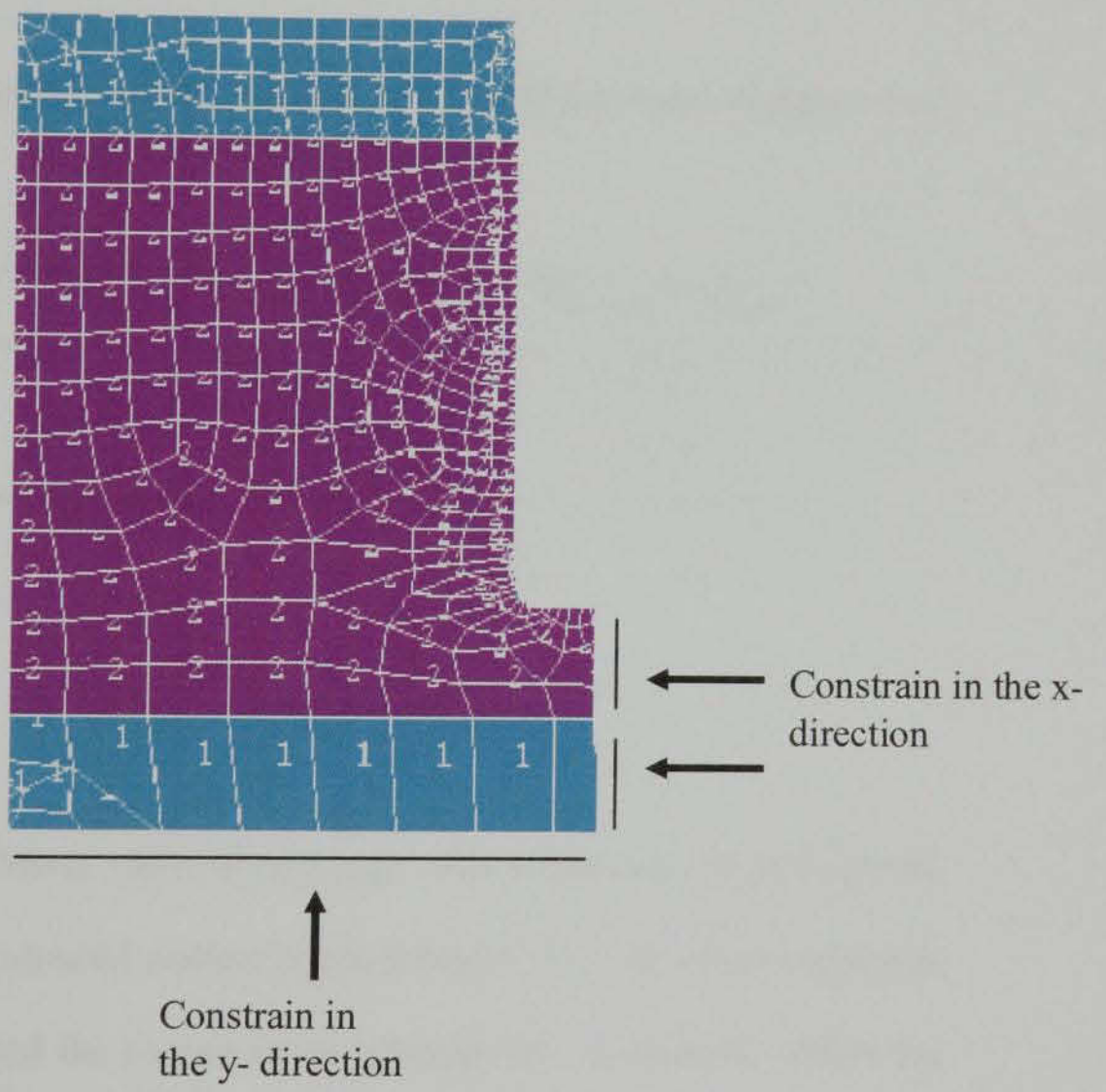

Figure 3.4 The boundary condition. Two lines that made the cancellous and the cortical bone apical to the osteotomy preparation were constrained in the x-direction and one line which made the lower border of the mandible was constrained in the y-direction.

3.2.3 Material Properties

Materials (cortical and cancellous bone) used in the model were considered as homogenous, isotropic, and linearly elastic. The model was assumed to be linearly elastic which means that when it was displaced it was elastically but not plastically deformed. The elastic properties of the cortical and cancellous bone were obtained from literature and used in the current study are represented in Table 3.2.

Table 3.2 Mechanical properties of the cortical and cancellous bone (Çağlar *et al.* 2006).

Material	Young's modulus (MPa)	Poisson's ratio
Cortical bone	13700	0.30
Cancellous bone	1370	0.30

3.3 Solution

Von Mises stress and Von Mises strain distributions within the bone were recorded, calculated and presented in colourful contour bands (Figure 3.5). Von Mises stress was selected because it represented the overall stress intensity and distribution within the model.

3.4 Results

3.4.1 Sub-model 1

The calculated Von Mises stresses reported in the x and y axes shown in Figure 3.1. The x-axis is perpendicular to the mandible while the y-axis is parallel to the long axis of the mandibular section. The predicted stresses were presented in Mega Pascal units (MPa) and the predicted strains in percentages.

3.4.1.1 The area close to the implant surface

3.4.1.1.1 Displaced keypoints and maximum Von Mises stresses:

3.4.1.1.1.1 Displacement of the 1st keypoint

The 1st keypoint, which was located at the crest of the alveolar bone, was displaced -0.375mm in the x direction. The stresses due to the applied displacement were predicted (Figure 3.5) and a maximum Von Mises stress of 489.859 MPa was observed in the crest of the alveolar bone around the 1st keypoint (Figure 3.5).

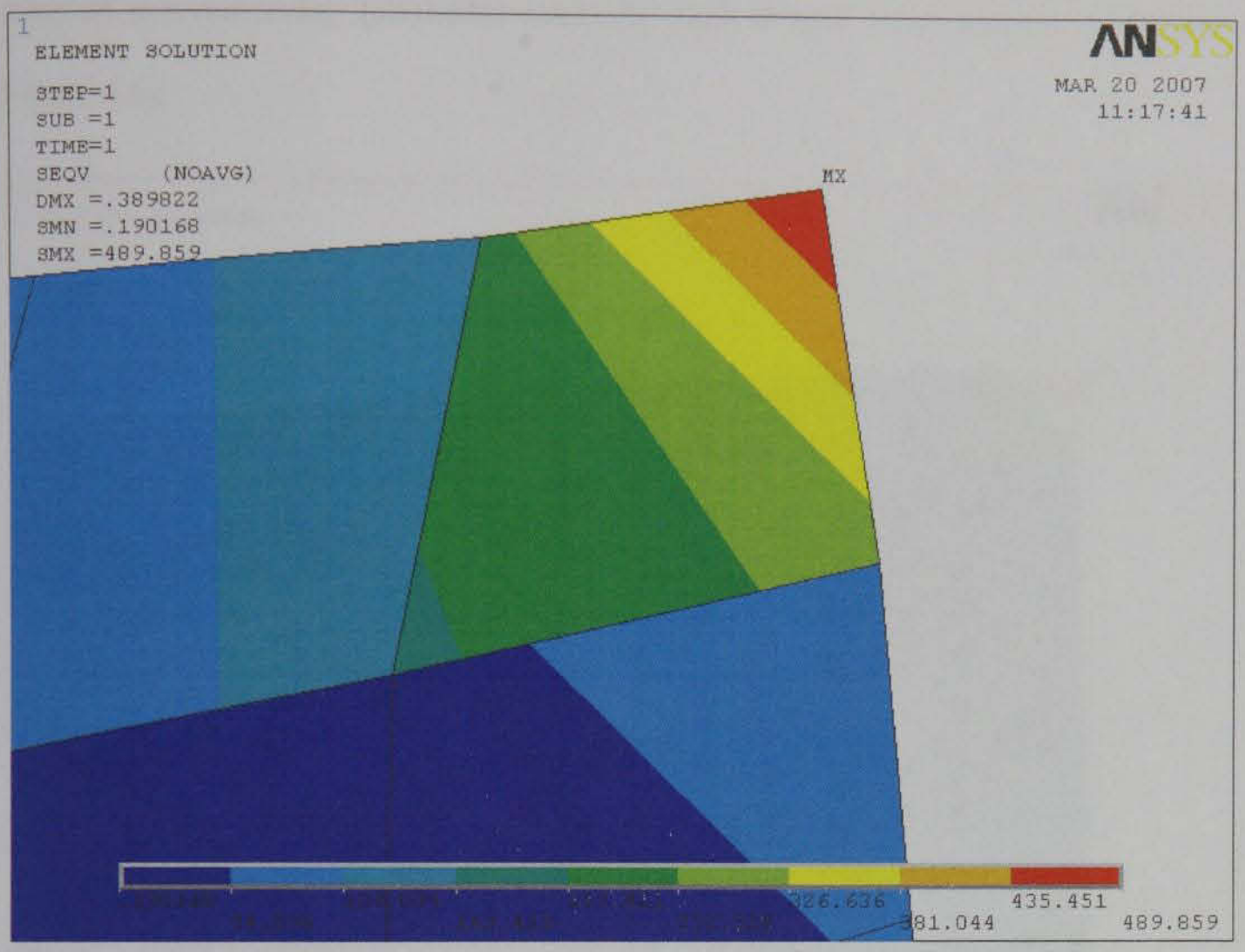

Figure 3.5 Maximum Von Mises stresses when keypoint no.1 was displaced. The maximum Von Mises stress (489.859 MPa) was located at the crest of the alveolar bone around the 1st keypoint. The predicted stresses were presented in Mega Pascal units (Mpa).

3.4.1.1.1.2 Displacement of the 1st and 4th keypoints

The two keypoints were displaced -0.375 mm in the x direction. The observed stresses suddenly increased. The maximum Von Mises stress value was recorded around the first keypoint (the crest of the alveolar bone) with a value of 1275MPa. Von Mises

stress of a lower value (283MPa) could be seen around the displaced 4th keypoint (Figure 3.6).

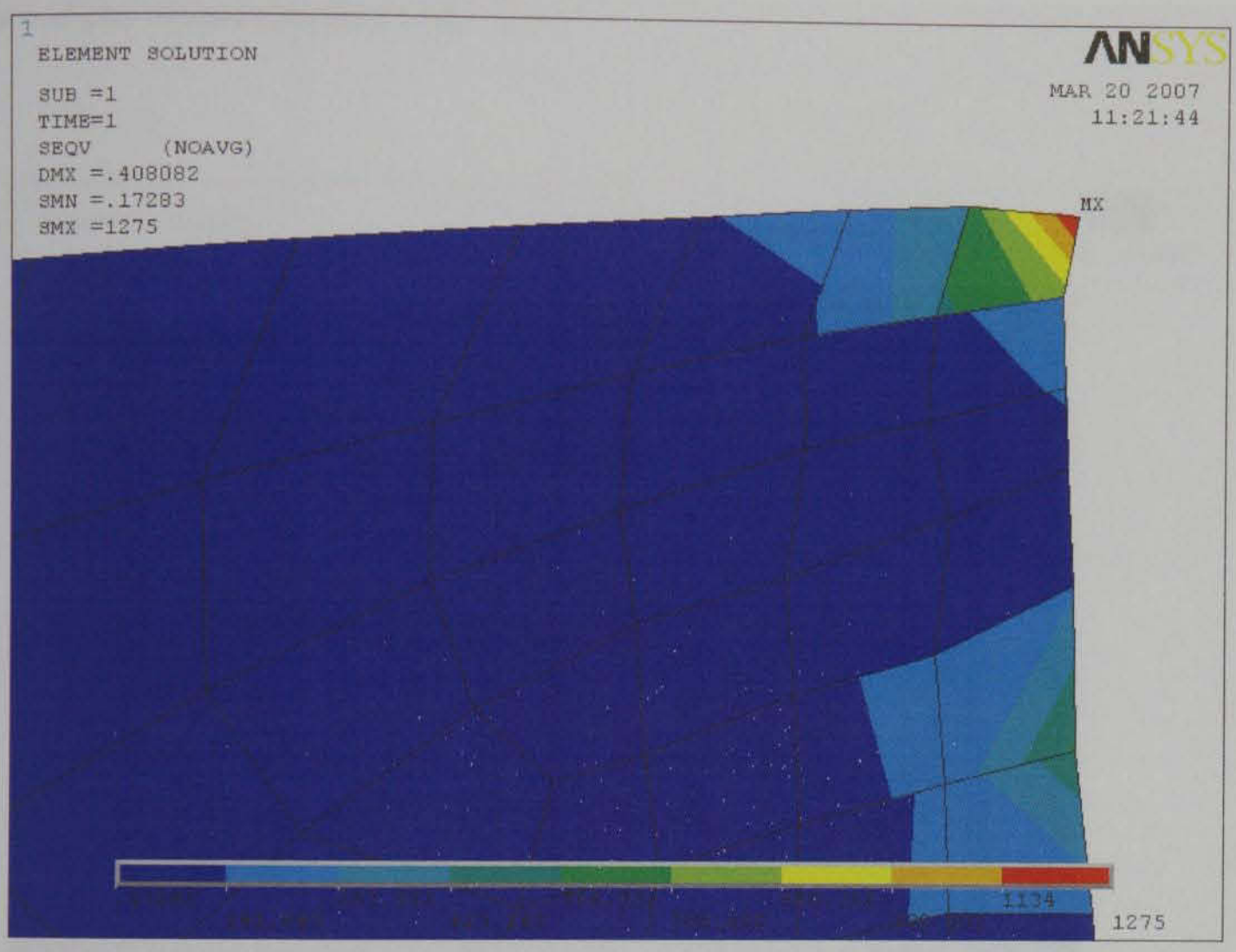

Figure 3.6 Maximum Von Mises stresses when the 1st and 4th keypoints were displaced. The maximum Von Mises stress (1275MPa) was located at the crest of the alveolar bone around the 1st keypoint. A lower stress (283MPa) could be seen around the 4th keypoint. The predicted stresses were presented in Mega Pascal units (MPa).

3.4.1.1.1.3 Displacement of the 1st, 4th and 7th keypoints

The predicted maximum Von Mises stresses increased gradually and reached 1555MPa which was located around the 1st and 7th keypoint. The 7th keypoint was located at

1.2mm from the crest of the alveolar bone. Maximum Von Mises stresses around the 4th keypoint was 345MPa (Figure 3.7 and 3.8). A lower stress could be seen along the apical part of the osteotomy wall.

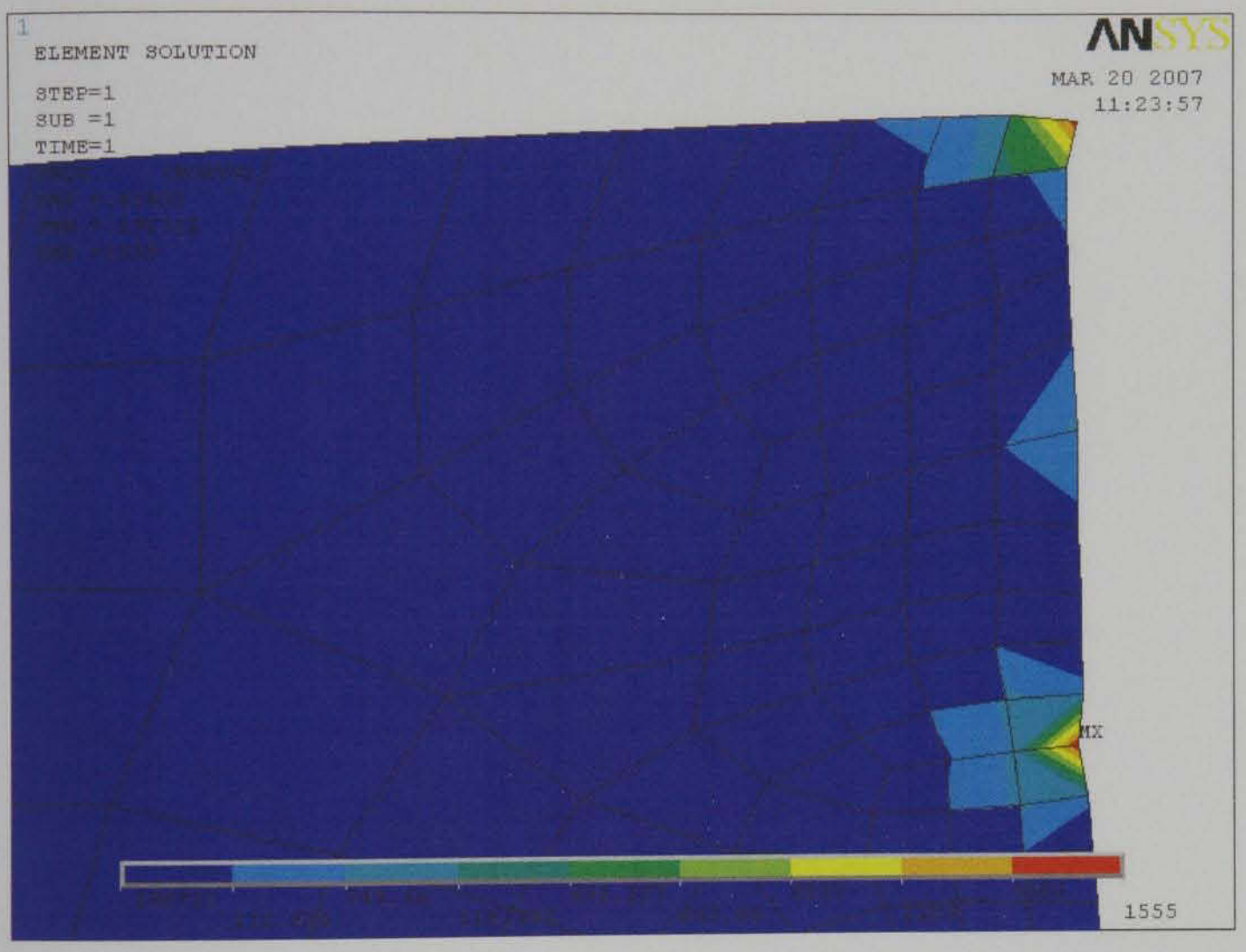

Figure 3.7 Maximum Von Mises stresses when the keypoint no. 1, 4 and 7 were displaced. The maximum Von Mises stress (1555MPa) was located close to the displaced 1st and 7th keypoints. A lower Von Mises stress (345MPa) could be seen around the 4th keypoint. The predicted stresses were presented in Mega Pascal units (MPa).

1.2mm from the crest of the alveolar bone. Maximum Von Mises stresses around the 4th keypoint was 345MPa (Figure 3.7 and 3.8). A lower stress could be seen along the apical part of the osteotomy wall.

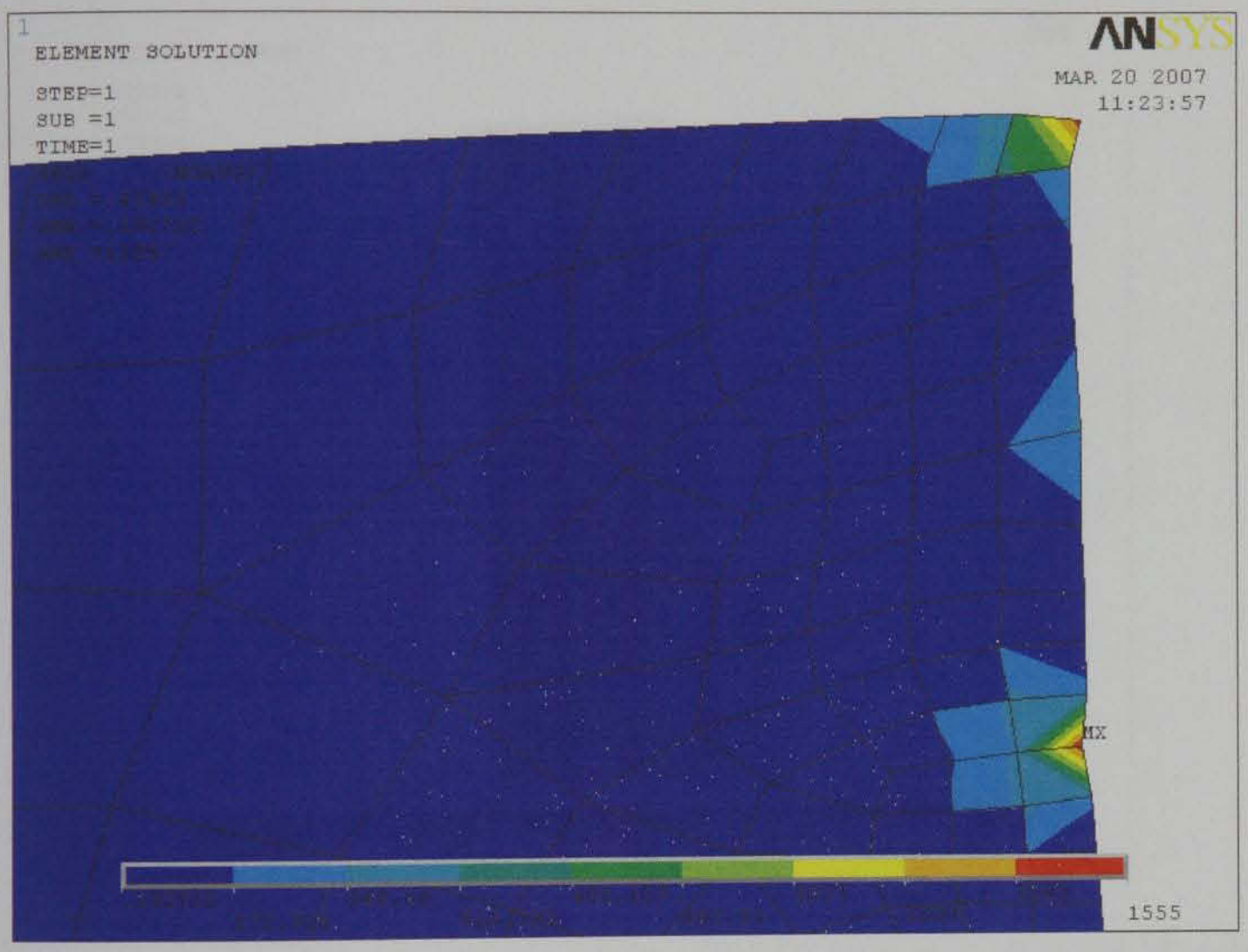

Figure 3.7 Maximum Von Mises stresses when the keypoint no. 1, 4 and 7 were displaced. The maximum Von Mises stress (1555MPa) was located close to the displaced 1st and 7th keypoints. A lower Von Mises stress (345MPa) could be seen around the 4th keypoint. The predicted stresses were presented in Mega Pascal units (MPa).

stresses at the area coronal to the 10th Keypoint had lower stress values (717Mpa around the 1st keypoint and 358Mpa around the 4th keypoint). Different Von Mises values could be seen around the different involved keypoints (Figure 3.9).

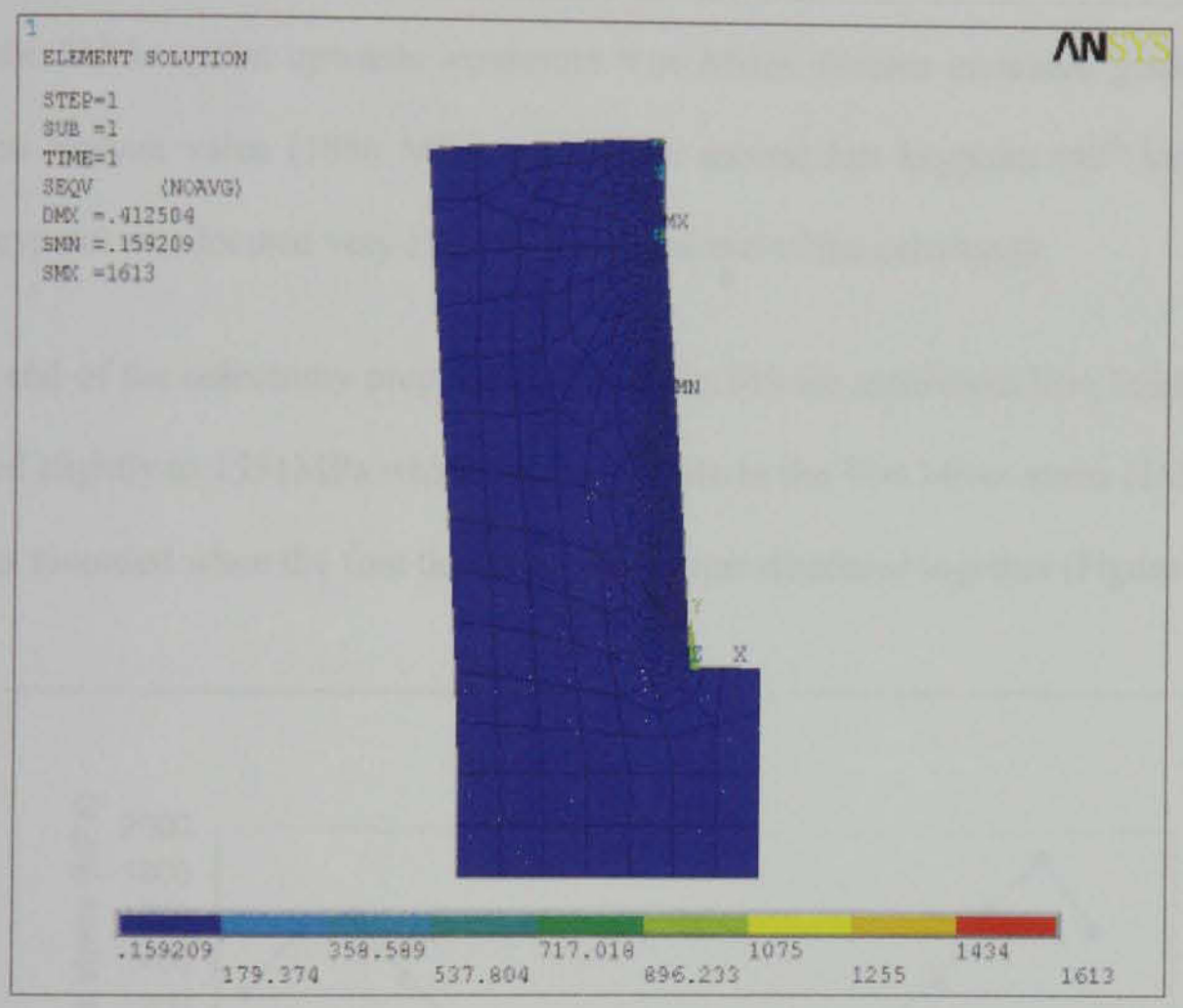

Figure 3.9 Maximum Von Mises stresses when the keypoint no. 1, 4, 7 and 10 were displaced. The maximum Von Mises stress (1613MPa) was located close to the displaced keypoint number 10. A lower stress (717MPa) could be observed around the 1st keypoint and 358MPa around the 4th keypoint. The predicted stresses were presented in Mega Pascal units (MPa).

After the 10th keypoint, the maximum stress gradually decreased to reach 772.019MPa at the 28th keypoint (Figure 3.10).

However, when keypoints number 16, 19, 22, and 25 were displaced, the maximum stress was found around the first keypoint (at the crest). From the 25th keypoint onwards the maximum Von Mises stress was always observed around the last displaced keypoint.

From the 31st keypoint upwards maximum Von Mises stresses increased gradually to reach its highest value (1880 MPa) around the second last keypoint (49th keypoint). This keypoint was located very close to the apical end of the osteotomy.

At the end of the osteotomy preparation (keypoint 51) the maximum Von Mises stress declined slightly to 1551MPa which was very close to the Von Mises stress (1555MPa) that was recorded when the first three keypoints were displaced together (Figure 3.10).

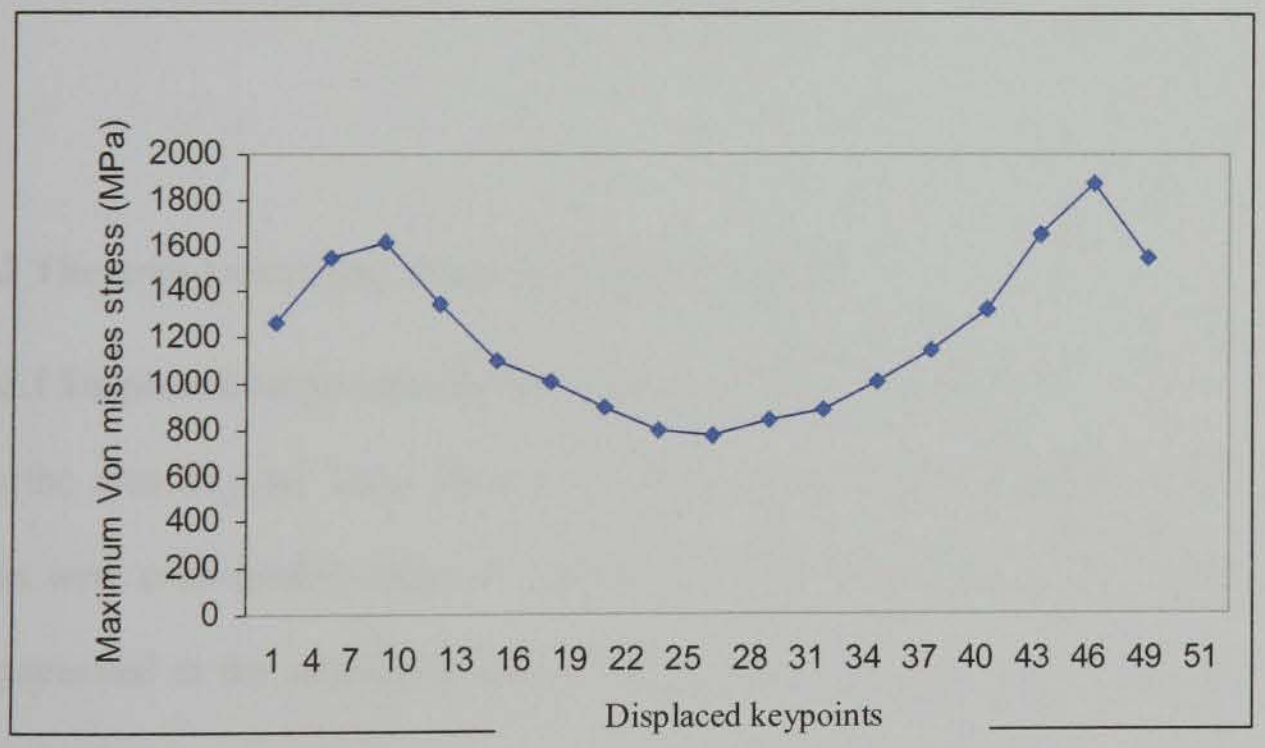

Figure 3.10 Maximum Von Mises stresses of the 5 mm FEM when the osteotomy diameter was 3mm and the keypoints were displaced -0.375mm in the x-direction.

In general, the curve could be divided into three main parts as follows (Figure 3.10):

1. It ascended gradually between the first and the 10th keypoint (ranging from 489.859 to 1613 MPa).
2. It descended gradually from the 13th to the 28th keypoint (maximum Von Mises stress ranged from 1345-772.019 MPa). At the 28th keypoint the maximum Von Mises stress reached 772.019MPa and then increase gradually afterward.
3. When the 31st keypoint and the other keypoints up to the 49th keypoint were displaced, the maximum Von Mises stresses increased gradually to reach their highest value (1880MPa) around the 49th.
4. When the last keypoint (51st keypoint) was also displaced, the maximum Von Mises stress decreased to 1551 MPa. (Figure 3.10).

3.4.1.2 The area 1mm away from the implant surface

3.4.1.2.1 Displaced keypoints and maximum Von Mises stresses

When the area beyond 1mm from the implant surface was studied the Von Mises stresses were considerably reduced. This indicates that most of the predicted stresses were generated in the osteotomy wall and reduced significantly in area away from the implant surface.

Comparison between the area that was close to the implant surface and formed the osteotomy wall and that was 1mm away from the implant surface is presented in Figure 3.11 and Table 3.3.

When all of the keypoints (including keypoint 51) were displaced, the generated stresses were similar (1551MPa) irrespective to the area examined.

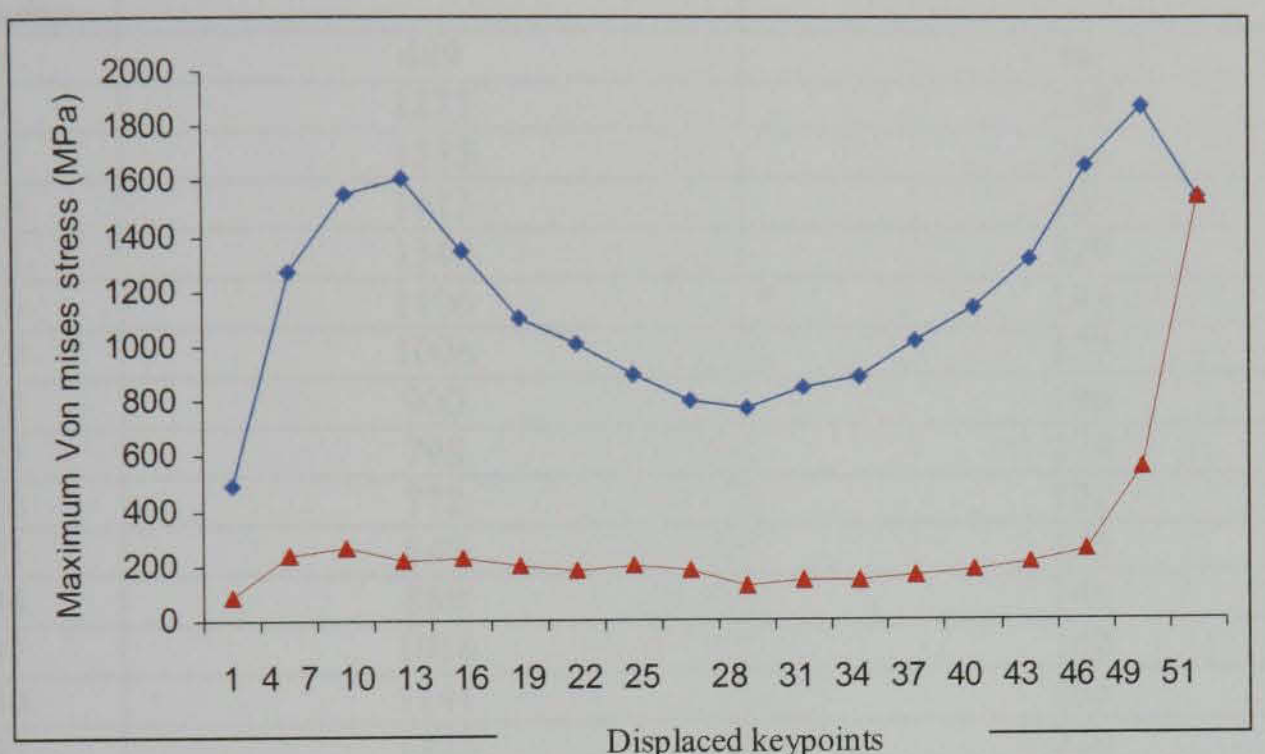

Figure 3.11 Comparisons between maximum Von Mises stresses that were predicted to occur in the area close to the implant surface (blue) with those predicted in the area beyond 1mm from the implant surface (red).

Table 3.3 Comparisons between maximum Von Mises stresses generated in the area close to the implant surface with those generated in the area beyond 1mm from the implant surface.

Maximum Von Misses stresses (Mpa)		
Displaced Keypoints	**Area close to the implant surface**	**Area ~1mm away from the implant surface**
1	489	88
4	1275	236
7	1555	264
10	1613	220
13	1345	229
16	1106	195
19	1006	177
22	900	196
25	798	179
28	772	122
31	847	145
34	889	146
37	1016	162
40	1141	183
43	1323	210
46	1656	251
49	1880	555
51	1551	1551

Displaced keypoints and maximum Von Mises strains (Area close to the implant:

3.4.1.2.1.1 Displacement of the 1st keypoint

When this keypoint was displaced in a similar manner and value as previously described the maximum Von Mises strain (4%) was observed at the apical end of the osteotomy preparation. A lower value of 2% was observed at the crest of the alveolar bone. Different strain levels were observed within cancellous bone while cortical bone

was minimally strained ($0.139E^{-4}$) (Figure 3.12). Strain values of 0.00486 and 0.0097 can be seen in the cancellous bone in the area away from the implant surface.

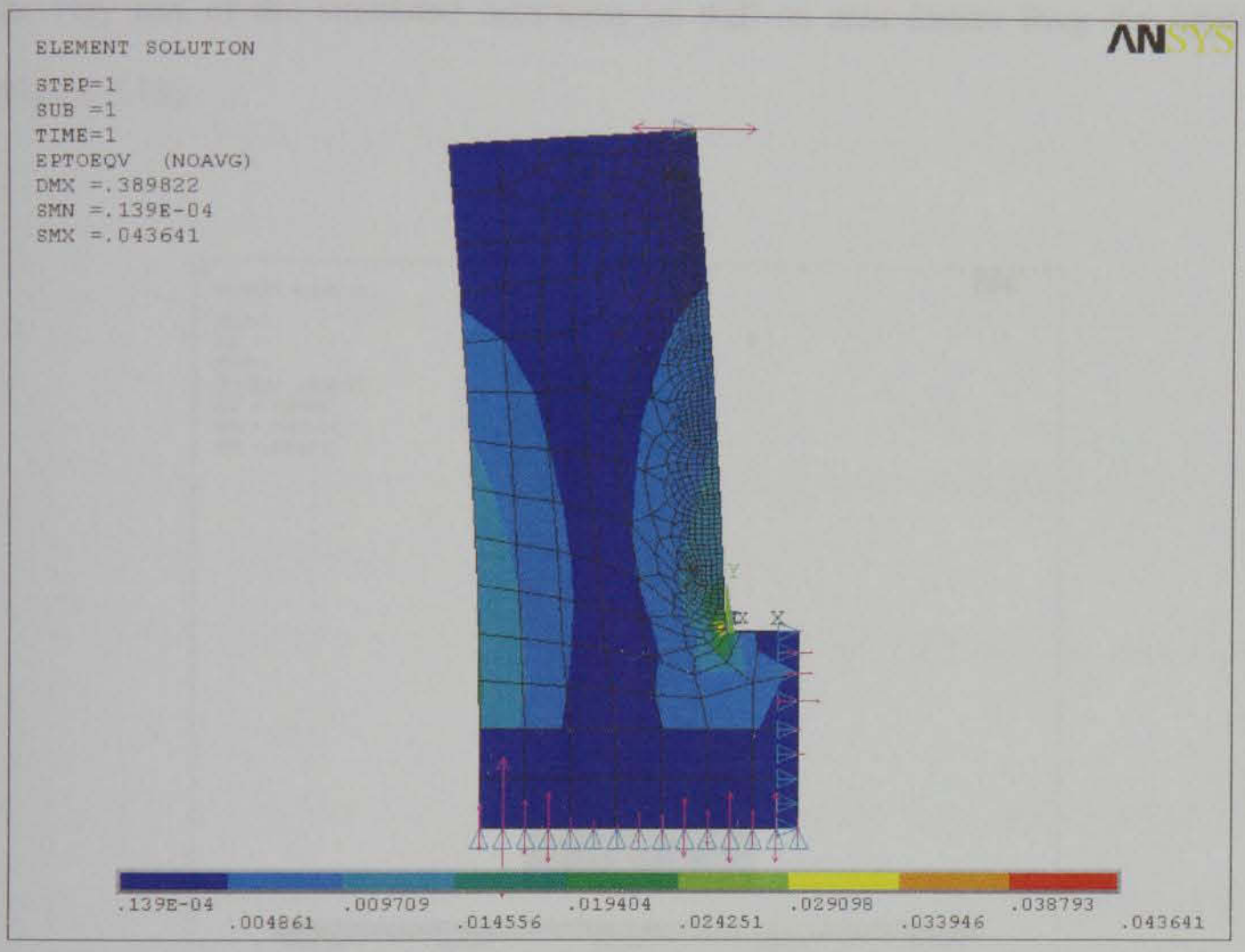

Figure 3.12 Maximum Von Mises strains. The displacement of keypoint no.1. The maximum strain was located at the apical end of the osteotomy preparation. The predicted strains were presented in percentages.

3.4.1.2.1.2 Displacement of the 1st and 4th keypoint

When these two keypoints were displaced together the maximum Von Mises strain raised gradually. High maximum Von Mises strains could be seen around these two keypoints as well as at the apical end of the osteotomy. However, the maximum Von

Mises strain was observed around the first keypoint (at the crest of the alveolar bone) with a value of 9.3% (Figure 3.13). A strain of a lower value ($0.126E^{-4}$) could be seen involved in most of the simulated bone, while a strain of 0.0204 could be observed at the very end of the simulated osteotomy as well an area distant from the implant (Figure 3.13).

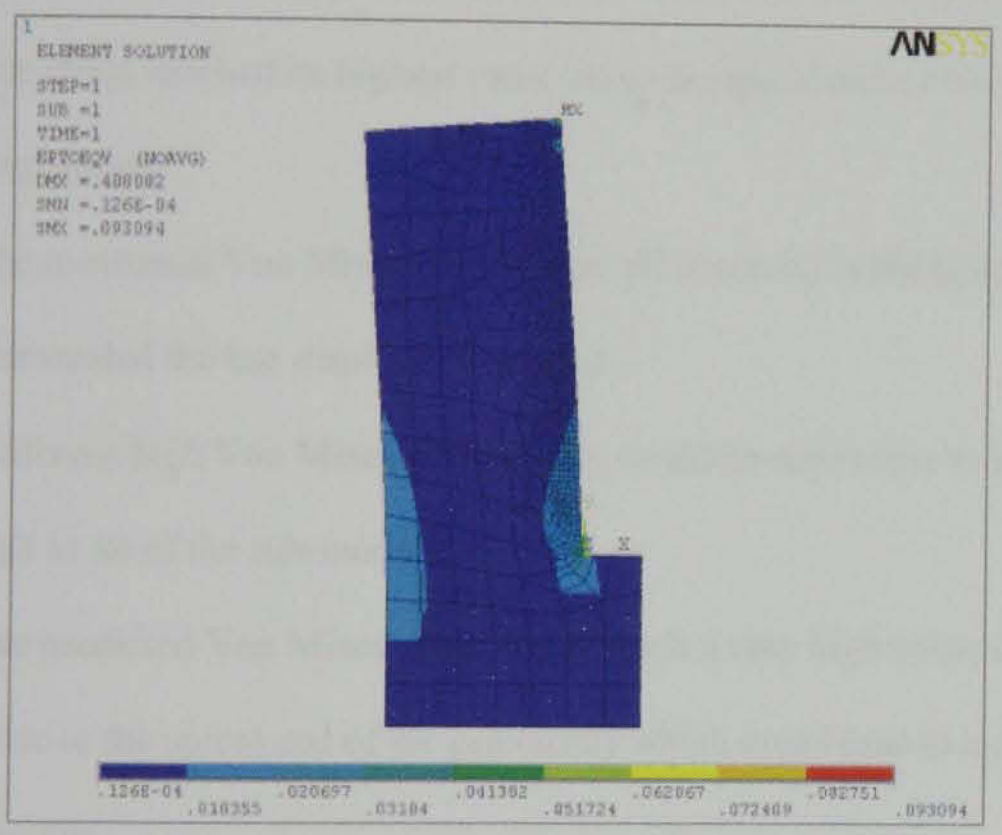

Figure 3.13 Maximum Von Mises strains when the keypoints no 1 and 4 were displaced. The maximum Von Mises strain (9.3%) was located at the crest around the 1st keypoint. The predicted strains were presented in percentages.

3.4.1.2.1.3 Displacement of the 1st and 4th and other keypoints

As the other keypoints were displaced, the maximum Von Mises strain increased gradually (almost linearly) to reach its highest value when keypoint number 49 was

displaced. The maximum Von Mises strain value was **1.372**. However, when the last keypoint (keypoint number 51) was displaced the maximum Von Mises strain slightly decreased to a value of 1.132.

In general, the following points could be observed from the curve (Figure 3.14).

1. The strains increased gradually as more keypoints were displaced.
2. The strain reached its highest value close the apical end of the osteotomy preparation.
3. The maximum Von Mises strains were all observed in the bone which surrounded the last displaced keypoint.
4. Different high Von Mises strain values could be seen close to the osteotomy wall in all of the sub-models.
5. The predicted Von Mises strain could reach a very high value i.e 113% close to the apical end of the osteotomy which could lead to a catastrophic fracture.

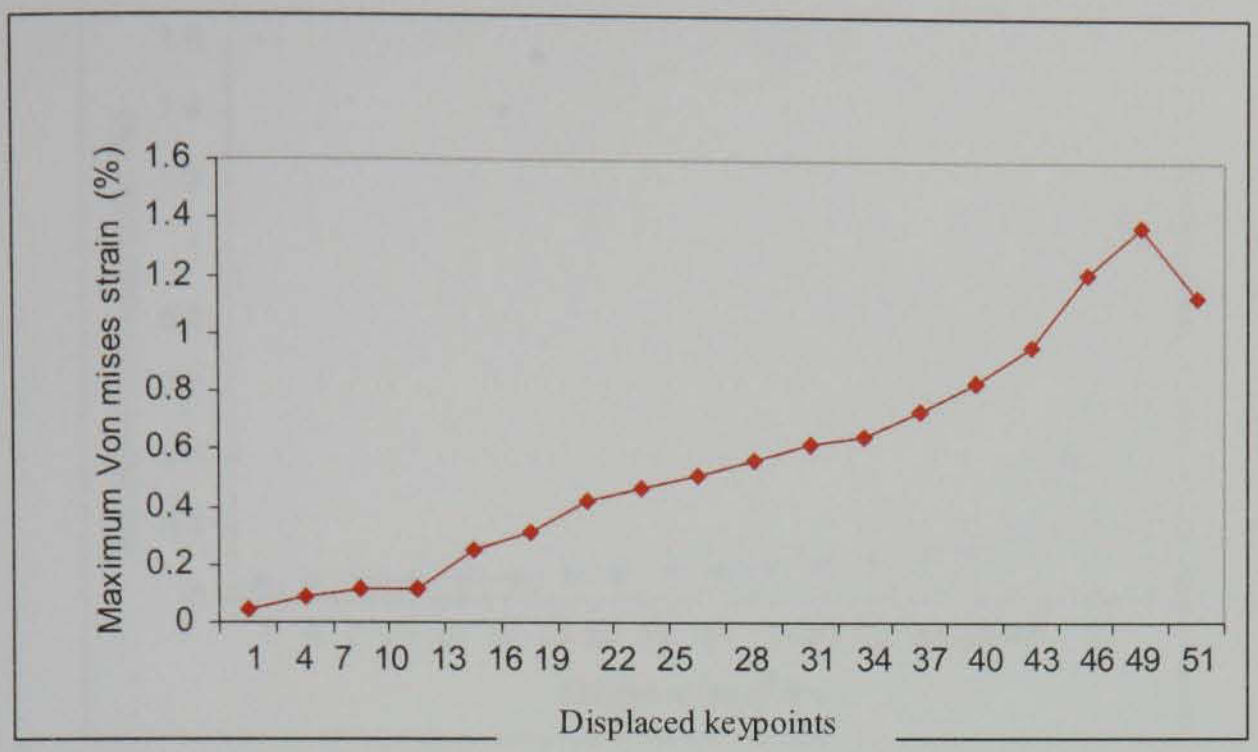

Figure 3.14 Maximum Von Mises strains in the area close to the implant surface when the osteotomy diameter was 3mm and the keypoints were displaced by –0.375mm in the x-direction. The predicted strains were presented in percentages.

3.4.1.3 The area 1mm away from the implant surface

3.4.1.3.1 Displaced keypoints and maximum Von Mises strains

When the area beyond 1mm from the implant surface was studied the Von Mises strains were noticeably reduced (Figure 3.15).

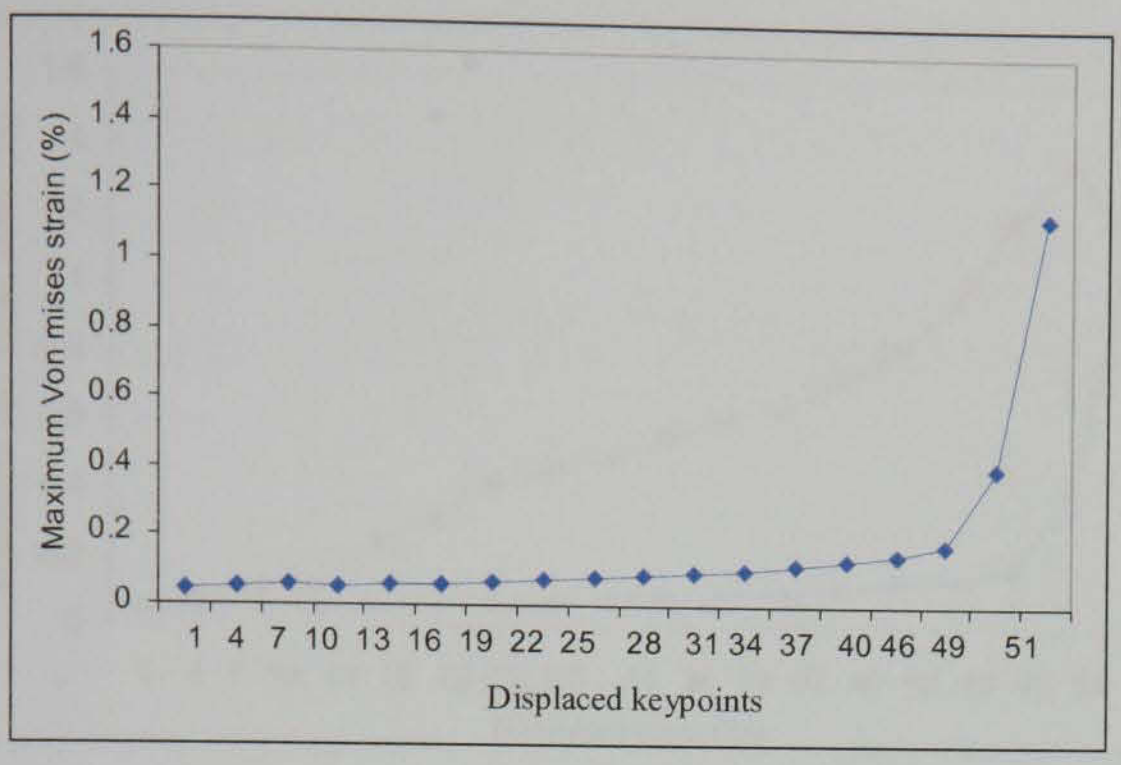

Figure 3.15 Maximum Von Mises strains that were generated in the area beyond 1mm from the implant.

When the keypoint no. 51 was displaced, the generated stresses were similar (1551MPa) irrespective of the area examined.

Comparisons between the predicted maximum Von Mises strains that were generated at the area which was close to the implant surface with those generated at areas located 1mm away from the implant are presented in Figure 3.16 and Table 3.4.

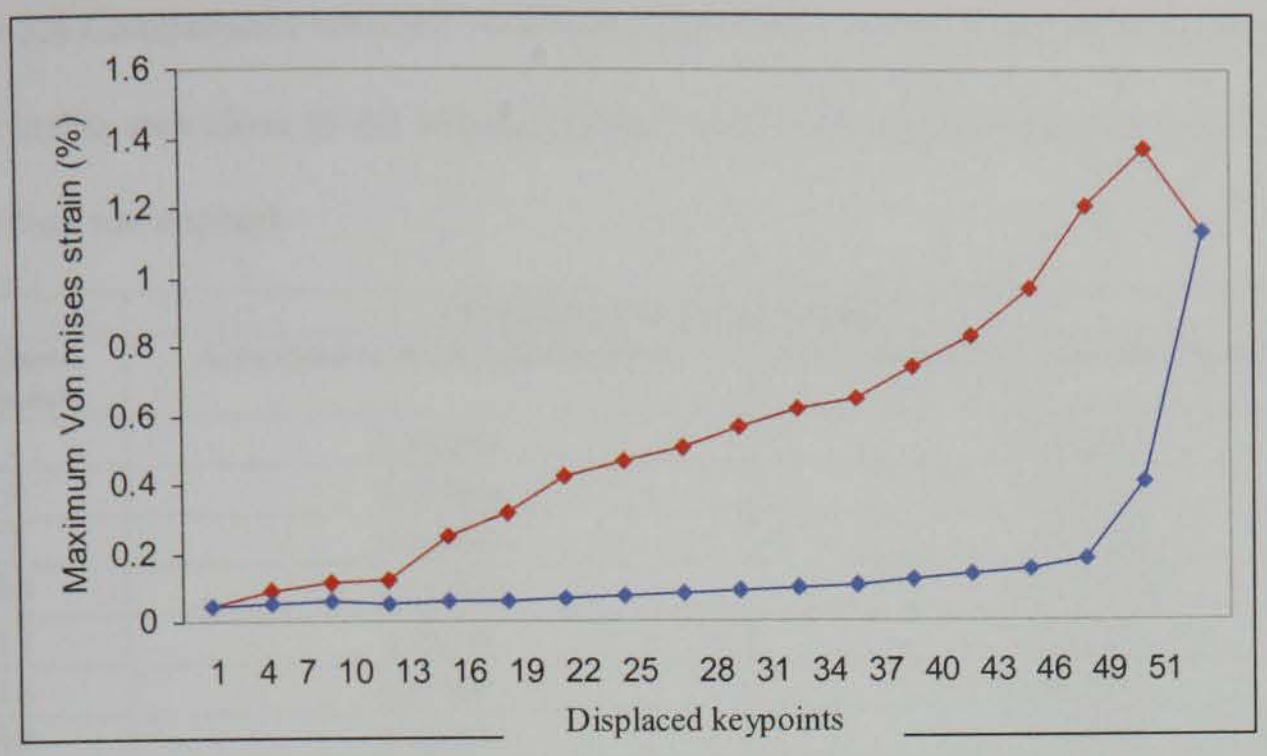

Figure 3.16 Maximum Von Mises strains that were generated in the area close to the implant surface (red) and those generated in the area beyond 1mm from the implant (blue).

Table 3.4 Comparisons between maximum Von Mises strains which were predicted to occur in the area close to the implant surface with those predicted in the area beyond 1mm from the implant

Maximum Von Misses strains		
Displaced Keypoints	**Area close to the implant surface**	**Area ~1mm away from the implant surface**
1	0.043641	0.043641
4	0.093094	0.049802
7	0.113489	0.057252
10	0.117744	0.0517568
13	0.25243	0.061373
16	0.319087	0.062871
19	0.423644	0.067717
22	0.465769	0.073589
25	0.508545	0.080324
28	0.563517	0.087967
31	0.618526	0.096613
34	0.649512	0.106768
37	0.741455	0.118722
40	0.832604	0.133616
43	0.965547	0.153513
46	1.209	0.183257
49	1.372	0.405617
51	1.132	1.132

3.4.2 Sub-model 2

When the surrounding bone was 5mm in thickness, the osteotomy diameter was increased to 3.25mm and the keypoints were displaced by -0.25mm, the maximum Von Mises stresses that were generated at the area close to the implant and those 1mm away from the implant surface showed the same trend that was observed in sub-model 1. However, the predicted Von Mises stresses decreased (Figure 3.17). This is because the bone was displaced to a lesser degree when compared with sub-model 1.

The predicted strains were also greater than those observed in sub-model 1 (Figure 3.18). The predicted strains were initially close to that generated in sub-model 1 (from the 1st keypoint to the 4th keypoint), then they increased but in a lesser steep manner when compared with sub-model 1(Figure 3.18).

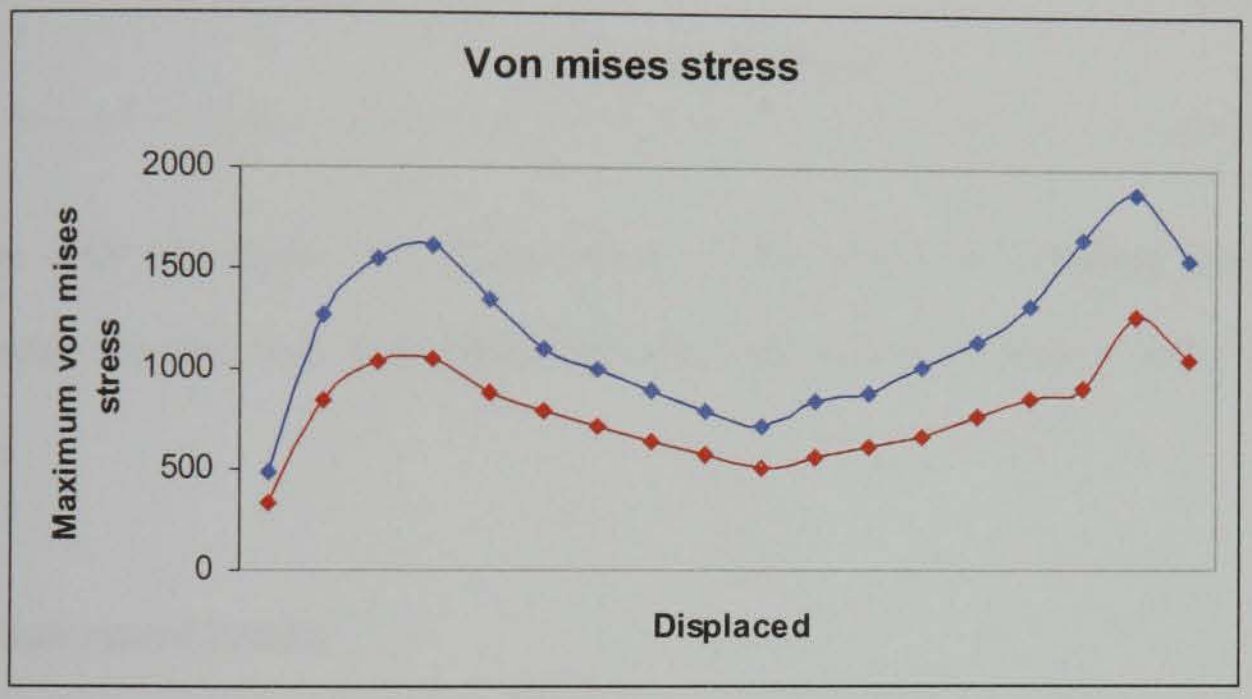

Figure 3.17 Comparisons between maximum Von Mises stresses of the 5mm FEM with the osteotomy diameter of 3mm (blue) and 3.25mm (red).

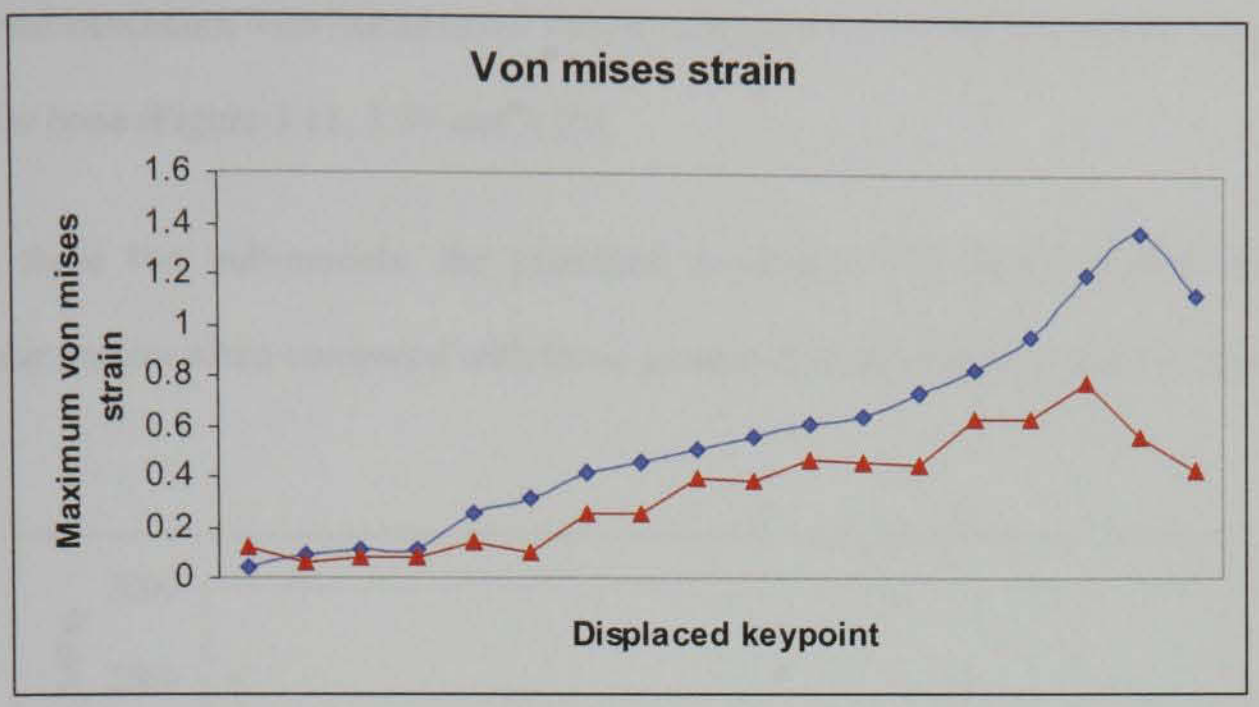

Figure 3.18 Maximum Von Mises strains of the displaced keypoints when the osteotomy diameter was 3mm (Blue) and when the osteotomy diameter was 3.25mm (Red).

3.4.3 Sub-model 3 and 4

From Figure 3.19 and Table 3.5, the following points could be proposed:

1) Sub-model 3 had higher Von Mises stress values than sub-model 4.

2) Maximum Von Mises stresses at each displaced keypoint were higher in sub-model 3 than in sub-model 4.

3) Sub-model 3 and 4 had greater maximum Von Mises stresses than that derived from sub-model 1 and 2 (Figure 3.11).

4) The highest predicted maximum Von Mises stress values which were observed in sub-models 3 and 4 were derived when the 1st keypoint was displaced; this keypoint was located at the crest of the simulated alveolar bone and the wall of the osteotomy preparation. This in contrast with sub-model 1 and sub-model 2 where the lowest

predicted maximum Von Mises stress values were observed at the crest of the simulated alveolar bone (Figure 3.11, 3.19 and 3.20).

5) In these two sub-models, the predicted maximum Von Mises stresses had an irregular pattern when compared with those generated in sub-model 1 and sub-model 2.

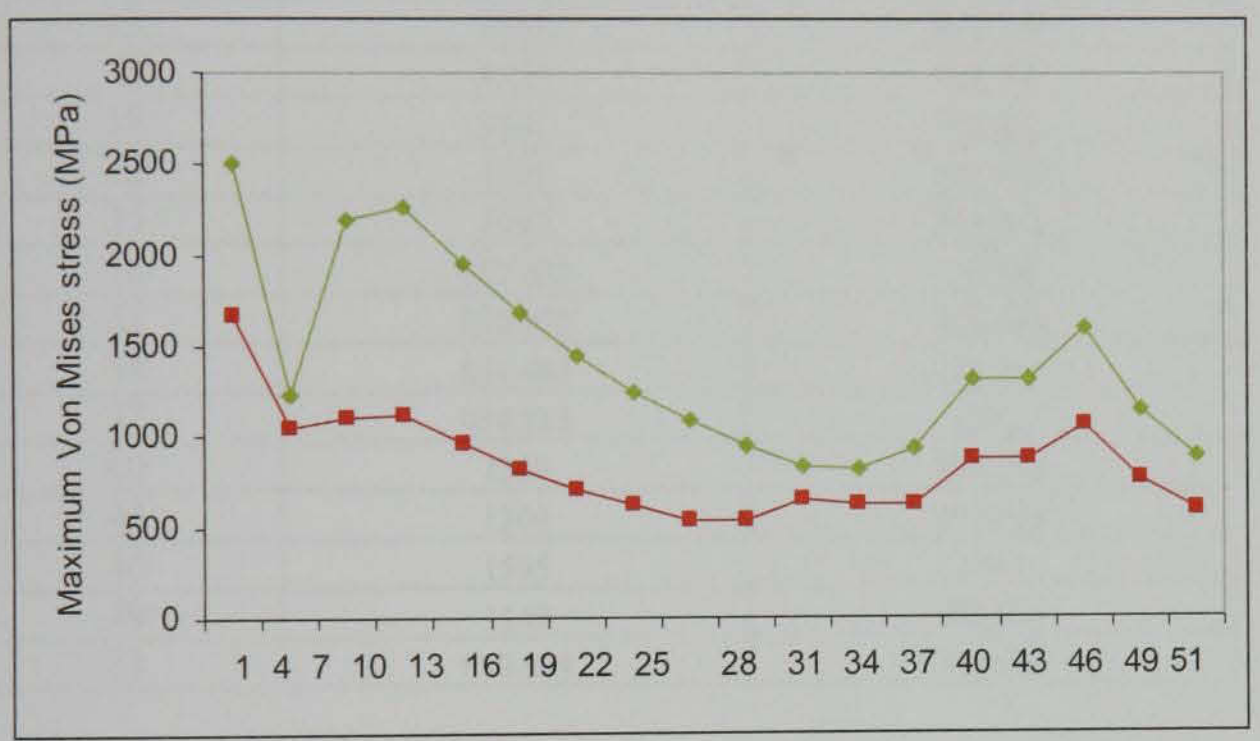

Figure 3.19 Maximum Von Mises stresses of sub-model 3 (green) and sub-model 4 (red).

Table 3.5 Comparisons between maximum Von Mises stresses generated in sub-model 3 with those generated in sub-model 4

Maximum Von Misses stresses		
Displaced Keypoints	**Sub-model 3**	**Sub-model 4**
1	2503	1673
4	1233	1043
7	2196	1101
10	2269	1112
13	1954	961.719
16	1677	819.951
19	1447	711.856
22	1251	617.837
25	1093	534.561
28	952.302	534.561
31	838.978	646.866
34	821.483	627.348
37	934.813	623.2
40	1309	872.594
43	1309	872.894
46	1595	1063
49	1149	766.326
51	890.994	593.996

From Figure 3.20 and Table 3.6, the following points could be suggested:

1) Sub-model 3 had a higher Von Mises strain values than sub-model 4.

2) Both curves followed the same pattern.

3) Sub-model 3 and 4 had greater maximum Von Mises strains than those derived from sub-model 1 and 2.

4) In these two sub-models, the predicted maximum Von Mises stresses had an irregular pattern when compared with those generated in sub-models 1 and 2.

5) The predicted Von Mises stresses were located at the crest of the simulated alveolar bone.

6) At keypoint 28 the predicted strains were very close to each other in both sub-models, 0.47657 for sub-model 3 and 0.472165 for sub-model 4.

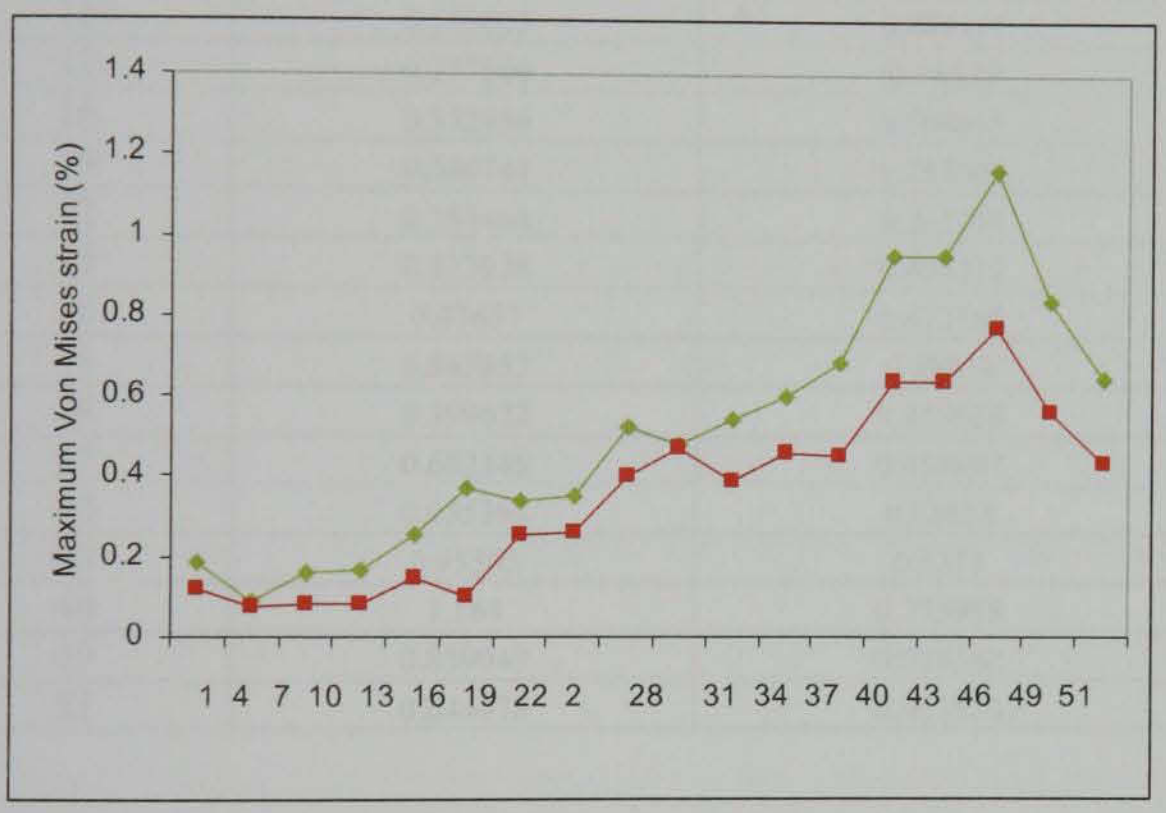

Figure 3.20 Maximum Von Mises strains derived from sub-model 3 (green) and sub-model 4 (red).

Table 3.6 Comparisons between maximum Von Mises strains generated in sub-model 3 with those generated in sub-model 4

	Maximum Von Misses strains	
Displaced Keypoints	**Sub-model 3**	**Sub-model 4**
1	0.182704	0.122094
4	0.090033	0.076144
7	0.160287	0.080346
10	0.165623	0.081191
13	0.257604	0.14522
16	0.372936	0.104675
19	0.340741	0.257502
22	0.353464	0.261289
25	0.522926	0.404222
28	0.47657	0.472165
31	0.545852	0.39019
34	0.599622	0.457918
37	0.682346	0.454897
40	0.955394	0.63693
43	0.95565	0.6371
46	1.164	0.775988
49	0.839043	0.559362
51	0.644978	0.433574

3.5 Discussion

Mismatches between the implant diameter and the osteotomy preparation leads to the generation of stresses and strains in the peri-implant bone. These stresses and strains could significantly rise to reach a high value that exceeds the bone elastic limit and leads to plastic deformation, which could cause the bone to fail.

The area close to the implant surface and that made up the osteotomy wall was strained above the 4000με (0.4%) that was postulated as the mild overload level beyond which irreversible bone damage could occur (Wiskott & Belser 1999). Bone damage and failure of bovine cortical bone have been studied in static tensile experiments and have shown large variations of stress failure from 100 to 200MPa, and failure strain from 0.4 to 4% (Pithioux *et al.* 2004).

However, how much stresses and how far bone is strained during implant placement is a matter of speculation. Nkenke and coworkers (2002) used an osteotome method for implant placement in rabbit. By the osteotome method, bone density and volume is increased and consequently will enhance implant initial stability (Nkenke *et al.* 2002, Strietzel *et al.* 2002, Neugebauer *et al.* 2006). However, peri-implant bone should not be stressed or strained beyond its biological limit which if it is exceeded will jeopardize angiogenesis and endanger bone cell activities. Nkenke *et al.* (2002) recommended that compression forces (used in the osteotome method) of 20MPa should not be exceeded.

The observed maximum stresses were seen close to the osteotomy wall and around the displaced keypoints. This observation is in accordance with the first study, which reported the generation of the diffuse damage (contact damage) in bone that made up the osteotomy wall and was in close contact with the implant surface.

The predicted stresses in the area beyond the 1mm area close to the implant surface were found to decrease considerably. This is also in accordance with the first study where the number of the observed microcracks was very low. It reasonable to suggest that the stresses were generated due to the implant placement being high in the area

close to the implant surface and led to local high stresses that could have led to the generation of diffuse damage areas while the stresses in the area beyond the previous area were not significantly high to generate bone damage such as microcracks.

Regarding the strains that were generated in both areas; they were high in the area close the implant and significantly lower in the area beyond the implant surface.

In the present study, maximum Von Mises stresses and strains were most commonly seen when the surrounding bone thickness increased from 5mm to 10mm. This observation may indicate differences in stress and strain generation according to constrain conditions. For instance, the generated stresses and strains when an implant is being placed in a partially edentulous jaw may differ compared to that placed in an edentulous jaw.

In the area farther from the implant surface, the predicted stresses and strains were low compared with those in the area close to the implant. However, the stress values ranged from 88MPa to 1551MPa. These values (except the lower range) are higher than the ultimate compressive stress of cortical bone as was described by (Reilly & Burstein 1975).

Regarding strain values, all strain values were higher than the upper limit of the range (0.4% to 4%) which was the limit at which bone may fail (Pithioux *et al.* 2004).

In the current study, the highest predicted maximum Von Mises stress values which were observed in sub-models 3 and 4 were derived when the 1st keypoint was displaced; this keypoint was located at the crest of the simulated alveolar bone and the

wall of the osteotomy preparation. This in contrast with sub-models 1 and 2 where the lowest predicted maximum Von Mises stress values were observed at the crest of the simulated alveolar bone. This in part may explain the early crestal bone loss observed in clinical studies.

However, this study dealt only with one factor that may influence the bone reaction to the implant placement procedure and other factors such as the osteotomy preparation procedure, implant surface topography and host response should not be ignored.

Comparison between the results of the present study and other studies is not possible because to my knowledge this issue has not been addressed in literature.

3.6 Clinical implications

In this simulation, the disparities in diameters between implant and osteotomy were 0.5mm and 0.75mm. From the obtained results, it is reasonable to assume that mismatches between implant and osteotomy should be kept as low as possible compatible with obtaining adequate primary stability as the potential catastrophic damage was demonstrated with the larger mismatches.

It may be important to prepare the osteotomy preparation deep enough and to use a shorter implant than the osteotomy to avoid generation of high stresses and strains at the apical end of the osteotomy while the implant threads are being engaged with the osteotomy wall.

Chapter 4. Intracortical bone remodelling during early stages of bone healing around self tapping endosseous implants

4.1 Introduction

Histomorphometric measurements of bone modelling and remodelling involves the application of the probability theory to geometry, through the use of estimates rather than exact measurements (Nölke1995). The dynamic nature of bone can be studied when fluorochrome chelating agents are administrated during bone remodelling activity.

Fluorochromes such as alizarin complexone are used as bone labels to study bone remodelling cycles due to their ability to chelate exposed calcium at the bone/osteoid (non-mineralised bone) interface. Each fluorochrome agent can be seen as a coulred band using fluorescent microscopy. It is acknowledged that if sequential doses of fluorescent chelating agents are given and spaced by a certain number of days, several fluorescent bands will be observed which are separated by a distance equivalent to the net amount of bone formed in that period (Suzuki & Mathews 1966, Módis *et al.* 1969, Nölke1995, Vajda *et al.* 1999; Moore, 2000, Lee *et al.* 2002, Lee *et al.* 2003).

The aims of the study are:

1) To describe the histological features of bone remodelling activity at areas ≤ one millimetre from the implant surfaces for different healing periods.

2) To study remodelling cycles in the area one millimetre away from implant surfaces at baseline, 3, and 6 weeks following implant placement using the same bone labelling technique.

3) To investigate quantitatively bone formation rates that occur in the area one millimetre away from implant surfaces at baseline, 3, 6 and 10 weeks following implant placement using sequential bone labelling.

All implant sites were prepared according to the technique described for *Group III* in the previous study (osteotomy preparation without tapping and receiving an implant).

4.2 Materials and Methods

The protocol followed was in accordance with the animal research policies of the Department of Health and Children in Ireland.

Four beagle dogs, about two years old and weighing approximately 16kg were included in the study.

General anaesthesia was administered as described in Chapter 2.

- The mandibular premolar regions of each dog were used for the study.
- All mandibular premolars were extracted.

After three months of healing, general anaesthesia was administered and implant surgery carried out. One implant was placed in each animal at baseline, 3, 6 and 9 weeks (Table 4.1) and the implant sites were rotated so as to balance the experimental design between animals and the different implant locations (Table 4.2).

All implants were "ITI Implants": (Dental Implant System®, (Straumann, Walenburg, Switzerland; Solid-screw; 8x4.1mm). The implant surgery was performed in accordance with the recommendations of the manufacturer. All implant were placed using a one stage technique. The border between the rough and smooth implant surface was positioned at the level of the alveolar bone crest.

Figure 4.1 ITI implant used in the study.

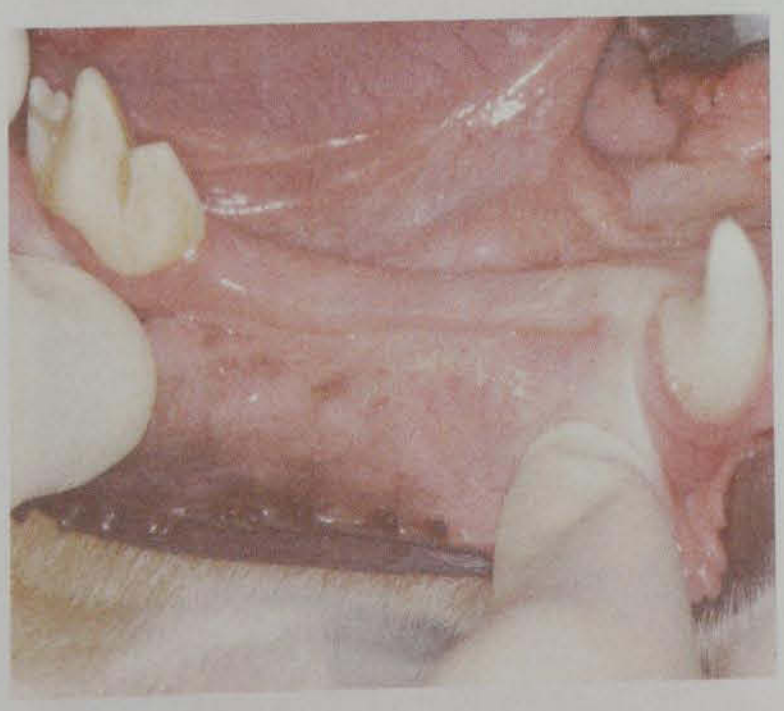

Figure 4.2 The experiment site.

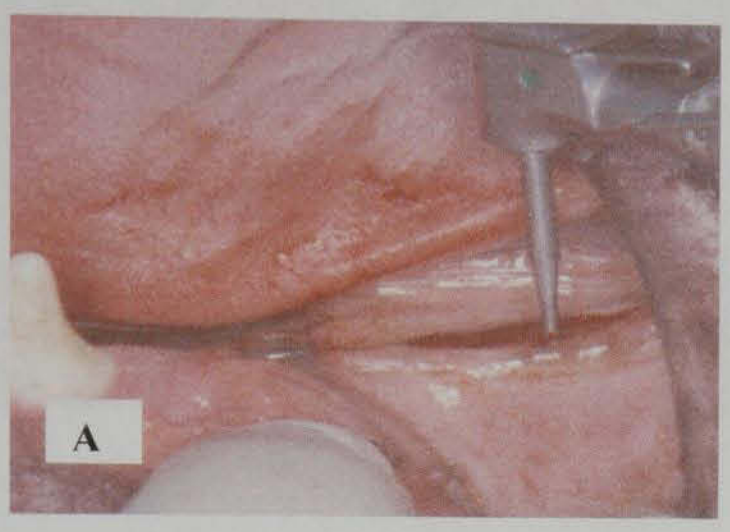
A

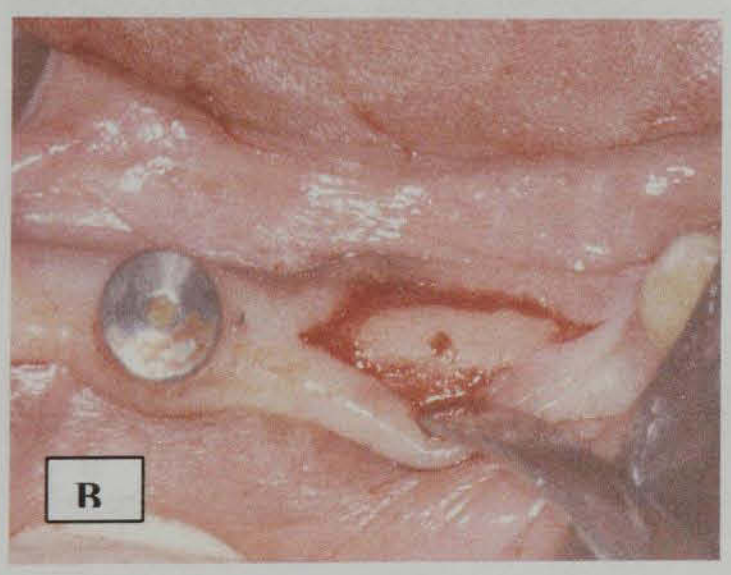
B

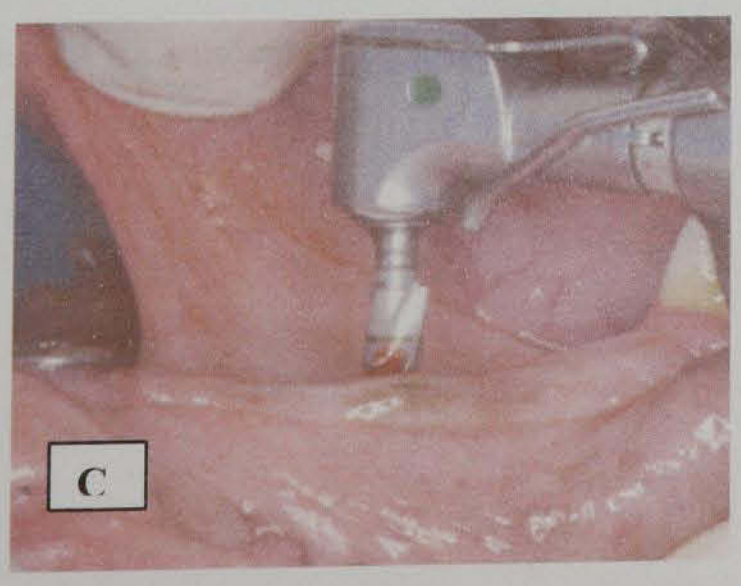
C

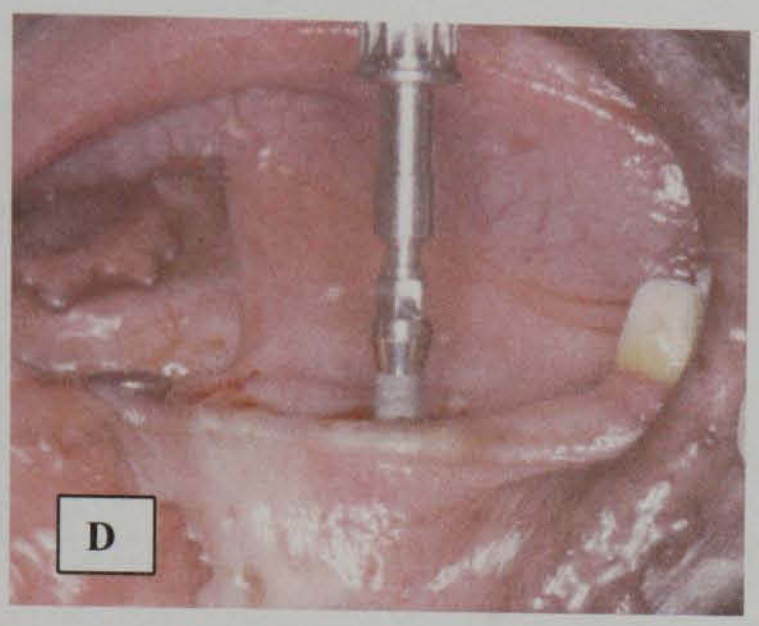

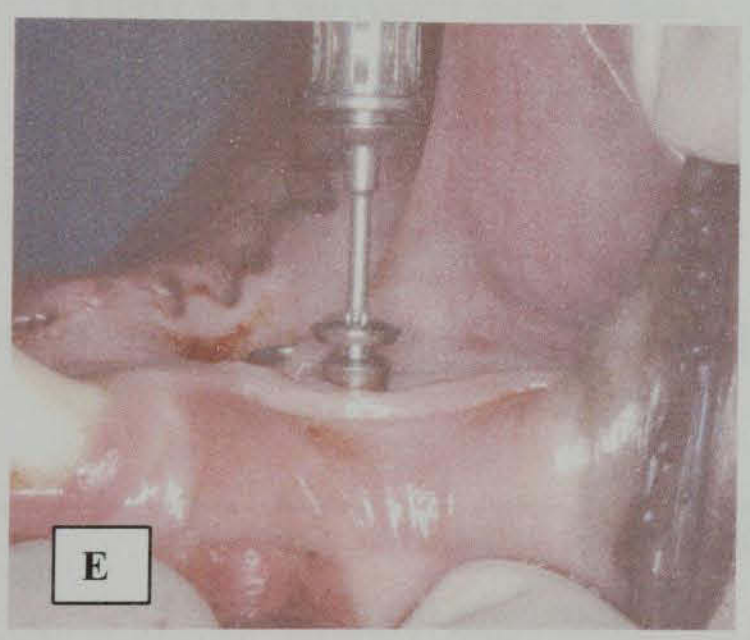

Figure 4.3 The surgical procedure. A) Marking of the implant site using a round bur. B) The marking produced by the bur. C) The drill used in preparation of the osteotomy. D) Insertion of the implant. E) Placement of the cover screw.

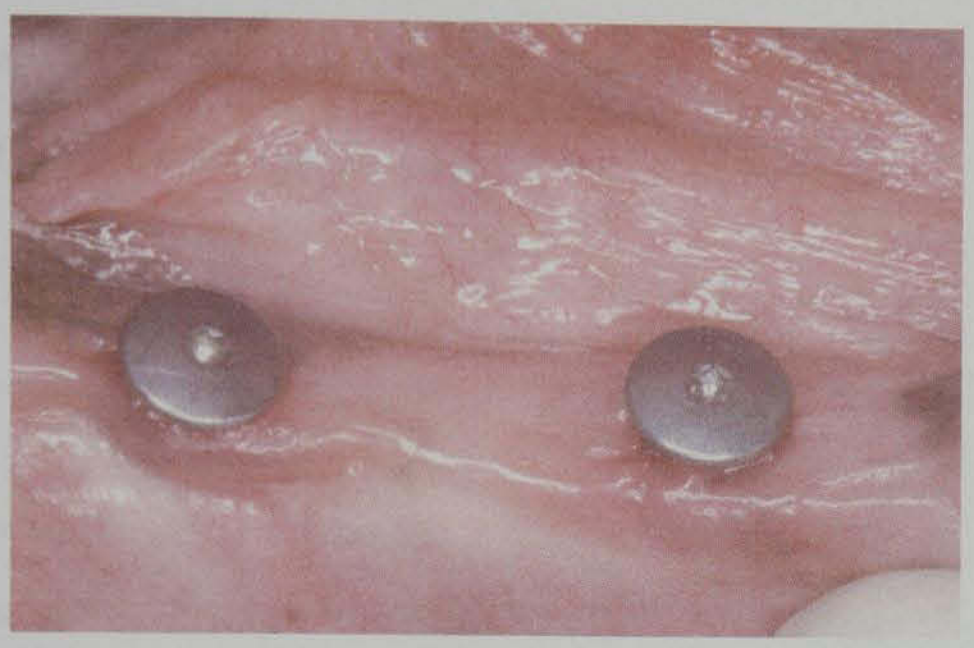

Figure 4.4 Two healed implant sites.

Table 4.1 Distribution of implants according to dog number, side, region and time-lapse.

		Regions of implant and time of implant placement	
Dog' Number	Dog' side	$1^{st} - 2^{nd}$ Premolar	3rd– 4^{th} Premolar
Dog 1	Left	Baseline	3-week
Dog 1	Right	6-week	9-week
Dog 2	Left	9-week	Baseline
Dog 2	Right	3-week	6-week
Dog 3	Left	6-week	9-week
Dog 3	Right	Baseline	3-week
Dog 4	Left	3-week	6-week
Dog 4	Right	9-week	Baseline

Four different fluorochromes were given at different times in order to study bone remodelling activities around dental implants. One day after the implant placement Alizarin was administrated intravenously at baseline, 3-, and 6-week and another fluorochrome (Oxytetracycline) one week after the placement of the last implant (Week 10). (Table 4.2 and Figures 4.5 and 4.6).

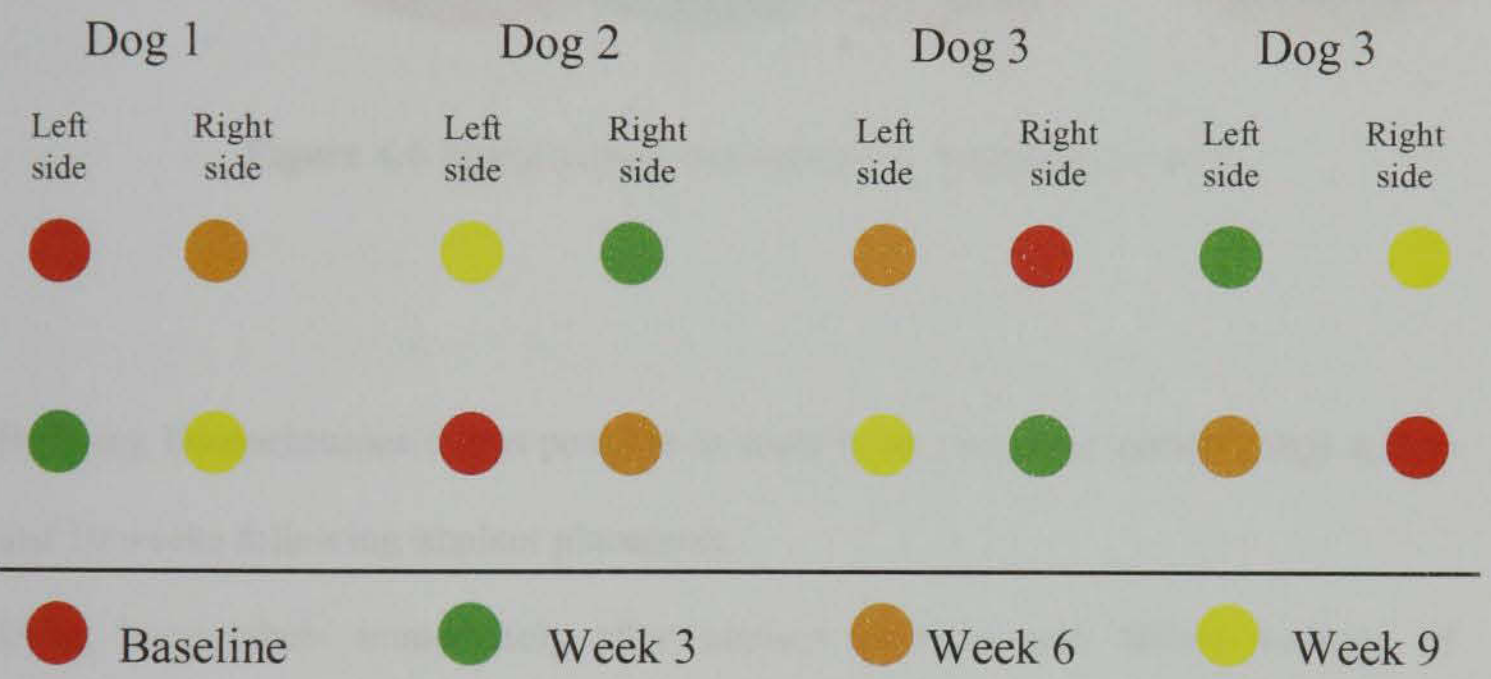

Figure 4.5 Flow chart of the study. Each implant time was represented by four slides.

Table 4.2 Dosages of bone fluorochromes and their excitation, emission maxima and colour (modified from Rahn, 1977; Rost, 1995; O'Brien 2000; Lee *et al.* 2002).

Fluorochrome	**Dosage (mg/kg) (intravenous)**	**Excitation wavelength (nm)**	**Emission wavelength (nm)**	**colour**
Alizarin	30	580	625	Red
Calcein	10	495	540	Green
Xylenol orange	90	377	615	Orange
Oxytetracycline	20	390	520	Yellow

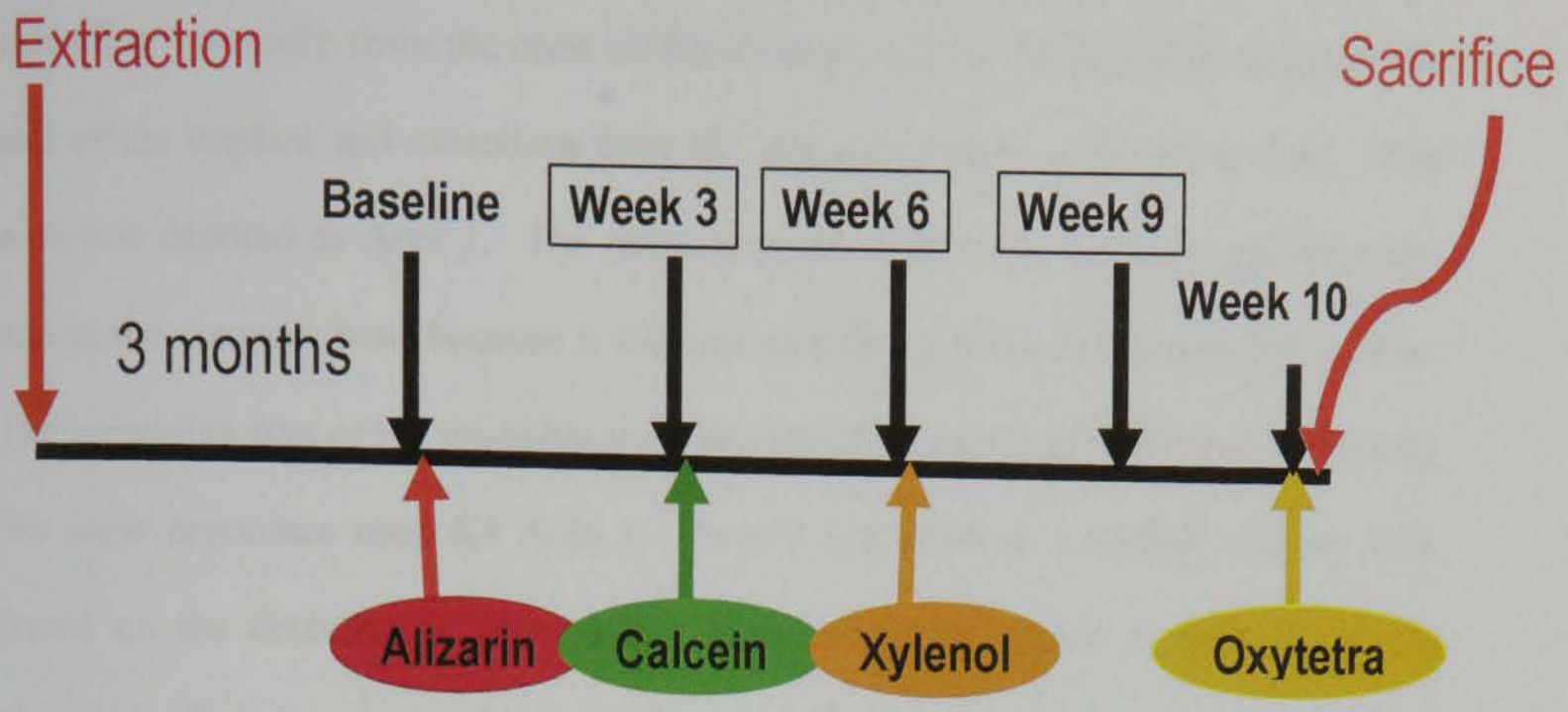

Figure 4.6 Study outline: animals n = 4; implants n = 16.

By using fluorochromes it was possible to study bone turn-over (remodelling) at 3, 6 and 10 weeks following implant placement.

Using bone labels immediately after implant insertion also allows marking of osteogenic surfaces by incorporating these labels at bone forming sites (Garetto *et al.* 1995). Therefore, immediately after surgery for each time point, one of the following bone labels was intravenously injected (Sun *et al.*1992; Hoshaw *et al.*1994; Garetto *et al.* 1995). The dose of the first three agents [(Alizarin (25 mg/kg), calcein (10 mg/kg) and xylenol orange (90 mg/kg)] were used according to the protocol observed by Lee and coworkers (2002), while the dose of the oxytetracycline was reduced to a concentration of 20 mg/kg because one dog died while the oxytetracycline was being injected. Thus oxytetracycline was given to the remaining three dogs one week after the insertion of the last implants (i.e. 10 weeks after the baseline) and the dogs were sacrificed one day after the last injection; at 71 days after the baseline time.

In the present study all measurements were carried out at the peri-implant bone area extending vertically from the crest of the alveolar bone to about 2 mm apical to the end of the implant and extending from the implant surface to the periostium. This area was denoted as Area 1. The measurements were made buccally and lingually and in the compact bone because it was not possible to do so in the cancellous bone. The remaining part of the mandible was considered as area 2 and was measured using the same procedure used for Area 1. Area 2 was used as a control (Figure 4.7). Based on the detection of bone labels, each secondary osteon in both areas was observed. Two lines crossing each other at right angles through the middle of each osteon; one parallel to the long axis of the implant and the other perpendicular to it served as reference points. The distance between each two consecutive labels on these lines was measured and four measurements were made for each osteon and the mean computed (Figure 4.9). All clearly visible secondary osteons were recorded and computed.

4.2.1 Cutting and grinding procedures

Each mandible was then sectioned at the area between the first and second molars using a diamond disc (Superflex®, Edenta AG, Switzerland) mounted in a straight hand piece at 100r.p.s. using water as a coolant.

Each mandible was then divided into two halves at the central incisors region using a scalpel.

Each half was stored in absolute alcohol (Ethanol, Aldrich Chemical Company, Inc 1001 West Saint Paul Avenue, Milwaukee, W1 53233, USA) until the time of the embedding procedure.

Block biopsies were harvested using a Minitom® cutting tool (Struers, Copenhagen, Denmark). Each block contained the implant and about 3 mm of the surrounding bone mesially and distally. The blocks were then rinsed in running water and were embedded in clear methylmethacrylate (as described in chapter 2).

The embedded blocks were mounted on the Minitom® to obtain a thickness of approximately 300μm. The implant sites were oriented so that the diamond saw was parallel to the experiment site and perpendicular to the body of the mandible. The cuts were made vertically through the centre of the experiment sites. Three sections (of 300μm thickness) were obtained; one in the centre, one mesial and one distal.

The obtained slides were ground manually to obtain a thickness of approximately 100-150μm using sandpaper under running water. Slides were washed using washing up liquid and then washed with distilled water, dried using tissue paper and mounted on glass slides using a mounting medium DPX® (Eukitt's mounting medium, Germany) under a glass cover slip.

4.2.2 Histological analysis

Measurements were carried out in the peri-implant bone area which extended:

- Vertically from the crest of the alveolar ridge to 2 mm apical to the end of the implant
- Horizontally extended from the implant surface to the periostium.

This area was represented as "Area 1".

The remaining part of the mandible was considered as "Area 2" and was measured using the same procedure used to measure Area 1.

An area close to the implant surface (≤ 1mm) was denoted as the interfacial zone.

The measurements were made buccally and lingually in the compact bone as it was not possible to do so in the cancellous bone.

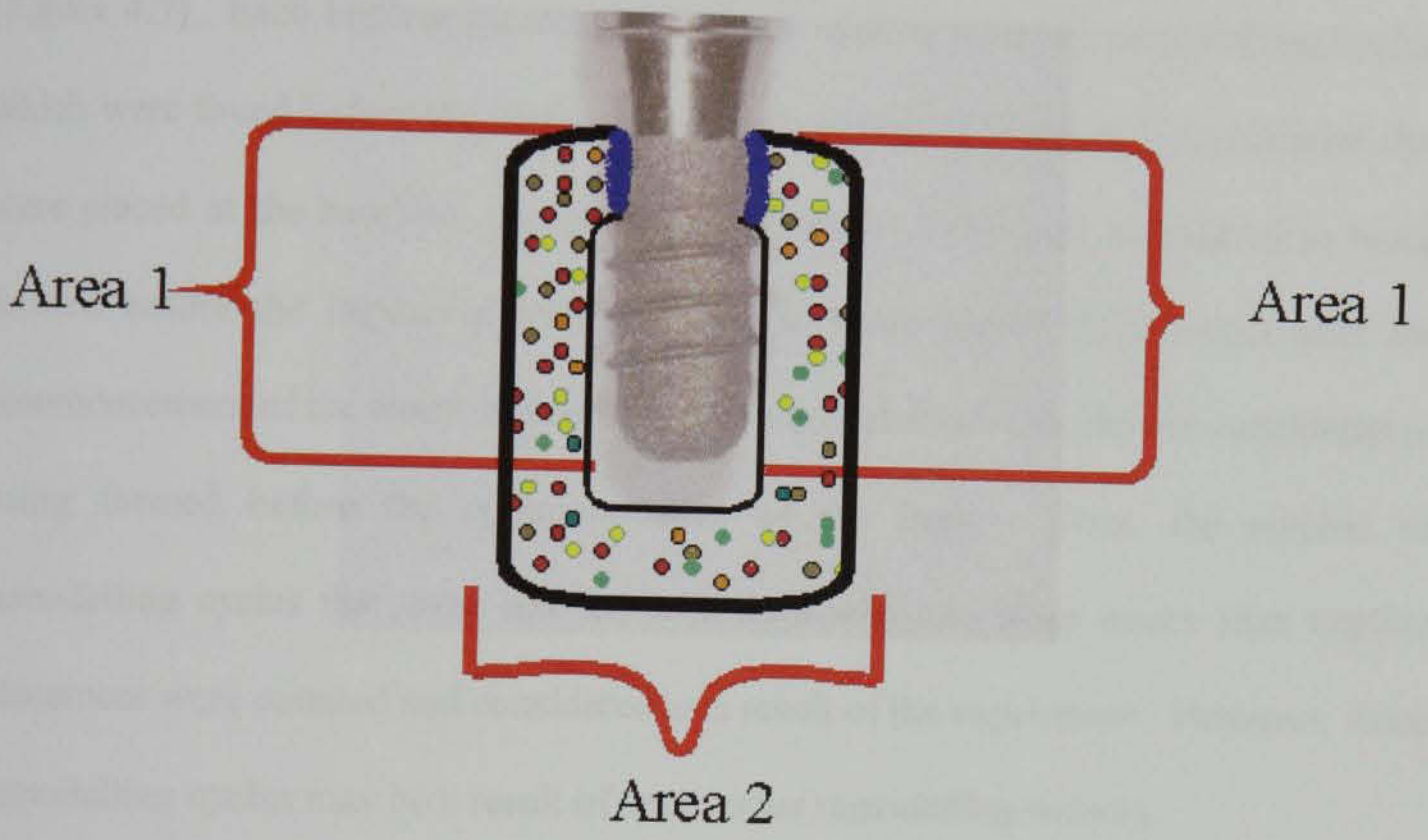

Figure 4.7 A schematic representation of the implant and the surrounding bone. The blue areas represent the interfacial zone.

The histological sections were magnified under epifluorescent microscopy by 100 times and images were captured with a CCD Digital Microscope Camera (Olympus Optical Co., Ltd, London EC1Y, United Kingdom) – UV (365nm) and Blue incident light (450nm). The images were saved on the computer hardware.

Forming osteons were identified by the presence of a fluorochrome label that indicated the time of bone formation.

All osteons found in both areas and labelled with fluorochromes were photographed and counted.

Number of remodelling cycles per unit area and bone formation rate was calculated as following:

A) Number of remodelling cycles (events) per unit area

This represented the number of fluorochromes that were found around each implant (Figure 4.7). Each implant placement time was used to count the remodelling cycles, which were found before the implant placement period. For instance, in implants that were placed at the baseline, alizarin labelled osteons (red) were considered as being formed before the implant placement while in those placed three weeks after the commencement of the study, the osteons that were labelled with alizarin considered as being formed before the commencement of the study. Thus, the number of remodelling cycles that were labelled with fluorochromes three weeks after implant placement were counted and considered as a result of the experiment. However, these remodelling cycles may be a result of continuous remodelling activity.

The number of remodelling cycles that are marked with each label were counted and compared with other groups (Figure 4.8).

However, the cycles that were stained with tetracycline were discarded because it was very difficult to distinguish between resorption cavities and cycles that were stained with tetracycline. So remodelling cycles that occurred in week 10 were not recorded.

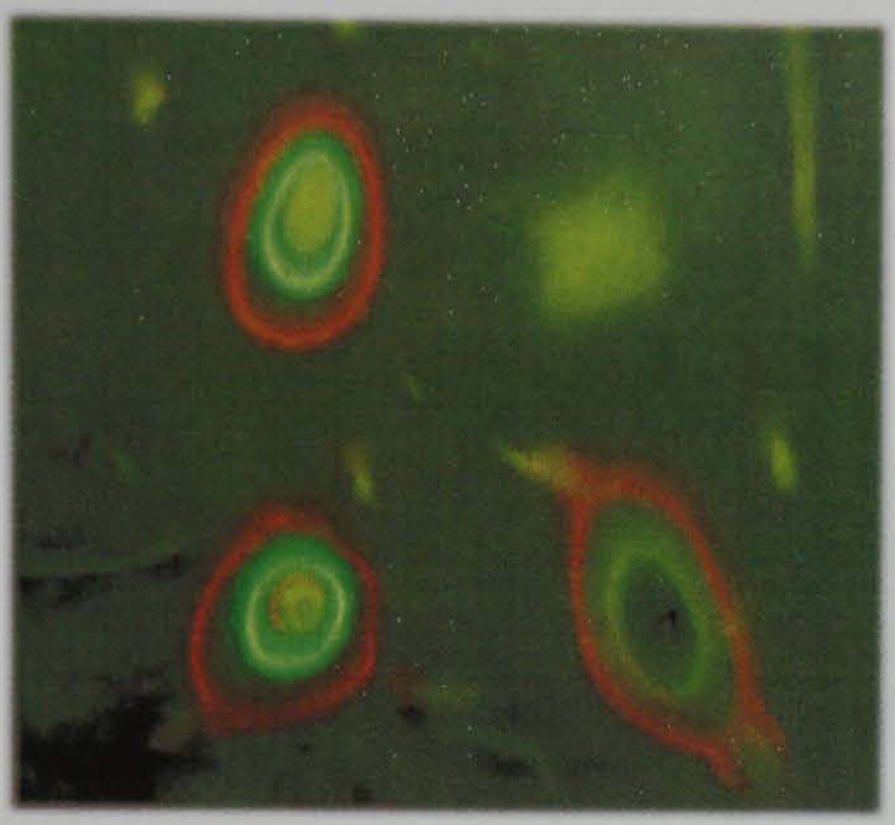

Figure 4.8 Number of remodelling cycles: Two cycles labelled with alizarin (red), two with calcein (green), two with xylenol (orange) and three with tetracycline (yellow). Observe the difficulty in distinguishing between alizarin (red) and xylenol orange (orange).

B) Bone formation rate (micron/ day)

The distance between each two consecutive labels was measured. Two lines crossing each other at right angles were drawn on each osteon; one parallel to the long axis of the implant and the other perpendicular to it. The distance between each two consecutive labels on these lines was measured (Figure 4.9).

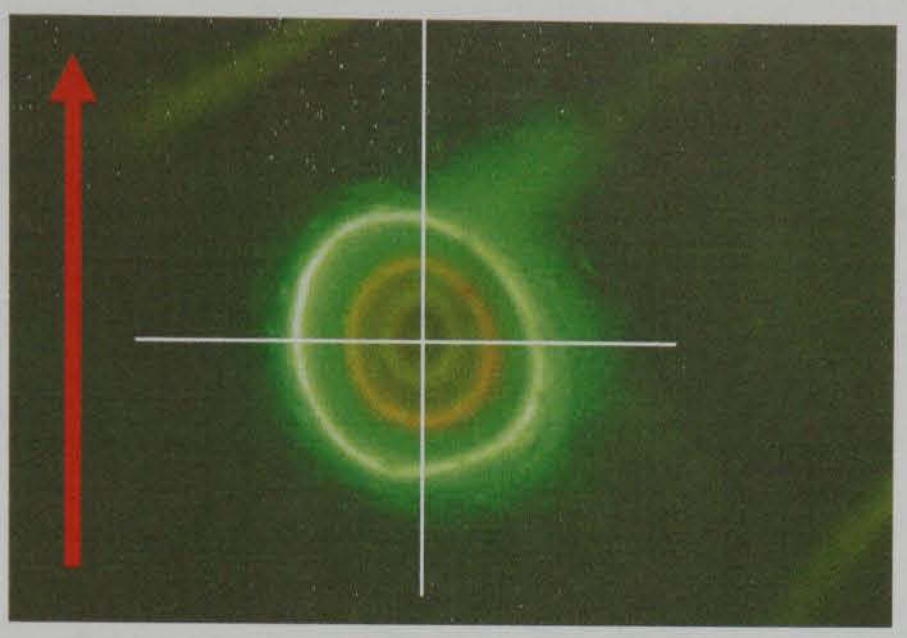

Figure 4.9 A figure of a secondary osteon illustrating the points at which the distance between the successive labels was measured. The vertical line is parallel to the long axis of the implant. The red arrow represents the long axis of the implant. The secondary osteon is labelled with three fluorochromes calcein (green), xylenol (orange) and tetracycline (yellow).

As osteons refill from the periphery towards the central Haversian canal, the mean distance between the inner surfaces of successive fluorochromes divided by the time between labels was used to calculate the linear appositional rate (μm/day) (Nölke 1995).

The amount of bone that formed per day was calculated as the linear distance between the two successive labels divided by the time (i.e. 21 days) between the first and the second, the second and the third. However, the time between the third and the forth label was 28 days. Consequently, the distance between the two of them was divided by 28. In some osteons certain labels could not be detected which indicated that bone

may have not formed at that time. In these situations the distance was calculated and divided by the number of days, which separated them (Table 4.3).

The label substitution phenomenon in which the second label covers the previous one was not found to occur *in vivo*.

Bone surrounding an implant that was labelled with different fluorochrome chelating agents can be seen in Figure 4.10.

Table 4.3 Representation of the period at which the bone labels are detected and the number of days by which the distance between succeeding labels was divided.

Period	day 1- day 21	day 21- day 42	day 42- cay 70	day 1- day 42	day 21- day 70	day 1- day 70
Number of days	21	21	28	42	48	70

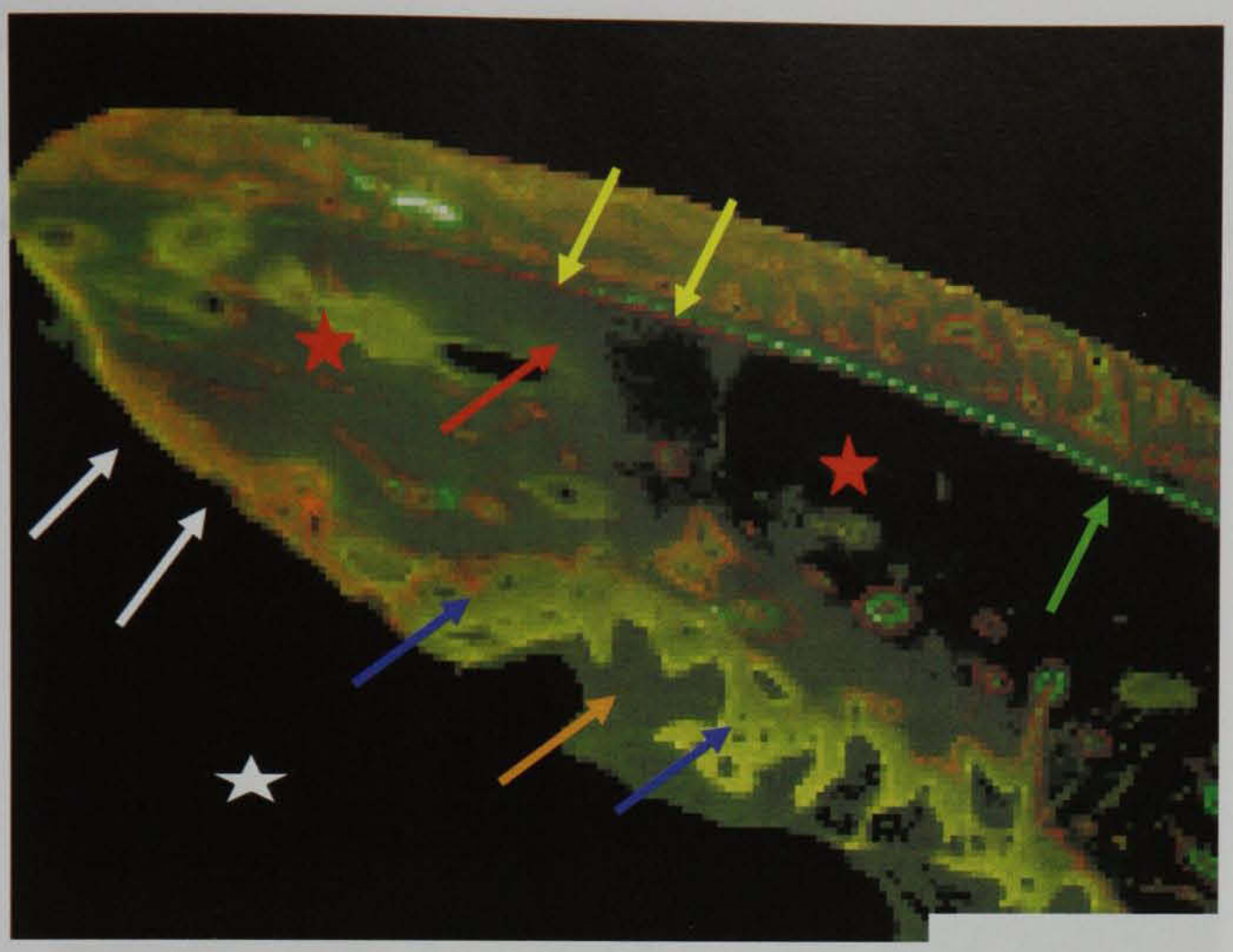

Figure 4.10 An implant placed three weeks after commencement of the study. Alizarin chelating agent separated old bone (red star) from newly formed subperiosteal bone (yellow arrows). Green arrows indicating calcein chelating agent (given week 3). Newly formed bone (white arrows) is interposed between the implant surface (white star) and old bone (red star). Fibrous tissue (orange arrow) is interposed between the implant surface and old bone (red star). Newly formed bone (blue arrow) was labelled with tetracycline chelating agent. Blue incident light (450nm). Scale bar = 1mm.

4.3 Results

4.3.1 Histological description

Sixteen slides were obtained and analyzed. Four slides were obtained from each dog. One slide represented each implant site.

There was an area close to the implant surface extending a few microns from it and characterized by either:

- Diffusely stained areas close to the implant surfaces and were associated with implants placed at the 9th week of the experiment (Figure 4.11).
- Woven and fibrolamellar bone were seen as a mixture of different fluorochromes in the interfacial zone (Figure 4.12 and 4.13).

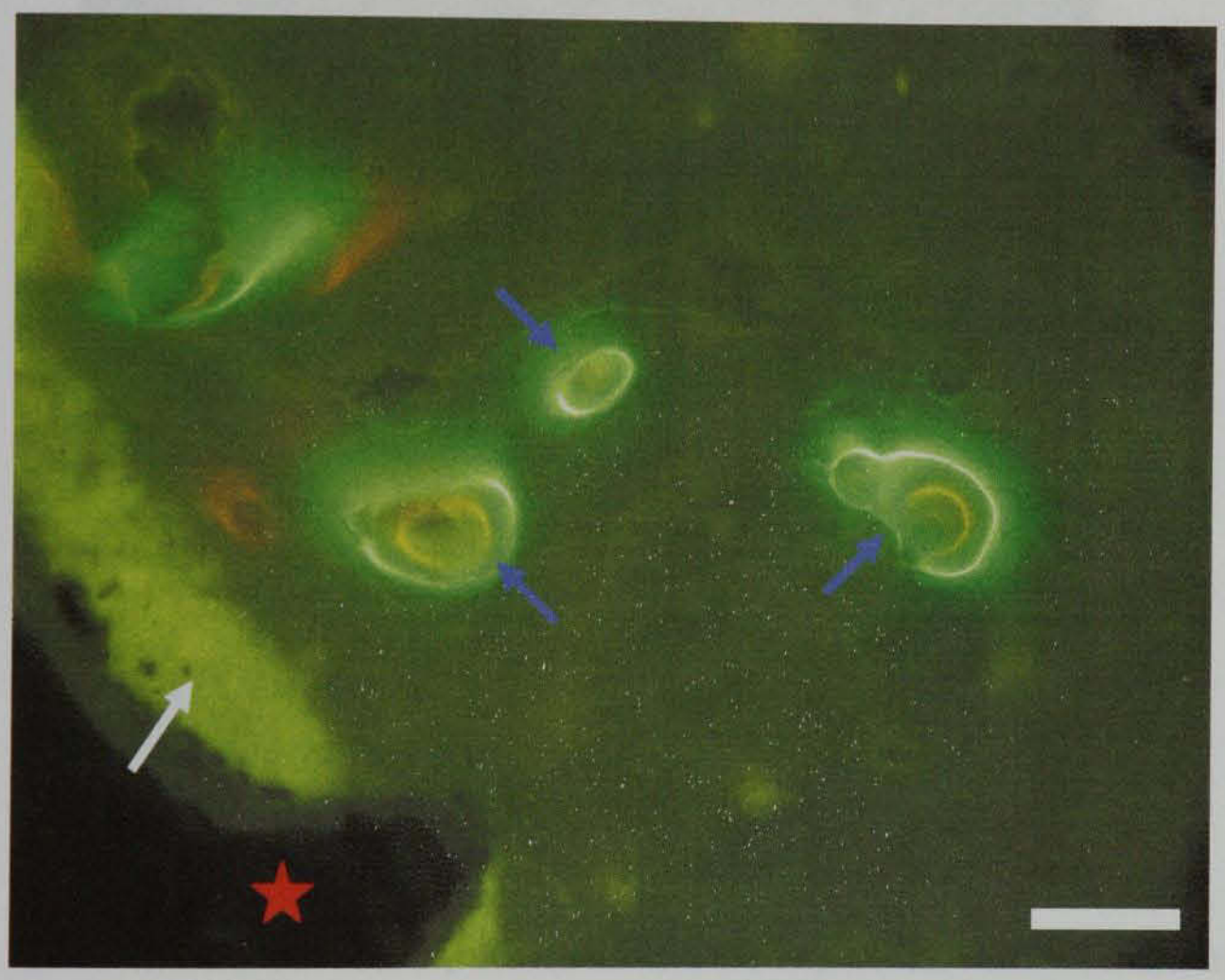

Figure 4.11 Diffuse stained area (white arrow) in the interfacial zone, secondary osteons (blue arrows) and the implant thread (red star). The implant was placed nine weeks after the commencement of the study. Scale bar = 200μm.

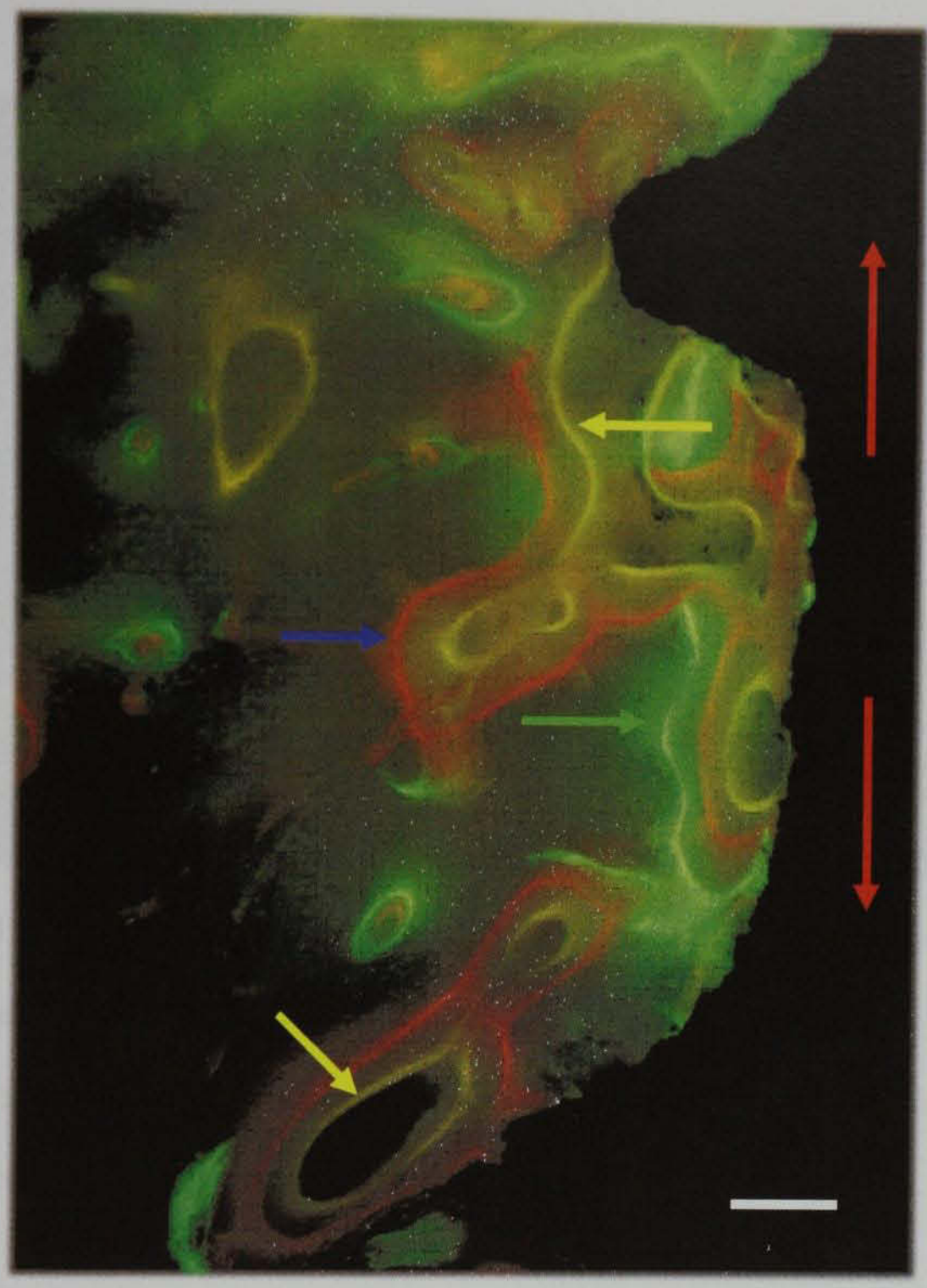

Figure 4.12 Fibrolamellar bone formation around the implant labelled with chelating fluorochromes: oxytetracycline (yellow arrow), xylenol (blue arrow) and calcein (green arrow). Note the presence of contact osteogenesis; bone was formed from the old bone towards the implant surface. Blue incident light (450nm). The implant is denoted by the red arrows. Scale bar =200μm.

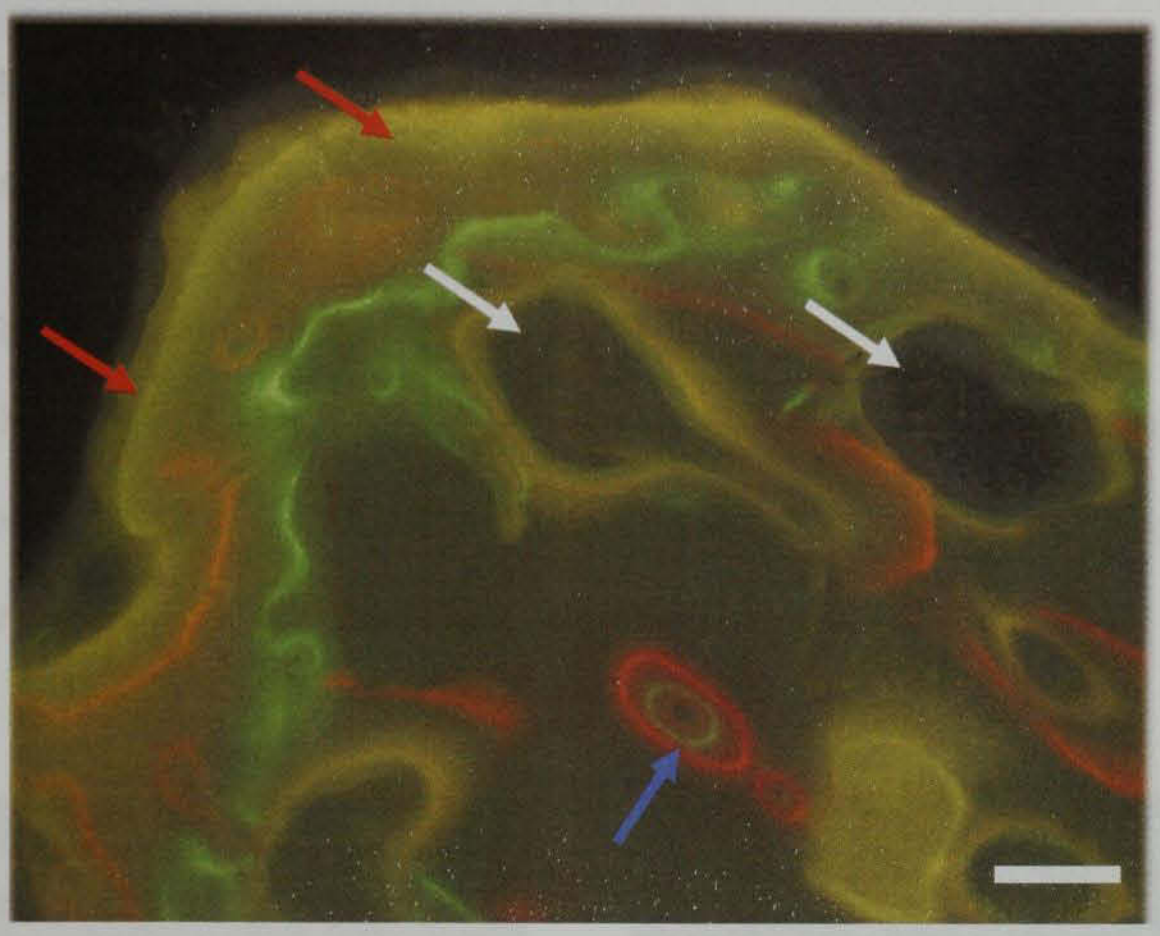

Figure 4.13 Refilling or secondary osteon (blue arrow) labelled at the base line with alizarin (red), at three weeks with calcein (green) and at six weeks with xylenol orange (orange). Resorption spaces labelled with tetracycline were denoted by white arrows. Note tetracycline stains the crest of alveolar ridge (red arrows). Scale bar =200μm.

It was planed to inject the oxytetracycline one day after the placement of the last implant using the same protocol used in the first study in order to label bone that is being formed during this time as well as to mark microcracks that have been present at the time of injection. However, one dog died while the oxytetracycline was being administered. So the dose was reduced to 20mg/kg and was given one week later (ten weeks after starting the study). See the study design.

4.3.1 Histological description

4.3.1.1 Bone formation around implants placed at baseline (implants remained 10 weeks)

New bone formation in the area ≤ 1mm:

Woven bone stained with calcein (green), xylenol (orange) and tetracycline (yellow) and fibrolamellar bone labelled with xylenol (orange) can be observed (Figure 4.14). Lamellar bone seen as fine orange lines within woven bone.

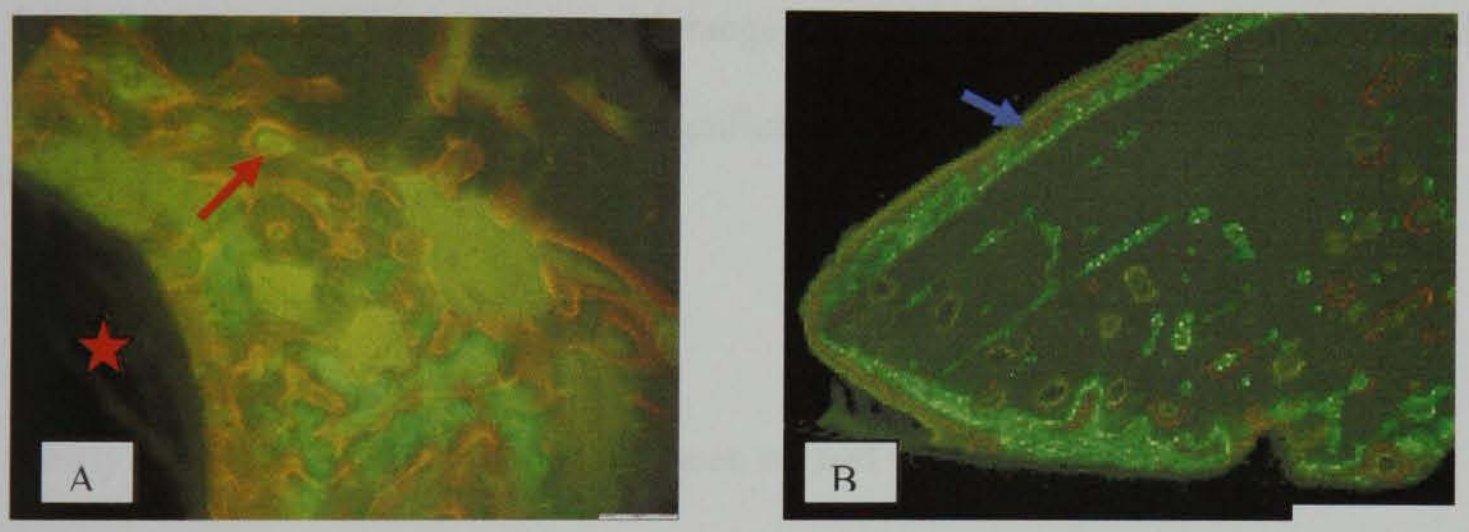

Figure 4.14. Woven bone (green, orange and yellow) can be seen in the area close to the implant surface. Fibrolamellar bone can be observed (red arrow) (A). The implant is marked with a red star. Fibrolamellar bone was interposed between the implant surface and old bone is stained green with calcein (B). Subperiosteal fibrolamellar (blue arrow). Blue incident light (450nm). Magnification X100. Scale bar = 200μm.

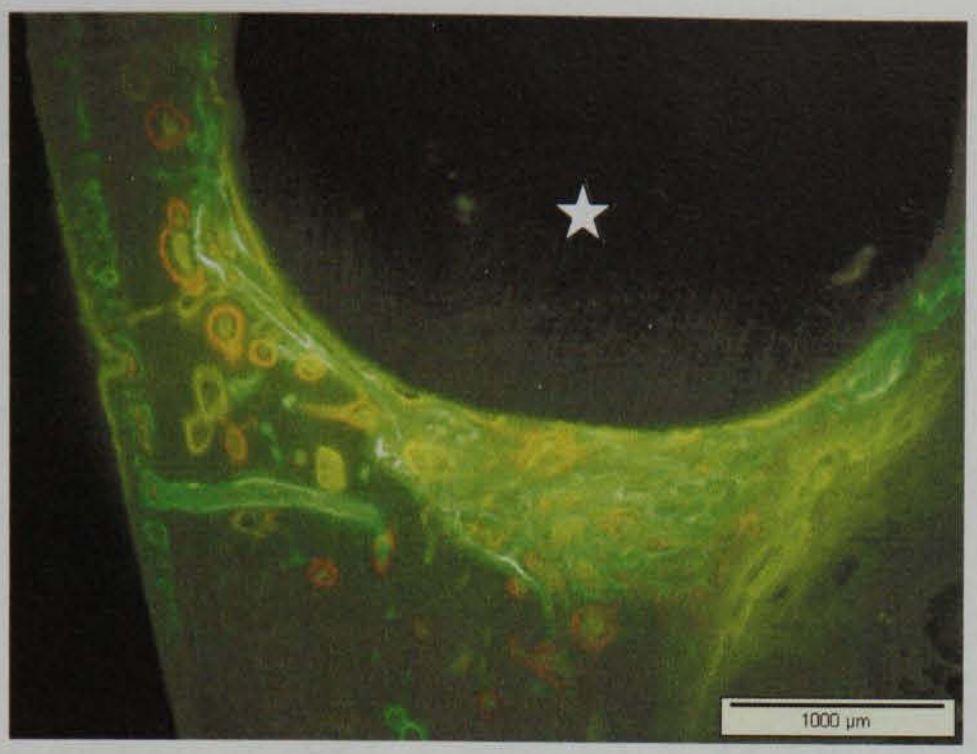

Figure 4.15 New woven bone covers the apical end of the implant (white star). It is labeled with calcein (green), xylenol (orange) and tetracycline (yellow) and examined under blue incident light (450nm). Magnification X100. Scale bar = 1mm.

Newly formed subperiosteal bone was seen stained with calcein (green), xylenol (orange) and tetracycline (yellow) indicating that this bone formed at 3, 6 and 10 weeks after commencement of the study. Primary osteons labeled with calcein, xylenol and tetracycline could be seen (Figure 4.16). The outer layer of this bone is labeled with tetracycline. Alizarin stained bone could not be found.

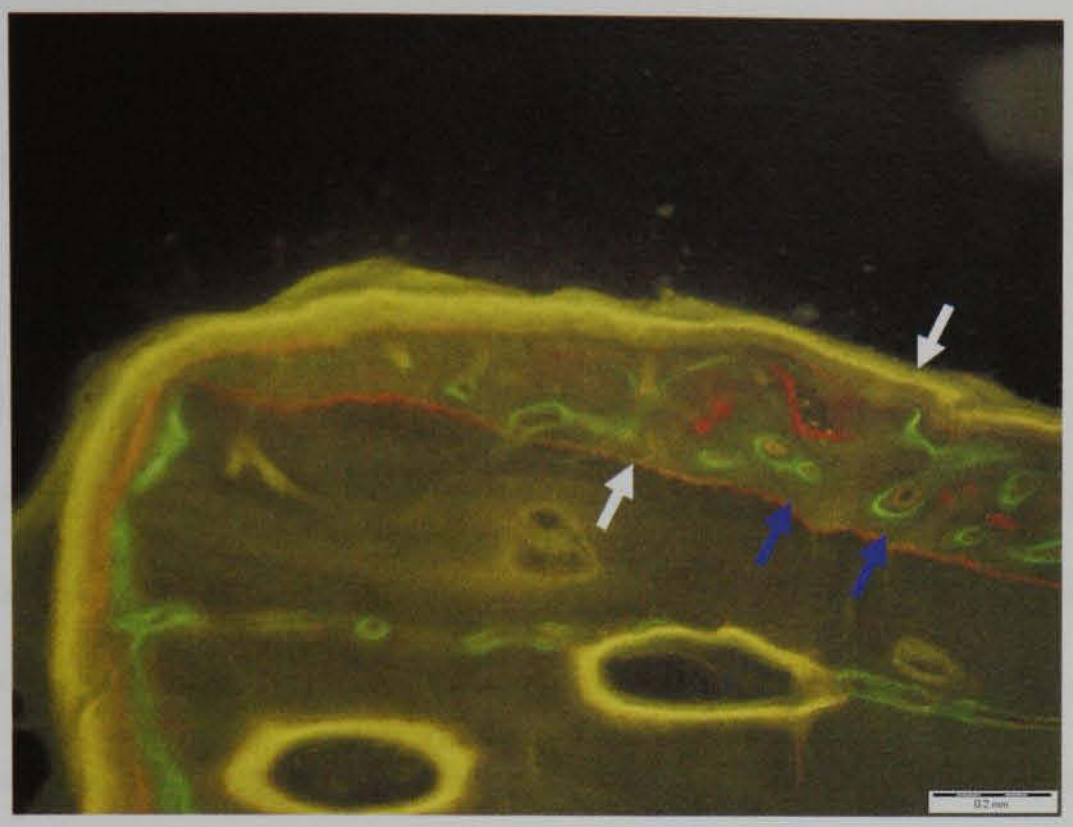

Figure 4.16 Subperiosteal bone (white arrows) formed around the implant placed at the baseline. Subperiosteal bone was separated from old bone with a red line (alizarin). Blue incident light (450nm). Magnification X100. Scale bar = 200μm.

Endosteal bone could be seen occasionally covering the apical part of the implant which was placed at baseline. It was labeled with three labels; calcein, xylenol and tetracycline.

4.3.1.2 Bone formation around implants placed at week 3 (implants remained 7 weeks)

New bone formation in the area ≤ 1mm:

An area of new bone stained with only two bone labels (xylenol and tetracycline) could be seen (Figure 4.17 and 4.18). This means that the bone formed after implant insertion. Osteons that were labelled with the two mentioned bone labels could be seen (Figure 4.17). Resorption spaces could also be observed. Secondary osteons labelled with alizarin and other labels could be seen in the old bone in the area away from the implant surface.

Woven bone was seen in the area close to the implant even after 7 weeks healing time.

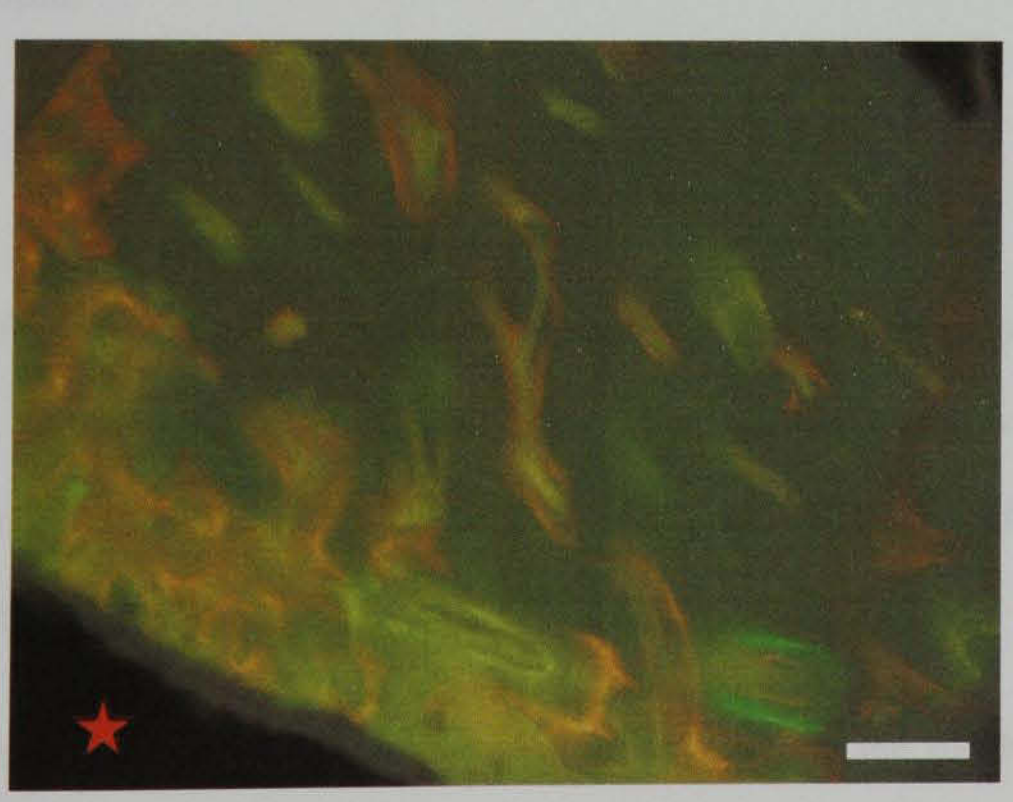

Figure 4.17 Only xylenol orange and tetracycline stained newly formed bone could be seen in the area close to the implant surface (red star). Magnification x100. Scale bar = 200μm.

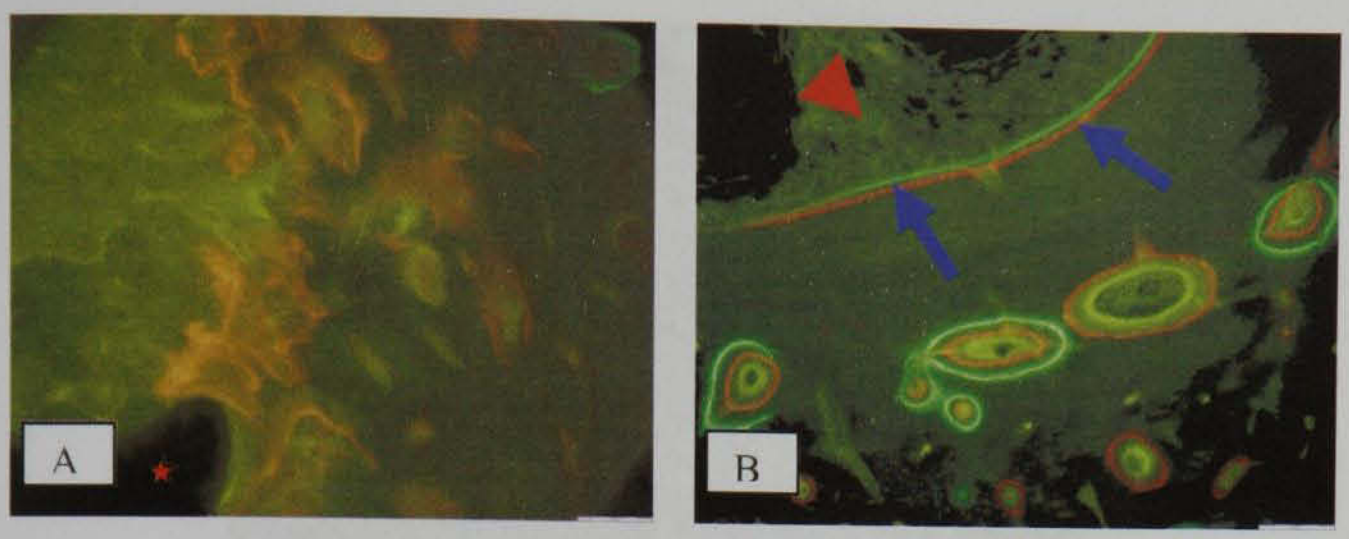

Figure 4.18 (A) Woven bone (yellow and orange) can be seen in area close to the implant surface after 7 weeks healing period. (B) A remote area away from the implant surface (Area 2). Note the two labels; alizarin (red) and calcein (green) indicating that bone was formed inwards from the cortical toward the cancellous bone. Blue arrows show this direction. Cancellous bone (red head arrow). The implant thread (red star). Scale bar =200μm.

Subperiosteal

A thin layer of this bone can be seen stained mainly with xylenol orange and tetracycline (Figures 4.19, 4.20 and 4.21). Neither Alizarin nor calcein were seen which indicates that bone formed three weeks after implant placement (6 weeks after the study commencement) (Figure 4.19).

The new formed subperiosteal bone was seen separated from the old bone by a red (alizarin) or green (calcein) labels (Figure 4.19). This may reflect the effect of surgery which was carried out earlier on the adjacent area six weeks before (Regional Acceleratory Phenomenon).

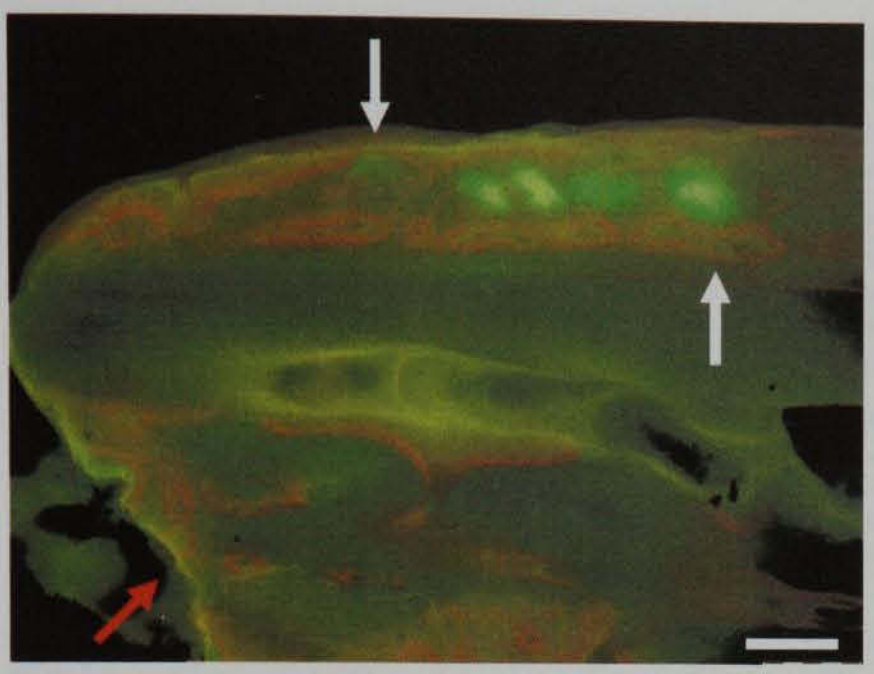

Figure 4.19 Subperiosteal bone formed around the implant placed at week 3 (white arrows). Resorption spaces can also be observed (red arrows) in the area > 1mm away from the implant surface. The spots of green label may be a result of the cutting and grinding process. Blue incident light (450nm). Scale bar= 200μm.

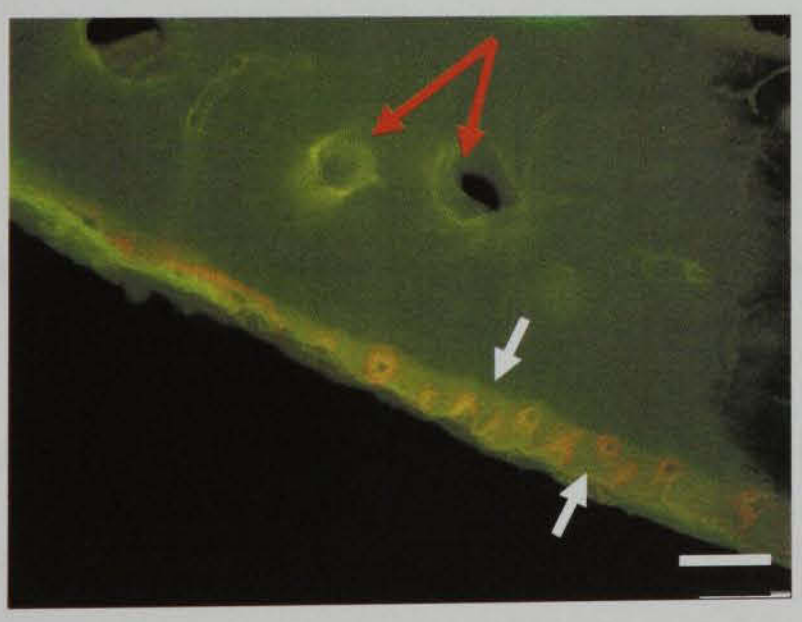

Figure 4.20 Subperiosteal bone formed around the implant placed at week 3 (white arrows). Resorption spaces can also be observed (red arrows) in the area > 1mm away from the implant surface. Blue incident light (450nm). Scale bar= 200μm.

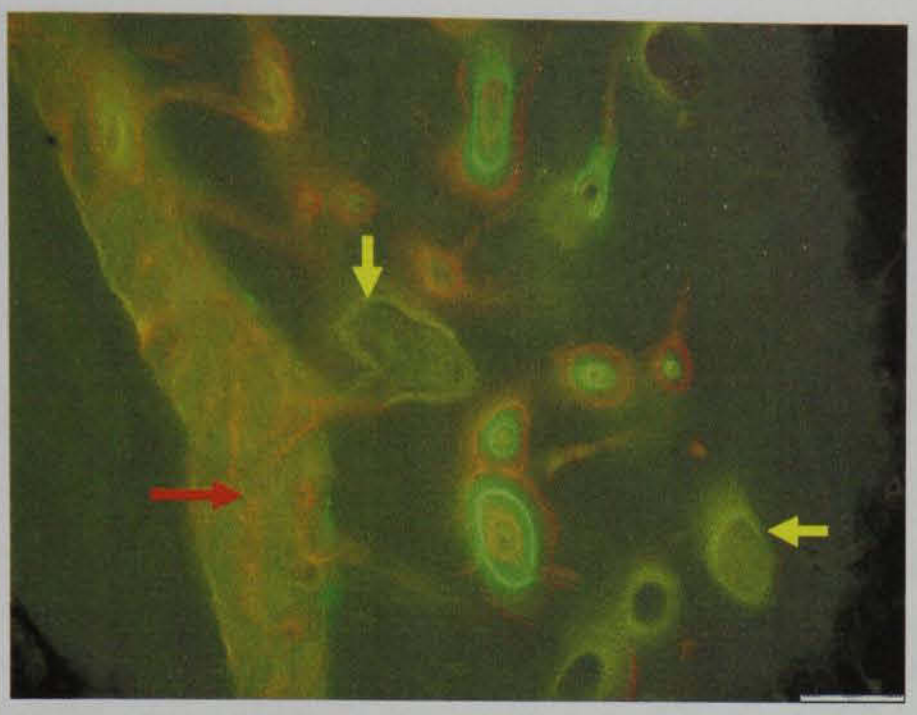

Figure 4.21 Subperiosteal bone (red arrow) formed around the implant placed at week 3. Secondary osteons labelled with alizarin (red), calcein (green), xylenol (orange) and tetracycline were seen in the old bone away from the implant. Resorption spaces labeled with tetracycline were marked with yellow arrows. Blue incident light (450nm). Scale bar= 200μm.

4.3.1.3 Bone formation around implants placed at week 6 (implants remained 4 weeks)

An area diffusely labelled with tetracycline (yellow) could be observed. A secondary osteon labelled with calcein which might have been damaged as a result of the surgery (Figure 4.22). Trace amount of xylenol orange still can be seen close to the implant surface. This may indicate that damaged bone was not completely resorbed.

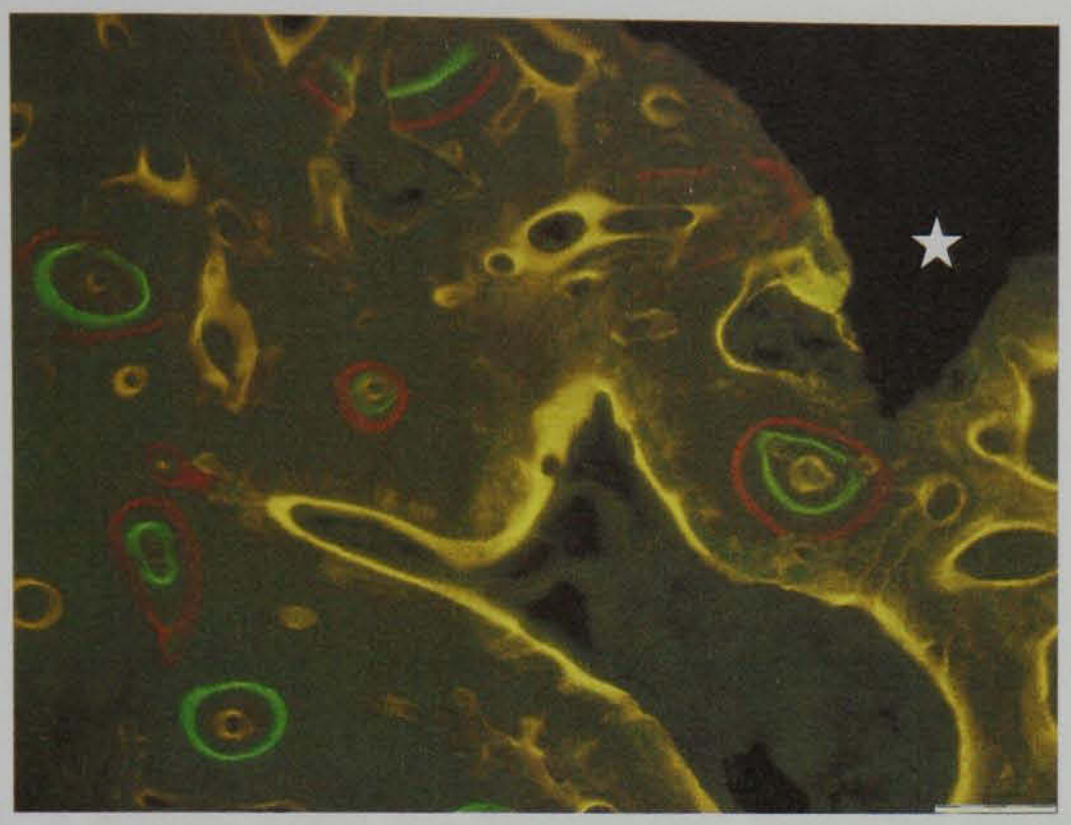

Figure 4.22 Tetracycline stained area close to the implant surface. Resorption spaces stained with tetracycline can be seen. Implant thread (white star). Blue incident light (450nm). Scale bar 200μm.

4.3.1.4 Bone formation around implants placed at week 9 (implants remained 1 week)

Only diffusely stained tetracycline area can be observed (Figure 4.23). This area represented the damage caused by the surgery as was explained earlier in study 1.

No new bone could be seen in the area close to the implant or in subperiosteal region.

Figure 4.23. A diffusely stained area represents bone damage that was caused by the surgical procedure. The implant thread is marked with a red star. Blue incident light (450nm). Magnification x100. Scale bar = 200μm.

Comments

According to the materials and methods used in the present study the following points could be emphasized:

1) The surgical procedure leads to bone damage in the area close to the implant surface. This damage was stained by tetracycline. This damage was seen one day after implant placement and remained up to at least one week after the implant surgery (Figure 4.23).

2) Bone close to the implant surface could be observed as it was labelled by the bone labels that had been given three weeks after implant placement except the implant that was placed at week 9.

3) The newly formed bone was woven bone type (Figure 4.18) in the early stage which then changed into fibrolamellar bone (Figure 4.19). Woven bone was seen around the implants placed 3 to 4 weeks before the animals were sacrificed. This bone was osteonless and not well organized which indicated that it was formed in a quick manner as a response to the surgery

4) When the implants were left to heal for 6 weeks or more the new formed bone looked more organized and a few secondary osteons could be observed labelled with green, orange and yellow.

5) The newly formed bone was always labelled with the bone labels that were given at 3 weeks after the implant placed. For instances, around the implants placed at the baseline the newly formed bone stained with calcein, xylenol and tetracycline (Figure 4.14 and 4.15). While around the implants that were placed at week 3, the new bone labelled with xylenol and tetracycline (Figure 4.17 and 4.18).

6) Subperiosteal bone was seen on the buccal and lingual surface of the alveolar bone around the early placed implants (Figure 4.16 and 4.19) but not around the implants that were placed at week 9 (Figure 4.23).

7) Subperiosteal bone was observed as early as 3 weeks after implant insertion (Figure 4.10).

8) Subperiosteal bone is woven bone in its early stage which is then transformed into fibrolamellar during the study period.

9) Subperiosteal bone could be seen separated from the old bone by the bone label given at the time of implant placement. For example, around the implant placed at the baseline

the periosteal bone was separated by a red mark (alizarin) (Figure 4.16) while those placed at week 3 were separated by green (calcein) (4.19 and 4.21).

10) In Area 2, cortical bone could be seen separated from cancellous bone using different bone labels (Figure 4.18).

11) Endosteal bone could be seen extending to cover the apical end of the implants. This phenomenon was seen around a few implants only.

4.3.2 Number of remodelling cycles (events) per unit area

4.3.2.1 Implant placed at the baseline

Neither the time at which an implant was placed nor jaw area were significant (p=0.886). The results of the effect tests are shown in Table 4.4. and are also displayed graphically in Figures 4.24 and 4.25.

Table 4.4 Effect tests for time of implant placement and jaw area.

Source	F ratio	*p* value
Time of implant placement	0.122	0.886
Jaw Area	0.021	0.886

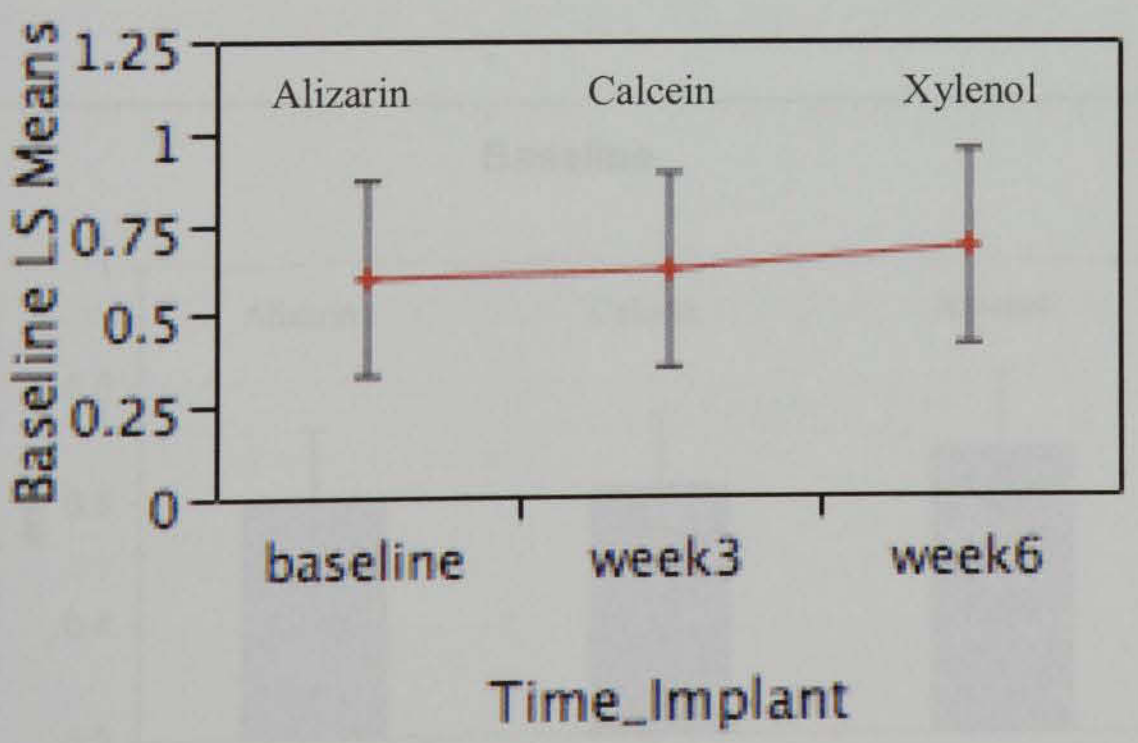

Figure 4.24 Least square means plots for the effects of implant placement time for implants that were placed at baseline.

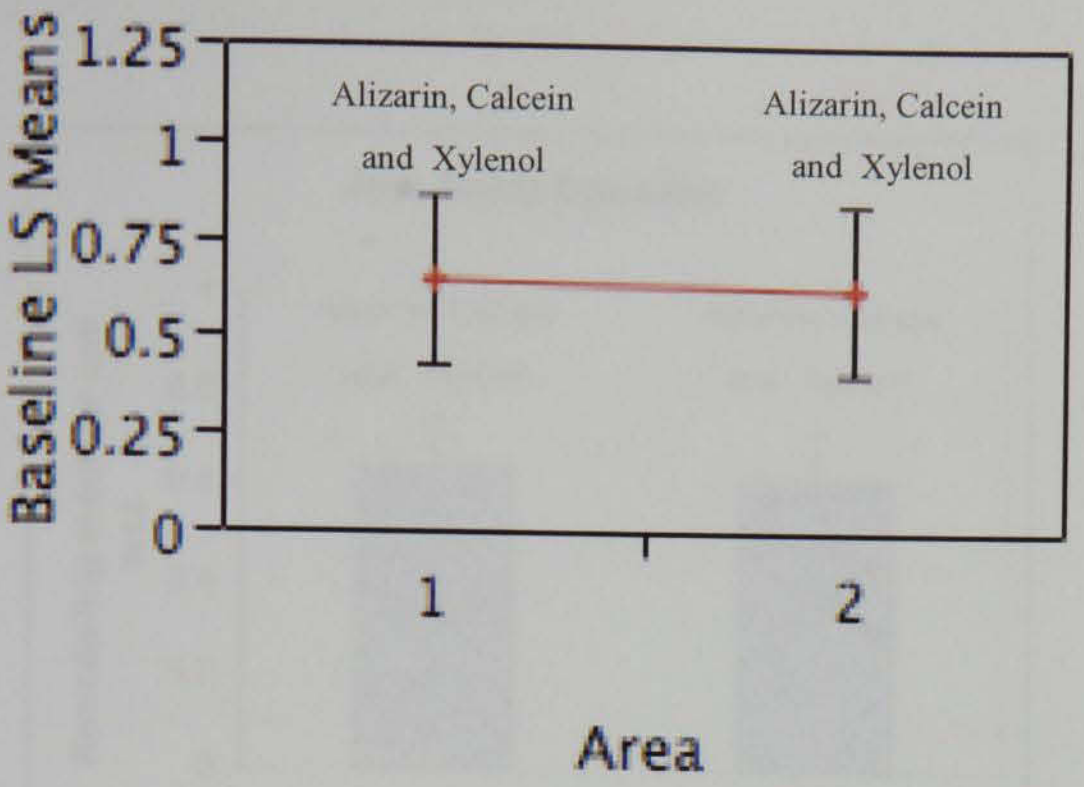

Figure 4.25 Least square means plots for the effects area within the jaw for implants that were placed at baseline.

Figure 4.26 shows means and standard errors of the baseline, week 3 and week 6 for the implants that were placed at baseline while means and standard errors of jaw area are displayed in Figure 4.27.

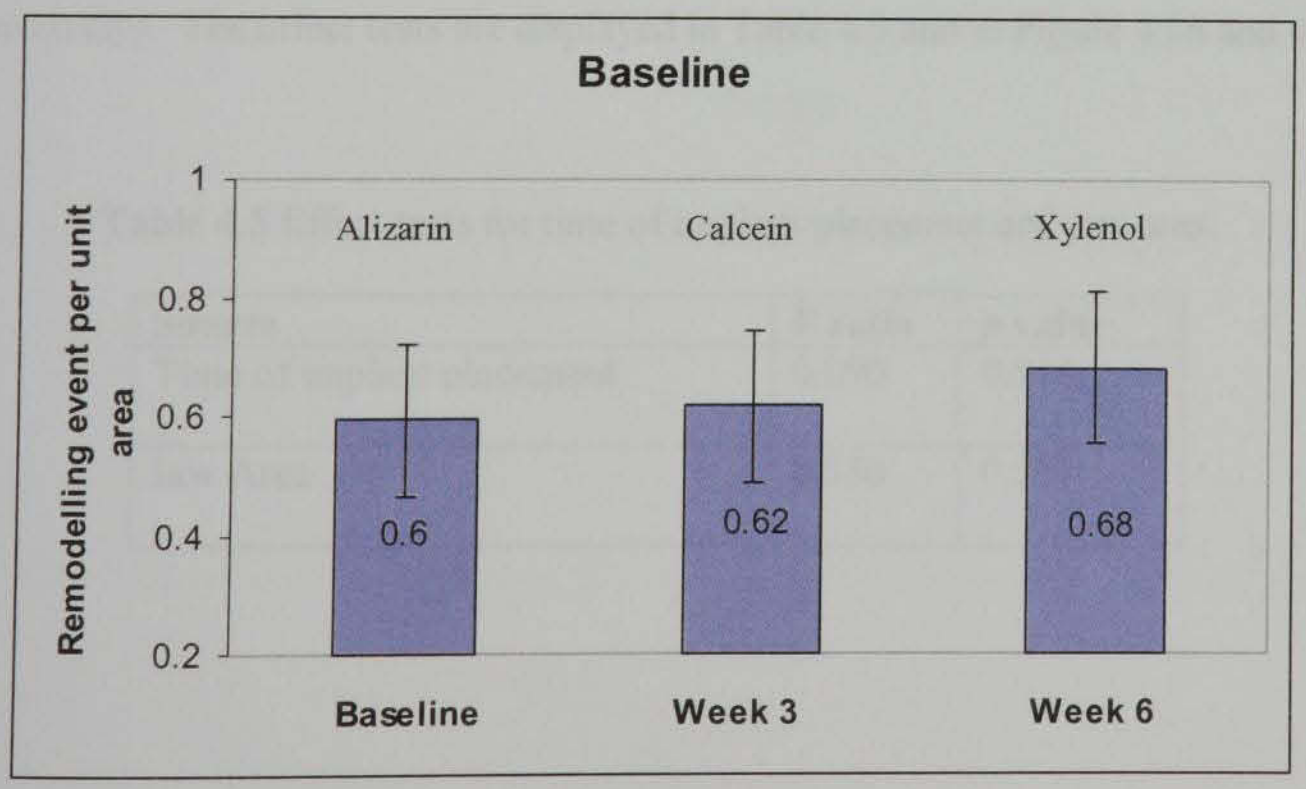

Figure 4.26 Means and standard errors of remodelling cycles at baseline, week 3 and week 6 for the implants that were placed at baseline.

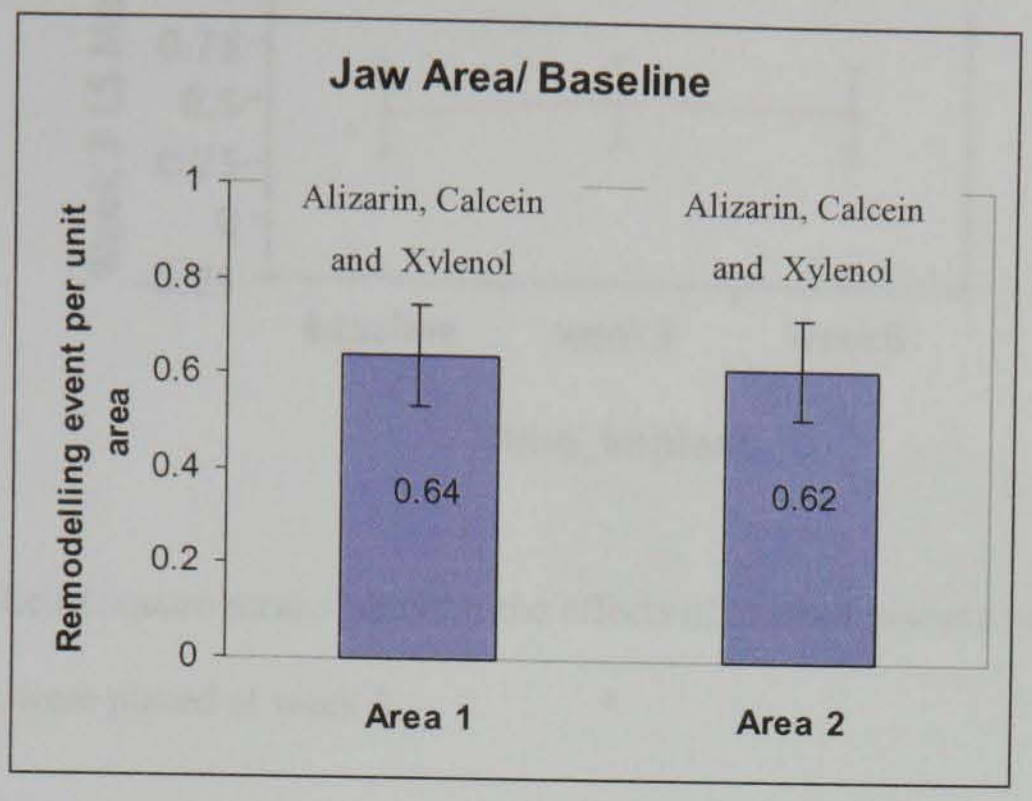

Figure 4.27 Means and standard errors of remodelling cycles for Jaw area for the implants placed at baseline.

4.3.2.2 Implants placed at Week 3

Neither time of implant placement nor jaw area were significant (p=0.914 and 0.561 respectively). The effect tests are displayed in Table 4.5 and in Figure 4.28 and 4.29.

Table 4.5 Effect tests for time of implant placement and jaw area.

Source	F ratio	*p* value
Time of implant placement	0.090	0.914
Jaw Area	0.350	0.561

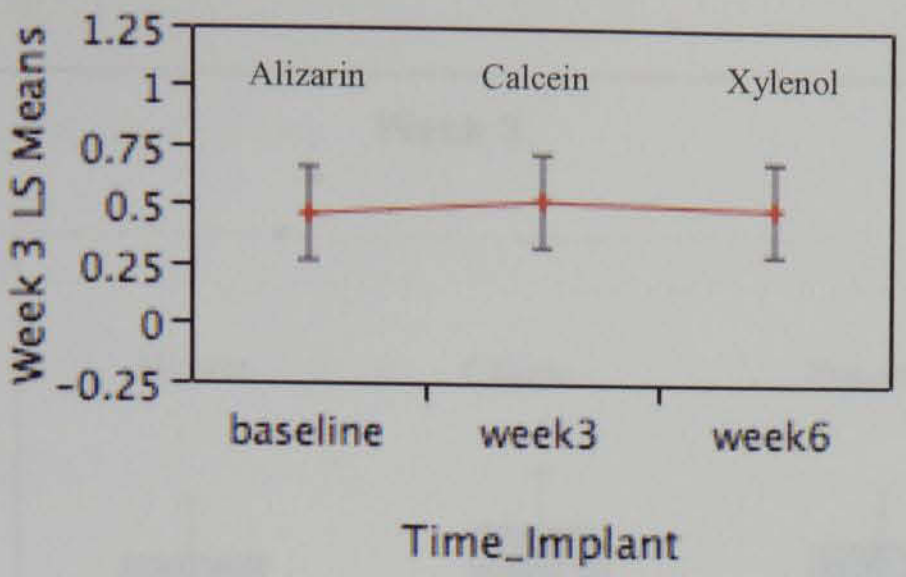

Figure 4.28 Least square means plots for the effects of implant placement time for implants that were placed at week 3.

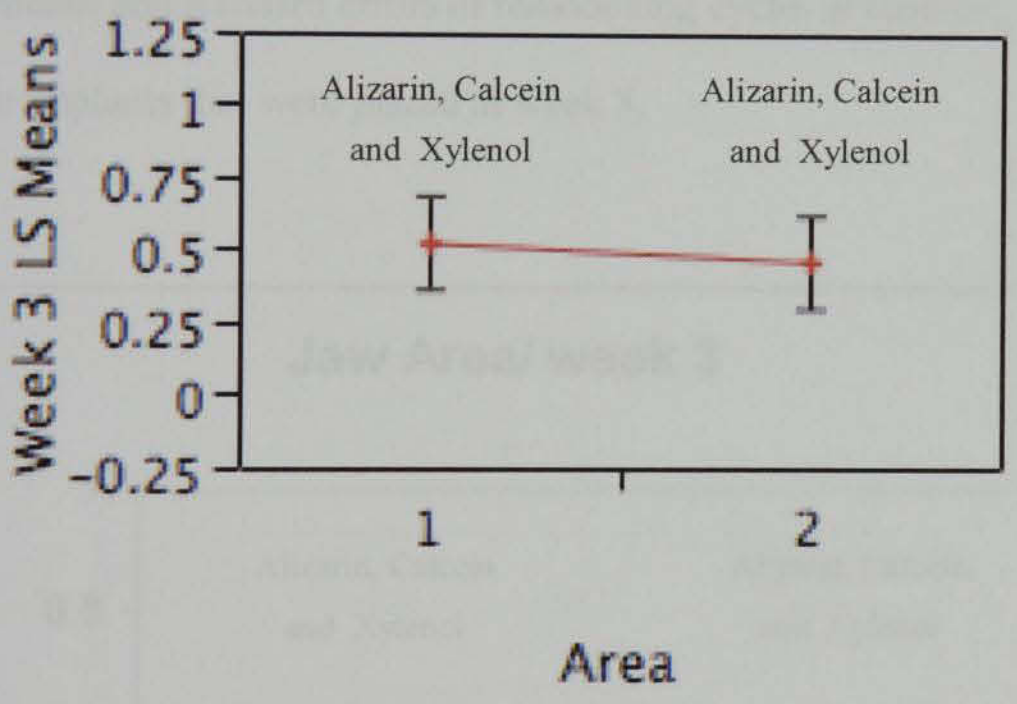

Figure 4.29 Least square means plots for the effects area within the jaw for implants that were placed at baseline.

Figure 4.30 shows means and standard errors of the baseline, week 3 and week 6 for the implants that were placed at week 3.

Means and standard errors of jaw area are displayed in figure 4.31.

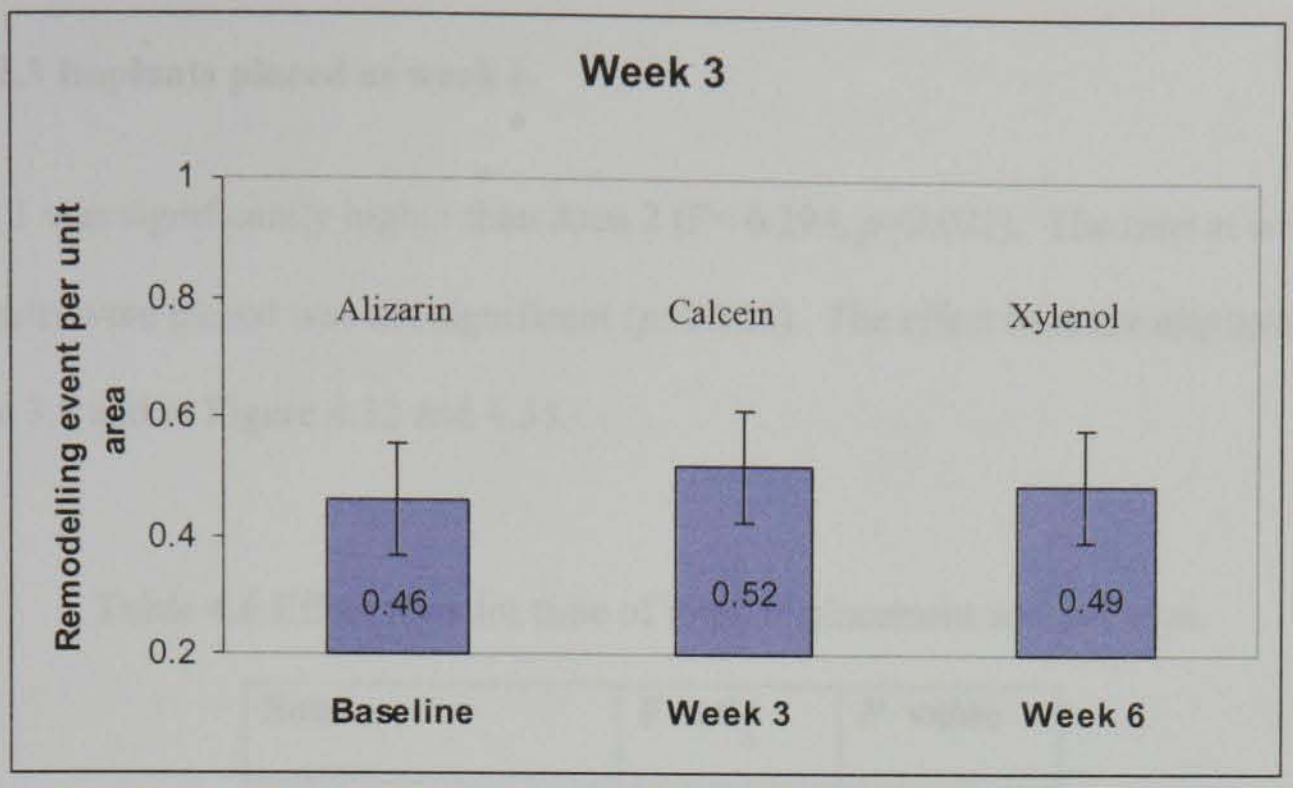

Figure 4.30 Means and standard errors of remodelling cycles at baseline, week 3 and week 6 for the implants that were placed at week 3.

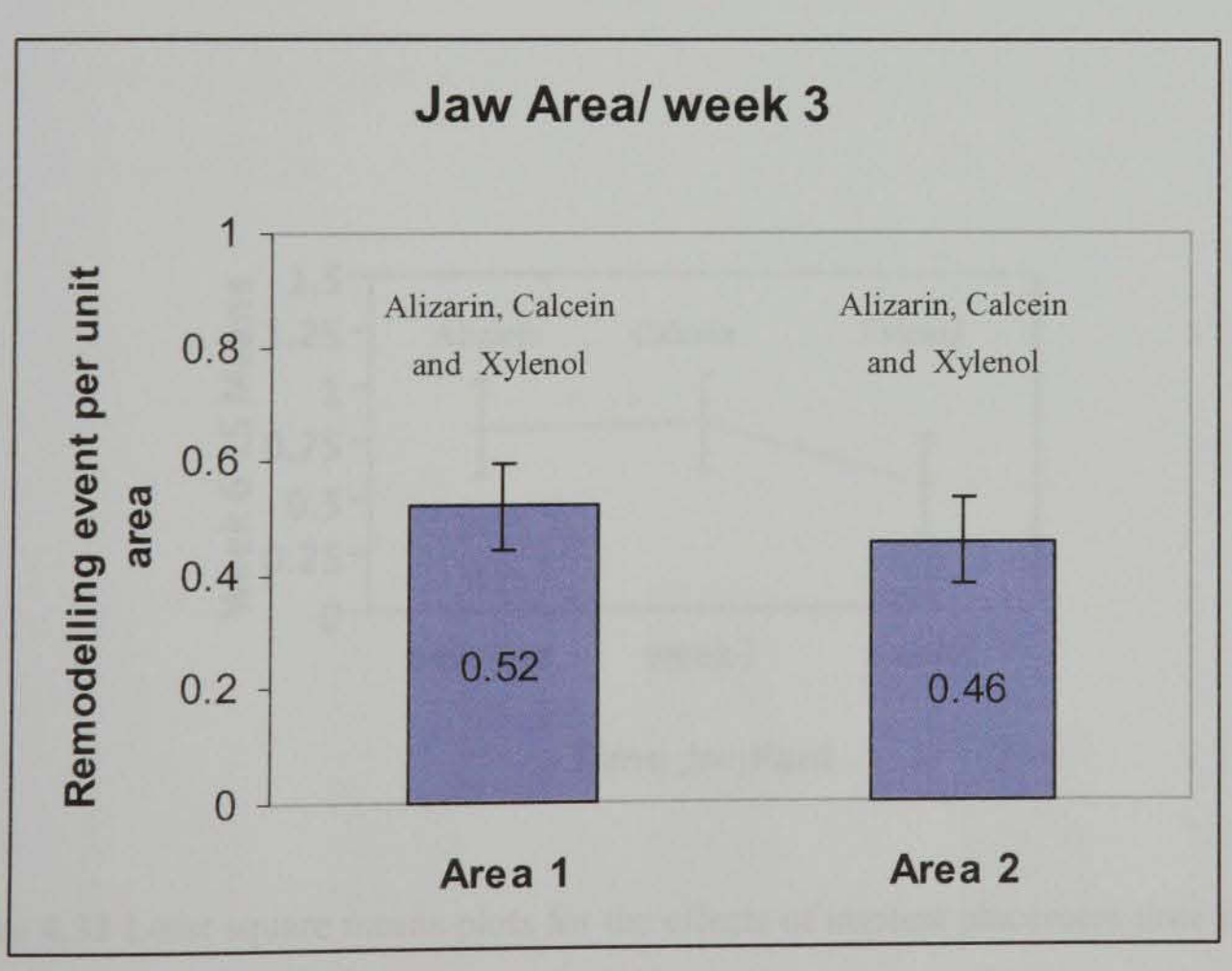

Figure 4.31 Means and standard errors of remodelling cycles for jaw area for implants that were placed at week 3.

4.3.2.3 Implants placed at week 6

Area 1 was significantly higher than Area 2 (F= 6.294, p=0.021). The time at which implants were placed was not significant (p=0.125). The effect tests are displayed in Table 3.6 and in Figure 4.32 and 4.33.

Table 4.6 Effect tests for time of implant placement and jaw area.

Source	**F ratio**	***P* value**
Time of implant placement	2.310	0.125
Jaw Area	6.294	0.021

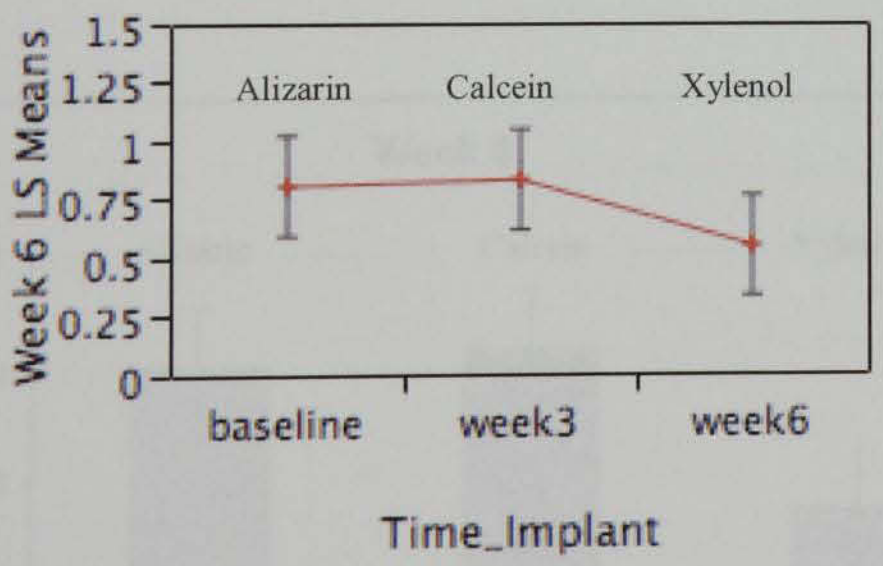

Figure 4.32 Least square means plots for the effects of implant placement time for implants that were placed at week 6.

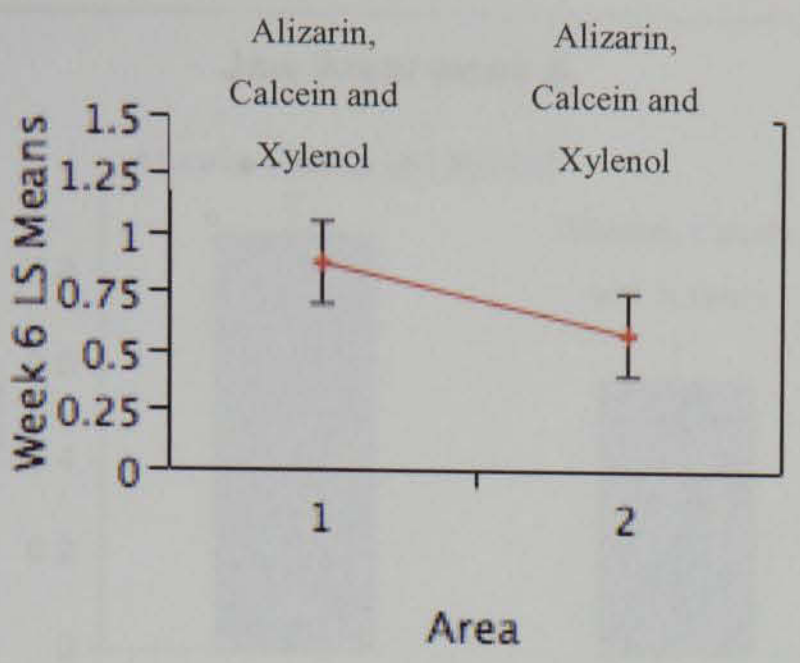

Figure 4.33 Least square means plots for the effects area within the jaw for implants that were placed at week 6.

Figure 4.34 shows means and standard errors of the baseline, week 3 and week 6 for the implants that were placed at week 6. Means and standard errors of jaw area are displayed in figure 4.35.

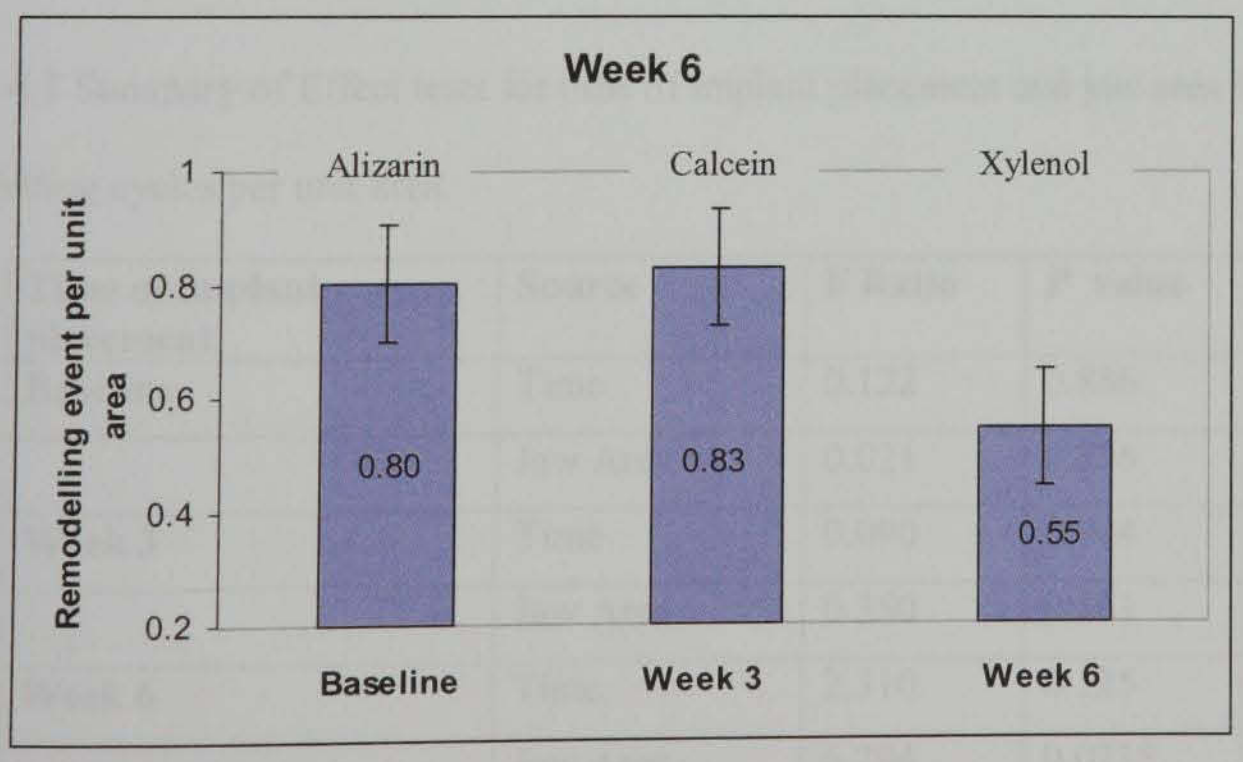

Figure 4.34 Means and standard errors of remodelling cycles at baseline, week 3 and week 6 for the implants that were placed at week 6.

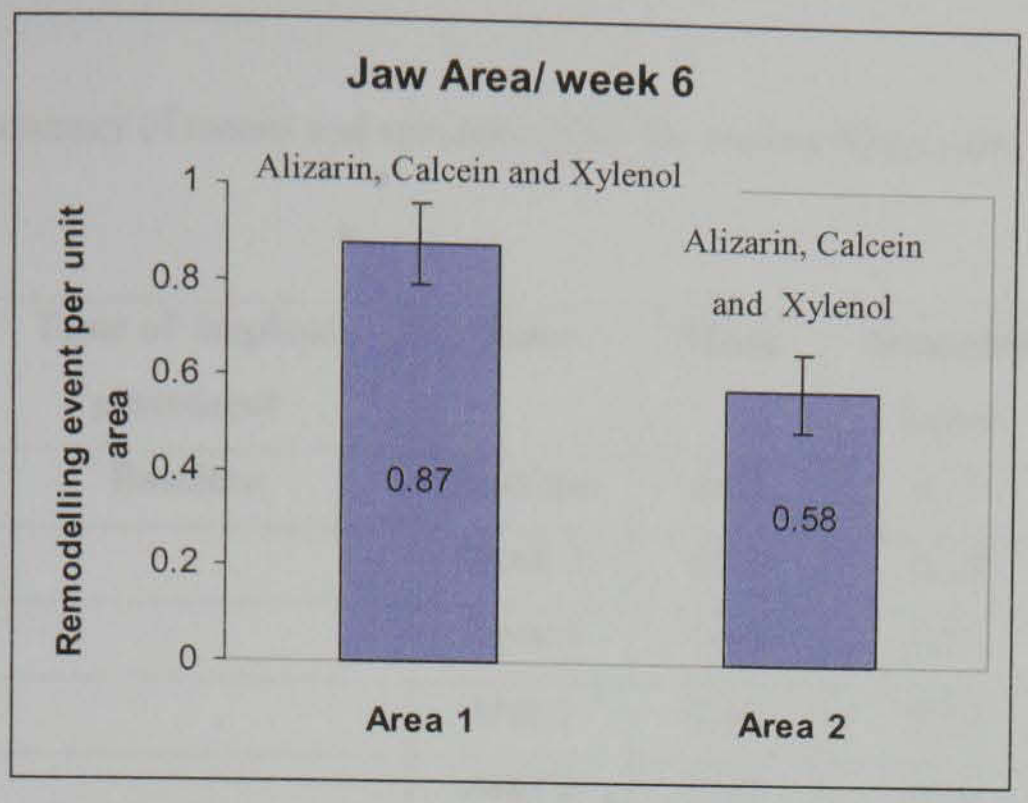

Figure 4.35 Means and standard errors of remodelling cycles for jaw area for implants that were placed at week 6.

A summary of Effect tests for time of implant placement and jaw area is displayed in Table 4.7. Table 4.8 outlines the means and standard errors for the three experiment periods.

Table 4.7 Summary of Effect tests for time of implant placement and jaw area for remodelling cycles per unit area.

Time of implant placement	**Source**	**F Ratio**	***P* value**
Baseline	Time	0.122	0.886
	Jaw Area	0.021	0.886
Week 3	Time	0.090	0.914
	Jaw Area	0.350	0.561
Week 6	Time	2.310	0.125
	Jaw Area	6.294	0.021*

*indicates significant at $p = 0.05$.

Table 4.8 Summary of means and standard errors for remodelling cycles per unit area.

Time of implant placement	Time	Mean	Standard Error
Baseline	Baseline	0.60	0.13
	Week 3	0.62	0.13
	Week 6	0.68	0.13
	Area 1	0.64	0.10
	Area 2	0.62	0.10
Week 3	Baseline	0.46	0.09
	Week 3	0.52	0.09
	Week 6	0.49	0.09
	Area 1	0.52	0.08
	Area 2	0.46	0.47
Week 6	Baseline	0.80	0.12
	Week 3	0.83	0.12
	Week 6	0.55	0.12
	Area 1	0.87	0.08
	Area 2	0.58	0.08

4.3.3 Bone formation rate (microns/day)

4.3.3.1 Results for implants placed at day 1

Four implants were placed at day 1. For these implants, it was possible to follow bone remodelling activity up to 10 weeks. The fluorochrome markers allow quantification of bone formation from 0-3, 3-6 and 6-10 weeks. A regression model was used to analyse the simultaneous effects of jaw side, region of jaw and area within region of the jaw on the amount of bone formation.

4.3.3.1.1 Bone formation rate (microns/day) between day 1 and day 21.

4.3.3.1.1.1 Effect of jaw side

The mean bone formation rate for the right side of the jaws (1.54μm/day) was higher than that for the left side (1.50μm/day). Although the difference was statistically significant (F =4.777, p= 0.03), the magnitude of the difference was low (0.04μm/day) and so the biological significance of the difference may not be important (Figure 4.36).

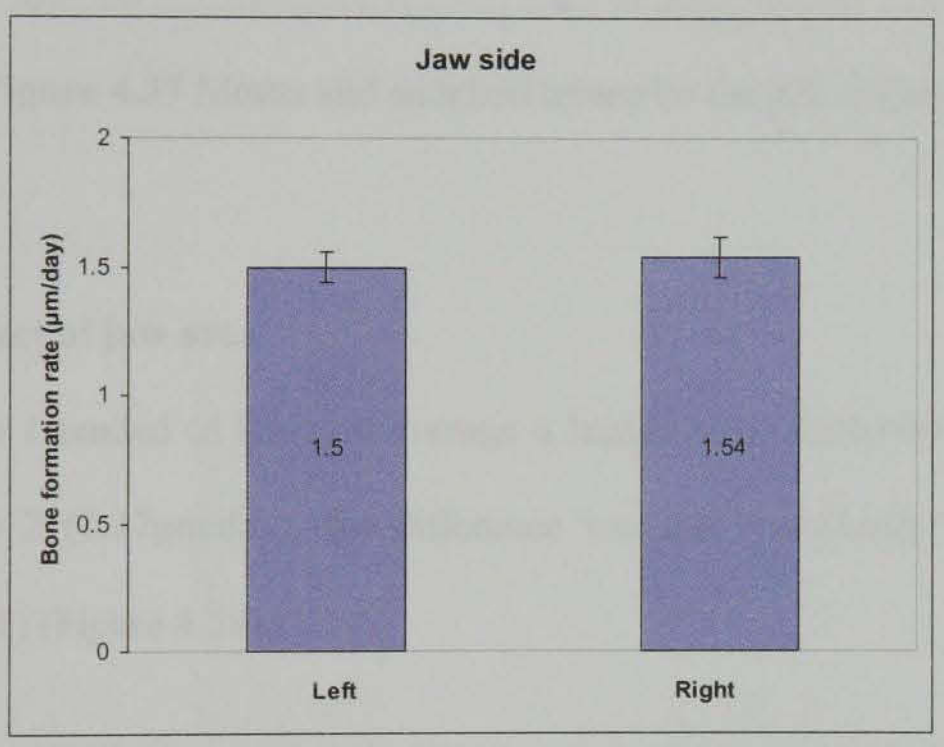

Figure 4.36 Means and standard errors for the left and right sides of the jaws.

4.3.3.1.1.2 Effect of jaw region

The mean bone formation rate for the 1st and 2nd premolar regions (1.66μm/ day) was greater than that for the 3rd and 4th premolar regions (1.48μm/ day). The mean difference between these two jaw regions was 0.18μm/ day. This difference was statistically significant (F= 7.522, p= 0.007) (Figure 4.37).

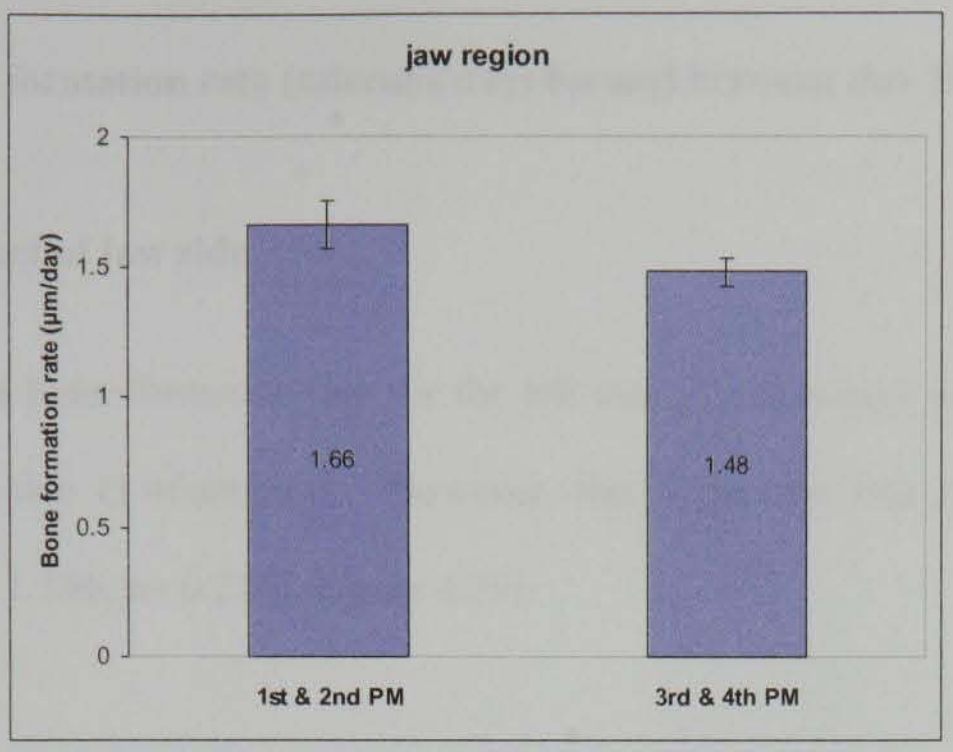

Figure 4.37 Means and standard errors for the jaw regions.

4.3.3.1.1.3 Effect of jaw area

Although Area 1 tended to have on average a higher bone formation rate (1.62µm/day) than area 2 (1.47µm/day), the difference was not statistically significant (F= 2.991, p= 0.085) (Figure 4.38).

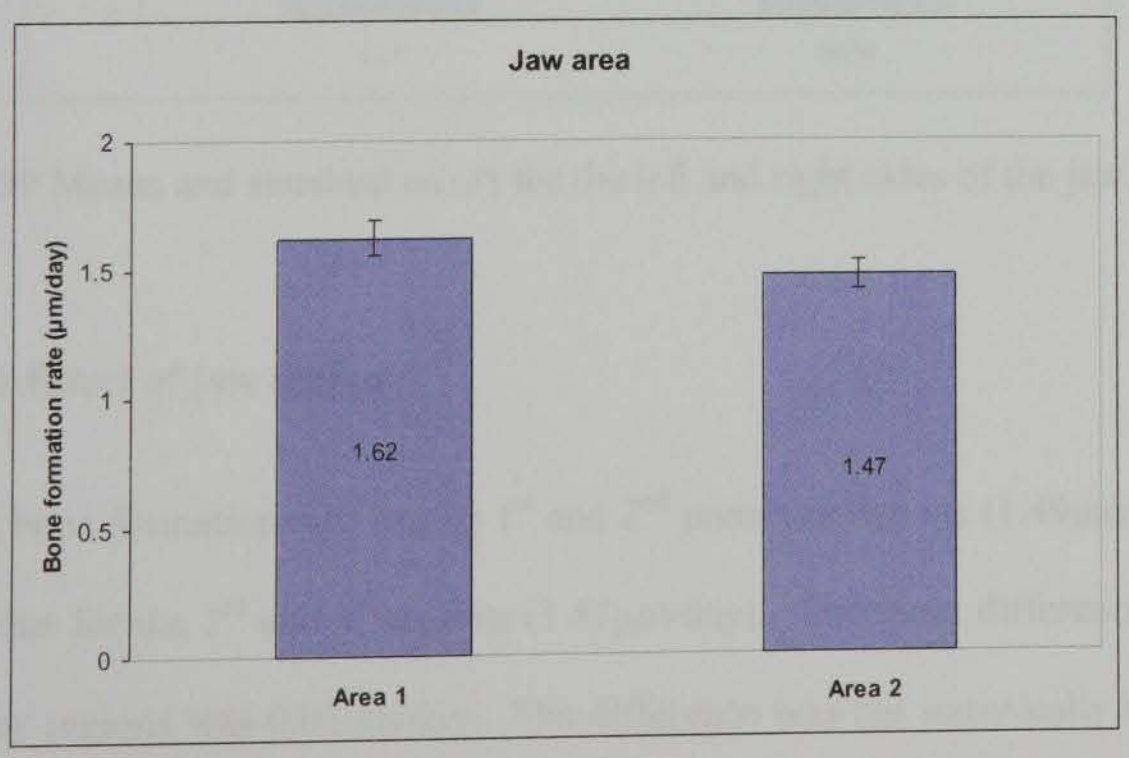

Figure 4.38 Means and standard errors for area 1 and 2.

4.3.3.1.2 Bone formation rate (microns/day) formed between day 21 and day 42.

4.3.3.1.2.1 Effect of jaw side

On average the bone formation rate for the left side (1.53μm/day) was greater than that for right side (1.46μm/day). However, this difference was not statistically significant (F= 1.556, p= 0.214) (Figure 4.39).

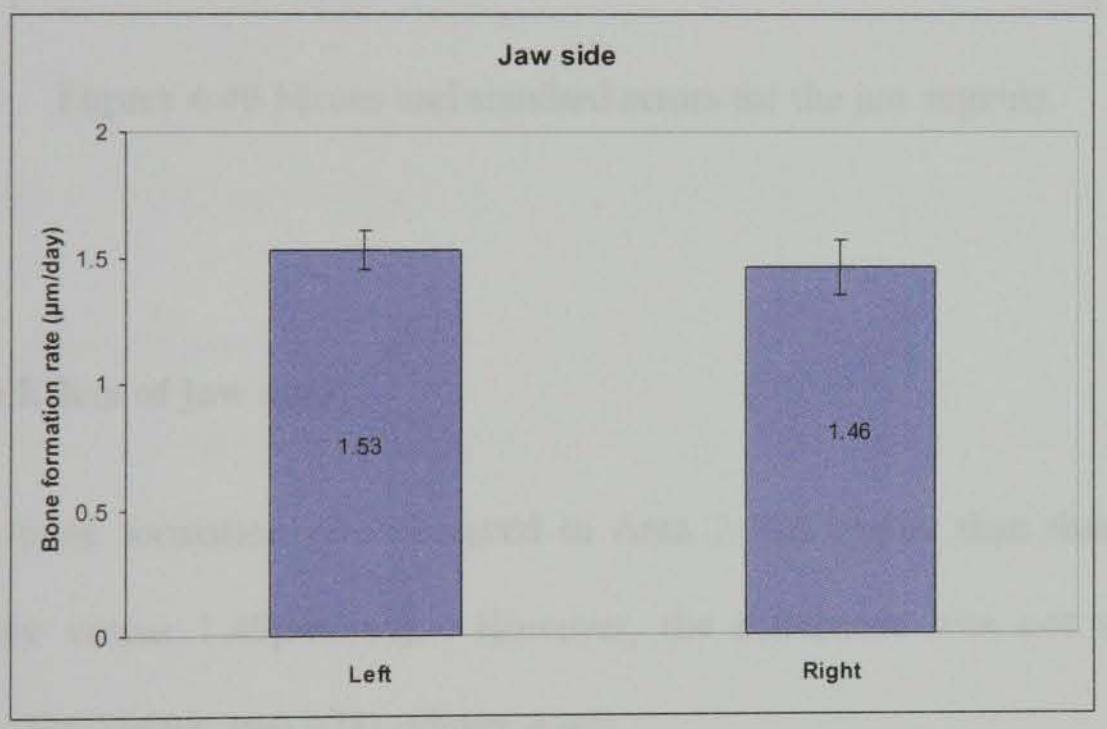

Figure 4.39 Means and standard errors for the left and right sides of the jaw.

4.3.3.1.2.2 Effect of jaw region

The mean bone formation rate for the 1st and 2nd premolar regions (1.49μm/ day) was less than that for the 3rd and 4th regions (1.51μm/day). The mean difference between the two jaw regions was 0.02μm/day. The difference was not statistically significant (F= 1.054, p= 0.306) (Figure 4.40).

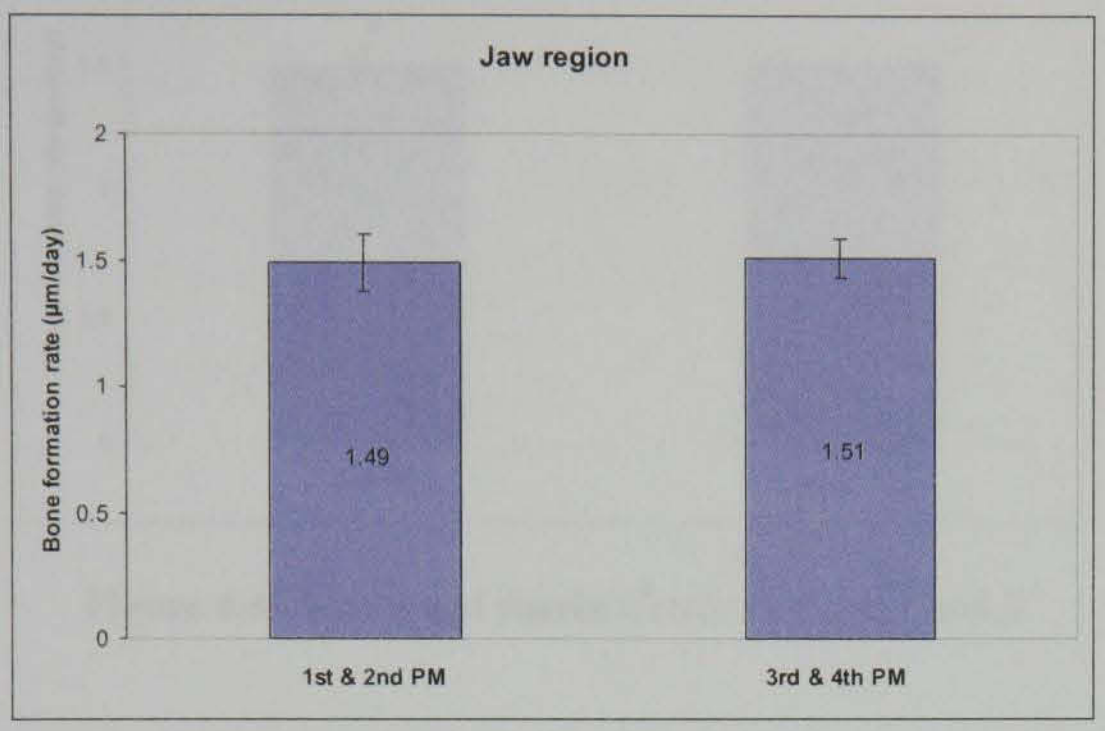

Figure 4.40 Means and standard errors for the jaw regions.

4.3.3.1.2.3 Effect of jaw area

The mean bone formation rate observed in Area 2 was higher than that in area 1 (1.51µm/day versus 1.49µm/day). However, the difference was not statistically significant (F= 0.0008, p=0.978) (Figure 4.41).

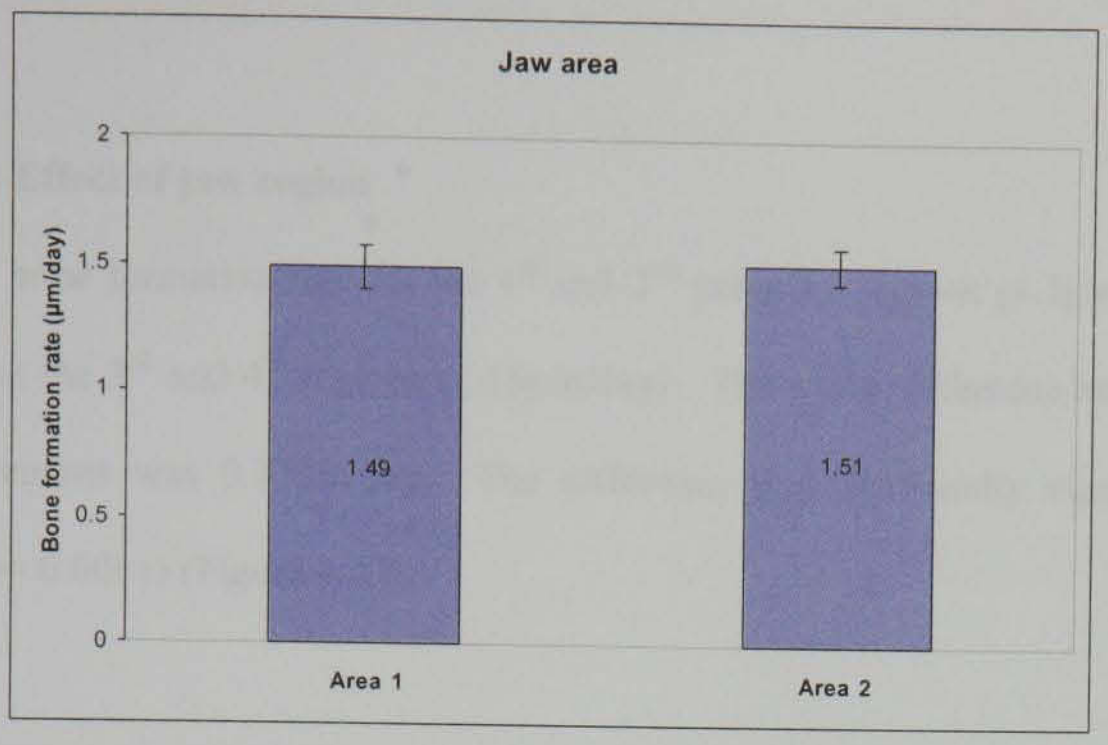

Figure 4.41 Means and standard errors for area 1 and 2.

4.3.3.1.3 Bone formation rate (microns/day) formed between day 42 and day 70.

4.3.3.1.3.1 Effect of jaw side

The bone formation rate for the left side was greater than that for the right side 1.34 and 1.18µm/day respectively. However, this difference was not statistically significant (F =1.377, p= 0.241) (Figure 4.42).

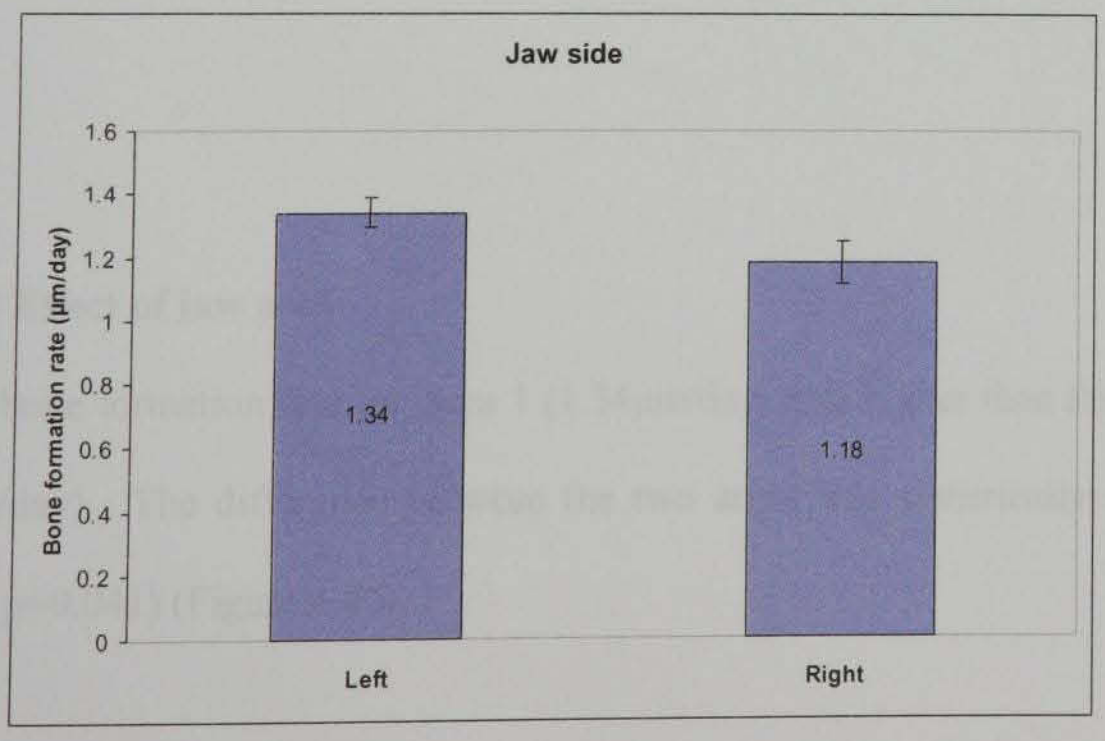

Figure 4.42 Means and standard errors for the jaw sides.

4.3.3.1.3.2 Effect of jaw region

The mean bone formation rate for the 1st and 2nd premolar regions (1.5μm/day) was greater than the 3rd and 4th regions (1.15μm/day). The mean difference between the two jaw regions was 0.35μm/day. The difference was statistically significant (F =16.584, p= 0.0001) (Figure 4.43).

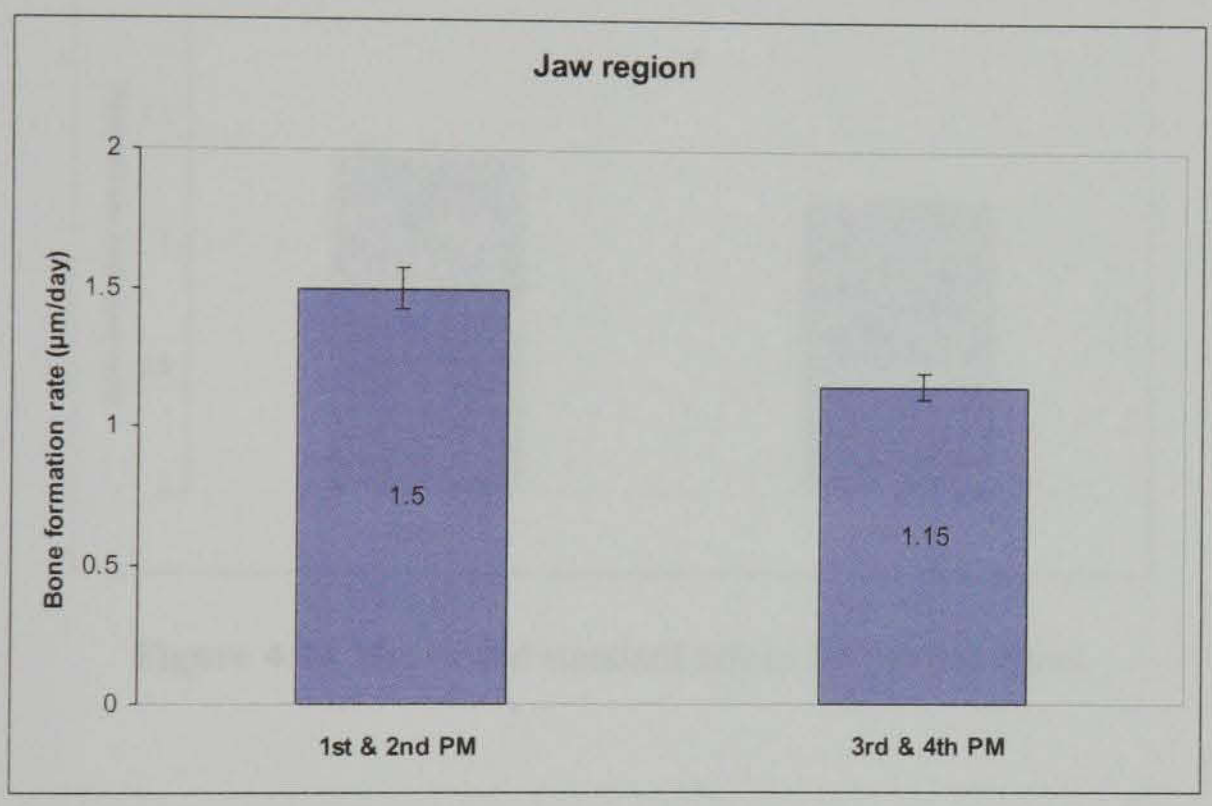

Figure 4.43 Means and standard errors for the jaw regions.

4.3.3.1.3.3 Effect of jaw area

The mean bone formation rate for Area 1 (1.34μm/day) was higher than that for Area 2 (1.17μm/day). The difference between the two areas was statistically significant (F= 4.194, p=0.041) (Figure 4.44).

A summary of effect tests, mean formation rate per day and mean difference for implants placed at day 1 of the study is displayed in Table 4.9.

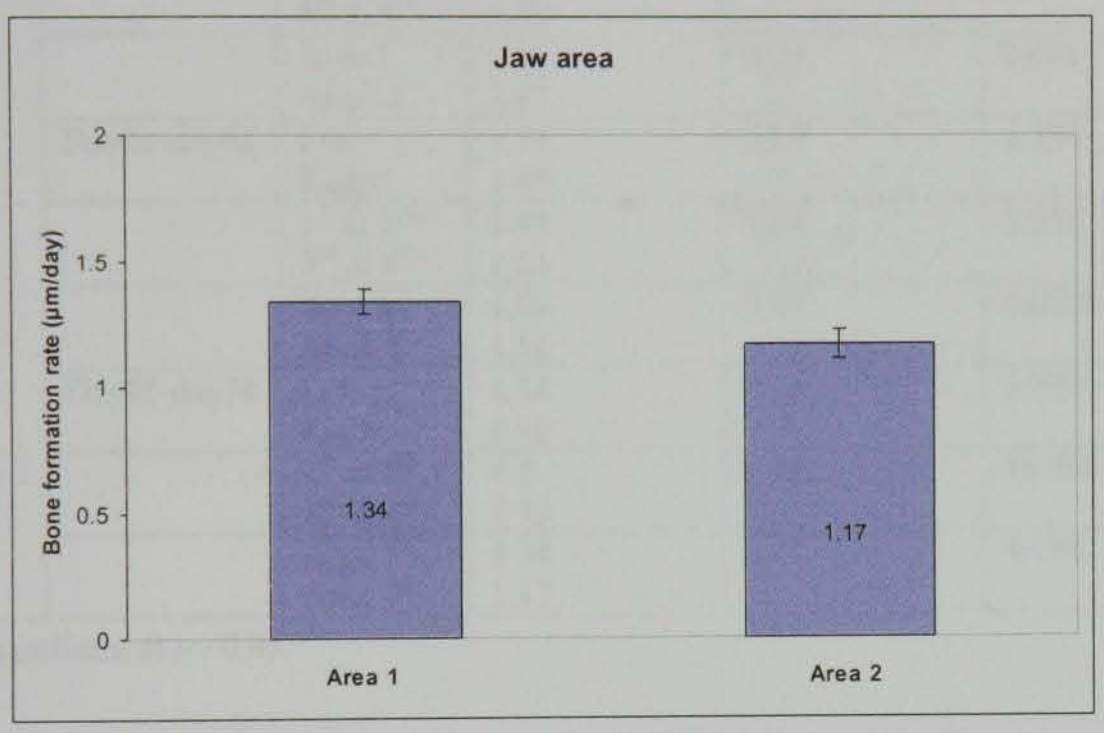

Figure 4.44 Means and standard errors for the jaw areas.

Table 4.9 Summary of effect tests, mean formation rate per day and mean difference for implants placed at day 1 of the study.

Time of implant placement	Duration	Source	Bone formation rate (µm/day)	Difference (µm)	F Ratio	*p*-value
Day 1	Day1-day21	Left Right	1.54 1.5	0.04	4.777	0.03*
		1st & 2nd 3rd & 4th	1.66 1.48	0.18	7.522	0.007*
		Area 1 Area 2	1.62 1.47	0.15	2.991	0.085
	Day21-day42	Left Right	1.53 1.46	0.07	1.556	0.214
		1st & 2nd 3rd & 4th	1.49 1.51	0.02	1.054	0.306
		Area 1 Area 2	1.49 1.51	0.02	0.0008	0.978
	Day42-day70	Left Right	1.34 1.18	0.16	1.377	0.241
		1st & 2nd 3rd & 4th	1.5 1.15	0.35	16.584	0.0001*
		Area 1 Area 2	1.34 1.17	0.17	4.194	0.041*

*indicates significant at $p = 0.05$.

4.3.3.2 Results for implants placed at day 21

4.3.3.2.1 Bone formation rate (microns/day) between day 1 and day 21.

4.3.3.2.1.1 Effect of jaw side

On average the mean bone formation rate for the right side of the jaws (1.33µm/day) was higher than that for the left side (1.22µm/day). This difference was not statistically significant ($F = 3.104$, $p = 0.080$), the magnitude of the difference was low (0.11µm/day) and so the biological significance of the difference may not be important (Figure 4.45).

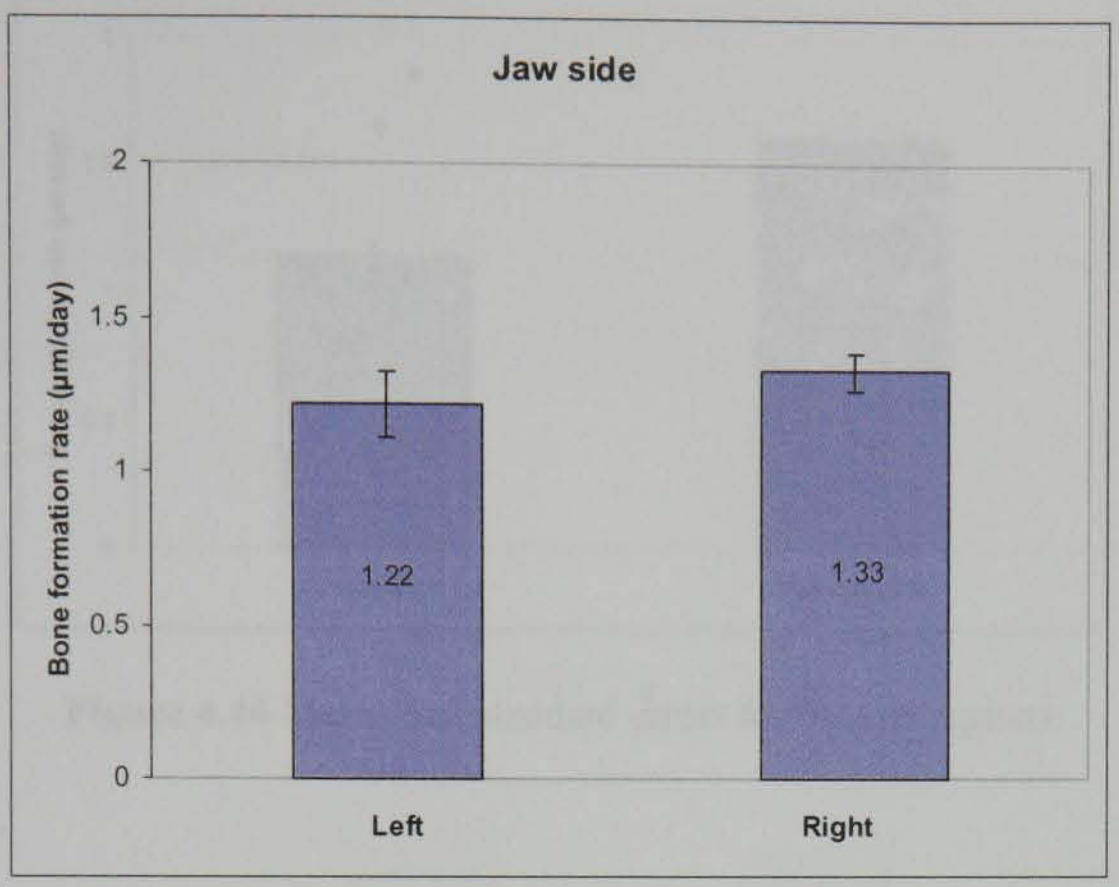

Figure 4.45 Means and standard errors for the left and right sides of the jaws.

4.3.3.2.1.2 Effect of jaw region

The mean bone formation rate for the 3rd and 4th premolar regions (1.62µm/day) was greater than that for the 1st and 2nd premolar regions (1.14µm/day). The mean difference between these two jaw regions was 0.48µm/day. This difference was statistically significant (F =7.186, p= 0.0001) (Figure 4.46).

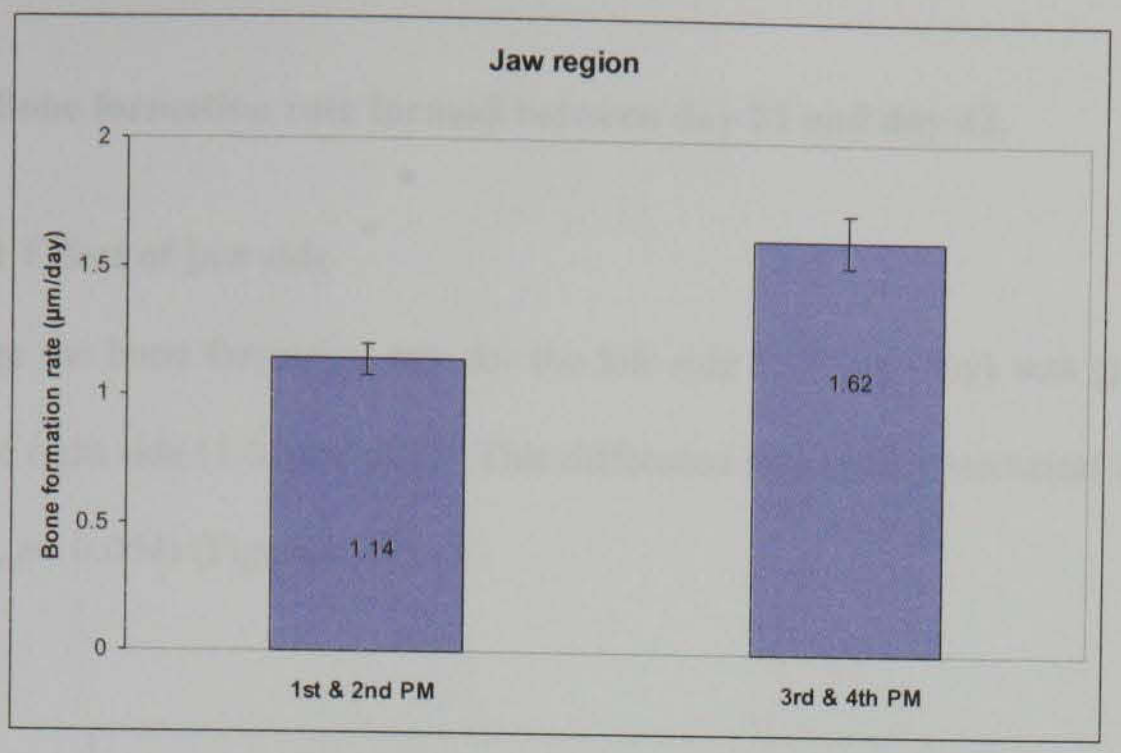

Figure 4.46 Means and standard errors for the jaw regions.

4.3.3.2.1.3 Effect of jaw area

Although Area 1 tended to have on average a higher bone formation rate (1.41µm/day) than area 2 (1.19µm/day), the difference was statistically significant (F= 5.323, p= 0.023) (Figure 4.47).

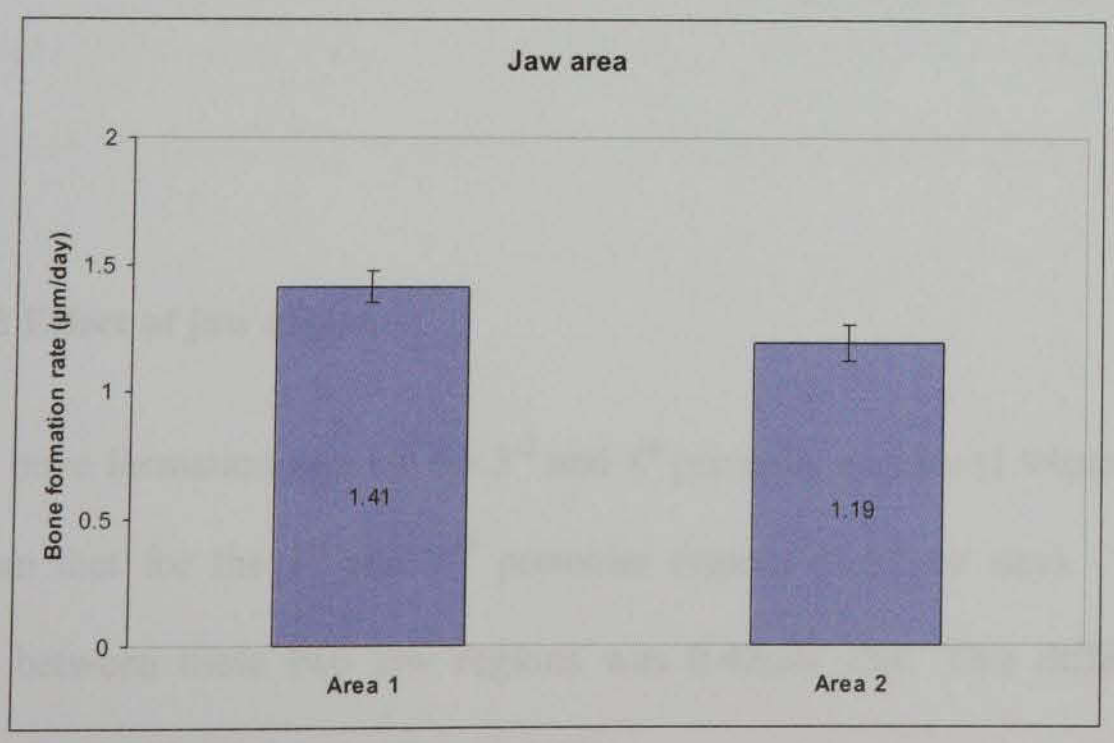

Figure 4.47 Means and standard errors for the areas within jaw areas.

4.3.3.2.2 Bone formation rate formed between day 21 and day 42.

4.3.3.2.2.1 Effect of jaw side

On average the bone formation rate for the left side (1.71μm/ day) was greater than that for the right side (1.62μm/ day). This difference approaches statistical significant (F= 3.825, p= 0.054) (Figure 4.48).

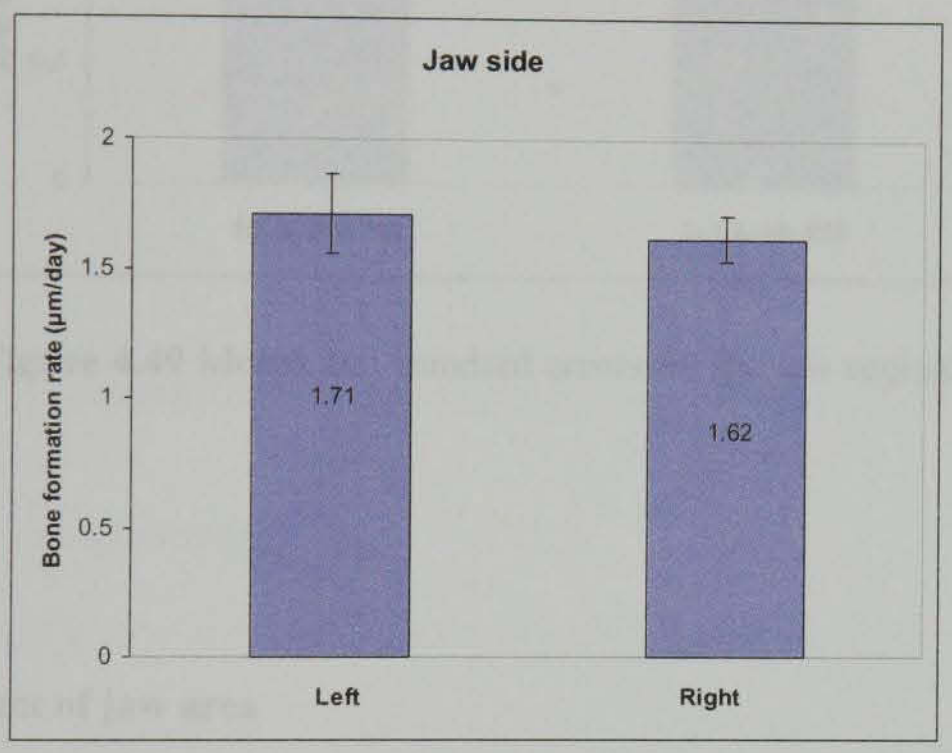

Figure 4.48 Means and standard errors for the left and right sides of the jaw.

4.3.3.2.2.2 Effect of jaw region

The mean bone formation rate for the 3rd and 4th premolar regions (1.94μm/ day) was greater than that for the 1st and 2nd premolar regions (1.52μm/ day). The mean difference between these two jaw regions was 0.42μm/ day. This difference was significant (F =7.522, p= 0.001) (Figure 4.49).

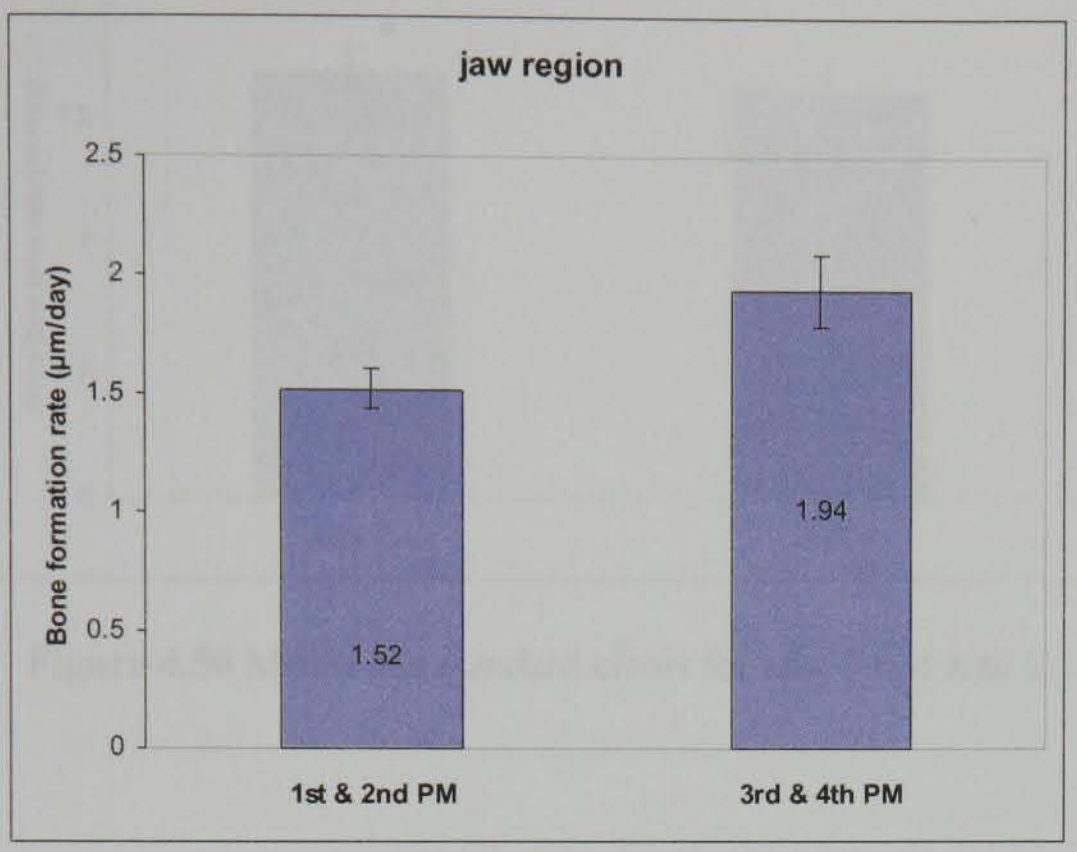

Figure 4.49 Means and standard errors for the jaw regions.

4.3.3.2.2.3 Effect of jaw area

The mean bone formation rate for Area 1 (1.66µm/day) was greater than that Area 2 (1.60µm/day). The mean difference between these two areas was 0.06µm/day. This difference was not statistically significant (F =0.0142, p= 0.905) (Figure 4.50).

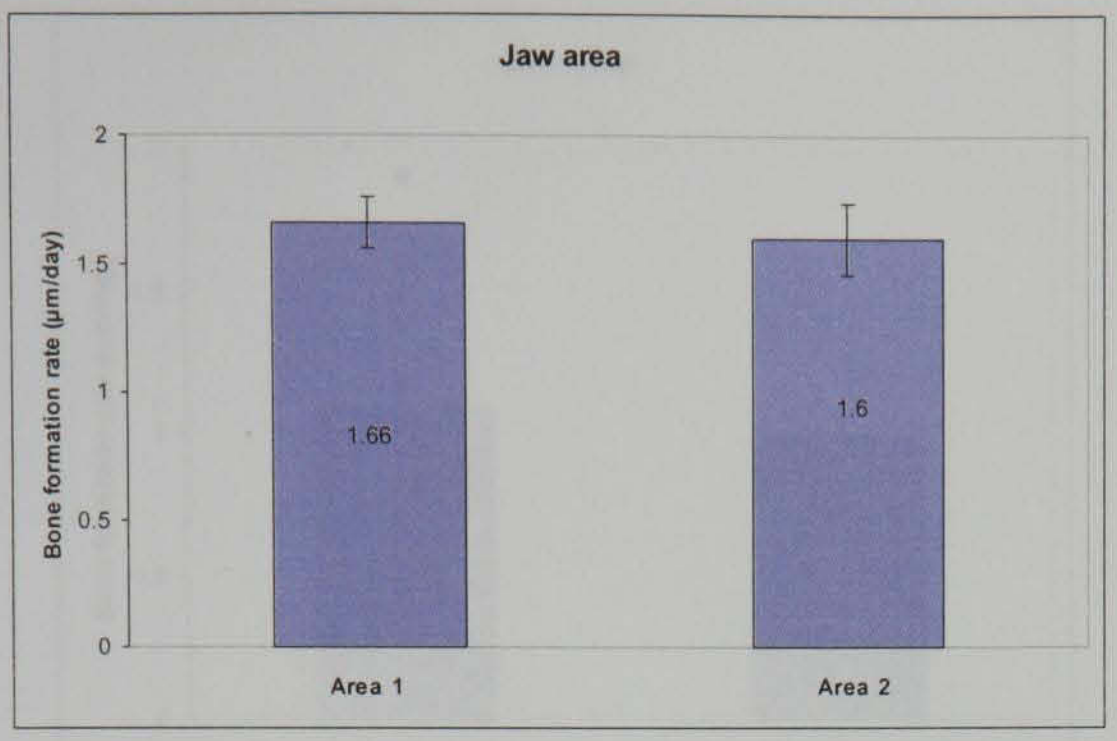

Figure 4.50 Means and standard errors for area 1 and area 2.

4.3.3.2.3 Bone formation rate (microns/day) formed between day 42 and day 70.

4.3.3.2.3.1 Effect of jaw side

The bone formation rate for the left side was greater than that for the right side 1.09 and 1.00µm/day respectively. However, this difference was not statistically significant (F =3.028, p= 0.084) (Figure 4.51).

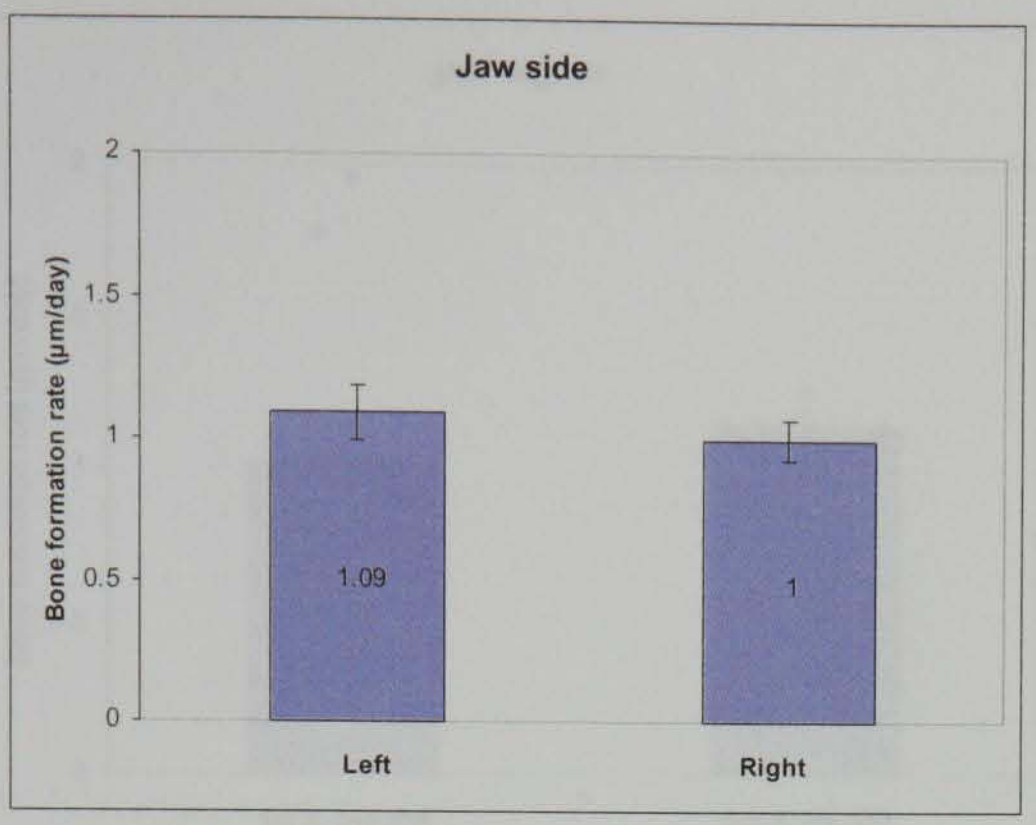

Figure 4.51 Means and standard errors for the jaw sides.

4.3.3.2.3.2 Effect of jaw region

The mean bone formation rate for the 1st and 2nd premolar regions (1.02µm/ day) was less than that for the 3rd and 4th premolar regions (1.15µm/day). The mean difference between the two jaw regions was 0.13µm/day. This difference was not statistically significant (F= 3.333, p= 0.070) (Figure 4.52).

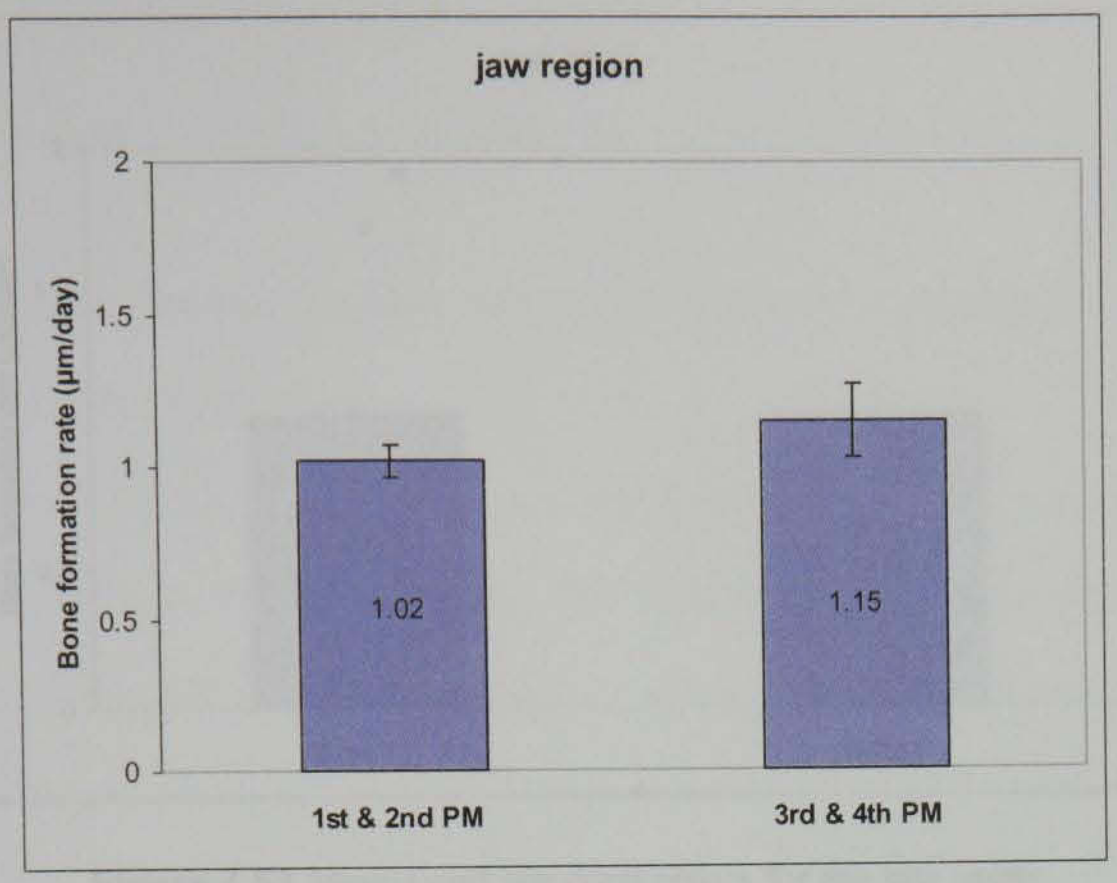

Figure 4.52 Means and standard errors for the jaw regions.

4.3.3.2.3.3 Effect of jaw area

The mean bone formation rate for Area 1 (1.04µm) was lower than that for Area 2 (1.05µm/ day). The difference between the two areas was not statistically significant (F= 0.069, p= 0.793) (Figure 4.53).

A summary of effect tests, mean formation rate per day and mean difference for implants placed at day 21 of the study is shown in Table 4.10.

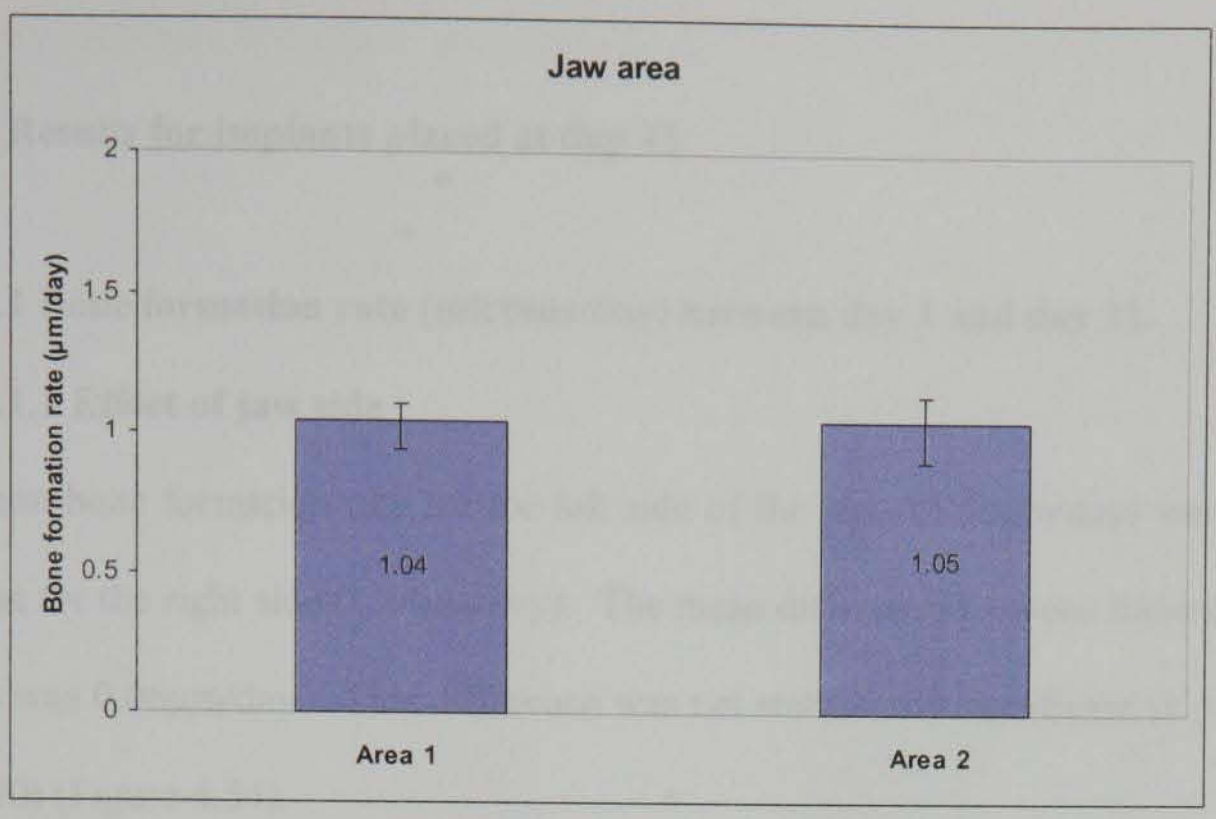

Figure 4.53 Means and standard errors for the jaw areas.

Table 4.10 Summary of effect tests, mean formation rate per day and mean difference for implants placed at day 21 of the study.

Time of implant placement	Duration	Source	Bone formation rate (µm/day)	Difference (µm)	F Ratio	*p*-value
Day 21	Day1-day21	Left Right	1.33 1.22	0.11	3.104	0.08
		1st & 2nd 3rd & 4th	1.14 1.62	0.48	7.186	0.0001*
		Area 1 Area 2	1.41 1.19	0.22	5.323	0.023*
	Day21-day42	Left Right	1.71 1.62	0.09	3.825	0.054
		1st & 2nd 3rd & 4th	1.52 1.94	0.42	7.522	0.001*
		Area 1 Area 2	1.66 1.60	0.06	0.0142	0.905
	Day42-day70	Left Right	1.09 1.00	0.09	3.028	0.084
		1st & 2nd 3rd & 4th	1.02 1.15	0.13	3.333	0.07
		Area 1 Area 2	1.04 1.05	0.01	0.069	0.793

*indicates significant at $p = 0.05$.

4.3.3.3 Results for implants placed at day 42

4.3.3.3.1 Bone formation rate (microns/day) between day 1 and day 21.

4.3.3.3.1.1 Effect of jaw side

The mean bone formation rate for the left side of the jaws (1.50μm/day) was higher than that for the right side (1.44μm/day). The mean difference between these two jaw regions was 0.06μm/day. This difference was not statistically significant (F = 0.291, p= 0.590) (Figure 4.54).

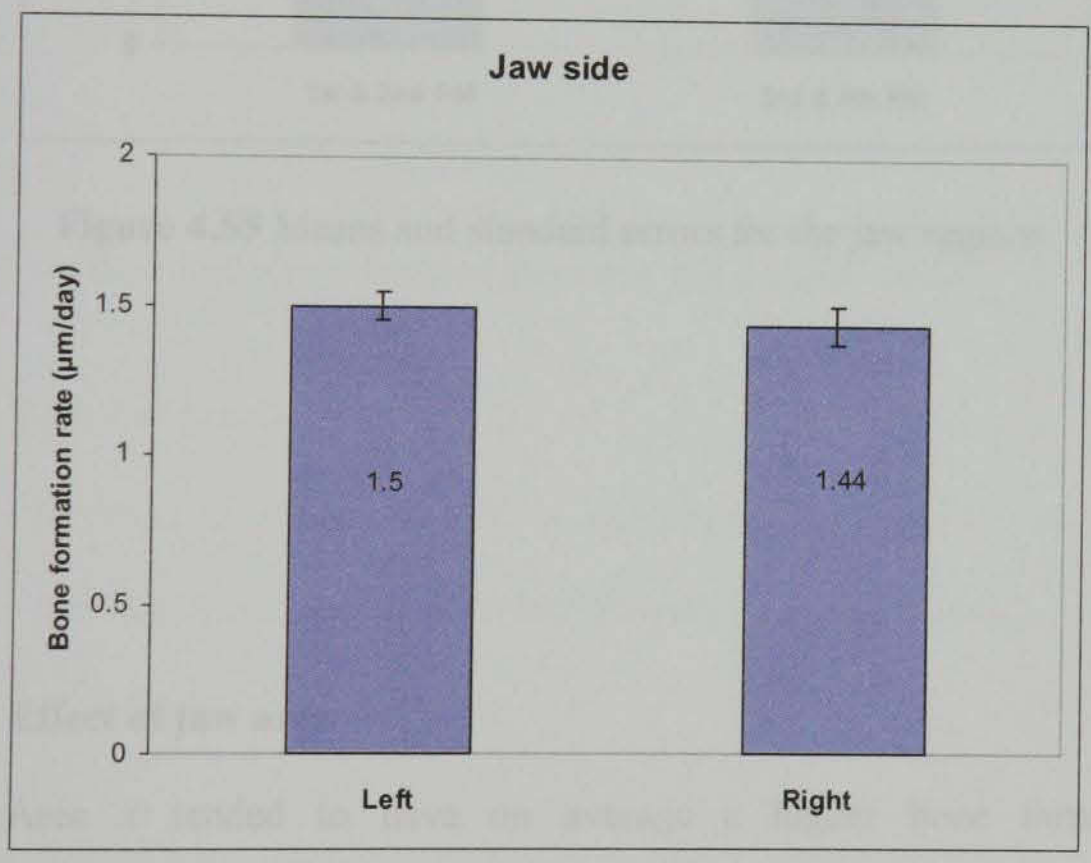

Figure 4.54 Means and standard errors for the left and right sides of the jaws.

4.3.3.3.1.2 Effect of jaw region

The mean bone formation rate for the 1st and 2nd premolar regions (1.54μm/day) was greater than that for the 3rd and 4th premolar regions (1.38μm/day). The mean

difference between these two jaw regions was 0.16μm/day. This difference was statistically significant (F= 3.584, p= 0.06) (Figure 4.55).

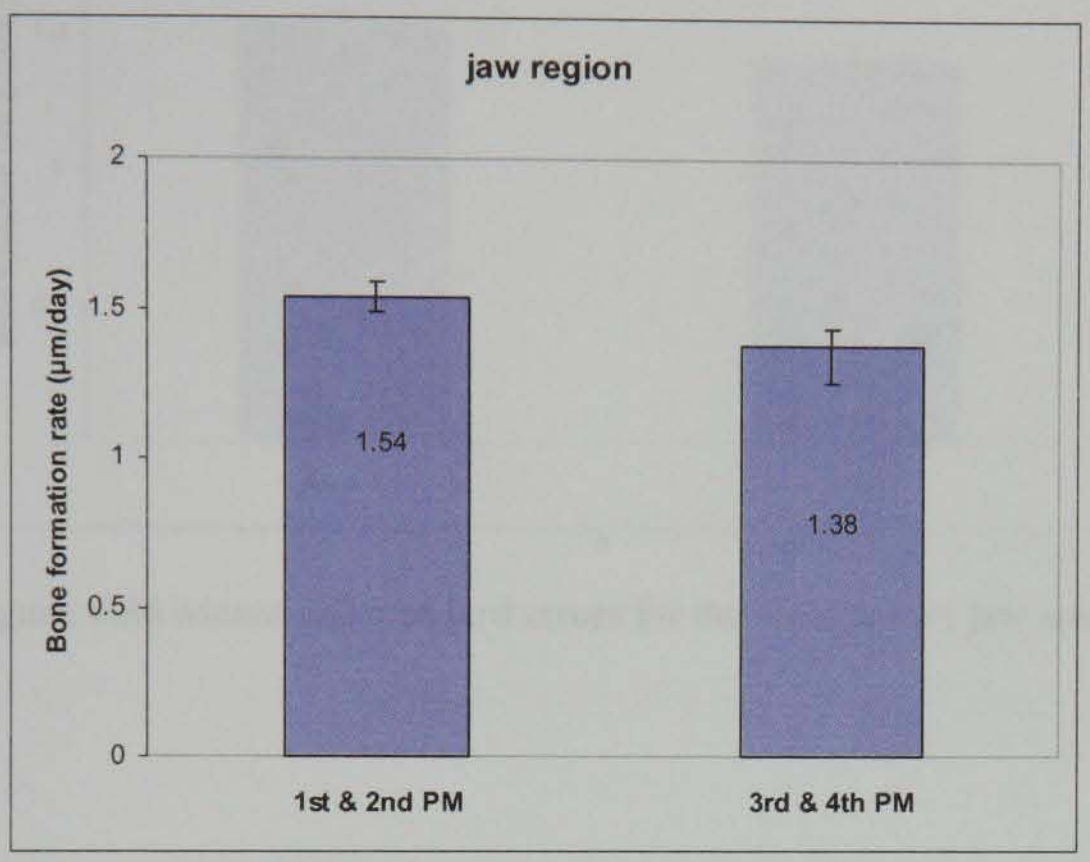

Figure 4.55 Means and standard errors for the jaw regions.

4.3.3.3.1.3 Effect of jaw area

Although Area 1 tended to have on average a higher bone formation rate (1.53μm/day) than area 2 (1.41μm/day), the difference was not statistically significant (F =2.155, p= 0.143) (Figure 4.56).

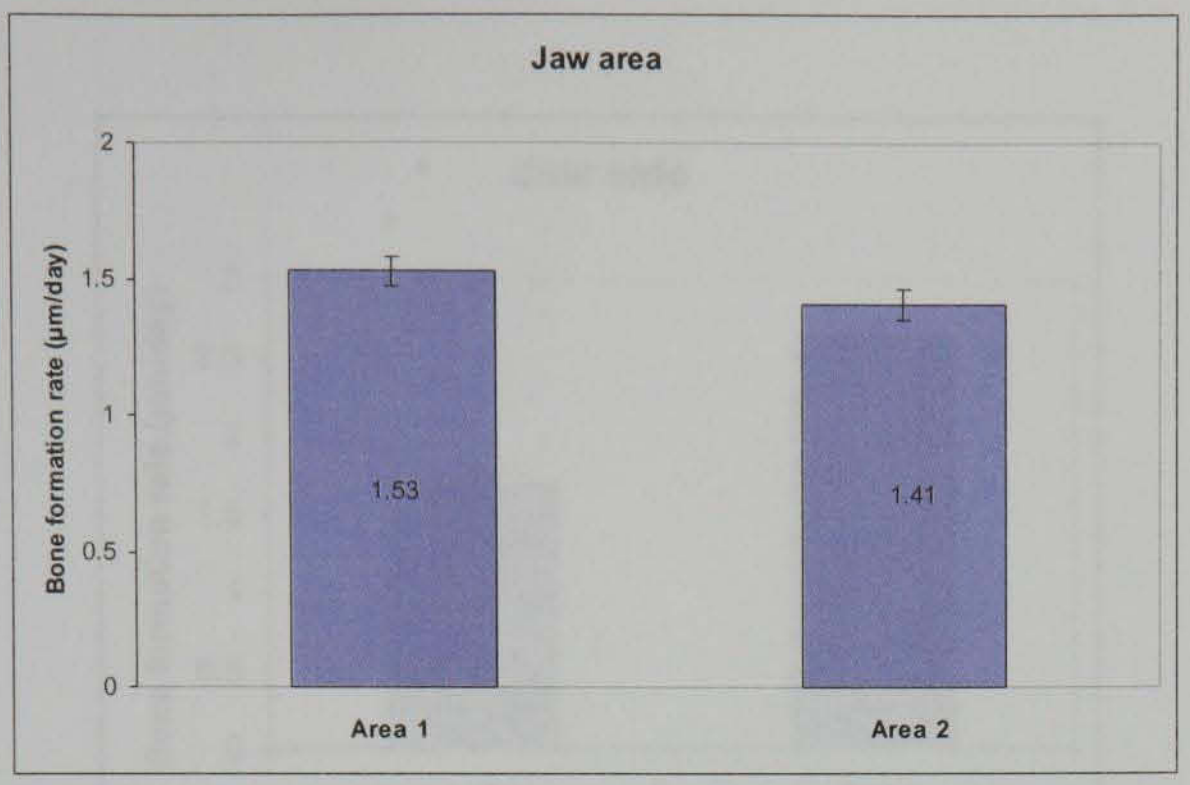

Figure 4.56 Means and standard errors for the areas within jaw areas.

4.3.3.3.2 Bone formation rate formed between day 21 and day 42

4.3.3.3.2.1 Effect of jaw side

On average the bone formation rate for the right side (2.64µm/day) was greater than that for the left side (1.69µm/day). This difference was not statistically significant (F= 0.666, p= 0.415) (Figure 4.57).

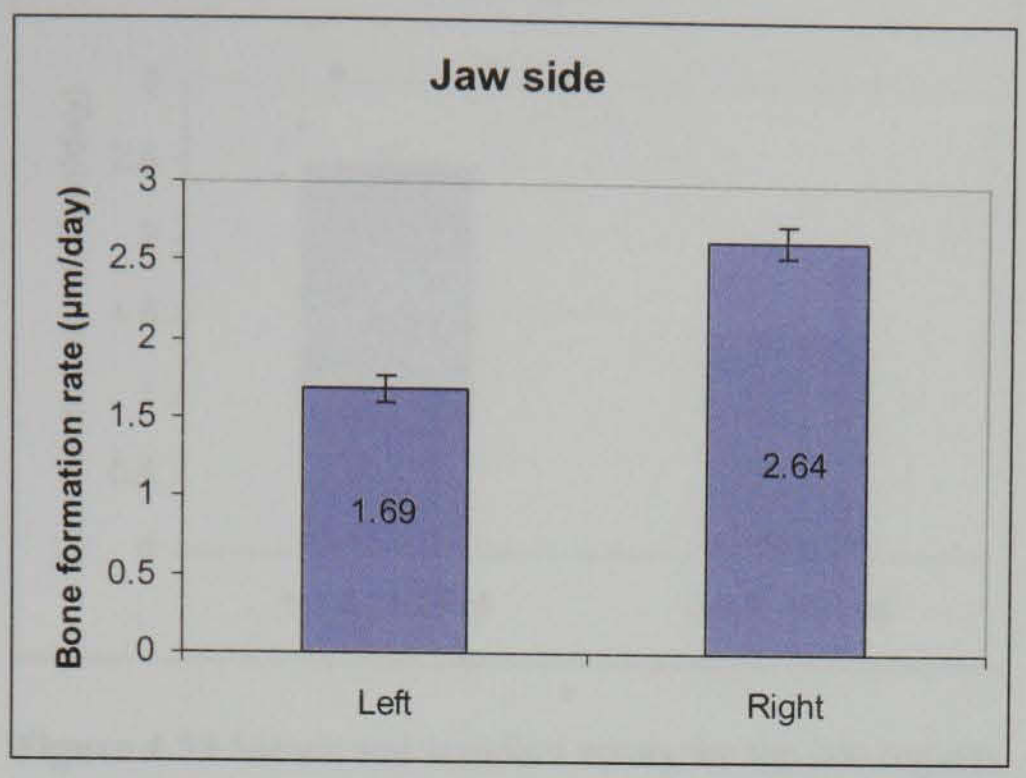

Figure 4.57 Means and standard errors for the left and right sides of the jaw.

4.3.3.3.2.2 Effect of jaw region

The mean bone formation rate for the 1st and 2nd premolar regions (2.48µm/day) was greater than that for the 3rd and 4th premolar regions (1.42µm/day). The mean difference between these two jaw regions was 1.06µm/day. This difference was not significant (F= 0.520, p= 0.472) (Figure 4.58).

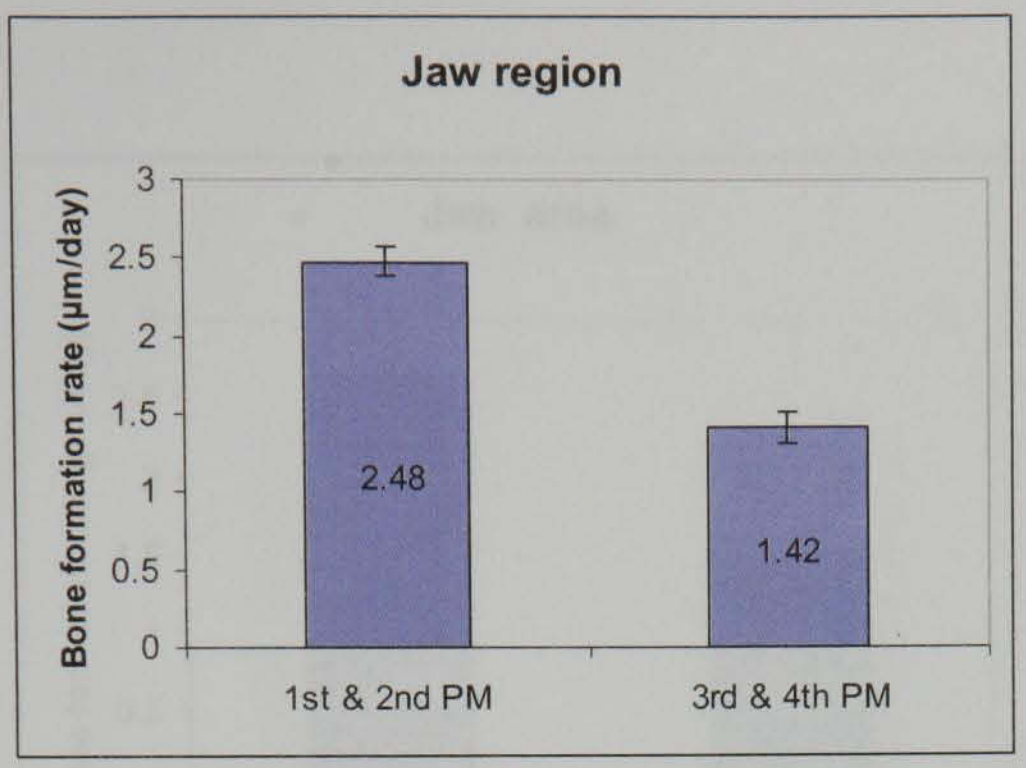

Figure 4.58 Means and standard errors for the jaw regions.

4.3.3.3.2.3 Effect of jaw area

The mean bone formation rate for Area 1 (2.65µm/day) was greater than that for Area 2 (1.51µm/day). The mean difference between these two areas was 1.14µm/day. This difference was not statistically significant (F =0.654, p= 0.420) (Figure 4.59).

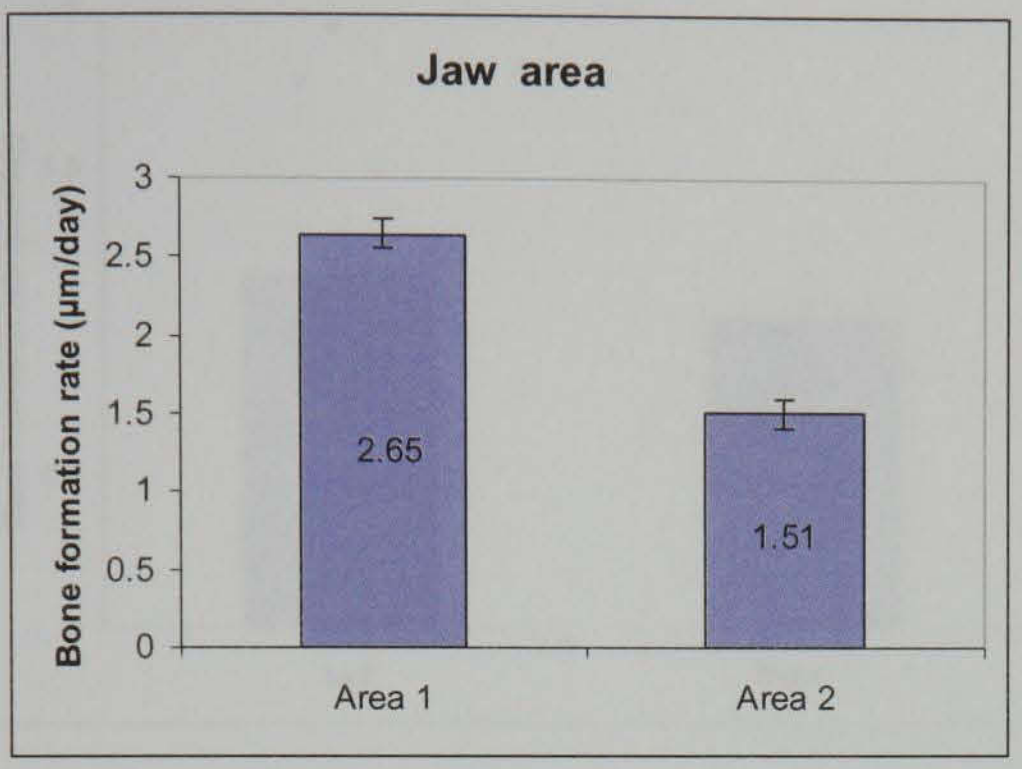

Figure 4.59 Means and standard errors for the areas within jaw areas.

4.3.3.3.3 Bone formation rate (microns/day) formed between day 42 and day 70

4.3.3.3.3.1 Effect of jaw side

The bone formation rate for the right side was greater than that for the left side 1.15 and 1.01µm/ day respectively. However, this difference was not statistically significant (F =3.0, p= 0.084) (Figure 4.60).

Figure 4.60 Means and standard errors for the jaw sides.

4.3.3.3.3.2 Effect of jaw region

The mean bone formation rate for the 1st and 2nd premolar regions (1.1µm/day) was greater than that for the 3rd and 4th premolar regions (1.06µm/day). The mean difference between the two jaw regions was 0.04µm/ day. This difference was not statistically significant (F =0.212, p= 0.646) (Figure 4.61).

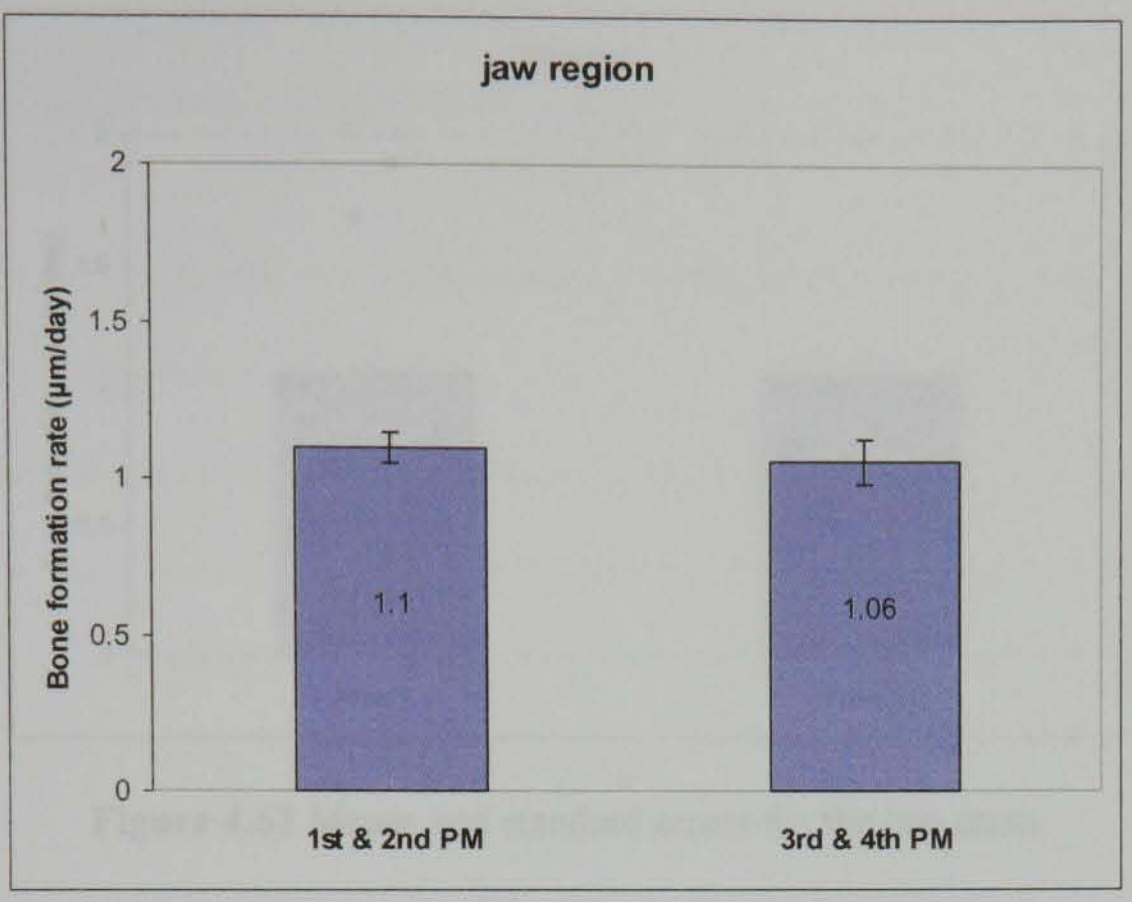

Figure 4.61 Means and standard errors for the jaw regions.

4.3.3.3.3.3 Effect of jaw area

The mean bone formation rate for Area 1 (1.09µm/day) was higher than that for Area 2 (1.08µm/day). The difference between the two areas was not statistically significant (F =0.025, p= 0.876) (Figure 4.62).

Summary of effect tests, mean formation rate per day and mean difference for implants placed at day 42 of the study is displayed in Table 4.11.

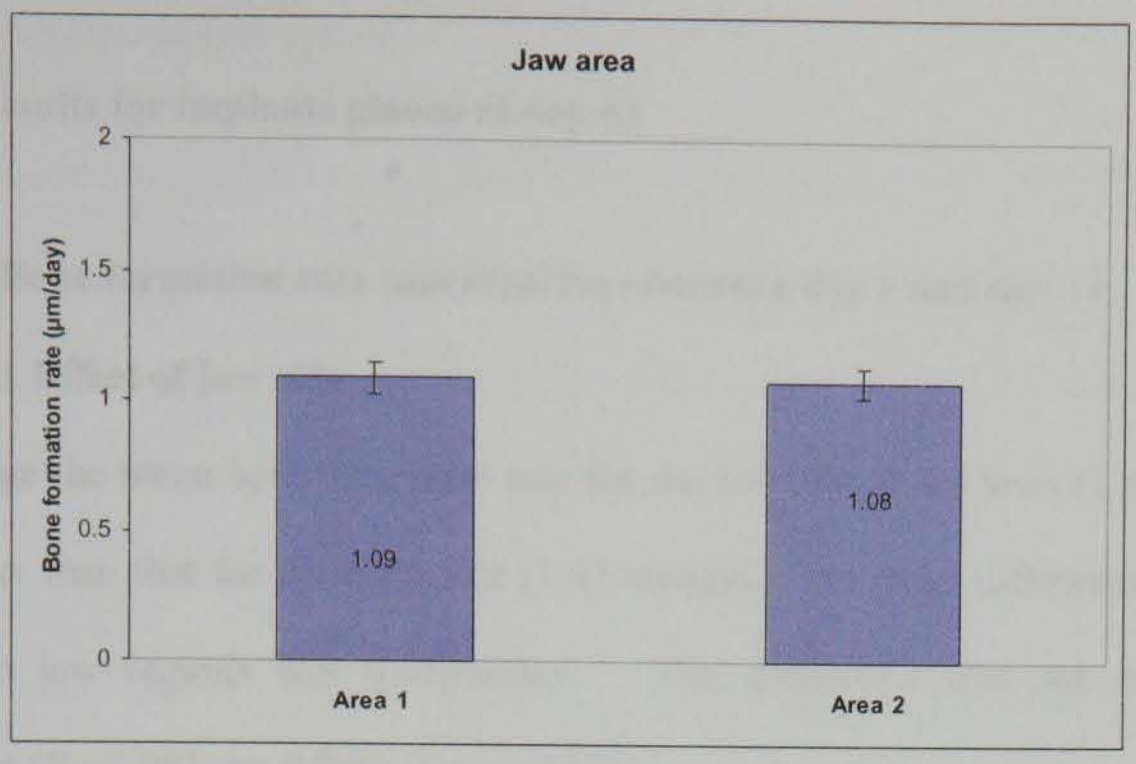

Figure 4.62 Means and standard errors for the jaw areas.

Table 4.11 Summary of effect tests, mean formation rate per day and mean difference for implants placed at day 42 of the study.

Time of implant placement	Duration	Source	Bone formation rate (µm/day)	Difference (µm)	F Ratio	*p*-value
Day 42	Day1-day21	Left Right	1.50 144	0.06	0.291	0.590
		1st & 2nd 3rd & 4th	1.54 1.38	0.16	3.584	0.06
		Area 1 Area 2	1.53 1.41	0.12	2.155	0.143
	Day21-day42	Left Right	1.69 2.64	0.95	0.666	0.415
		1st & 2nd 3rd & 4th	2.48 1.42	1.06	0.520	0.472
		Area 1 Area 2	2.65 1.51	1.14	0.654	0.420
	Day42-day70	Left Right	1.15 1.01	0.14	3.0	0.084
		1st & 2nd 3rd & 4th	1.10 1.06	0.04	0.212	0.646
		Area 1 Area 2	1.09 1.08	0.01	0.025	0.876

4.3.3.4 Results for implants placed at day 63

4.3.3.4.1 Bone formation rate (microns/day) between day 1 and day 21

4.3.3.4.1.1 Effect of jaw side

On average the mean bone formation rate for the left side of the jaws (1.48μm/day) was higher than that for the right side (1.47μm/day). The mean difference between these two jaw regions was 0.01μm/day. This difference was not statistically significant (F =1.081, p= 0.299) (Figure 4.63).

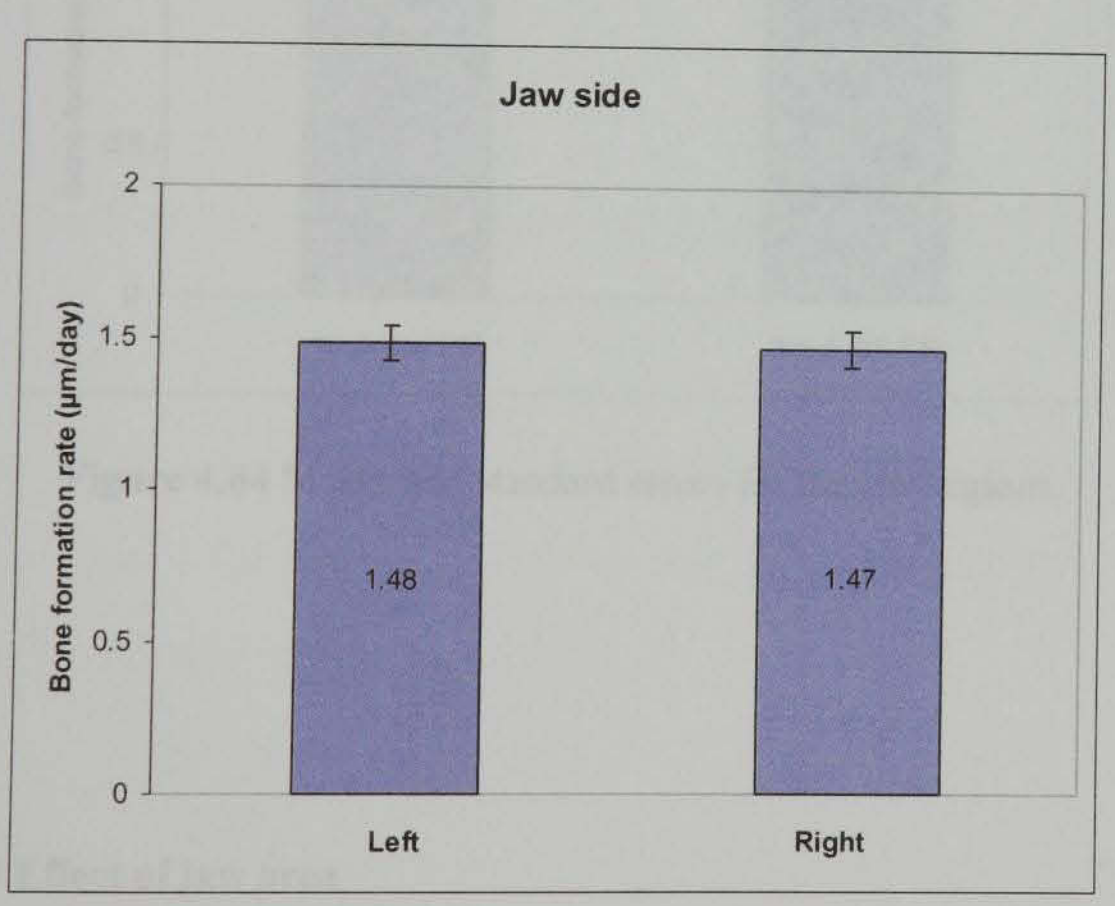

Figure 4.63 Means and standard errors for the left and right sides of the jaws.

4.3.3.4.1.2 Effect of jaw region

The mean bone formation rate for the 3rd and 4th premolar regions (1.51μm/day) was greater than that for the 1st and 2nd premolar regions (1.33μm/day). The mean difference between these two jaw regions was 0.18μm/ day. This difference was statistically significant (F =4.428, p= 0.036) (Figure 4.64).

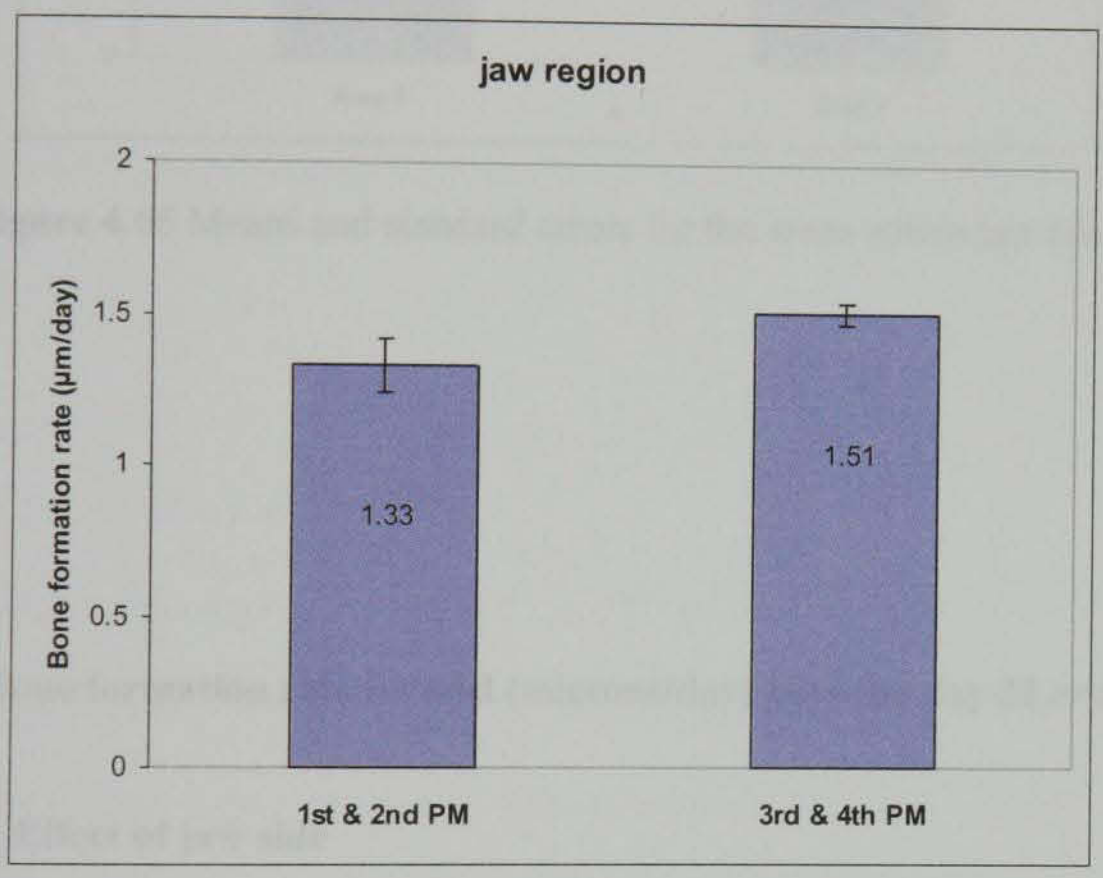

Figure 4.64 Means and standard errors for the jaw regions.

4.3.3.4.1.3 Effect of jaw area

Although Area 1 tended to have on average a higher bone formation rate (1.59μm/day) than area 2 (1.35μm/day), the difference was statistically significant (F =10.577, p= 0.001) (Figure 4.65).

Figure 4.65 Means and standard errors for the areas within jaw areas.

4.3.3.4.2 Bone formation rate formed (microns/day) between day 21 and day 42.

4.3.3.4.2.1 Effect of jaw side

On average the bone formation rate for the left side (1.70µm/day) was greater than that for right side (1.38µm/day). However, this difference was not statistically significant (F= 0.070, p= 0.791) (Figure 4.66).

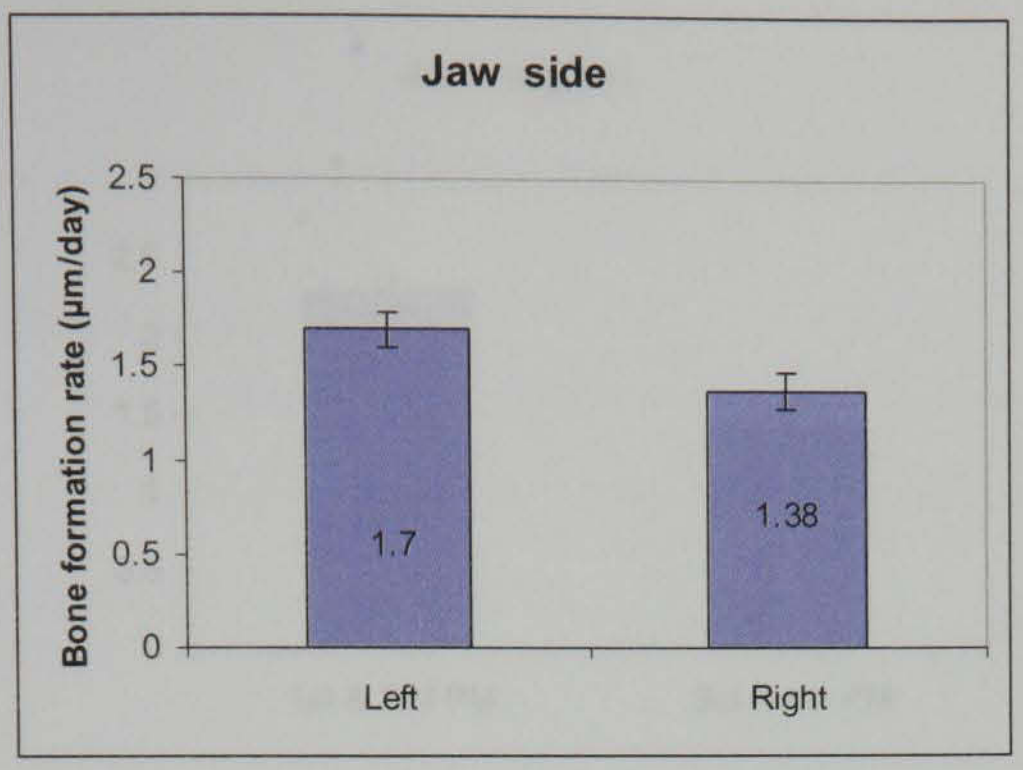

Figure 4.66 Means and standard errors for the left and right sides of the jaw.

4.3.3.4.2.2 Effect of jaw region

The mean bone formation rate for the 1st and 2nd premolar regions (2.28µm/day) was less than that for the 3rd and 4th regions (1.41µm/day). The mean difference between the two jaw regions was 0.87µm/day. However, this difference was not statistically significant (F= 1.856, p= 0.174) (Figure 4.67).

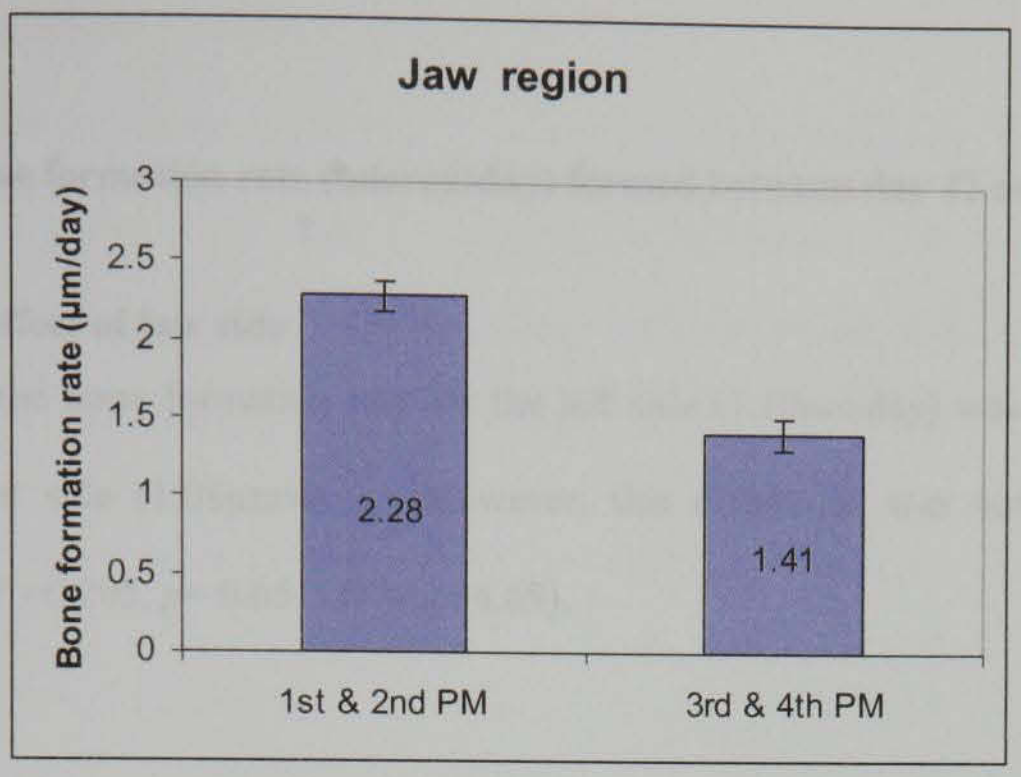

Figure 4.67 Means and standard errors for the jaw regions.

4.3.3.4.2.3 Effect of jaw area

The mean bone formation rate for Area 1 (1.72µm/day) was higher than that for Area 2 (1.29µm/day). The difference between the two areas was not statistically significant (F= 1.390, p=0.240) (Figure 4.68).

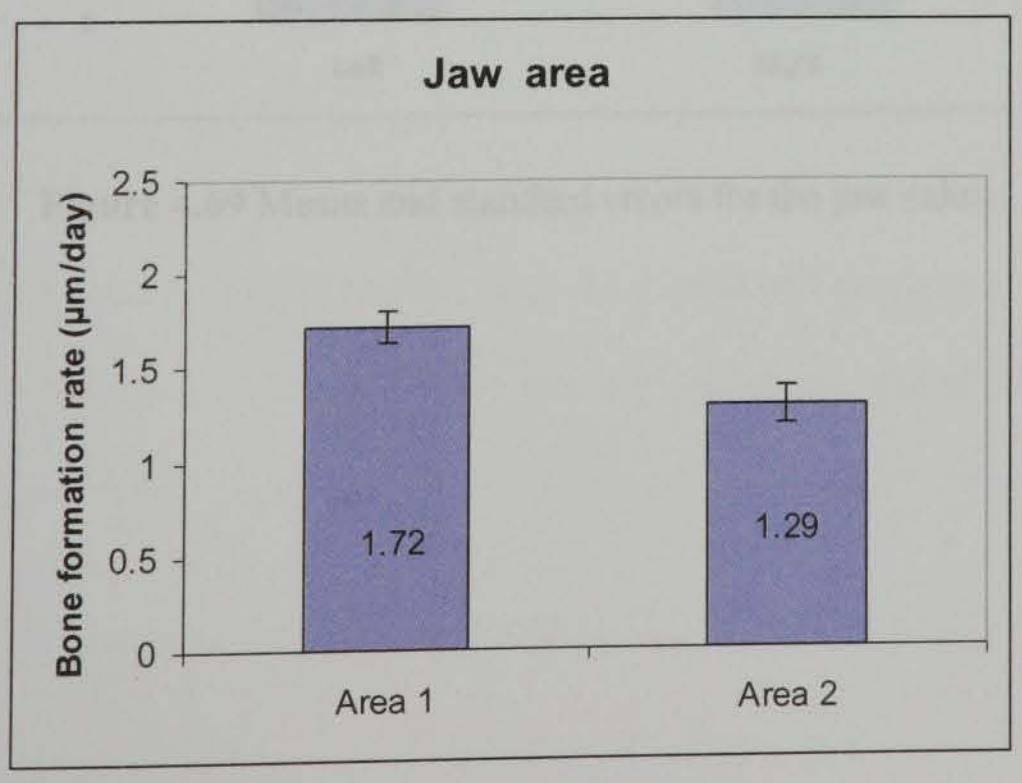

Figure 4.68 Means and standard errors for area 1 and 2.

4.3.3.4.3 Bone formation rate (micron/day) formed between day 42 and day 70

4.3.3.4.3.1 Effect of jaw side

On average the bone formation rate for the left side (1.10μm/day) was greater than that for right side (1.08μm/day). However, this difference was not statistically significant (F =0.205, p= 0.651) (Figure 4.69).

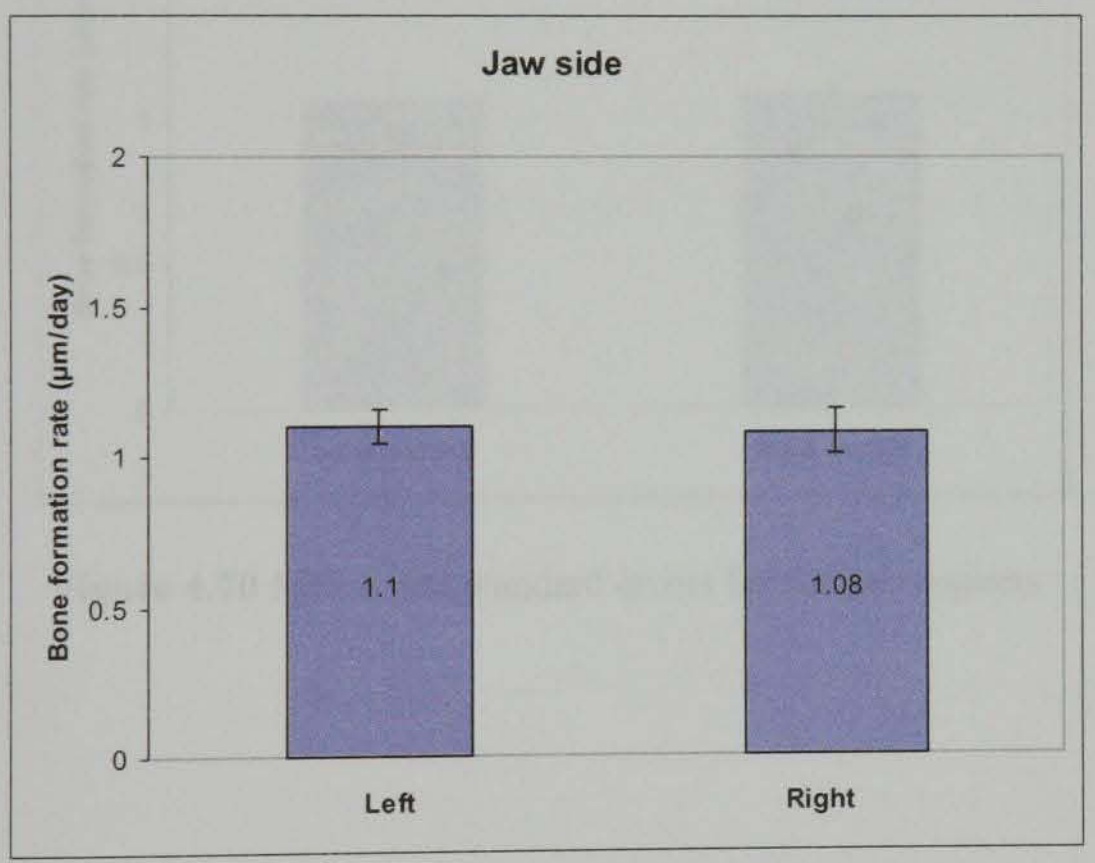

Figure 4.69 Means and standard errors for the jaw sides.

4.3.3.4.3.2 Effect of jaw region

The mean bone formation rate for the 3rd and 4th premolar regions (1.09μm/day) was greater than that for the 1st and 2nd regions (1.07μm/day). The mean difference between the two jaw regions was 0.02μm/day. The difference was not statistically significant (F= 0.227, p= 0.634) (Figure 4.70).

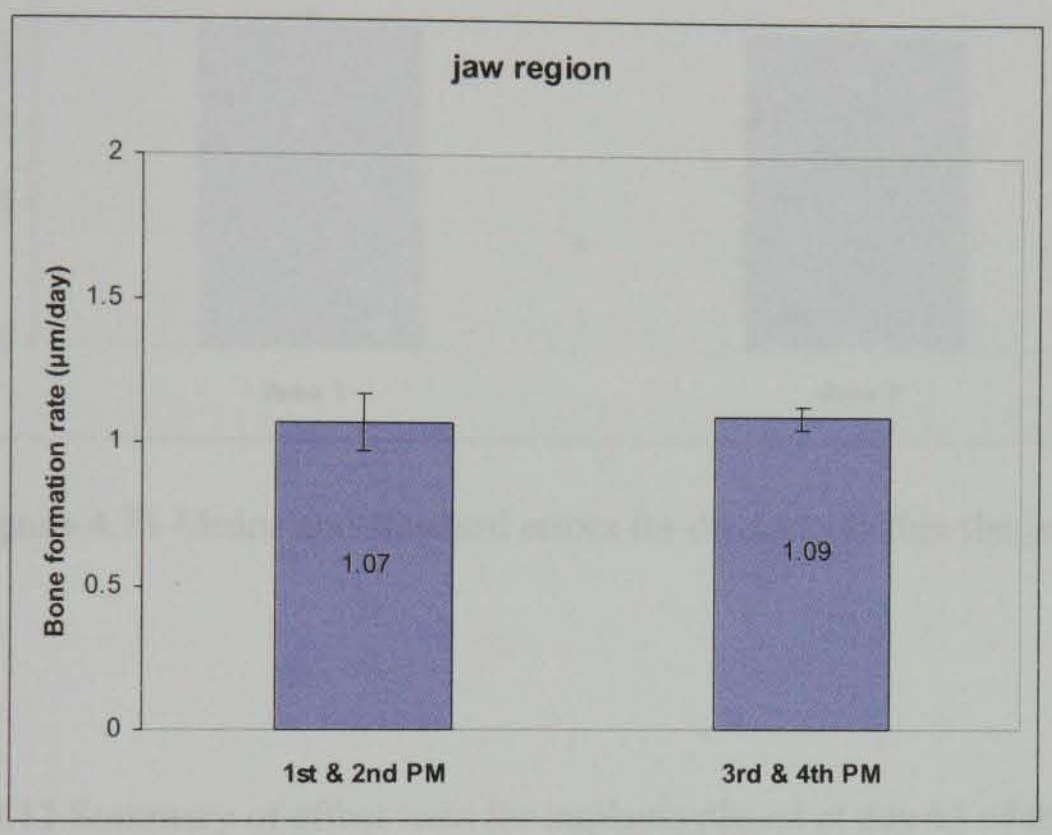

Figure 4.70 Means and standard errors for the jaw regions.

4.3.3.4.3.3 Effect of jaw area

On average the bone formation rate for Area 1 (1.1μm/day) was greater than that for right side (1.08μm/day). This difference was not statistically significant (F= 0.102, p= 0.750) (Figure 4.71).

A summary of effect tests for implants placed at day 63 of the study is shown in Table 4.12.

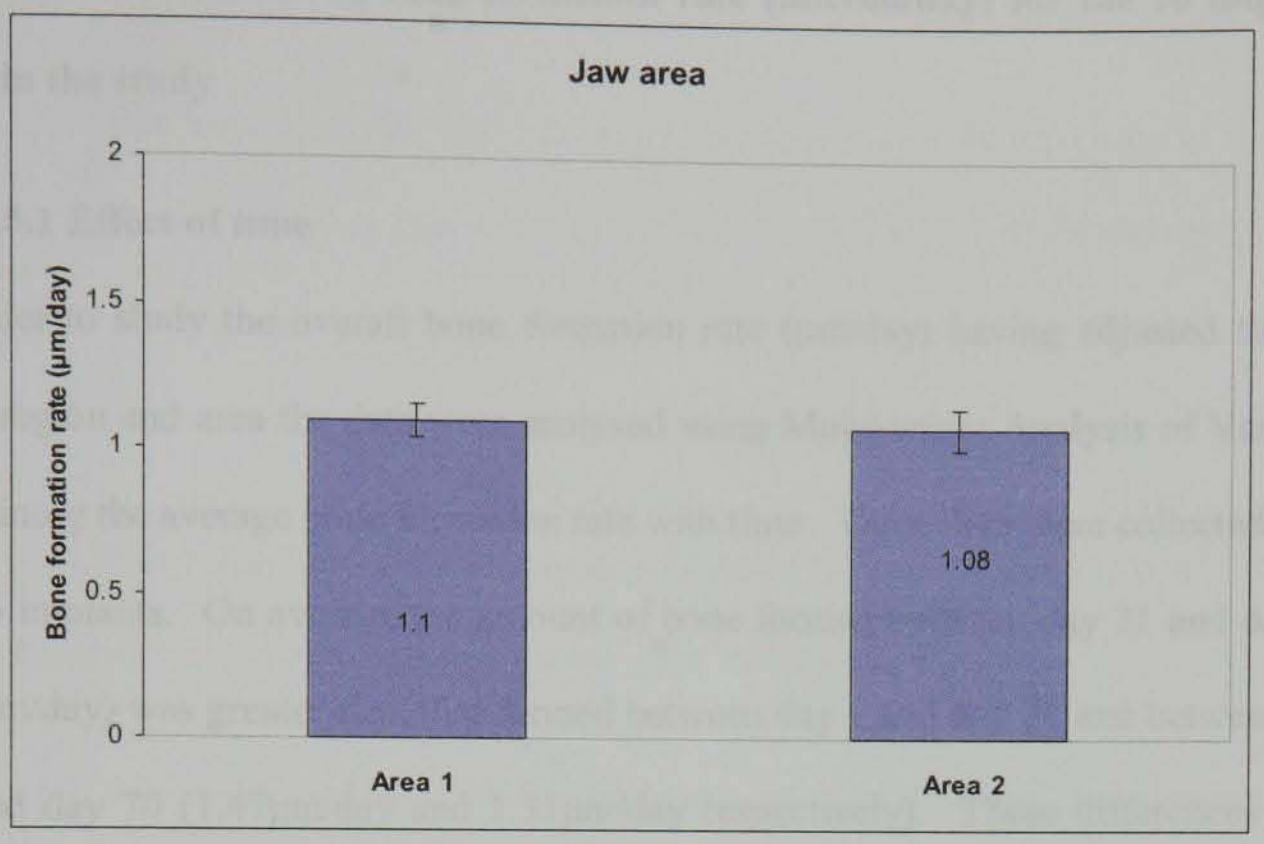

Figure 4.71 Means and standard errors for the areas within the jaw.

Table 4.12 Summary of effect tests for implants placed at day 63 of the study

Time of implant placement	Duration	Source	Bone formation rate (µm/day)	Difference (µm)	F Ratio	*p*-value
Day 63	Day1-day21	Left Right	1.48 1.47	0.01	1.081	0.299
		1st & 2nd 3rd & 4th	1.33 1.51	0.18	4.428	0.036*
		Area 1 Area 2	1.59 1.35	0.24	10.577	.0013*
	Day21-day42	Left Right	1.70 1.38	0.32	0.070	0.791
		1st & 2nd 3rd & 4th	2.28 1.41	0.87	1.856	0.174
		Area 1 Area 2	1.71 1.29	0.43	1.390	0.240
	Day42-day70	Left Right	1.10 1.08	0.02	0.205	0.651
		1st & 2nd 3rd & 4th	1.07 1.09	0.02	0.227	0.634
		Area 1 Area 2	1.10 1.08	0.02	0.102	0.750

* indicates significant at $p = 0.05$.

4.3.3.5 Overall results of bone formation rate (micron/day) for the 16 implants used in the study

4.3.3.5.1 Effect of time

In order to study the overall bone formation rate (μm/day) having adjusted for jaw side, region and area the data were analysed using Multivariant Analysis of Variance examining the average bone formation rate with time. These data were collected from all 16 implants. On average the amount of bone formed between day 21 and day 42 (1.7μm/day) was greater than that formed between day 1 and day 21 and between day 42 and day 70 (1.47μm/day and 1.31μm/day respectively). These differences were statistically significant overtime (F=144.18, $p< 0.0001$) (Figure 4.72).

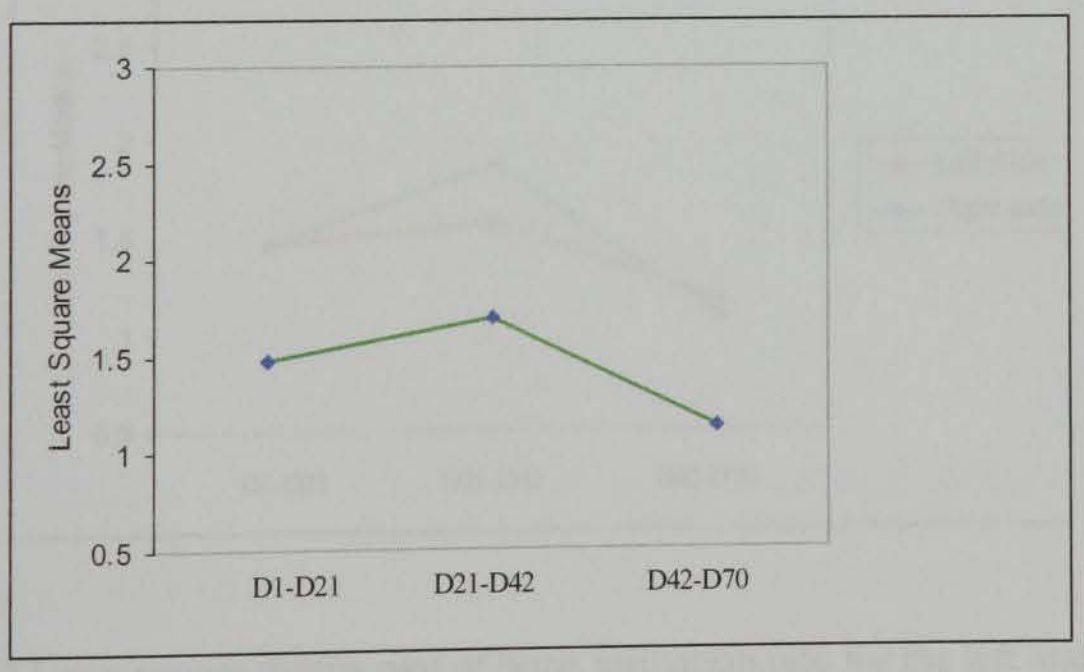

Figure 4.72 Overall least square means of bone formation rate for the different healing times (D = Day).

4.3.3.5.2 Effect of jaw side

The mean bone formation rate between day 1 and day 21 for the right side of the jaws (1.46μm/day) was equal to that for the left side (1.46μm/day) while the mean bone formation rate between day 21 and day 42 for the right was greater than that for the left side (1.88μm/day and 1.58μm/day respectively).

The mean bone formation rate between day 42 and day 70 for the left side of the jaws (1.17μm/day) was greater than that for the right side (1.08μm/day).

In general, the amount of bone formation increased with time and then decreased at the end of the study (Figure 4.73).

These differences were statistically significant (F=104.71, p<0.0001).

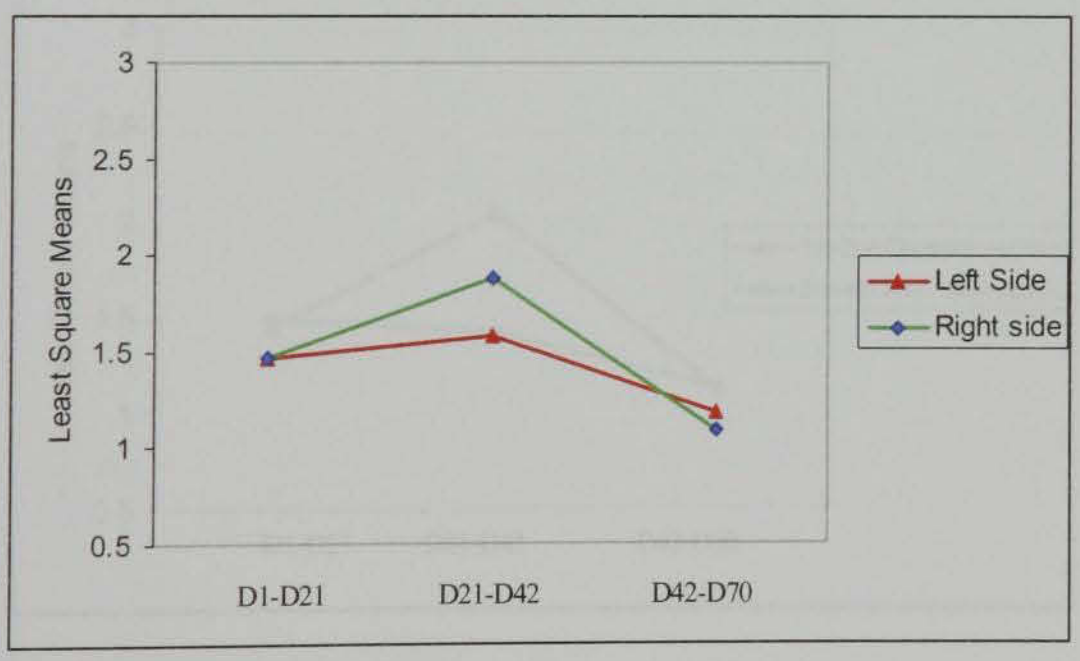

Figure 4.73 Least square means plot of bone formation rate for the left and right sides of the jaws (D = Day).

4.3.3.5.3 Effect of jaw region

The mean bone formation rate between day 1 and day 21 for the 3rd and 4th premolar regions (1.44μm/day) was less than that for the 1st and 2nd premolar regions (1.49μm/day (Figure 4.74).

The mean difference between bone formation rate that formed between day 42 and day 70 for the 1st and 2nd premolar regions and the 3rd and 4th premolar regions was 0.02μm/day).

In general, the amount of bone formation increased with time and then decreases at the end of the study. These differences were statistically significant ($F = 172.30$, $p < 0.0001$).

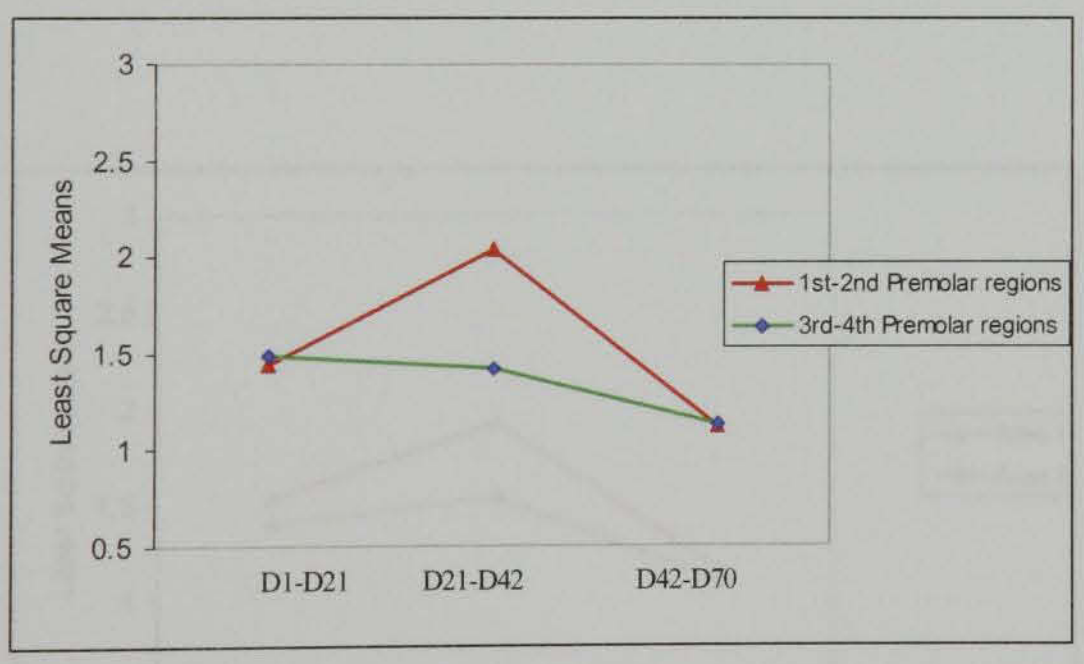

Figure 4.74 Least square means plot for the jaw regions (D = Day).

4.3.3.5.4 Effect of jaw area

The mean bone formation rate between day 1 and day 21 for Area 1 (1.54μm/day) was greater than that for Area 2 (1.39μm/day) (Figure 4.75).

The mean bone formation rate between day 21 and day 42 for Area 1 (1.93μm/day) was greater than that for Area 2 (1.53μm/day).

The mean bone formation rate between day 42 and day 70 for Area 1 (1.16μm/day) was greater than that for Area 2 (1.10μm/day (Figure 4.75).

In general, the amount of bone formation in Area 1 was always greater than that in Area 2. The amount of bone increased with time and then decreases at the end of the study. These differences were statistically significant ($F = 97.032$, $p < 0.0001$).

Summary of effect tests for the 16 implants used in the study is displayed in Table 4.13.

Figure 4.75 Least square means plot for area 1 and 2 (D = Day).

Table 4.13 Summary of effect tests for the 16 implants used in the study; time, jaw side, region within the jaw and area within the jaw.

Source	F Ratio	*p*-value
Time	144.18	0.0001
Jaw side	104.71	0.0001
Jaw region	172.30	0.0001
Jaw area	97.032	0.0001

4.4 Discussion

Bone remodelling is an essential mechanism for replacing immature, damaged, or over-stressed bone on a continuous basis (Roberts *et al.* 1984). Despite the use of the optimal surgical technique for preparation of the osteotomy site compact bone adjacent to implant (up to 1 millimetre) undergoes necrosis (Eriksson & Albrektsson 1983, Eriksson & Albrektsson 1984) which concurred with the findings of the first study presented in this thesis. Remodelling starts at the area adjacent to the implant surface in order to replace the necrotic bone, which unavoidably occurs in the implant surrounding bone, probably as a result of severed blood vessels, trauma caused by the drilling procedure and heat generation at the time of implant surgery (Eriksson & Albrektsson 1983, Clokie & Warshawsky 1995). The sequence of such necrosis may be reflected in one of the following three outcomes: 1) formation of fibrous tissue; 2) necrotic bone remains as a sequestrum without repair or 3) bone remodelling and formation of new bone (Albrektsson 1985).

The dynamic nature of bone can be studied when fluorochrome chelating agents are given during bone remodelling activity (Nölke1995, Lee 1997, O'Brien 2000, O'Brien *et al.* 2000, Lee *et al.* 2002, Lee *et al.* 2003).

Bone modelling in the form of subperiosteal and endosteal woven bone was previously reported to occur around implants placed in four species including humans (Garetto *et al.* 1995). In the present study the newly formed subperiosteal bone was found to cover the buccal and lingual surface of the alveolar bone and extend apically by varying amounts. Subperiosteal bone was found to form around implants that were placed at baseline, week 3 and week 6. However, this new bone could not be seen around implants placed one week before the dogs were sacrificed (week10). This

infers that this bone formation probably initiated between one and three weeks following implant placement.

This new subperosteal bone which formed seven weeks before the animals were scarificed was more mature than that formed at four weeks as reflected by the formation of fibrolamellar bone. However, whether this subperiosteal bone would resorb (model) or will remodel to a more mature bone, cannot be determined in the present study due to the limited study duration.

Newly formed bone in the interfacial area (≤ 1mm from implant surface) was seen as a mixture of different fluorescents and could be differentiated by its maturity. This area was separated from the old bone with a label that was given one day after the placement of the implant. Bone was found to form around implants that were placed at the baseline, 3- and 6-weeks after the commencement of the study. Sometimes, new bone could be seen extending from the apical part of the implants and to line the marrow space. It was also found to form on the buccal and the lingual surfaces.

Fluorochromes such as alizarin complexone are usually used as bone labels to study bone remodelling events due to their ability to chelate exposed calcium at the bone/osteoid (un-mineralised bone) interface. Each fluorochromic agent can be seen as a fluorescent band using the fluorescent microscopy. It is acknowledged that if sequential doses of fluorescent chelating agents are given and spaced by a certain number of days, several fluorescent bands will be observed which are separated by a distance equivalent to the net amount of bone formed in that period (Suzuki & Mathews 1966, Módis *et al.* 1969, Nölke1995, Vajda *et al.* 1999; Moore, 2000, Lee *et al.* 2002, Lee *et al.* 2003).

From the present and previous studies (Roberts 1988, Garetto *et al.* 1995, Davies 1998, Raghavendra *et al.* 2005), it seems that implant placement leads to a localised increase in remodelling activity in a limited area close to the implant surface. It also leads to acceleration in remodelling activity in an area distant from the implant surface which may be due to Regional Acceleratory phenomena which leads to acceleration of this response when bone is exposed to trauma (sham surgery). The present study in accordance with Garetto and coworkers (1995) who reported that after implant placement the remodelling activity adjacent to the implant (within 1 mm) is greatest and substantially decreased with increasing distance from the implant-bone interface. This phenomenon seems to occur irrespective of implant design. This elevation in remodelling activity,which may be in the early healing stage, is attributed to the surgical procedure and to the material biocompatibility and host response (Garetto *et al.* 1995). However, host bone response to implant placement is characterised by sub-periosteal and endosteal bone formation as already reported by Roberts (1988) and Garetto and associates (1995).

Hoshaw *et al.* (1994a) used male canine tibia and demonstrated that bone formed on the original periosteal and endosteal surfaces in both loaded and control implants. Hoshaw *et al.* (1994a) demonstrated what they believed was evidence of microdamage after implant loading. This damage may stimulate remodelling activities. In this study the small amount of detected microdamage may be attributed to the inability of the histological technique used to detect microdamage and/or healing of this damage, as the animals were sacrificed 12 weeks after load application.

It may be argued that elevation of remodelling activity in an area adjacent to the implant surface is the key to maintaining a long term rigid bone-implant connection

and is also required to repair the damage generated during the implant surgery and is the initial step which will lead to a rigid bone-implant interface.

The surgical procedure led to bony responses not only close to the implant surface but also in areas away from the implant surface (Area 2) including the area located apical to the implant. However, in this area the remodelling activity was obvious as several remodelling cycles and several new secondary osteons were observed. Nevertheless, bone remodelling in Area 1 was faster in the earlier stage than it was in Area 2 and more bone was found to form in Area 1 than in Area 2 as reflected by the bone formation rate.

All measurements were carried out by one investigator. It may be important to note that intra-examiner reproducibility was not investigated which may have been a limitation of the study.

4.5 Collective results obtained from the three studies

From the results of the three studies, it may be concluded that implant surgery could cause bone damage principally in the area close to the implant surface. This damage induces bone remodelling in order to replace the damaged bone. The newly formed bone in its early stage is woven bone which is replaced by more mature lamellar bone. It may be reasonable to suggest that subperiosteal bone is formed as a result of the surgery; however, its fate is not known.

Figure 4.76 below shows the effect of implant surgery as indicated by the generation of a diffusely stained area which represents damage that occurred as a result of surgery. It also represents high stresses that were predicted using FEM when the implant diameter was greater than the diameter of the osteotomy preparation. The last

part of the figure shows high remodelling activity close to the implant surface which may be induced by the generated damage in order to repair it.

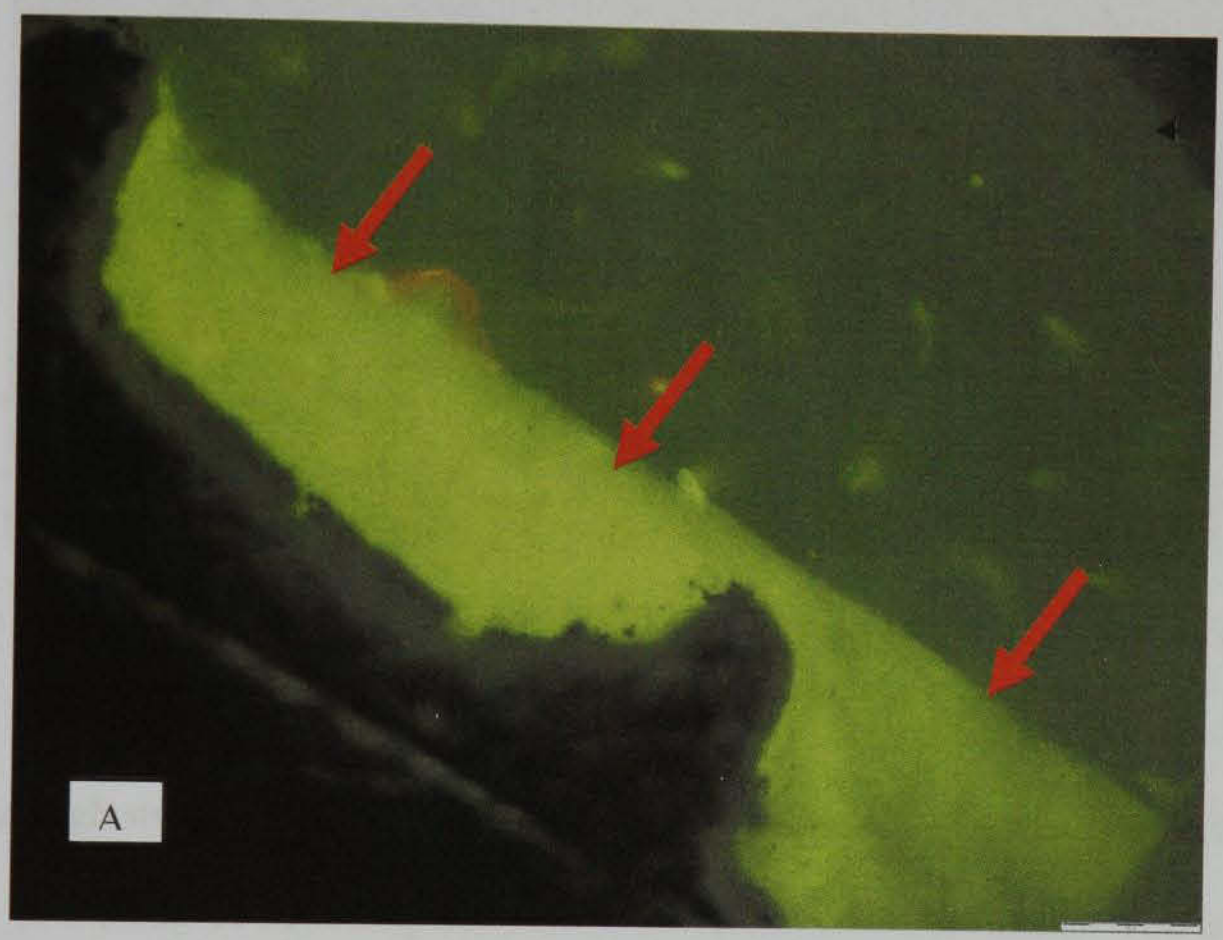

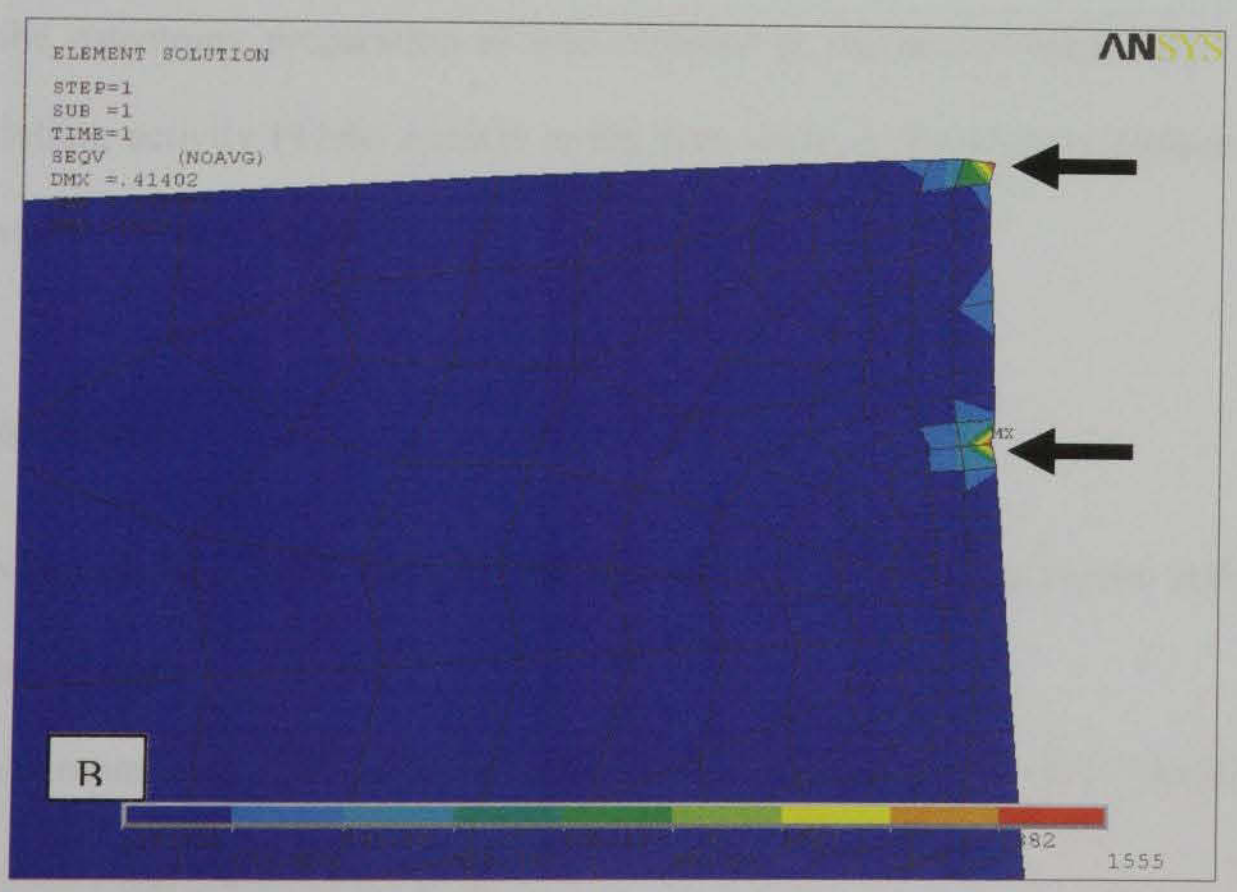

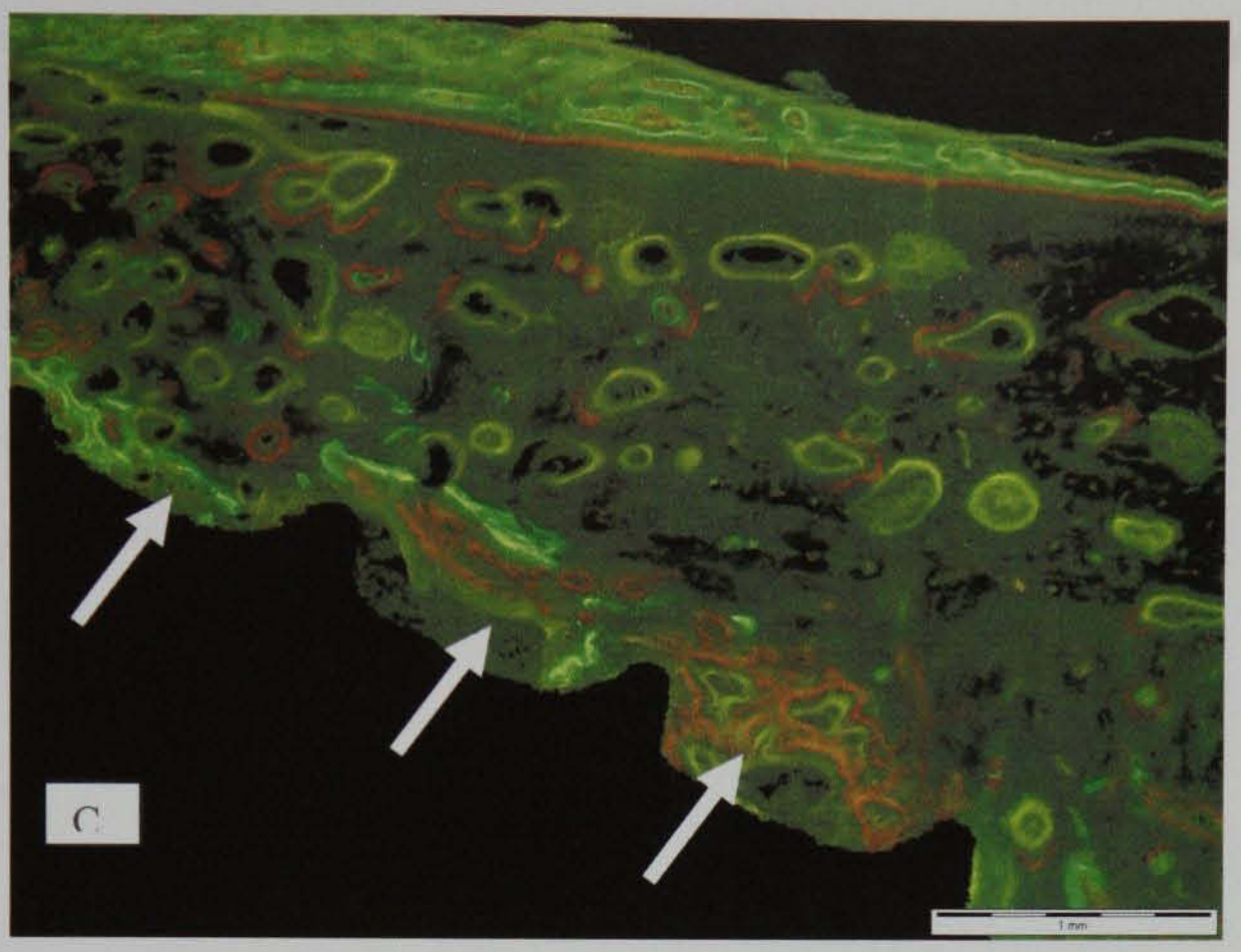

Figure 4.76 A diffusely stained area (red arrows) represents bone damage that was caused by the surgical procedure as was reported in the first study (A). FE model showing high stresses (black arrows) can be predicted in the area close to the implant surface as a result of bone displacement due to insertion of an implant that is wider than the osteotomy preparation as was reported in the second study (B). High remodelling activity (white arrows) in the area close to the implant surface as was observed in the third study (C).

4.6 Conclusions

Fluorochromes are useful materials in studying bone remodelling around endosseous implants in dogs.

The maximum bone remodelling was found to occur in dogs between 3 weeks and 6 weeks following implant placement.

Bone remodelling in Area 1 was faster in the earlier stage than in Area 2.

More bone was formed in Area 1 than in Area 2.

Woven bone was formed in the interfacial area during the early healing stage in a dog model.

For a better understanding of bone remodelling, the duration of the experimental period should be extended in future studies.

References

Aaron JE, Makins NB, Francis RM, Peacock M. Staining of calcification front in human bone using contrasting fluorochromes *in vitro*. Journal of Histochemistry and Cytochemistry 1984; 32: 1251-1261.

Abrahamsson I, Berglundh T, Linder E, Lang NP, Lindhe J. Early bone formation adjacent to rough and turned endosseous implant surfaces. An experimental study in the dog. Clinical Oral Implants Research 2004; 15: 381-392.

Abron A, Hopfensperger M, Thompson J, Cooper LF. Evaluation of a predictive model for implant surface topography effects on early osseointegration in the rat tibia model. Journal of Prosthetic Dentistry 2001; 85: 40-46.

Adell R, Lekholm U, Rockler B, Brånemark PI. A 15-year study of osseointegrated implants in the treatment of the edentulous jaw. International Journal of Oral Surgery 1981 10:387-416.

Adell R, Lekholm U, Rockler B, Brånemark PI, Lindhe J, Eriksson B, Sbordone L. Marginal tissue reaction at osseointegrated titanium fixtures (1). A 3-year longitudinal prospective study. International Journal of Oral and Maxillofacial Surgery 1986; 15: 39-52.

Adkins KF. Alizarin red as an intravital fluorochrome in mineralising tissues. Stain Technology 1965; 40: 69-70.

Akagawa Y, Satomi K, Nikai H, Tsuru H. Initial interface between submerged hydroxyapatite-coated titanium alloy implant and mandibular bone after nontapping and tapping insertion in monkeys. Journal of Prosthetic Dentistry 1990, 63:559-564.

Akagawa Y, Sato Y, Teixeira N, Shindoi N, Wadamoto M. A mimic osseointegrated implant model for three-dimensional finite element analysis. Journal of Oral Rehabilitation 2003; 30: 41-45.

Akkus O, Rimnac CM: Cortical bone tissue resists fatigue fracture by deceleration and arrest of microcrack growth. Journal of Biomechanics 2001, 34:757–764.

Albrektsson T, Brånemark P-I, Hansson HA, Lindstrom J. Osseointegrated titanium implants. Requirements for ensuring a long-lasting, direct bone-to-implant anchorage in man. Acta Orthopaedica Scandinavica 1981; 52: 155-170.

Albrektsson T, Brånemark P-I, Hansson HA, Kasemo B, Larsson K, Lundström I, McQueen DH, Skalak R. The interface zone of inorganic implants *in vivo*: titanium implants in bone. Annals Biomedical Engineering 1983; 11: 1-27.

Albrektsson T. Bone tissue response. In, P Brånemark, G Zarb, T Albrektsson. Tissue-Integrated Prostheses. Osseointegration in Clinical Dentistry. 1st ed, Quintessence Publishing Co. 1985, 129-143.

Albrektsson T, Jacobsson M. Bone metal interface in osseointegration. Journal of Prosthetic Dentistry 1987; 57: 597-607.

Albrektsson CB, Johansson T. A removal torque and Histomorphometric study of commercially pure niobium and titanium implants in rabbit bone. Clinical Oral Implants Research 1991; 2: 24-29.

Albrektsson T, Isidor F. Consensus report of session IV. In, NP Lang, T Karring. Proceedings of the First European workshop on Periodontology. Quintessence Publishing Co. London 1994, 365-369.

Albrektsson T. Hydroxyapatite-coated implants: A case against their use. Journal of Maxillofacial Surgery 1998; 56: 1312-1326.

Albrektsson T, Johansson C, Lundgren A-K, Sul Y-T, Gottlow J. Experimental studies on oxidized implants. A histomorphomertical and biomechanical analysis. Applied Osseointegration Research 2000a; 1: 21-24.

Albrektsson T, Johansson C, Lundgren A-K, Sul Y-T, Gottlow J. Expiremntal studies on oxidised implants. A histomorphometrical and biomechanical analysis. Applied Osseointegration Research 2000b; 1: 21-24.

Al-Sayyed A, Deporter DA, Pilliar RM, Watson PA, Pharoah M, Berhane K, Carter S. Predictable crestal bone remodelling around two porous-coated titanium alloy dental implant designs. A radiographic study in dogs. Clinical Oral Implants Research. 1994; 5: 131-141.

Anselme K, Sharrock P, Hardouin P, Dard M. In vitro growth of human adult bone-derived cells on hydroxyapatite plasma sprayed coatings. Journal of Biomedical Materials Research 1997; 34: 247-259.

Ascenzi A, Bonucci E. Relationship between ultrastructure and "pin test" in osteons, Clinical Orthopaedic and Related Research 1976; 121: 275-294.

Ask M, Lausmaa J, Kasemo B. Preparation and surface spectroscopic characterisation of oxide films on Ti6 Al 4V. Applied Surface Science 1989; 35: 283-301.

Assael LA. New foundations in understanding osteonecrosis of the jaws. Journal of Oral and Maxillofacial Surgery 2004; 62: 125-126.

Assenza B, Scarano A, Petrone G, Iezzi G, Thams U, San Roman F, Piattelli A. Crestal Bone Remodelling in Loaded and Unloaded Implants and the Microgap: A Histologic Study. Implant Dentistry 2003; 12: 235-241.

Barbier L, Schepers E. Adaptive bone remodelling around oral implants under axial and nonaxial loading conditions in the dog mandible. International Journal of Oral and Maxillofacial Implants 1997; 12: 215-223.

Barbier L, Vander Sloten J, Krzesinski G, Scepers E. Finite element analysis of non-axial loading of oral implants in the mandible of the dog. Journal of Oral Rehabilitation 1998; 25: 847-858.

Bentolila V, Boyce TM, Fyhrie DP, Drumb R, Skerry TM, Schaffler MB. Intracortical remodelling in adult rat long bones after fatigue loading. Bone 1998; 23: 275-281.

Berglundh T, Abrahamsson I, Lang NP, Lindhe J. De novo alveolar bone formation adjacent to endosseous implants. Clinical Oral Implants Research 2003; 14: 251-262.

Bianco PD, Ducheyne P, Cuckler JM. Titanium serum and urine levels in rabbits with a titanium implant in the absence of wear. Biomaterials 1996; 17: 1937-1942.

Block MS, Kent JN, Kay JF. Evaluation of hydroxyapatite-coated titanium dental implants in dogs. Journal of Oral and Maxillofacial Surgery 1987; 45: 601-607.

Block MS, Gardiner D, Kent JN, Misiek DJ, Finger IM, Guerra L. Hydroxyapatite-coated implants in the posterior mandible: 10-year observation. International Journal of Oral and Maxillofacial Implants 1996; 11: 626-633.

Blumenthal NC, Cosma V. Inhibition of apatite formation by titanium and vanadium ions. Journal of Biomedical Materials Research 1989; 23 (A1 Supplement): 13-22.

Botticelli D, Berglundh T, Buser D, Linhe J. Appositional bone formation in marginal defects at implants. An experimental study in the dog. Clinical Oral Implants Research 2003; 14: 1-9.

Boyce TM, Fyhrie DP, Glotkowski MC, Radin EL, Schaffler MB. Damage type and strain mode association in human compact bone bending fatigue. Journal of Orthopaedic Research 1998; 16: 322-329.

Bozkaya D, Muftu S, Muftu A. Evaluation of load transfer characteristics of five different implants in compact bone at different load levels by finite elements analysis. Journal of Prosthetic Dentistry 2004; 92: 523-530.

Brånemark P. Introduction to osseointegration. In, P Brånemark, G Zarb, T Albrektsson. Tissue-Integrated Prostheses. Osseointegration in Clinical Dentistry. 1st ed, Quintessence Publishing Co 1985, 11-76.

Brisman DL. The effect of speed, pressure, and time on bone temperature during the drilling of implant sites. International Journal of Oral and Maxillofacial Implants 1996; 11: 35-37.

Brunski JB, Hoshaw SJ. Bone modelling and remodelling in relation to maintenance of attachment at bone-dental implant interface. In, Z Davidovitch, the Biological Mechanism of Tooth Eruption, Resorption and Replacement by implants. Harvard Society for the advancement of Orthodontic, Boston Massachusetts, 1994; 667-680.

Brunski JB, Puleo DA, Nanci A. Biomaterials and biomechanics of oral and maxillofacial implants: current status and future developments. International Journal of Oral and Maxillofacial Implants 2000; 15: 15-46.

Büchter A, Kleinheinz J, Wiesmann HP, Kersken J, Niekemper M, von Weyhrother H,Joos U, Meyer U. Biological and biomechanical evaluation of bone remodelling and implant stability after using an osteotome technique. Clinical Oral Implants Research 2005; 16:1-8.

Burger EH, Klein-Nulend J. Mechanotransduction in bone-role of the lacuno-canalicular network. The FASEB Journal 1999; 13: S101-S112.

Burr DB, Martin RB, Schaffler MB, Radin EL. Bone remodelling in response to in vivo microdamage. Journal of Biomechanics 1985; 18: 189-200.

Burr DB, Schaffler MB, Yang KH, Wu DD, Lukoschek M, Kandzari D, Sivaneri N, Blaha JD, Radin EL. The effects of altered strain environments on bone tissue kinetics. Bone 1988; 10: 215-221.

Burr DB, Stafford T. Validity of the bulk-staining technique to seprate artifactual from *in vivo* bone microdamage. Clinical Orthopaedics and Related Research 1990; 260: 305-308.

Burr DB, Hooser M. Alterations to the en bloc basic fuchsin staining protocol for the demonstration of microdamage produced *in vivo*. Bone 1995; 17: 431-433.

Burr DB, Forwood MR, Fyhrie DP, Martin RB, Schaffler MB, Turner CH. Bone microdamage and skeletal fragility in osteoporotic and stress fracture. Journal of Bone and Mineral Research 1997; 12: 6-15.

Burr DB, Turner CH, Naick P, Forwood MR, Ambrosius W, Hasan MS, Pidaparti R. Does microdamage accumulation affect the mechanical properties of bone? Journal of Biomechanics 1998; 31:337-345.

Burr DB. Targeted and non-targeted remodelling. Bone 2002; 30: 2-4.

Burr DB. Bone quality: understanding what matters. Journal of Musculoskeletal and Neuronal Interactions 2004; 4: 184-186.

Buser D, Schenk RK, Steinmann S, Fiorellini JP, Fox CH, Stich H. Influence of surface characteristics on bone integration of titanium implants. A histomorphometric study in miniature pigs. Journal of Biomedical Materials Research 1991; 25: 889-902.

Carr AB, Gerard DA, Larson PE. Quantitative histomorphometric description of implant anchorage for three types of dental implants following three months of healing in baboon. International Journal of Oral and Maxillofacial Implants 1997; 12: 777-784.

Carr AB, Gerard DA, Larson PE. Quantitative histomorphometric description of implant anchorage for three types of dental implants following six months of healing in baboon. International Journal of Oral and Maxillofacial Implants 2000; 15; 785-791.

Carter DR, Hayes WC, Schurman DJ. Fatigue life of compact bone-II. Effects of microstructure and density. Journal of Biomechanics 1976; 9: 211-218.

Carter DR, Hayes WC. Compact bone fatigue damage: a microscopic examination. Clinical Orthopaedics and Related Research 1977; 127: 265-274.

Carter DR, Spengler DM. Mechanical properties and composition of cortical bone. Clinical Orthopaedics and Related Research 1978; 135: 192-217.

Carvalho L, Ramos A, Simões JA. Finite element analysis of a dental implant system with an elastomeric barrier. 2003 Summer Bioengineering Conference, June 25-29, Sonesta Beach Resort in Key Biscayne, Florida.

Castellani R, de Ruijter JE, Jansen JA. Response of rat bone marrow cells to differently roughened titanium discs. Clinical Oral Implants Research 1999; 10: 369-378.

Caulier H, van der Waerden JP, Wolke JG, Kalk W, Naert I, Jansen JA. A histological and histomorphometrical evaluation of the application of screw-designed calciumphosphate (Ca-P)-caoted implants in the cancellous maxillary bone of the goat. Journal of Biomedical Materials Research 1997; 35: 19-30.

Chamay A. Mechanical and morphological aspects of experimental overload and fatigue in bone. Journal of Biomechanics 1970; 3: 263-270.

Chang YL, Lew D, Park JB, Keller JC. Biomechanical and morphometric analysis of hydroxyapatite-coated implants with varying crystallinity. Journal of Oral and Maxillofacial Surgery 1999; 57:1096-1108.

Chappard D, Aguado E, Huré G, Grizon F, Basle MF. The early remodeling phases around titanium implants: A histomorphometric assessment of bone quality in a 3- and 6-month study in sheep. International Journal of Oral and Maxillofacial Implants 1999; 14: 189-196.

Chehroudi B, McDonnell D, Brunette DM. The effect of micromachined surfaces on formation of bonelike tissue on subcutaneous implants as assessed by radiography and computer image processing. Journal of Biomedical Materials Research 1997; 34: 279-290.

Chen J, Lu X, Paydar N, Akay HU, Roberts WE. Mechanical simulation of human mandible with and without an endosseous implants. Medical Engineering and Physics 1994; 16: 53-61.

Chen J, Chen K, Garetto LP, Roberts WE. Mechanical response to functional and therapeutic loading of a retromolar endosseous implant used for orthodontic anchorage to mesially translate mandibular molars. Implant Dentistry 1995; 4: 246-258.

Chen J, Esterle M, Roberts E. Mechanical response to functional loading around the threads of retromolar endosseous implants utilised for orthodontic anchorage: coordinated histomorphometric and finite element analysis. International Journal of Maxillofacial Implants 1999; 14: 282-289.

Chou C-T, Morris HF, Ochi S, Walker L DesRosiers D. AICRG, Part II: Crestal bone loss associated with Ankylos implants: Loading to 36 months. Journal of Oral Implantology (Special issue) 2004; 30: 134–143.

Clokie CML, Warshawsky H. Morphological and radioautographic studies of bone formation in relation to titanium implants using the rat tibia as a model. International Journal of Oral and Maxillofacial Implants 1995; 10: 155-165.

Cochran DL, Simpson J, Weber HP, Buser D. Attachment and growth of periodontal cells on smooth and rough titanium. International Journal of Oral and Maxillofacial Implants 1994; 9: 289-297.

Cohen R, McCabe RP, Kalscheur VL, Vanderby Jr R, Markel MD, Muir P. Microdamage at the pin-bone interface of external skeletal fixation pins after short-

term cyclical loading ex-vivo. Veterinary and Comparative Orthopaedics and Traumatology 2003; 16: 88-92.

Cook SD, Kay JF, Thomas KA, Jarcho M. Interface mechanics and histology of titanium and hydroxylapatite coated titanium for dental implant applications. International Journal of Oral and Maxillofacial Implants 1987; 2: 15-22.

Cook SD, Salkeld SL, Gaisser DM, Wagner WR. An *in vivo* analysis of an elliptical dental implant design. Journal of Oral Implantology 1993a; 19: 307-313.

Cook SD, Salkeld SL, Gaisser DM, Wagner WR. The effect of surface macrotexture on the mechanical and histologic characteristics of hydroxylapatite-coated dental implants. Journal of Oral Implantology 1993b; 19: 288-294.

Cooper LF. Biological determinants of bone formation for osseointegration: Clues for future clinical improvements. Journal of Prosthetic Dentistry 1998; 80: 439-449.

Cooper LF. A role for surface topography in creating and maintaining bone at titanium endosseous implants. Journal of Prosthetic Dentistry 2000; 84: 522-534.

Cordioli G, Majzoub Z, Piattelli A, Scarano A. Removal torque and histomorphometric investigation of 4 different titanium surface: an experimental study in the rabbit tibia. International Journal of Oral and Maxillofacial Implants 2000; 15: 668-674.

Currey JD. Effects of differences in mineralisationon and the mechanical properties of bone. Philosophical Transactions of the Royal Society of London. Series B, Biological Sciences 1984; 304: 509-518.

Currey JD. Physical characteristics affecting the tensile failure properties of compact bone. Journal of Biomechanics 1990; 23: 837-844.

Currey JD. Ontogenetic changes in compact bone material properties. In: Cowin SC eds. Bone mechanics handbook, CRC Press, Boca Raton, FL, 2001; 13-26.

Currey JD. The structure of bone tissue. In J Currey, Bones: Structure and mechanics. 1st ed. Princeton University Press 2002: 3-26.

Daculsi G, Le Geros RZ, Deudon C. Scanning and transmission electron microscopy, and electron probe analysis of the interface between implants and host bone. Osseo-coalescence versus osseo-integration. Scanning Microscopy 1990; 4:309-314.

Davies JE. Mechanisms of endosseous integration. The International Journal of Prosthodontics 1998; 11: 391-401.

de Bruijn JD, Klein CP, de Groot K, van Blitterswijk CA. The ultrastructure of the bone-hydroxyapatite interface in vitro. Journal of Biomedical Materials Research 1992; 26: 1365-1382.

de Groot K, Geesink RGT, Klein CPAT, Serkioin P. Plasma sprayed castings of hydroxyapatite. Journal of Biomedical Materials Research 1987; 21: 1275-1381.

de Lange GL, Donath K. Interface between bone tissue and implants of solid hydroxyapatite or hydroxapatite-coated titanium implants. Biomaterials 1989; 10: 121-125.

de Lange GL, de Putter C, de Wijs FLJA. Histological and ultrastructural appearance of the hydroxyapatite-bone surface. Journal of Biomedical Materials Research 1990; 24: 829-845.

Denissen HW, Kalk W, de Nieuport HM, Maltha JC, van de Hooff A. Mandibular bone response to plasma-sprayed coatings of hydroxyapatite. The International Journal of Prosthodontics 1990; 3: 53-58.

Duncan RL, Turner CH. Mechanotransduction and the functional response of bone to mechanical strain. Calcified Tissue International 1995; 57: 344-358.

Elias JJ, Brunski JB, Scarton HA. A dynamic modal testing technique for non-invasive assessment of bone-dental implants interfaces. International Journal of Oral and Maxillofacial Implants 1996; 11: 728-734.

Ellingsen JE. A study on the mechanism of protein adsorption to TiO_2. Biomaterials 1991, 12: 593-596.

Equivel-Upshaw J. Dental implants. In, KJ Anusavice, Phillips Science of Dental Materials. 11th ed, Philadelphia, WB Saunders 2003, 759-781.

Ericsson I, Johansson CB, Bystedt H, Norton MR. A histomorphometric evaluation of bone-to-implant contact on machine-prepared and roughened titanium dental implants. A pilot study in the dog. Clinical Oral Implants Research 1994; 5: 202-206.

Eriksson AR, Albrektsson T. Temperature threshold levels for heat-induced bone tissue injury: a vital-microscopic study in the rabbit. Journal of Prosthetic Dentistry 1983; 50:101-107.

Eriksson RA, Albrektsson T. The effect of heat on bone regeneration: an experimental study in the rabbit using the bone growth chamber. Journal of Oral and Maxillofacial Surgery 1984; 42: 705-711.

Esposito M, Hirsch JM, Lekholm U, Thomsen P. Biological factors contributing to failures of osseointegrated oral implants. (I) Success criteria and epidemiology. European Journal of Oral Sciences 1998a; 106: 527-551.

Esposito M, Hirsch JM, Lekholm U, Thomsen P. Biological factors contributing to failures of osseointegrated oral implants. (II) Etiopathogenesis. European Journal of Oral Sciences 1998b; 106: 721-764.

Esposito M, Lausmaa J, Hirsch J-M, Thomsen P. Surface analysis of failed oral titanium implants. Journal of Biomedical Materials Research 1999; 48: 559-568.

Fallon MD, Teitelbaum SD. The interpretation of fluorescent tetracycline markers in diagnosis of metabolic bone diseases. Human Pathology 1982; 13: 416-417.

Fantner GE, Rabinovych O, Schitter G, Thurner P, Kindt J, Finch, MM, Weaver JC, Golde LS, Morse DE, Lipman EA, Rangelow IW, Hansma PK. Hierarchical interconnections in the nano-composite material bone:Fibrillar cross-links resist fracture on several length scales. Composites Science and Technology 2006; 66: 1202 –1208.

Fazzalari NL, Forwood MR, Manthey BA, Smith K, Kolesik P. Three-dimensional conofocal images of microdamage in cancellous bone. Bone 1998, 23: 373–378.

Ferrigno N, Laureti M, Fanali S, Grippaudo G. A long-term follow-up study of non-submerged ITI implants in the treatment of totally edentulous jaws: Part 1: Ten-year

life table analysis of a prospective multicenter study with 1286 implants. Clinical Oral Implants Research 2002; 13: 260-273.

Ficarra G, Beninati F, Rubino I, Vannucchi A, Longo G, Tonelli P, Pini Prato G. Osteonecrosis of the jaws in periodontal patients with a history of bisphosphonates treatment. Journal of Clinical Periodontology 2005; 32:1123-1128.

Flint SR, Sharkey S, Galvin S. Warning: bisphosphonates and osteochemonecrosis of the jaws. Journal of the Irish Dental Association 2006; 52: 79-83.

Forwood MR, Parker AW. Microdamage in response to repetitive torsional loading in the rat tibia. Calcified Tissue International 1989; 45: 47-53.

Forwood MR, Burr DB, Takano Y, Eastman DF, Smith PN, Schardt JD. Risedronate treatment does not increase microdamage in the canine femoral neck. Bone 1995; 16: 643–650.

Forwood MR, Turner CH. Skeletal adaptations to mechanical usage: results from tibial loading studies in rats. Bone 1995; 17 (4 supl): 197s-205s.

Frank JD, Ryan M, Kalscheur VL, Ruaux-Mason CP, Hozak RR, Muir P. Ageing and accumulation of microdamage in canine bone. Bone 2002; 30: 201-206.

Friberg B, Sennerby L, Roos J, Lekholm U. Identification of bone quality in conjunction with insertion of titanium implants. A pilot study in jaw autopsy specimens. Clinical Oral Implants Research 1995; 6: 213–219.

Frost HM. Presence of microscopic cracks *in vivo* in bone. Henry Ford Hospital Medical Bulletin 1960; 8: 25-35.

Frost HM. Preparation of thin undecalcified bone sections by rapid manual method. Stain Technology 1985; 33: 273-277.

Frost HM. Bone "mass" and the "mechanostat": a proposal. The Anatomical Record 1987; 219: 1-9.

Frost HM. Transient-steady state phenomena in microdamage physiology: A proposed algorithm for lamellar bone. Calcified Tissue International 1989; 44: 367-381.

Frost HM. Some ABC's of skeletal pathophysiology. 5. Microdamage physiology. Calcified Tissue International 1991; 49: 229-231.

Frost HM. Wolf's law and bone's structural adaptations to mechanical usage: an overview for clinicians. The Angle Orthodontist 1994; 64: 175-188.

Futami T, Fujii N, Ohnishi H, Taguchi N, Kusakari H, Ohshima H, Maeda T. Tissue response to titanium implants in the rat maxilla: ultrastructural and histochemical observations of the bone-titanium interface. Journal of Periodontology 2000; 71: 287-298.

Fyhrie DP, Vashishth D. Bone stiffness predicts strength similarly for human vertebral cancellous bone in compression and cortical bone tissue in tension. Journal of Biomechanics 2000; 26: 169-173.

Gaggl A, Schultes G. Clinical experiences with a new maintenance-free shock absorbing element in titanium implants. Implant Dentistry 2001; 10: 246-253.

Galassini S, Egeni GP, Jaksic M, Moschini G, Passi P, Piattelli A, Zadro A. Biological phenomena in osseointegration of endosseous oral implants studied with

PIXE and micro-PIXE techniques. Dentistry Tomorrow (The international dental journal on line); Issue 1, December 1995.

Garetto LP, Chen J, Parr JA, Roberts WE. Remodelling dynamics of bone supporting rigidily fixed titanium implants: A histomorphometric comparison in four species including humans. Implant Dentistry 1995; 4: 235-243.

Geng J-P, Tan KBC, Liu G-R. Application of finite element analysis in implant dentistry: A review of the literature. Journal of Prosthetic Dentistry 2001; 85: 585-598.

Geramy A, Sharafoddin F. Abfraction: 3D analysis by means of the finite element method. Quintessence International 2003; 34: 526-533.

Giannobile WV, Finkelman RD, Lynch SE. Comparison of canine and non-human primate animal models for periodontal regenerative therapy: results following a single administration of PDGF/IGF-I. Journal of Periodontology 1994; 65: 1158-1168.

Giraud-Guille MM. Twisted plywood architecture of collagen fibrils in human compact bone osteons. Calcified Tissue International 1988; 42:167-180.

Gotfredsen K, Berglundh T, Lindhe J. Bone reactions adjacent to titanium implants with different surface characteristics subjected to static load. A study in the dog (II). Clinical Oral Implants Research 2001; 12: 196-201.

Gotfredsen K, Nimb L, Hjörting, Jensen JS, Holmén A. histomorhometric and removal torque analysis for Ti_2-blasted titanium implants. An experimental study on dogs. Clinical Oral Implants Research 1992; 3: 77-84.

Gotfredsen K, Wennerburg A, Johansson C, Skovgaard LT, Hjorting-Hansen E. Anchorage of Ti_2-blasted, HA-coated, and machined implants: an experimental study with rabbits. Journal of Biomedical Materials Research 1995; 29: 1223-1231.

Gottlander M, Albrektson T. Histomorphometric studies of hydroxyapatite-coated and uncoated CP titanium threaded implants in bone. International Journal of Oral and Maxillofacial Implants 1991; 6: 399-404.

Gottlander M, Johansson CB, Albrektsson T. Short- and Long-term animal studies with a plasma-sprayed calcium phosphate-coated implant. Clinical Oral Implants Research 1997; 8: 345-351.

Gottlow J, Johansson C, Albrektsson T, Lundgren A-K. Biomechanical and histologic evaluation of the TiUnite and Osseotite implant surfaces in rabbits after 6 weeks of healing. Applied Osseointegration Research 2000; 1: 25-27.

Gross KA, Berndt CC, Goldschlag DD, Iacono VJ. In vitro changes of hydroxyapatite coatings. International Journal of Oral and Maxillofacial Implants 1997; 12: 589-597.

Gross KA, Brendt CC, Iacono VJ. Variability of hydroxyapatite-coated dental implants. International Journal of Oral and Maxillofacial Implants 1998; 13: 601-610.

Guyton AC, Hall JE. Parathyroid Hormone, Calcitonin, Calcium and Phosphate Metabolis, Vitamin D, Bone, and Teeth. In AC Guyton and JE Hall, Textbook of Medical Physiology. 10th ed. Philadelphia, WB Saunders Co. 2000: 899-915.

Hansson HA, Albrektsson T, Brånemark PI. Structural aspects of the interface between tissue and titanium implants. Journal of Prosthetic Dentistry 1983; 50: 108-113.

Harris WH. A microscopic method of determining rates of bone growth. Nature 1960; 188: 1038-1039.

Heitz-Mayfield LJ, Schmid B, Weigel C, Gerber S, Bosshardt DD, Jönsson J, Lang NP. Does excessive occlusal load affect osseointegration? An experimental study in the dog. Clinical Oral Implants Research 2004; 15: 259-268.

Hellstein JW, Marek CL. Bisphosphonate osteochemonecrosis (bis-phossy jaw): is this phossy jaw of the 21st century? Journal of Oral and Maxillofacial Surgery 2005; 63: 682-689.

Hermann JS, Cochran DL, Nummikoski PV, Buser D. Crestal bone changes around titanium implants. A radiographic evaluation of unloaded nonsubmerged and submerged implants in the canine mandible. Journal of Periodontology 1997; 68: 1117-11130.

Hermann JS, Buser D, Schenk RK, Cochran DL. Crestal bone changes around titanium implants. A histometric evaluation of unloaded non-submerged and submerged implants in the canine mandible. Journal of Periodontology 2000; 71:1412-1424.

Hermann JS, Schoolfield JD, Schenk RK, Buser D, Cochran DL. Influence of the size of the microgap on crestal bone changes around titanium implants. A histometric evaluation of unloaded non-submerged implants in the canine mandible. Journal of Periodontolgy 2001; 72: 1372-1383.

Hernandez CJ, Beaupré GS, Carter DR. A model of mechanobiologic and metabolic influences on bone adaptation. Journal of Rehabilitation Research and Development 2000; 37: 235-244.

Hipp JA, Brunski JB, Cochran GVB, Higuchi KW. Investigation of "Osseointegration" by histomorphometric analysis of fixture-bone interfaces. Journal of Dental Research (Special Issue) 1987; 66: 186 (abstract No. 637).

Holmgren EP, Seckinger RJ, Kilgren LM, Mante F. Evaluating parameters of osseointegrated dental implants using finite element analysis--a two-dimensional comparative study examining the effects of implant diameter, implant shape, and load direction. The Journal of Oral Implantology 1998; 24: 80-88.

Hori M, Takahashi H, Konno T, Inoue J, Haba T. A classification of in vivo bone labels after double labelling in canine bones. Bone 1985; 6: 147-154.

Hoshaw SJ, Brunski JB, Chocran GVB. Mechanical loading of Brånemark implants affects interfacial bone modelling and remodelling. International Journal of Oral and Maxillofacial Implants 1994a; 9: 345-360.

Hoshaw SJ, Fyhrie DP, Schaffler MB. The effect of implant insertion and design on bone microdamage. The Biological Mechanism of Tooth Eruption, Resorption and Replacement. Edited by Davidovitch Z. Harvard Society for the advancement of Orthodontics, Boston Massachusetts 1994b; 735-741.

Hoshaw SJ, Watson JT, Schaffler MB, Fyhrie DP. Microdamage at bone-implant interfaces affects bone remodelling activity. Trans 41st Orthop Res Soc 1995; 188.

http://training.seer.cancer.gov/module_anatomy/unit3_2_bone_tissue.html.

Huiskes R, Ruimerman R, van Lenthe GH, Janssen JD. Effects of mechanical forces on maintenance and adaptation of form in trabecular bone. Nature 2000; 405: 704-706.

Huja SS, Katona TR, Burr DB, Garetto LP, Roberts WE. Microdamage adjacent to endosseous implants. Bone 1999a; 25: 217-222.

Huja SS, Hasan MS, Pidaparti R, Turner CH, Garetto LP, Burr DB. Development of a fluorescent light technique for evaluating microdamage in bone subjected to fatigue loading. Journal of Biomechanics 1999b; 32: 1243-1249.

Hürzeler MB, Quinones CR, Kohal RJ, Rohde M, Strub JR, Teuscher U, Caffesse RG. Changes in peri-implant tissues subjected to orthodontic forces and ligature breakdown in monkeys. Journal of Periodontology 1998; 69: 396-404.

Ishigaki S, Nakano T, Yamada S, Nakamura T, Takashima F. Biomechanical stress in bone surrounding an implant under simulated chewing. Clinical Oral Implants Research 2003, 14: 97-102.

Isidor F, Kabaaber S. Clinical condition of oral mucosal and bone at osseointegrated titanium implants. Journal of Dental Research 1988; 67: 53 (Abstract No.143).

Isidor F. Loss of osseointegration caused by occlusal load of oral implants. A clinical and radiographic study in monkeys. Clinical Oral Implants Research 1996; 7:143-152.

Isidor F. Histological evaluation of peri-implant bone at implants subjected to occlusal overload or plaque accumulation. Clinical Oral Implants research 1997; 8:1-9.

Ivanoff CJ, Sennerby L, Lekholm U. Influence of initial implant mobility on the integration of titanium implants. An experimental study in rabbits. Clinical oral Implants Research 1996; 7: 120-127.

Ivanoff CJ, Grondahl K, Sennerby L, Bergstrom C, Lekholm U. Influence of variations in implant diameter: a 3- 5-year retrospective clinical report. International Journal of Maxillofacial Implants 1999; 14: 173-180.

Jansen JA, van der Waerden JP, Wolke JG. Histological and histomorphometrical evaluation of the bone reaction to three different titanium alloy and hydroxyapatite coated implants. Journal of Applied Biomaterials 1993; 4: 213-219.

Jee WSS. Integrated Bone Tissue Physiology: Anatomy and Physiology. In: In: SC Cowin, Bone mechanics handbook. 2nd ed. CRC Press, Boca Raton, FL. 2001: Chapter 1, 2 -68.

Jepsen KJ, Davy DT, Akkus O. Observations of damage in bone. In: SC Cowin, Bone mechanics handbook, 2nd ed. CRC Press, Boca Raton, FL. 2001: Chapter 17,1-18.

Johansson C, Albrektsson T. Integration of screw implants in the rabbit: a 1-year follow-up of removal torque of titanium implants. International Journal of Oral and Maxillofacial Implants 1987; 2: 69-75.

Johansson C, Lausmaa J, Ask M, Hansson HA, Albrektsson T. Ultrastrucural differences of the interface zone between bone and Ti_6 AL_4V or commercially pure titanium. Journal of Biomedical Engineering 1989; 11: 3-8.

Junqueira LC, Carneiro J, Kelly RO. Basic Histology. 9thed. Beirut, Lebanon, Appleton and Lange; 1998;135-151.

Kapanen A. Biocompatibility of orthopaedic implants on bone formation cells. Thesis 2002, University of Oulu.

Kim Y, Le Geros R, Le Geros R. Characterisation of commercial HA-coated dental implants. Journal of Dental Research 1994; 73: 137 (Abstract 287).

Kiuru M. Magnetic resonance imaging of fatigue bone stress injury. Academic Dissertation 2002, Helsinki University Central Hospital, Department of Diagnostic Radiology, Helsinki, Finland.

Klokkevold PR, Nishimura RD, Adachi M, Caputo A. Osseointegration enhanced by chemical etching of titanium surface. A torque removal study in the rabbit. Clinical Oral Implants Research 1997; 8: 442-447.

Klokkevold PR., Johnson P, Dadgostari S, Caputo A, Davies JE, Nishimura RD. Early endosseous integration enhanced by dual acid etching of titanium: A torque removal study in the rabbit femur. Clinical Oral Implants Research 2001; 12: 350-357.

Knothe-Tate ML. Interstitial fluid flow. In, SC Cowin, Bone mechanics handbook. 2nd ed. CRC Press, Boca Raton, FL 2001, 1-29.

Knox R, Caudill R, Meffert R. Histologic evaluation of dental endosseous implants placed in surgically created extraction defects. The International Journal of Periodontics and Restorative Dentistry 1991; 11: 365-375.

Kolonidis SG. Effect of contamination of implant surfaces on re-osseointegration. A thesis submitted in partial fulfilment of degree of Master of Dental Surgery (Periodontology) 2001, University of Dublin.

Kotobuki N, Ioku K, Kawagoe D, Fujimori H, Goto S, Ohgushi H. Observation of osteogenic differentiation cascade of living mesenchymal stem cells on transparent hydroxyapatite ceramics. Biomaterials 2005; 26: 779-785.

Lai H, Zhang F, Zhang B, Yang C, Xue M. Influence of percentage of osseointegration on stress distribution around dental implants. The Chinese Journal of Dental Research 1998; 1: 7-11(Abstract).

Lanyon LE, Goodship AE, Pye CJ, MacFie JH. Mechanically adaptive bone remodelling. Journal of Biomechanics 1982; 15:141-154.

Lanyon LE. Functional strain in bone tissue as an objective, and controlling stimulus for adaptive bone remodelling. Biomechanics1987; 20: 1083-1093.

Larsson C. The interface between bone and implants with different surface oxide properties. Applied Osseointegration Research 2000; 1: 9-14.

Lazzara RJ, Porter SS, Testori T, Galante J, Zetterqvist LA. A prospective multicentre study evaluating loading of osseotite implants two months after placement. Journal of Esthetic Dentistry 1998; 10: 280-289.

Lazzara RJ, Testori T, Trisi P, Porter SS, Weinstein RL. A human histologic analysis of osseotite and machined surface using implants with two opposing surfaces. International Journal of Periodontics and Restorative Dentistry 1999; 19: 117-129.

Lee TC. Functional adaptation in compact bone. 1995, PhD. Thesis, University of Dublin.

Lee TC. Detection and accumulation of microdamage in bone. 1997, MD.Thesis, University of Dublin.

Lee TC, Myers ER, Hayes WC. Fluorescence-aided detection of microdamage in compact bone. Journal of Anatomy 1998; 193:179-184.

Lee TC, O'Brien FJ, Taylor D. The nature of fatigue damage in bone. International Journal of Fatigue 2000; 22: 84-853.

Lee TC, Staines A, Taylor D. Bone adaptation to load: microdamage as a stimulus for bone remodelling. Journal of Anatomy 2002; 201:437-446.

Lee TC, Mohsin S, Taylor D, Parkesh R, Gunnlaugsson T, O'Brien FJ, Giehl M, Gowin W. Detecting microdamage in bone. Journal of Anatomy 2003; 203: 161-172.

Lee TC, McHugh PE, O'Brien FJ, O'Mahony D, Taylor D, Bruzzi M, Rackard SM, Kennedy OD, Mahony NJ, Harrison N, Lohfield S, Brennan O, Gleeson J, Hazenberg JG, Mullins L, Tyndyk M, McNamara LM, Prendergast PJ. (2004) "Bone for life": osteoporosis, bone remodelling and computer simulation. In: Topics in Bio-Mechanical Engineering, P.J. Prendergast and P.E. McHugh (Eds). Trinity Centre for Bioengineering, Dublin and National Centre for Biomedical Engineering Science, Galway, Ireland pp: 58-93.

Lekholm U, Zarb GA. Patient selection and preparation. In, P Brånemark, G Zarb , T Albrektsson, Tissue-Integrated Prostheses. Osseointegration in Clinical Dentistry. 1st ed. Quintessence Publishing Co., 1985, 195–205.

Lemons JE, Dietsh-Misch F. Biomaterials for Dental Implants. In CE Misch, Implant Dentistry. 2nd ed. St Louis: Mosby, 1999: 271-302.

Lin JH, Russell G, Gertz B. Pharmacokinetics of alendronate: an overview. International Journal of Clinical Pracitice. Supplement 1999; 101: 18-26.

Linder L, Albrektsson T, Branemark PI, Hansson HA, Ivarsson B, Jonsson U, Lundström I. Electron microscopic analysis of the bone-titanium interface. Acta Orthopaedica Scandinavica 1983; 54: 45-52.

Lozada JL, Abbate MF, Pizzarello FA, James RA. Comparative three-dimensional analysis of two finite-element endosseous implant designs. Journal of Oral Implantology 1994; 20: 315-321.

Lubberts R, Turley PK. Force application to bioglass coated alumina implants of various sizes. Journal of Dental Research 1982; 61 (Special Issue): 339 (Abstract No.1447).

Lum LB. A biomechanical rationale for the use of short implants. The Journal of Oral Implantology 1991; 17: 126-131.

Lum LB, Osier JF. Load transfer from endosteal implants to supporting bone: an analysis using statics. Part two: Axial loading. Journal of Oral Implantology 1992; 18: 349-353.

Marcaccini A, Novaes AB, Souza SLS, Taba M, Grisi MFM. Immediate placement of implant into periodontally infected sites in dogs. Part 2: a fluorescence microscopy study. International Journal of Oral and Maxillofacial Implants 2003; 18: 812-819.

Marotti G, Muglia MA. A scanning electron microscope study of human bony lamellae. Proposal for a new model of collagen lamellar organization. Italian Journal of anatomy and embryology 1988; 93:163-175.

Martin RB, Burr DB. A hypothetical mechanism for the stimulation of osteonal remodelling by fatigued damage. Journal of Biomechanics 1982; 15: 137-139.

Martin RB, Burr DB. Structure, function and adaptation of compact bone. New York: Raven Press 1989:143-144.

Martin JY, Schwartz Z, Hummert Tw, Schraub DM, Simpson J, Lankford JJr, Dean DD, Cochran DL, Boyan BD. Effect of titanium surface roughness on proliferation, differentiation, and protein synthesis of human osteoblast-like cells (MG63). Journal of Biomedical Materials Research 1995; 29: 389-401.

Martin RB, Lau ST, Mathews PV, Gibson VA, Stover SM. Collagen fiber organization is related to mechanical properties and remodelling in equine bone. A comparison of two methods. Journal of Biomechanics 1996; 29: 1515-1521.

Martin RB, Burr DV, Sharkey NA. Skeletal biology. In RB Martin, Burr DB, N A Sharkey, Skeletal tissue mechanics. 1st ed. New York: spinger-Verlag 1998: 29-78.

Martin RB. Toward a unifying theory of bone remodelling. Bone 2000; 26: 1-6.

Martin RB. Is all cortical bone remodelling initiated by microdamage? Bone 2002; 30: 8-13.

Martin RB. Fatigue microdamage as an essential element of bone mechanics and biology. Calcified Tissue International 2003; 73:101-107.

Martinez H, Davarpanah M, Missika P, Celletti R, Lazzara R. Optimal implant stabilization in low density bone. Clinical Oral Implants Research 2001; 12: 423-432.

Marx RE. Pamidronate (Aredia) and zoledronate (Zometa) induced avascular necrosis of the jaws: a growing epidemic. Journal of Oral and Maxillofacial Surgery 2003; 61:1115-1117.

Mashiba T, Hirano T, Turner CH, Forwood MR, Johnston CC, Burr DB. Suppressed bone turnover by bisphosphonates increases microdamage accumulation and reduces some biomechanical properties in dog rib. Journal of Bone and Mineral Research 2000; 15: 613-620.

Mashiba T, Turner CH, Hirano T, Forwood MR, Johnston CC, Burr DB. Effects of suppressed bone turnover by bisphosphonates on microdamage accumulation and biomechanical properties in clinically relevant skeletal sites in beagles. Bone 2001a; 28: 524–531.

Mashiba T, Turner CH, Hirano T, Forwood MR, Jacob DS, Johnston CC, Burr DB. Effects of high-dose etidronate treatment on microdamage accumulation and biomechanical properties in beagle bone before occurrence of spontaneous fractures. Bone 2001b; 29: 271-278.

Masuda T, Yliheikkilä PK, Felton DA, Cooper LF. Generalization regarding the process and phenomenon of osseointegration. Part I. In vivo studies. International Journal of Oral and Maxillofacial Implants 1998; 13: 17-29.

Matthews L, Hirsch C. Temperatures measured in human cortical bone when drilling. Journal of Bone and Joint Surgery 1972; 54: 297-308.

McMillan PJ, Riggs ML, Bogle GC, Crigger M. Variables that influence the relationship between osseointegration and bone adjacent to an implant. . International Journal of Oral and Maxillofacial Implants 2000; 15: 654-661.

Mellal A, Wiskott HW, Botsis J, Scherrer SS, Belser UC. Simulating effect of implant loading on surrounding bone. Comparsion of three numerical models and validation by in vivo data. Clinical Oral Implants Research 2004; 15: 239-248.

Melo MD, Obeid G. Osteonecrosis of the maxilla in a patient with a history of bisphosphanate therapy. Journal Del'Association Dentaire Canadienne 2005; 71: 111-113.

Melsen F, Moseklide L. Tetracycline double-labelling of ilac trabecular bone in 41 normal adults. Calcified Tissue Research 1978; 26: 99-102.

Mikuni-Takagaki Y. Mechanical responses and signal transduction pathways in stretched osteocytes. Journal of Bone and Mineral Metabolism 1999; 17: 57-60.

Milch RA, Rall DP, Tobie JE. Bone localization of the tetracyclines. Journal of National Cancer Institute 1957; 19: 87-93.

Milch RA, Rall DP, Tobie JE. Fluorescence of tetracycline antibiotics in bone. Journal of Bone and Joint Surgery 1958; 40-A: 897-910.

Miller SC. Hormonal regulation of osteogenesis. In, Z Davidovitch, The biological mechanism of tooth eruption, resorption and replacement by implants. EBSCO Media, Birmingham 1988, 71-79.

Minkin C, Marinho VC. Role of osteoclast at the bone-implant interface. Advance Dental Research 1999; 13: 49-56.

Misch CE, Qu M, Bidez MW. Mechanical properties of trabicular bone in the human mandible: Implications for dental implant treatment planning and surgical placement. Journal of Oral and Maxillofacial Surgery 1999; 57:700-706.

Misch CE, Bidez MW, Sharawy M. A bioengineered implant for a predetermined bone cellular response to loading forces. A literature review and case report. Journal of Periodontology 2001; 72: 1276-1286.

Miyata T, Kobayashi Y, Araki H, Motomura Y, Shin K. The influence of controlled occlusal overload on peri-impant tissue: A histologic study in monkeys. International Journal of Oral and Maxillofacial Implants 1998; 13: 677-683.

Miyata T, Kobayashi Y, Araki H, Ohto T, Shin K. The influence of controlled occlusal overload on peri-impant tissue. Part 3: A histologic study in monkeys. International Journal of Oral and Maxillofacial Implants 2000; 15:425-431.

Miyata T, Kobayashi Y, Araki H, Ohto T, Shin K. The influence of controlled occlusal overload on peri-impant tissue. Part 4: A histologic study in monkeys. International Journal of Oral and Maxillofacial Implants 2002; 17: 384-390.

Módis L, Petkó M, Földs I. Histochemical examination of supporting tissues by means of fluorescence. Acta Morphologica Academia Scientiarm Hungaricae 1969; 17: 156-166.

Mohsin S, Taylor D, Lee TC. Three dimensional reconstruction of Haversian systems in ovine compact bone. European Journal of Morphology 2002; 40: 309-315.

Mohsin S, O'Brien FJ, Lee CT. Osteonal crack barriers in ovine compact bone. Journal of Anatomy 2006; 208: 81-89.

Moore TLA, Gibson LJ. Fatigue microdamage in bovine trabecular bone. Journal of Biomechanical Engineering 2003; 125: 769-776.

Mori S, Burr DB. Increased intracortical remodelling following fatigue damage. Bone 1993; 14: 103-109.

Mori S, Harruff R, Ambrosius W, Burr. Trabecular bone volume and microdamage accumulation in the femoral heads of women with and without femoral neck fractures. Bone 1997; 21: 521-526.

Morris HF, Ochi S, Crum P, Orenstein IH, Winkler S. AICRG, Part I: A 6-year multicentered, multidisciplinary clinical study of a new and innovative implant design. Journal of Oral Implantology (Special issue) 2004; 30: 125–133.

Mosley JR. Osteoporosis and bone functional adaptation: Mechanobiological regulation of bone architecture in growing and adult bone, a review. Journal of Rehabilitation Research and Development 2000; 37: 189-199.

Naert I, Quirynen M, Theuniers G, van Steenberghe D. Prosthetic aspects of osseointegrated fixtures supporting overdentures. A 4-year study. Journal of Prosthetic Dentistry 1991; 65: 671-680.

Nagasato T, Kobayashi M, Tsuchiya Y, Kaneko T, Nakajima T. Finite element analysis of the stresses around endosseous implants in various reconstructed mandibular models. Journal of Craniomaxillofacial Sugery 2002; 30: 170-177.

Nalla RK, Kinney JH, Richie RO. Mechanistic fracture criteria for the failure of human cortical bone. Natural Materials 2003; 2: 164-168.

Nalla RK, Kruzic JJ, Kinney JH, Richie RO. Mechanistic aspects of fracture and R-curve behaviour in human cortical bone. Biomaterials 2005; 26: 217-231.

Nanci A, Whitson W, Bianco P. Bone. In: Ten Cate's Oral Histology: Development, structure and function. 6th e ed. Edited by Antonio Nancy. St Louis Mosby 2003: 111-144.

Neugebauer J, Traini T, Thamas U, Piattelli A, Zöller JE. Peri-implant bone organization under immediate loading circularly polarized light analysis: A minipig study. Journal of Periodontology 2006: 77: 152-160.

Nkenke E, Kloss F, Wiltfang J, Schultze-Mosgau, Radespiel-Tröger M, Loos K, Neukam FW. Histomorphometric and fluorescence microscopic analysis of bone after installation of implants using an osteome technique. Clinical Oral Implants Research 2002; 13: 595-602.

Nkenke E, Lehner B, Weinzierl K, Thams U, Neugebauer J, Steveling H, Radespiel-Troger M, Neukam FW. Bone contact, growth, and density around immediately loaded implants in the mandible of mini pigs. Clinical Oral Implants Research 2003; 14: 312-321.

Noble B. Bone microdamage and cell apoptosis. European cells and Materials 2003; 6: 46-56.

Nölke L. Tissue Kinetics in compact bone: a study using polyfluorchrome labelling. A dissertation submitted the National University of Ireland, in partial fulfilment of the requirements for the Degree of Medical Science. 1995. Department of Anatomy, Royal College of Surgeons, Dublin.

Norman TL, Wang Z. Microdamage of human cortical bone: incidence and morphology in long bones. Bone 1997; 20: 375-379.

Norman T, Parsamian G, Coleman C. In-vivo diffuse damage in human cortical bone does not compromise bone toughness. 47th Annual Meeting Orthopaedic Research Society, February 25-28, 2001, San Francisco, California.

O'Brien FJ, Taylor D, Dickson GR, Lee TC. Visualisation of three-dimensional microcracks in compact bone. Journal of Anatomy 2000, 197:413–420.

O'Brien FJ. Microcracks and fatigue behaviour of compact bone. 2000, PhD. Thesis, University of Dublin.

O'Brien FJ, Taylor D, Lee TC. The process of microcrack growth in compact bone. In: Proceedings of the ASME Summer Bioengineering Conference, Snowbird, Utah: 2001: 791-792.

O'Brien FJ, Taylor D, Lee TC. An improved labelling technique for monitoring microcrack growth in compact bone. Journal of Biomechanics 2002; 35: 523-526.

O'Brien FJ, Taylor D, Lee TC. Microcrack accumulation at different intervals during fatigue testing of compact bone. Journal of Biomechanics 2003; 36: 973-980.

O'Brien FJ, Taylor D, Lee TC: The effect of bone microstructure on the initiation and growth of microcracks. Journal of Orthopaedic Research 2005a, 23: 475–480.

O'Brien F, Brennan O, Kennedy O, and Lee TC. Microcracks in cortical bone: How do they affect bone biology? Current Osteoporosis Reports 2005b, 3:39–45.

O'Mahony AM, Williams JL, Spencer P. Anisotropic elasticity of cortical and cancellous bone in the posterior mandible increases peri-implant stress and strain under oblique loading. Clinical Oral Implants Research 2001; 12: 648-657.

O'Reilly P. Torsional fatigue of cortical bone. 2002, M.Sc Thesis, University of Dublin.

O'Sullivan D, Sennerby L, Meredith N. Measurements comparing the initial stability of five designs of dental implants: a human cadaver study. Clinical Implant Dentistry and Related Research 2000; 2: 85-92.

O'Sullivan D, Sennerby L, Jagger D, Meredith N. A comparasion of two methods of enhancing implant primary stability. Clinical Implant Dentistry and Related Research 2004; 6: 48-57.

Ochi S, Morris HF, Winkler S. The influence of implant type, material, coating, diameter, and length on periotest values at second-stage surgery: DICRG interim report no. 4. Dental Implant Clinical Research Group. Implant Dentistry 1994; 3:159-162.

Ogiso B, Hashimoto M, Valiquette N, Carter S, Pilliar RM, Deporter D. A rat model for studying mechanical forces around implants. Journal of Dental Research 1991; 70 (Special Issue): 400 (Abstract No. 1072).

Ogiso M, Tabata K, Kuo PT, Borgese D. A histologic comparison of the functional loading capacity of an occludeddense apatite implant and natural dentition. Journal of Prosthetic Dentistry 1994; 71: 581-588.

Oh TJ, Yoon J, Misch CE, Wang HL. The causes of early implant bone loss: myth or science? Journal of Periodontology 2002; 73:322-333.

Ohtsu A, Kusakari H, Maeda T, Takano Y. A histological investigation on tissue response to titanium implants in cortical bone of the rat femur. Journal of Periodontology 1997; 68: 270-283.

Olerud S, Lorenz GL. Triple fluorochrome labelling in bone formation and bone resorption. The Journal of Bone and Joint Surgery 1970; 52-A: 274-278.

Parfitt AM. Targeted and non-targeted bone remodelling: relationship to BMU origination and progression. Bone 2002; 30: 5-7.

Petrie CS, Williams JL. Comparative evaluation of implant designs: influence of diameter, length, and taper on strains in the alveolar crest. A three-dimensional finite-element analysis. Clinical Oral Implants Research 2005; 16: 486-494.

Piattelli A, Cordioli GP, Trisi P, Passi P, Favero GA, Meffert RM. Light and conofocal laser scanning microscopic evaluation of hydroxyapatite resorption patterns of medullary and cortical bone. International Journal of Oral and Maxillofacial Implants 1993; 8: 309-315.

Pithioux M, Subit D, Chabrand P. Compact bones failure models in quasi-static and dynamic solicitations. Medical Engineering and Physics 2004; 26: 647-653.

Prendergast PJ, Huiskes R. Microdamage and osteocyte-lacuna strain in bone: a microstructural finite element analysis. Journal of Biomechanical Engineering 1996, 118:240-246.

Puleo DA, Nanci A. Understanding and controlling the bone-implant interface. Biomaterial/ Biological Engeneering Society 1999; 20: 2311-2321.

Quirynen M, Naert I, van Steenberghe D. Fixture design and overload influence marginal bone loss and fixture success in the Brånemark system. Clinical Oral Implants Research 1992; 3: 104-111.

Raghavendra S, Wood MC, Taylor TD. Early wound healing around endosseous implants: A review of the literature. International Journal of Oral and Maxillofacial Implants 2005; 20: 425-431.

Rahn BA. Polychrome fluorescence labelling of bone formation instrumental aspects and experimental use. Zeiss Information 1977; 22: 36-39.

Ralston SH. Structure and metabolism of bone. Medicine 2005; 33: 58-60.

Reilly DT, Burstein AH. The elastic and ultimate properties of compact bone tissue. Journal of Biomechanics 1975; 8: 393-405.

Reilly GC, Currey JD. The development of microcracking and failure in bone depends on the loading mode to which it is adapted. Journal of Experimental Biology 1999; 202: 543-552.

Reilly GC, Currey JD. The effects of damage and microcracking on the impact strength of bone. Journal of Biomechanics 2000; 33: 337-343.

Riggs CM, Lanyon LE, Boyde A. Functional association between collagen fibre orientation and locomotor strain direction in cortical bone of the equine radius. Anatomy and Embryology 1993; 187: 231-238.

Ritchie RO, Kinney JH, Kruzic JJ, Nalla RK. A fracture mechanics and mechanistic approach to the failure of cortical bone. Fatigue Fract Mater Sruct 2005; 28: 345-371.

Roberts WE, Smith RK, Zilberman Y, Mozsary PG, Smith RS. Osseous adaptation to continuous loading of rigid endosseous implants. American Journal of Orthodontics 1984; 86: 95-111.

Roberts WE. Bone tissue interface. Journal of Dental Education 1988; 52:804-809.

Rost FWD. Fluorescence Microscopy. Cambridge University Press, New York, 1992, Volume I: 256.

Rost FWD. Fluorescence Microscopy. Fluorescence Microscopy. Cambridge University Press, New York, 1995, Volume II: 456.

Rubin CT, Sommerfeldt DW, Judex S, Qin Y-X. (2001). http://www.bme.sunysb.edu/bme/people/faculty/docs/crubin/2001-DDT-bone-adapt.pdf.

Ruggeiro SL, Mehrotra B, Rosenberg TJ, Engroff SL. Osteonecrosis of the jaws associated with the use of bisphosphonates: a review of 63 cases. Journal of Oral and Maxillofacial Surgery 2004; 62: 527-534.

Ruggeiro SL, Mehrotra B. Ten years of alendronate treatment for osteoporosis in postmenopausal women. The New England Journal of Medicine 2004; 350:1189-1199.

Russell GG, Croucher PI, Rogers MJ. Bisphosphonates: Pharmacology, mechanics of action and clinical uses. Osteoporosis International 1999; 2: S66-S80.

Sandén B (2001). Fixation of spinal implants. clinical and experimental studies on the effects of hydroxyapatite coating. Comprehensive Summaries of Uppsala. Dissertations from the Faculty of Medicine 1085.

Sanz M, Alandez J, Lazaro P, Calvo JL, Quirynen M, van Steenberghe D. Histo-pathologic characteristics of peri-implant soft tissues in Brånemark implants with 2 distinct clinical and radiological patterns. Clinical Oral Implants Research 1991; 2: 128-134.

Satomi K, Akagawa Y, Nikai H, Tsuru H. Bone-implant interface structures after nontapping and tapping insertion of screw-type titanium alloy endosseous implants. Journal of Prosthetic Dentistry 1988; 59: 339-342.

Säuberlich S, Klee D, Richter E-J, Höcker H, Speakermann H. Cell culture tests for assessing the tolerance of soft tissue to variously modified titanium surfaces. Clinical Oral Implants Research 1999; 10: 379-393.

Scannell PT, Prendergast PJ. Simulation of changes in bone around hip replacement implants. The Engineers Journal 2005; 59: 372-377.

Schaffler MB, Burr DB, Frederickson RG. Morphology of the osteonal cement line in human bone. Anatomical Record 1987; 217: 223-238.

Schaffler MB, Radin EL, Burr DB. Mechanical and morphological effects of strain rate on fatigue of compact bone. Bone 1989; 10; 207-214.

Schaffler MB, Pitchford WC, Choi K, Riddle JM. Examination of compact bone microdamage using black-scattered electron microscopy. Bone 1994; 15: 483-488.

Schaffler MB, Choi K, Milgrom C Ageing and matrix microdamage accumulation in human compact bone. Bone 1995; 17: 521-525.

Schaffler MB, Boyce TM, Fyhrie DP. Tissue and matrix failure modes in human compact bone during tensile fatigue. Trans Orthopaedic Research Society 1996; 21: 57.

Schliephake H, Reiss G, Urban R, Neukam FW, Guckel S. Metal release from titanium fixtures during placement in the mandible: an experimental study. International Journal of Oral and Maxillofacial Implants 1993; 8: 502-511.

Scully C, Cawson, R A. Medical problems in dentistry. 4th ed, Wright , Oxford 1998, 316.

Sennerby L, Ericson LE, Thomsen P, Lekholm U, Astrand P. Structure of the bone-titanium interface in retrieved clinical oral implants. Clinical Oral Implants Research 1991; 2:103-111.

Sennerby L, Thomsen P, Ericson LE. Early tissue response to titanium implants inserted in rabbit bone. Part I. Light microscopic observations. Journal of Material Sciences: Materials in Medicine 1993; 4: 240-250.

Sennerby L, Roos J. Surgical determinants of clinical success of osseointegrated oral implants: A review of the literature. The International Journal of Prosthodontics 1998; 11: 408-420.

Shirakura M, Fujii N, Ohnishi H, Taguchi Y, Ohshima H, Nomura S, Maeda T. Tissue response to titanium implantation in the rat maxilla, with special reference to the effects of surface conditions on bone formation. Clinical Oral Implants Research 2003; 14: 687-696.

Siddiqui AA, Ismail JY, Kukunas S. Immediate loading of dental implants in the edentulous mandible: a preliminary case report from an international prospective multicenter study. Compendium of Continuing Education in Dentistry 2001; 22:867-870.

Silva ECCM, Ulm F-J. A bio-chemo-mechanics approach to bone resorption and fracture. 15th ASCE Engineering Mechanics Conference, June 2-5, 2002, Colombia University, New York.

Sobelman OS, Gibeling JC, Stover SM, Hazelwood SJ, Yeh OC, Shelton DR, Martin RB: Do microcracks decrease or increase fatigue resistance in cortical bone? Journal of Biomechanics 2004, 37:1295–1303.

Sommerfeldt DW, Rubin CT. Biology of bone and how it orchestrates the form and function of the skeleton. European Spine Journal 2001; 10: S86-S95.

Srinivasan S, Gross TS. Canalicular fluid flow induced by bending of a long bone. Medical Engineering and Physics 2000; 22: 127-133.

Stanford CM, Brand RA. Toward an understanding of implant occlusion and strain adaptive bone modelling and remodelling. Journal of Prosthetic Dentistry 1999; 81: 553-561.

Stanford CM. Biomechanical and functional behaviour of implants. Advance Dental Research 1999; 13: 88-92.

Stark WJ, Epker BN. Failure of osteointegrated implants after diphosphonate therapy for osteoporosis: A case report. International Journal of Oral and Maxillofacial Implants 1995; 10:74-78.

Steflik DE, Noel C, McBrayer C, Lake FT, Parr GR, Sisk AL, Hanes PJ. Histologic observations of bone remodelling adjacent to endosteal dental implants. Journal of Oral Implantology 1995; 21: 96-106.

Steflik DE, Lake FT, Sisk AL, Parr GR, Hanes PJ, Davis HC, Adams BO, Yavari J. A comparative investigation in dogs: 2-year morphometric results of the dental implant-bone interface. International Journal of Oral and Maxillofacial Implants 1996; 11: 15-25.

Steigenga JT, Al-Shammari KF, Nociti FH, Misch CE, Wang HL. Dental implant design and its relationship to long-term implant success. Implant Dentistry 2003; 12: 306-317.

Steigenga JT, Al-Shammari KF, Misch CE, Nociti FH, Wang HL. Effects of implant thread geometry on percentage of osseointegration and resistance to reverse torque in the tibia of rabbits. Journal of Periodontology 2004; 75: 1233-1241.

Stewart DJ. The re-incorporation in calcified tissues of tetracycline released following its deposition in the bone rats. Archives of Oral Biology 1973; 18: 759-764.

Stover SM, Martin RB, Pool RR, Taylor KT, Harrington TM. *In vivo* labelling of microdamage in cortical bone tissue. Proceedings of the Orthopaedic Research Society 1993; 18: 541.

Strietzel FP, Nowak M, Küchler I, Friedmann A. Peri-implant alveolar bone loss with respect to bone quality after use of the osteotome technique. Results of a retrospective study. Clinical Oral Implants Research 2002; 13: 508-513.

Strnad SZ, Strnad J, Povysil C, Urban K. Effect of plasma-sprayed hydroxyapatite coating on the osteoconductvity of commercially pure titanium implants. International Journal of Oral and Maxillofacial Implants 2000; 15: 483-490.

Sun F, Mosekilde L. Tetracycline double-labelling of trabecular bone in 41 normal adults. Calcified Tissue Research 1978; 26: 99-102.

Sun TC, Mori S, Roper J, Brown C, Hooser T, Burr DB. Do different fluorochrome labels give equivalent histomorphometric information? Bone 1992; 13: 443-446.

Suzuki HK, Mathews A. Two-colour fluorescence labelling of mineralising tissues with tetracycline and 2,4-bis[N, N′ -Di-(Carbomethyl) aminometyl] fluorescin. Stain Technology 1966; 41: 57-60.

Sykaras N, Iacopino AM, Marker VA, Triplett RG, Woody RD. Implant materials, designs, and surface topographies: their effect on osseointegration. A literature review. International Journal of Oral and Maxillofacial Implants 2000; 15: 675-690.

Tada S, Stegaroiu R, Kitamura E, Miyakawa O, Kusakari H. Influence of implant design and bone quality on stress/strain distribution in bone around implants: a 3-dimensional finite element analysis. International Journal of Oral and Maxillofacial Implants 2003; 18: 357-368.

Takeshita F, Ayukawa Y, Iyama S, Murai K, Suetsugu T. Long-term evaluation of bone-titanium interface in rat tibiae using light microscopy, transmission electron microscopy, and image processing. Journal of Biomedical Materials Research 1997; 37: 235-242.

Taylor D, Lee TC. Measuring the shape and size of microcrack in bone. Journal of Biomechanics 1998; 31: 1177-1180.

Taylor D. Microcrack growth parameters for compact bone deduced from stiffness variations. Journal of Biomechanics 1998; 31:587-592.

Tehemar SH. Factors affecting heat generation during implant site preparation: a review of biologic observations and future considerations. International Journal of Oral and Maxillofacial Implants 1999; 14: 127-136.

Teixeira ER, Sato Y, Akagawa Y, Shindoi N. A comparative evaluation of mandibular finite element models with different lengths and elements for implant biomechanics. Journal of Oral Rehabilitation 1998; 25: 299-303.

Testori T, Szmukler-Moncler S, Francetti L, Del Fabbro M, Scarano A, Piattelli A, Weinstein RL. Immediate loading of Osseotite implants: a case report and histologic analysis after 4 months of occlusal loading. International Journal of Periodontics and Restorative Dentistry 2001; 21 451-459.

Thomas KA, Kay JF, Cook SD, Jarcho M. The effect of surface macrotexture and hydroxylapatite coating on the mechanical strengths and histologic profiles of titanium implant materials. Journal of Biomedical Materials Research 1987; 21:1395-1414.

Thomas KA. Hydroxyapatite coatings. Orthopaedics 1994; 17: 267-278.

Treharne RW, Brighton CT. The use and possible misuse of tetracycline as a vital stain. Clinical Orthopaedic and Related Research 1979; 140: 240-246.

Tricker ND, Dixon RB, Garetto LP. Cortical bone turnover and mineral apposition in dentate dog mandible. Journal of Dental Research 1977; 76 (Special issue): 201.

Trisi P, Rebaudi A. Progressive bone adaptation of titanium implants during and after orthodontic load in humans. The International Journal of Periodontics and Restorative Dentistry 2002; 22: 31-43.

Trisi P, Rebaudi A. Peri-implant bone reaction to immediate, early, and delayed orthodontic loading in humans. The International Journal of Periodontics and Restorative Dentistry 2005; 25: 317-329.

Tufekci E, Brantley WA, Mitchell JC, McGlumphy EA. Microstructures of plasma sprayed hydroxyapatite-coated Ti-6Al-4V dental implants. International Journal of Oral and Maxillofacial Implants 1997; 12: 25-31.

Turner CH, Burr DB. Basic biomechanical measurements of bone: a tutorial. Bone 1993; 14: 595-608.

Turner CH. Biomechanics of bone: determinants of skeletal fragility and bone quality. Osteoporosis International 2002; 13: 97-104.

Turner C H . Biomechanical aspects of bone formation. In, F Bronner and M Farach-Carson eds: Bone formation. Springer, 2004, 1, 79-105.

Uehara T, Takaoka K, Ito K. Histological evidence of osseointegration in human retrieved fractured hydroxyapatite-coated screw-type implants: a case report. Clinical Oral Implants Research 2004; 15: 540-545.

Vaillancourt H, Pilliar RM, McCammond D. Finite element analysis of crestal bone loss around porous-coated dental implants. Journal of Applied Biomaterials 1995; 6: 267-282.

Vajda EG, Kneissel M, Muggenburg B, Miller SC. Increased intracortical bone remodeling during lactation in beagle dogs. Biology of Reproduction 1999; 61: 1439-1444.

Vashishth D, Behiri JC, Bonfield W. Crack growth resistance in cortical bone: concept of microcrack toughening. Journal of Biomechanics 1997; 30: 763-769.

Vashishth D, Verborgt O, Divine G, Schaffler MB, Fyhrie DP. Decline in osteocyte lacunar density in human cortical bone is associated with accumulation of microcracks with age. Bone 2000; 26: 375–380.

Vashishth D, Kim D, Rho J. The influence of tensile and compressive damage on bending fatigue of human cortical bone. Proceeding of the Second Joint EMBS/BMES Conference, Houston, TX, USA. October 23-26. 2002.

Vashishth D, Tanner KE, Bonfield. Experimental validation of a microcracking-based toughening mechanism for cortical bone. Journal of Biomechanics 2003; 26: 121-124.

Verborgt O, Gibson GJ, Schaffler MB. Loss of osteocyte integrity in association with microdamage and bone remodelling after fatigue *in vivo*. Journal of Bone and Mineral Research 2000; 15: 60-67.

Wachtel E F, Keaveny T M. Dependence of trabecular damage on mechanical strain. Journal of Orthopaedic Research 1997; 15: 781-787.

Wang X. A model of energy dissipation in the post-yield deformation of bone. 2003 Summer Bioengineering Conference, June 25-29, Sonesta Beach Resort in Key Biscayne, Florida.

Watzek G, Gruber R. Morphologic and cellular parameters of bone quality. Applied Osseointegration Research; 2002; 3: 3-8.

Weinbaum S, Cowin SC, Zeng Y. A model for the excitation of osteocytes by mechanical loading-induced bone fluid shear stresses. Journal of Biomechanics 1994; 27: 339-360.

Weinlaender M, Beumer J 3rd, Kenney EB, Lekovic V, Holmes R, Moy PK, Plenk H Jr. Histomorphometric and fluorescence microscopic evaluation of interfacial bone healing around 3 different dental implants before and after radiation therapy. International Journal of Oral and Maxillofacial Implants 2006; 21: 212-224.

Wennerburg A, Albrektsson T, Andersson B, Krol JJ. A histomorphometric and removal torque study of screw-shaped titanium implants with three different surface topographies. Clinical Oral Implants Research 1995; 6: 24-30.

Wennerburg A, Albrektsson T, Andersson B. Bone tissue response to commercially pure titanium implants blasted with fine and coarse particles of aluminium oxide. International Journal of Oral and Maxillofacial Implants 1996; 11: 38-45.

Wennerburg A, Ektessabi A, Albrektsson T, Johansson C. Andersson B. A 1-year follow-up of implants of differing surface roughness placed in rabbit bone. International Journal of Oral and Maxillofacial Implants 1997; 12: 486-494.

Wenzel TE, Schaffler MB, Fyhrie DP. In vivo trabecular microcracks in human vertebral bone. Bone 1996; 19: 89-95.

Wie H, Herø H, Solheim T, Kleven E, Rørvik AM, Haanaes HR. Bonding capacity in bone of HIP-processed HA-coated titanium: mechanical and histological investigations. Journal of Biomedical Materials Research 1995; 29:1443-1449.

Wie H, Herø H, Solheim T. Hot isostatic pressing-processed hydroxyapatite-coated titanium implants: light microscopic and scanning electron microscopy investigations. International Journal of Oral and Maxillofacial Implants 1998; 13: 837-844.

Wiskott HW, Besler UC. Lack of integration of smooth titanium surfaces: a working hypothesis based on strains generated in the surrounding bone. Clinical Oral Implants Research 1999; 10: 429-44.

Wong M, Eulenberger J, Schenk R, Hunziker E. Effects of surface topology on the osseointegration of implant in trabecular bone. Journal of Biomedical Materials Research 1995; 29: 1567-1575.

Yacker MJ, Klein M. The effect of irrigation on osteotomy depth and bur diameter. International Journal of Oral and Maxillofacial Implants 1996; 11: 634-638.

Zarb GA, Albrektsson T. Osseointegration: a requiem for the periodontal ligament. International Journal of Periodontics and Restorative Dentistry 1991; 11: 88-91.

Zioupos P, Currey JD, Sedman AJ. An examination of the micromechanics of failure of bone and antler by acoustic emission tests and laser scanning conofocal microscopy. Medical Engineering and Physics 1994; 16: 203-212.

Zioupos P, Currey JD. The extent of microcracking and the morphology of microcracks in damaged bone. Journal of Materials Science 1994; 29: 978-986.

Zioupos P. Accumulation of *in vivo* fatigue microdamage and its relation to biomechanical properties in ageing human cortical bone. Journal of Microscopy 2001a; 201: 270-278.

Zioupos P. Ageing Human Bone: Factors affecting its biomechanical properties and the role of collagen. Journal of Biomaterials Applications 2001b; 15: 187-229.

Zurita V, Le Geros R, Le Geros JP, Wang J. Disolution of "Hydroxyapatite" coatings on implant materials. Journal of Dental Research 1994; 73: 137 (Abstract No. 288).